FORMATION AND REACTIVITY OF SOME METAL BORIDES AND CARBIDES

A Thesis presented for the Research Degree of

DOCTOR OF PHILOSOPHY

of the

COUNCIL FOR NATIONAL ACADEMIC AWARDS

LONDON

by

ASGHAR ALI CHAUDHRY

John Graymore Chemistry Laboratories,
Department of Mathematical and
Physical Sciences,
Plymouth Polytechnic,
PLYMOUTH,
PL4 8AA,
Devon.

November 1973

A B S T R A C T

Most recent developments in the production, properties and applications of borides and carbides are reviewed.

The reactivity and sintering of finely-divided boron carbide with metal additives has been investigated. The additives (Fe, Ti, Zr, V, Nb, Ta, Mo, W and Al) generally promote sintering of the boron carbide. Their effectiveness is reduced occasionally when there is some surface activation caused by the metals reacting with the boron carbide to form metal borides and carbides of different crystal lattice type and molecular volume. The more metallic character of the bonding in the metal borides and carbides enhances surface and crystal lattice diffusion at the grain boundaries of the more covalent boron carbide. Iron is much more effective than the other metal additives tested in promoting sintering of the boron carbide at 1800°C since it forms the lowest-melting borides. It also enhances sintering during hot pressing of boron carbide at this temperature, but even with pressures up to one ton in^{-2} ($1.54 \times 10^7 Nm^{-2}$) the densification does not exceed 60% of theoretical. Further research on hot pressing of more ionic borides such as CaB_6 indicates that for most borides and carbides, including boron carbide, final consolidation of the material is not achieved until a temperature of about 90% of the melting point (in K) is reached.

Various metal foils e.g. Fe, Ti, Zr, V, Nb, Ta, Cr, Mo and W were coated with a dispersion of boron carbide and heated under argon at fixed temperatures for 5 hours. This produced mixed phases of borides and carbides which varied in their composition and pene-

tration according to the metal substrate. Microhardness measurements showed that the coatings were harder than the surfaces of the original metals.

Factors influencing the oxidation of the metals, metal borides and carbides and unreacted boron carbide in the above metal coatings have been investigated. The oxidations are often controlled by solid-state diffusion processes, giving parabolic kinetics which become linear if the material sinters extensively. The Tammann temperatures of the reactants and products are significant in the sintering and agglomeration of the oxidised material.

ACKNOWLEDGEMENTS

The author wishes to express his sincere thanks to Dr. D.R. Glasson and Dr. J.A. Jones for their helpful advice, guidance and constant supervision throughout the course of this work. He is grateful also to Dr. S.A.A. Jayaweera for his advice, co-operation and valuable discussions.

He is grateful to Mr. K.J. Matterson, Borax Consolidated Ltd., Chessington, for industrial supervision and Dr. R.H. Biddulph and Dr. C. Brown for their constructive and valuable suggestions; also to Mr. L. Bullock, Diamond Products Research Laboratories, Torpoint, Cornwall, and to Mr. Matterson, for hot pressing facilities; to Mr. D. Short for assistance with the metallographic examinations and to Mr. D. Sargent and Dr. B.J. Brockington for assistance in the use of the scanning electron microscope at the Royal Naval Engineering College, Manadon, Plymouth.

He would like to thank the Governors of the Polytechnic for granting him a research assistantship.

He is grateful to Dr. A.B. Meggy and Dr. C.M. Gillett for allowing the use of research facilities. His thanks are also due to the Polytechnic Library staff for their assistance and the Computer staff for programming facilities.

He is thankful to Mrs. A. Harman for her special care in typing the manuscript.

CONTENTS

CHAPTER 1

GENERAL INTRODUCTION

During the last fifteen years an increasing industrial demand for refractory hard materials, especially in the fields of Aviation, Space and Nuclear Industries, has intensified the research on borides and carbides. Among the most desirable properties of these materials are their high melting point and thermal stability, hardness, as well as specific electrical and magnetic properties. In addition to their very high melting point, modern refractories are recognised by a combination of other important properties such as hot hardness (hardness at high temperatures), resistivity to highly reactive agents, low vapour pressure and evaporation rates. Dependence of these properties of refractory borides and carbides on their electronic structure is explained (Shaffer & Samsonov, 1964a).

The refractory borides and carbides that have attracted extensive research studies are those of transition metals, lanthanides, actinides, and aluminium (Schwarzkopf & Kieffer, 1953, Samsonov, 1964a). The electrons of the incomplete d- and f- levels of the transition metals take part in the formation of chemical bonds in the crystal lattices of these compounds (Samsonov, 1967). The refractory metal borides and carbides possess most of the properties of metals and alloys and they exhibit heterodesmic chemical bonding, properties of each type being characterised by their crystal structure. Binder metals such as chromium, cobalt and nickel are used in the formation of 'hard metals', i.e. cemented carbides and borides (Schwarzkopf & Kieffer, 1960). Some of the borides and carbides exhibit metalloid

properties, e.g. they are semiconductors and have high electrical resistance. These are compounds of boron and carbon with each other and with other non-metals such as N, S, P and Si. These compounds are characterised also by the heterodesmic chemical bonding in their crystal lattices, but with covalent bonding predominating. This contributes semiconductor properties and high electrical resistance at room temperature. They exhibit layer, chain or skeletal structure patterns and they decompose either at their melting points or slightly higher temperature.

Nevertheless, some borides and carbides are intermediate between the above-mentioned metallic and non-metallic groups as regards their refractory properties.

Aims of the present work

Although other workers have prepared borides and carbides for use as refractories, their investigations have been mainly empirical and viewed from a commercial angle. Their aim has been to form products with improved properties, e.g. with higher microhardness values. Systematic investigations correlating crystallographic properties with time and temperature of formation have not been carried out before.

One of the aims of the present work has been to produce metal borides/carbides starting from boron carbide + metal, attempting to improve the properties of the finished product. Thus, the production of boride/carbide surfaces of metal foils with superior microhardness values was one of the objectives. Also the densification of boron carbide by pressureless sintering and hot-pressing with powdered metal additives was attempted. Densification usually leads to the improvement of mechanical properties.

In the reaction of boron carbide with metals, changes in crystallographic properties with temperature, reaction time and nature and amount of metal additive was investigated, attempting to optimise the reaction condtions. Previous workers have worked mostly with a single metal in each case. In the present work, the sintering behaviour of the products has been studied systematically over a wide range of metals.

The stability of the products was assessed by comparing their behaviour on oxidation with that of the original materials, viz. boron carbide and the metals. The oxidation of boron carbide of submicron size has been studied previously in these laboratories. In the present work, the investigation has been extended to the

material above this range. Oxidation studies were also carried out on titanium metal and some related products.

The structure of the work

The work is presented in two parts - dissertation (Part I) and thesis (Part II).

Part I gives the general background to the work. This includes a review of studies carried out by previous workers on the formation and reactivity of borides and the theoretical background related to certain aspects of the work. In Chapter 3 the experimental techniques are summarised and a brief description of the underlying theoretical principles is given.

In Part II, the results of the present work are described and discussed in relation to the theoretical principles and the results of previous workers.

P A R T I

DISSERTATION

Chapter 2 — Review of borides and carbides

Chapter 3 — Experimental techniques

CHAPTER 2

REVIEW OF BORIDES

2.1 Introduction

The formation and reactivity of borides was the subject of several reviews, e.g. Aronsson (1960), Thompson & Wood (1963), Thompson (1965, 1970a, 1970b, 1970c, 1971), Nowotny (1972). A comprehensive account of the subject was also given by Glasson and Jones (1969a). In this chapter the review has been updated.

Methods of production of borides are tabulated in the following section. The references include phase-diagram studies on metal-boron systems as well as patents on methods of producing borides, with improved properties.

Thermodynamic data for the formation of borides are presented in Section 2.3, and compared with that of other refractories. This is followed by discussion of the relationship between bonding and crystal structure of borides (Section 2.4). Studies on the properties of borides and carbides are tabulated in Section 2.5.

A comprehensive review of the theories of sintering is given in Section 2.6. This brings up-to-date an earlier review (Jones, 1970). The industrial applications of borides and carbides are classified and tabulated (Section 2.7).

2.2 Production techniques

Methods of production of borides and carbides were discussed by Schwarzkopf & Kieffer (1953), Samsonov (1956, 1959), Aronsson (1960), Thompson & Wood (1963), Thompson (1965, 1970a, 1970b, 1970c), Glasson & Jones (1969a), Nowotny (1972a), Storms (1967, 1972), Toth (1971) and Kosolapova (1971). Table 2.1 summarises studies carried out in recent years on various aspects of the production of borides.

Table 2.1

Borides

Boride	Nature of publication	Reference
Lithium boride	Magnesium boride + lithium fluoride	Maron & Germaide 1970
BaB_6	Mechanism of formation	Torker et al 1971
Ba, Ca, Sr (MB_6)	Me + B	Blizhakov & Peshev 1970
Aluminium and magnesium borides	Mixed ores	Vekshina et al 1971
AlB_{12}	Aluminothermic process	Samsonov & Neronov 1970
YB_2	Y + B	Markovski et al 1969
YB_{12}	Y + B	O, Dinstov & Paderno 1971
TiB_2	Single crystals in Al	Higashi & Atoda 1970
TiB_2	$BCl_3 + TiCl_4 + 5H_2$	Takahashi et al 1971
ZrB_2	Zr + B	Voroshilov & Kuz'ma 1969
Cr_4B, Cr_2, CrB, Cr_2B_4, CrB_2	Cr + B	Serebryakova & Samsonov 1967
NbB, Nb_2B, NbB, Ta_3B_4, TaB, Ta_2B, Cr_2B, CrB	Nb_2O_5 - NbB_2 Ta_2O_5 - TaB_2 Cr_2O_3 - CrB_2	Marek et al 1971
Molybdenum boride	Coatings	Karev et al 1967
Zirconium, Chromium, molybdenum borides	Carbothermic process	Meerson & Gorbunov 1969
Tungsten boride	Phase diagram up to 2370°C	Kuz'ma et al 1967
CaB_6, SrB_6, BaB_6, CeB_6, PrB_6, NdB_6, TiB_2, ZrB_2, HfB_2, VB_2, NdB_2, TaB_2, CrB_2, Mo_2B_5, W_2B_5	Borothermic reduction	Blizhakov & Peshev 1970
AlB_2, TiB_2	Vapour deposition	Blizhakov & Peshev 1970

Table 2.1 (cont'd)

Boride	Nature of publication	Reference
Niobium, tantalum, molybdenum and tungsten borides	Me + B	Samsonov et al 1970b
TiB_2, ZrB_2, HfB_2, VB_2, NbB_2, TaB_2, CrB_2, MoB, Mo_2B_5	Borides + C 2000-3000°C	Levinskii et al 1968
TiB_2, W_2B_5, chromium boride	Me + B	Oreshkin 1971
Borides of metal group IVA - VIA	In powder form from solution in molten zinc	Gurin et al 1971
Mn_4B, Mn_2B, MnB, Mn_3B_4, MnB_2, MnB_4	Mn + B, phase diagram	Markovskii & Bezruk 1967
Re_3B, Re_7B_3, Re_2B	Re + B	Portnoi & Romashov 1968
Fe_2B, FeB	Fe + B	Deger et al 1972
Fe_2B, FeB	Fe + B_4C + 1% NH_4Cl also Fe + B_4C + $Na_2B_4O_7$	Minkevich et al 1967
FeB	Boronizing by B_4C - alkali metal carbonate	Muta et al 1968
FeB	Boronizing by boron	Protasevich et al 1972
Fe_2B, FeB	Composition of hot bath for boronizing iron	Hosokawa & Kogakubu 1972
Co_2B, Co_3B	Cobalt borides + C)	Markovskii et al 1971
Nickel borides	Nickel borides + C)	
Vanadium, iron, cobalt Nickel Borides, CrB_4	BCl_3 + H_2 + MeS_x)	Cueilleron et al 1971
TiB_2, VB_2, CrB_2	B + MeS_x $\xrightarrow{700\text{-}1000^\circ C}$)	
LaB_6	La_2O_3 + B_2O_3	Meerson et al 1970
LaB_6	Production of complex shapes	Medvedev et al 1971
Ta_2B_2, TaB, Ta_3B_4, TaB_2, Mo_2B, -Mo_B	LaB_6 + Ta) LaB_6 + Mo)	Gert et al 1969

Table 2.1 (cont'd)

Boride	Nature of publication	Reference
LaB_4, CeB_4, PrB_4, LuB_4	Metal flux + B	Fisk et al 1972
SrB_6, LaB_6, YbB_6, ThB_6	Me + B or MeO_x + B_2O_3 + C	Etourneau et al 1970
SmB_6	$2Sm_2O_3$ + (6+4x) B	Niihara 1971
SmB_4, NiB, Ni_2B, Ni_4B_3	SmB_6 + Ni, phase diagram	Romashov et al 1970
Borides: general review of methods	D.C. plasma	De Vynck 1970, 1971
Boron carbide briquette	Hot pressing	Maire et al 1969 patent
Boron and boron carbide coatings on objects	Vapour deposition	Cochran & Stephenson 1970
Boronizing of forging dies	Article + B	Vincze 1969
Mixed borides		
Borides	**Nature of publication**	**Reference**
Aluminium, magnesium boride	Metals + B	Vekshina et al 1971
MoBC	Mo + B + C	Salibekov et al 1970
SrB_6 — LaB_6 BaB_6 — LaB_6	Borothermic process	Blizhakov & Peshev 1970
W-Cr-B, W-Mo-B	Phase diagrams	Telegus & Kuz'ma 1968
(Ti, Cr) borides	Alloy + B	Oreshkin et al 1971
$Fe-Fe_2B-Fe_3C$	Equilibrium phase diagram	Fomichev et al 1971
$Co_{11}B_2C$	Co+B+C or Co_2B+Co_3C+Co	Markovskii et al 1971
$B_{48}B_2C$	Pyrolysis of $BBr_3-CH_4-H_2$ on tantalum substrate	Ploog et al 1972
$B_{48}B_2N_2$	-do- - N_2-H_2 on BN substrate	Ploog et al 1972
$C - B_4C - X$ X = fluorides, V_2O_5, MgO, Al_2O_3, SiO_2	B_4C + C + oxide	Srbobran 1969

Table 2.1 (cont'd)

Carbides

Carbides	Nature of publication	Reference
Titanium, zirconium carbides	Me + C	Davydov et al 1970
IVA - VIA group metals carbides	In powder form from solution in molten zinc	Gurin et al 1971
General review of methods of production	D.C. plasma	De Vynck 1970, 1971
Preparation of boron carbide	By using a radio-frequency plasma	MacKinnon & Wickens 1973

2.3 Thermodynamics of boride and carbide formation

2.3.1 Ellingham diagrams

The variation of standard free energy of formation ΔG°_{T} and the production and stability of the various borides and carbides were correlated over wide ranges of temperature (Shaffer & Samsonov, 1964, JANAF tables 60-72). The temperature variation of ΔG°_{T} per g-atom of boron and carbon is compared for the formation of borides and carbides, figs. 2.1-2.3. The temperature variation of standard free energy is best represented by Ellingham diagrams (1944). Fig. 2.1 represents the free energy of formation of the boride, carbide and oxide of titanium. Plots for other metals give similar results. Fig. 2.2 compares the standard free energies of formation of different methods of formation of boron carbide. Fig. 2.3 compares the thermodynamic data for various methods of formation of titanium diboride.

Equilibrium compositions of the systems represented on Ellingham diagrams are readily readable over the desired temperature range by the Richardson & Grants (1954) nomographic scale. High temperature materials such as borides, carbides and other refractory materials have significantly large vapour pressures at moderate temperature, limiting their practical applications at higher temperatures. The Ellingham diagrams for these compounds are usually linear. Their slope depends upon whether thermodynamically the reaction proceeds in the forward or reverse direction as the temperature is increased and on volume changes accompanying the reaction. Other factors as the temperature-sensitivity of the extensive properties are approximately interbalanced:

$$\Delta G^{\circ}_{T} = \Delta H^{\circ}_{T} - T\Delta S^{\circ}$$

A plot of the free energies of formation of boride, carbide

and oxide, fig. 2.1, of titanium compares its relative affinities for boron, carbon and oxygen and gives important information about the co-existence of these compounds. The points of intersection of the curves show the equilibrium co-existence of each pair of compounds. At all other temperatures, the compound with the more negative free energy will be the more stable. This will determine the direction of the interconversion of the compounds at different temperatures.

Analysis of free energy data (Schwarzkopf & Glaser, 1953) shows that diborides of the fourth and fifth odd (A) metal subgroup have higher thermodynamic stability than of other metals. Diborides of other groups, e.g. MgB_2 and CrB_2, show a decreasing trend in stability as compared with group IV. Diborides of group IV transition metals and monoborides of group VI transition metals (Schwarzkopf & Glaser, 1953) are the most stable of all the borides. In group V different borides of the same transition metals have similar thermodynamic stability. For group IV, V and VI, the M-B bond strength, as deduced from a comparison of m.p. of borides, increases with the atomic weight of the metals in each period and decreases with atomic weight within each group.

Despite their usefulness, Ellingham diagrams have some inadequacies, viz.

(i) The distribution of the reactants and products between the different phases is not taken into account.

(ii) The formation of intermetallic compounds and other mixed phases between products and reactants is possible.

(iii) The compounds are assumed to be of definite composition, although in practice this may not be so for many refractories.

Fig. 2.1 Ellingham diagram for TiC, TiB_2, TiO_2

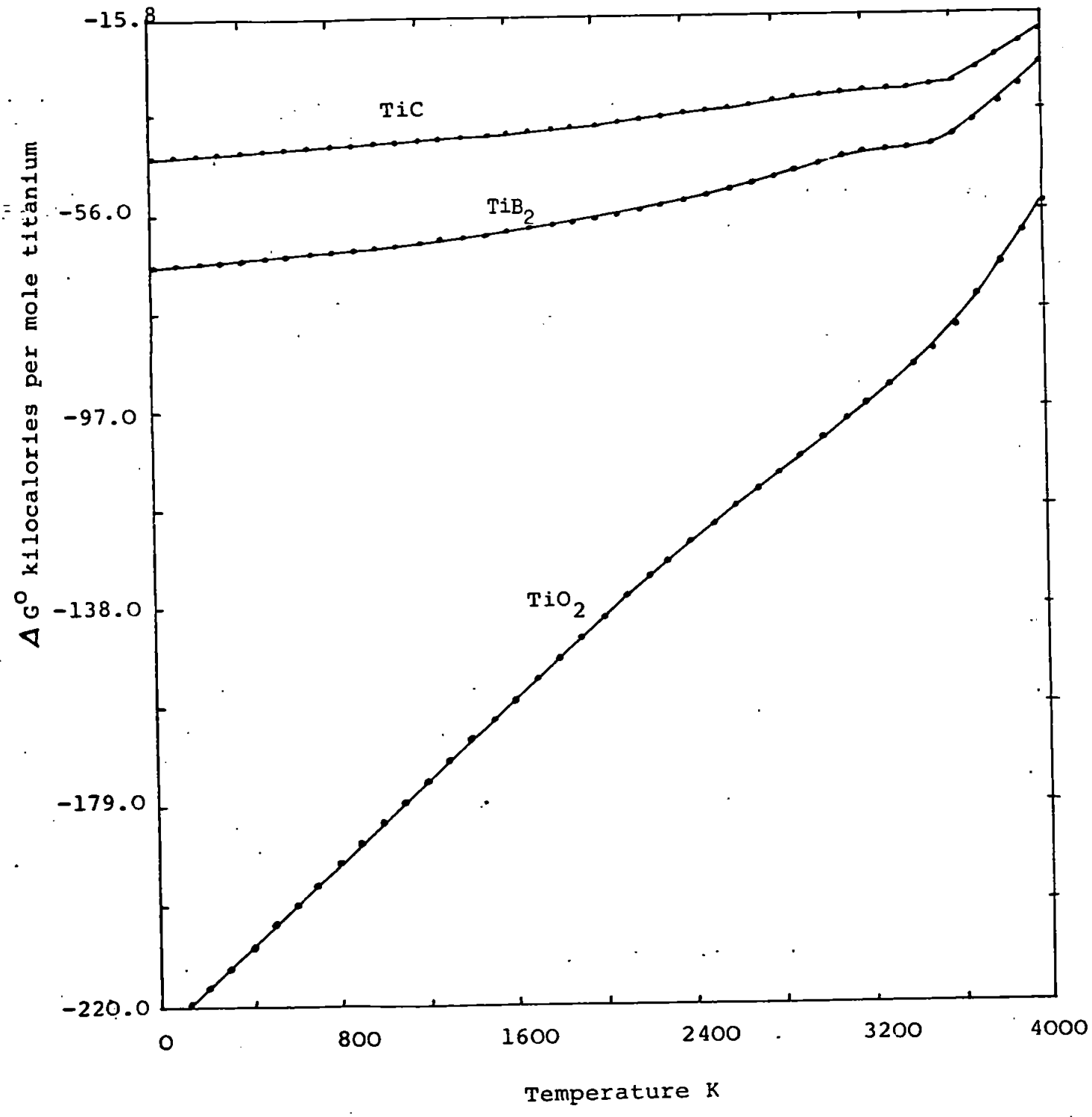

(After Schick, 1966)

(iv) They indicate only whether a process is thermodyanically feasible, but not whether it is kinetically favourable. In particular, solid-state reactions which are thermodynamically feasible are often kinetically unfavourable; this might apply to reactions involving borides and carbides.

(v) The free energy changes refer to standard states only, conditions never realised in dynamic systems.

However, these inadequacies do not diminish the value of the diagrams in terms of their ready evaluation and ease of interpretation. Sources for reliable thermodynamic information are the U.S. Bureau of Standards (Publication 1952, etc), JANAF Thermochemical tables and Supplement (1960-71), Schick (1966) and Wicks & Block (1965). The second most important thermodynamic function is the enthalpy change of the reaction. It shows the endothermicity or exothermicity of the process. It is applicable to open and closed processes, i.e. those involving formation of gaseous products from solids and condensation of initial gaseous reactants to form solids.

2.3.2 Application to production processes

Free energy changes have been plotted against temperature for six methods of production of boron carbide as shown in fig. 2.2. A brief discussion of this information for each reaction is given below:

(i) $2B_2O_3 + 7C = B_4C + 6CO(g)$

Thermodynamically feasible at temperatures $> 2320K$. The operating free energy

$$\Delta G_T = \Delta G^\circ_T + RT\ln p(CO)$$

shows that an 'open' system would be favourable. However, if the volatile nature of B_2O_3 is taken into consideration, the equation becomes:

Fig. 2.2 Ellingham Diagrams for Boron Carbide Formation

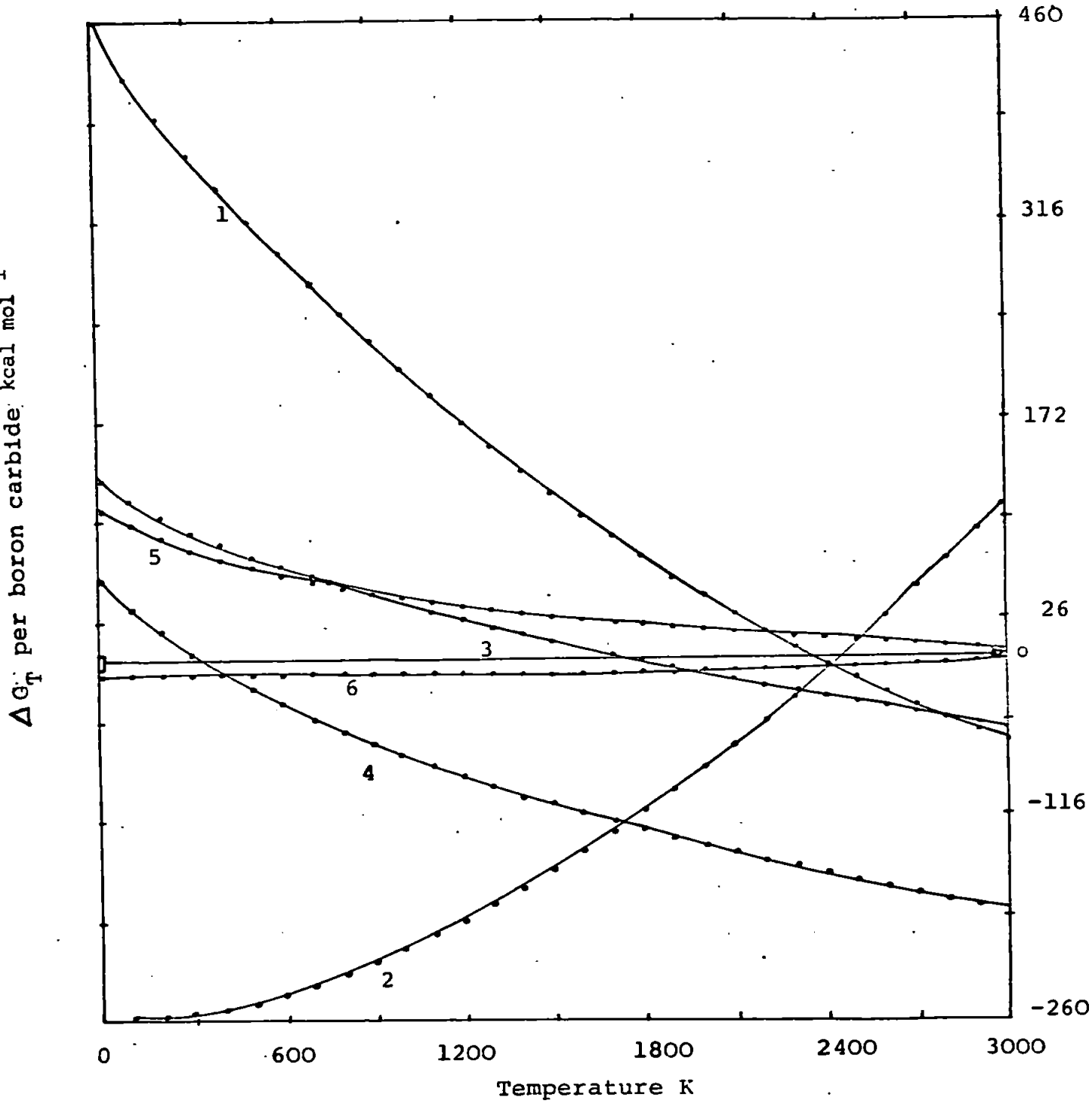

Numbers refer to reactions in table 2.2

(After Wicks & Block, 1965)

TABLE 2.2

BORON CARBIDE

Reaction	Feasibility Range K	Heat of Reaction kcal mol^{-1} 0...4000K	Eq. Constant 0...4000K
1. $2B_2O_3+7C = B_4C + 6CO$	>2300	448...-22	0...$1X10^7$
2. $2B_2O_3+6Mg+C = B_4C+6MgO$	0...2400	-252...-745	10^{39}...0
3. $4BCl_3+4H_2+CH_4 = B_4C+12HCl$	>1700	123...80	0...$1X10^6$
4. $4BCl_3+8H_2+CCl_4 = B_4C+16HCl$	>300	54...-56	0...10^{13}
5. $4BCl_3+6H_2+C = B_4C+12HCl$	>3300	106...50	0...3
6. $4B+C = B_4C$	0...3100	-10...-75	10^{28}...0

Fig. 2.3 Ellingham Diagrams for Titanium Diboride

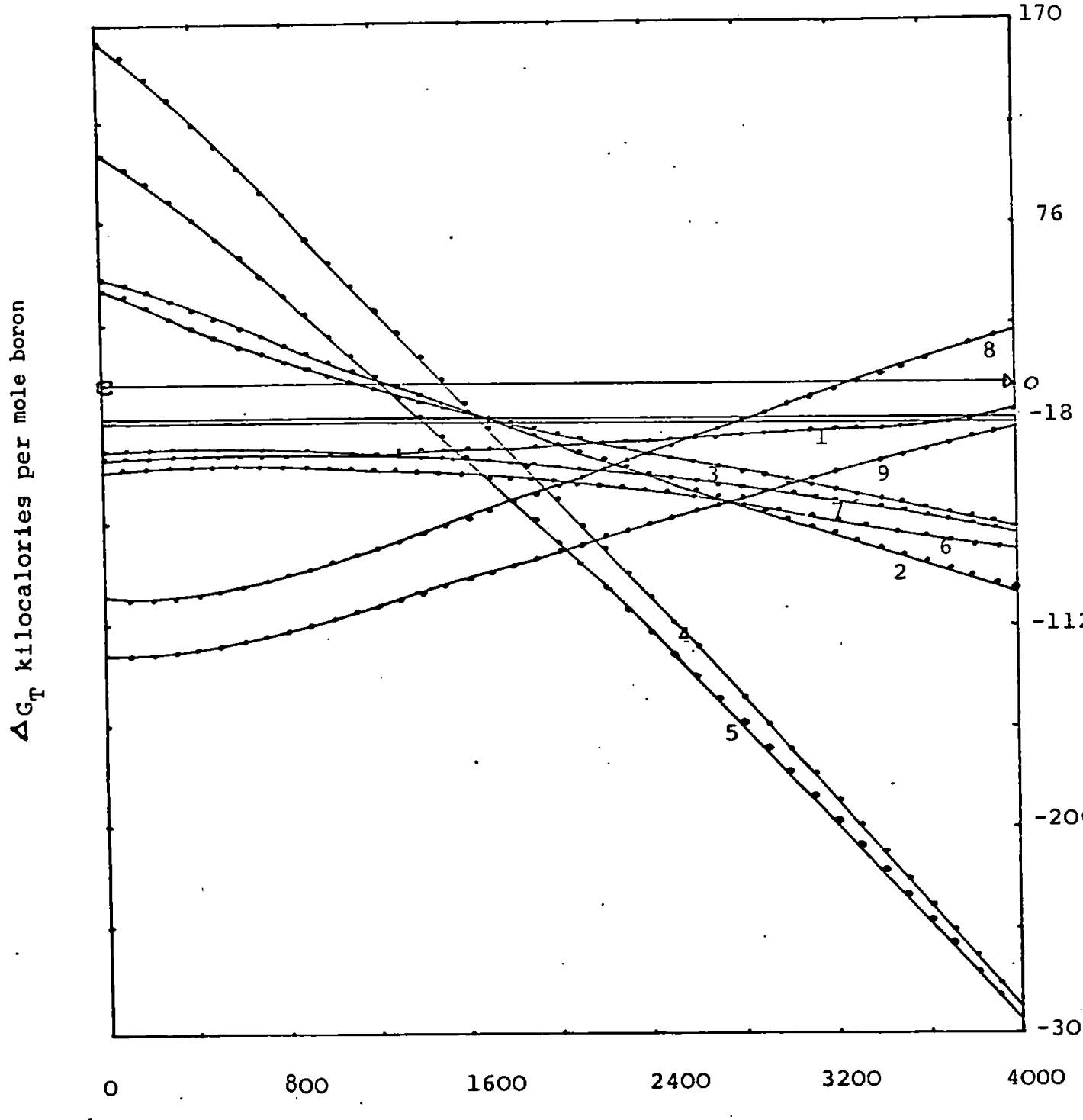

Numbers refer to reactions in table 2.3

(After Schick, 1966)

TABLE 2.3

TITANIUM DIBORIDE

Reaction	Feasibility Range	Heat of Reaction	Eqm. Constant
	K	k cal mol^{-1} 0...4000K	0...4000K
1. $Ti + 2B = TiB_2$	0...	-66...-403	$10^{37}...10^{2}$
2. $TiO_2 + 2B + 2C = TiB_2 + 2CO$	>1300	104...62	$0...4X10^{11}$
3. $TiCl_4 + 2BCl_3 + 5H_2 = TiB_2 + 10HCl$	> 1200	99...41	$0...3X10^{8}$
4. $TiO_2 + B_2O_3 + 5C = TiB_2 + 5CO$	> 1500	327...420	$0...10^{32}$
5. $2TiO_2 + B_4C + 3C = 2TiB_2 + 4CO$	> 1200	217...383	$0...10^{33}$
6. $3Ti + B_4C = 2TiB_2 + TiC$	0-----	-155...14	$10^{39}...10^{17}$
7. $2Ti + B_4C = 2TiB_2 + C$	0-----	-120...52	$10^{39}...10^{16}$
8. $3TiO_2 + 3B_2O_3 + 10Al = 3TiB_2 + 5Al_2O_3$	0...3200	-56...-659	$10^{39}...0$
9. $TiO_2 + B_2O_3 + 5Mg = TiB_2 + 5MgO$	0...	-243...232	$10^{39}...10^{3}$

$$\Delta G_T = \Delta G^\circ_T - RT\ln p(B_2O_3) + RT\ln p(CO)$$

Hence, an 'open' system may not be favourable, particularly at higher temperatures.

(ii) $2B_2O_3 + 6Mg + C = B_4C + 6MgO$

The reaction is thermodynamically feasible over the temperature range 0-2500°C (Glasson & Jones, 1969). The optimum operating temperature must be determined by the kinetics involved. The reaction is exothermic (i.e. ΔH_T is negative) and the operating free energy change is given by:

$$\Delta G_T = \Delta G^\circ_T - RT\ln p(B_2O_3) - RT\ln p(Mg)$$

This suggests that a 'closed' system is preferable; this is likely to favour the kinetics of the process.

(iii) $4BCl_3 + 4H_2 + CH_4 = B_4C + 12HCl$

This reaction is thermodynamically feasible above 1700K. The optimum operating temperature must be determined from the kinetics involved.

(iv) $4BCl_3 + 8H_2 + CCl_4 = B_4C + 16HCl$

The reaction is thermodynamically feasible at all temperatures greater than 300K.

(v) $4BCl_3 + 6H_2 + C = B_4C + 12HCl$

The reaction is thermodynamically feasible at temperatures greater than 3100K.

(vi) $4B + C = B_4C$

The reaction of elemental β- rhombohedral boron with graphite is thermodynamically feasible over the temperature range 0-3100K.

Thermodynamic functions for the metal borides of group IVA-VA have been computed over the temperature range 0-4000K. Free energy change values have been plotted to compare the various methods of formation for TiB_2. A table of free energy change, heat of reaction and equilibrium constants at different temperatures for one of these reactions is given in Appendix II. Complete tables are available for all methods of boride production for the metals titanium, zirconium, hafnium, niobium, tantalum and magnesium.

Fourth and fifth odd (A) subgroups metal carbides are of the highest stability, e.g. SiC and TiC. This systematically drops for carbides of lower groups, e.g. CuC_2 and AlC_3, and transition metal carbides in groups VI to VIII, e.g. WC.

A comparison of the relative reactivity of metals towards boron and carbon shows that borides are comparatively more stable than carbides and easily formed. This behaviour is attributed to the comparatively open structure of elemental boron compared with that of carbon. Boron retains its elemental groupings, while carbon lattices are disrupted during reaction. This makes ready ingress of the metal component possible to form the binary boride, e.g. AlB_{10} (but not AlB_{12}) (Will, 1966); also ScB_{12} and YB_{12} which have B_{12}-cubo-octahedra (Matkovich et al, 1965). The solubility of boron in transition metals is relatively low except when it substitutes an atomic site in the metal, thus causing shrinkage of the unit cell (Hansen & Anderko, 1958; Pearson, 1958; Aronsson, 1960) (e.g. with Mo- and W-B alloys). Any increase in the cell dimensions of the transition metals is an indication of the interstitial dissolution of boron except when such increases are due to the uptake of nitrogen or oxygen. These elements though more electronegative are small enough to be dissolved inter-

stitially. Homogeneity ranges of primary solid solutions are considerably affected by the free energy of intermediate phases. The interstitial solubility of non-metals in solid metals is controlled by electronic factors also. This is discussed in the next section .

2.4 The structure of boron carbide in relation to its reaction with metals

The crystallo-chemical structure of boron carbide and its reaction with titanium and chromium has been comprehensively reviewed by Jones (1970). A brief discussion of the structure of boron carbide and its relation to its properties and reaction with iron and other metals is presented below.

The structure of boron carbide with composition of $B_{12}C_3$ is ideally represented by regular icosahedra where 12 boron atoms are situated at the vertices and has interstitial spaces to accommodate up to 3 carbon atoms. The two end carbons in the -C-C-C- chain differ from the central carbon which may be replaced by boron atom giving the compound of composition $B_{13}C_2$. A homogeneous continuous mixture of these two compositions is considered to constitute the boron carbide compound. According to Fourier synthesis of electron densities of boron carbide two formulations are suggested: (i) $C_3^{2+}B_{12}^{2-}$; or (ii) $(CBC)^+(B_{11}C)^-$. Ordinarily a well-annealed boron carbide of B_4C composition is structurally formulated as $(CBC)^+(B_{11}C)^-$ to indicate probable charge transfer and is considered to be energetically preferred. The rhombohedral lattice constants of boron carbide are $a_R = 5.167 \pm 0.003$Å and $\alpha = 65.68 \pm 0.05$ and $a_o = 5.58$Å and $c_o = 12.00$Å for its hexagonal cell containing three rhombohedral unit structures.

Properties of boron carbide such as very high wear-resistance, abrasion-resistance, heat resistance and microhardness are explained

in terms of its electronic configuration (Oreshkin et al, 1970). Modern theory attributes its high abrasiveness to the fact that boron and carbon in its composition attain the electronic configuration having highest stability. Boron atoms having s^2p configuration in the ground state undergo $s \longrightarrow p$ transition to acquire sp^2 configuration. This tends to stabilize further to sp^3 configuration due to attraction of the electrons of carbon atoms with s^2p^2 configuration of valency electrons. Carbon undergoes s→p transition to acquire more stable configuration. Thus in the lattice of the boron carbide the boron atoms will have the stability of sp^3 configuration by exchange of electrons between boron atoms and due to breakdown of the sp^3 configuration of carbon atoms. As a result of shortage of electrons for transition to sp^3 configuration a part of the boron atoms remains with less stable sp^2 configuration. Thus compared with diamond and the analogous cubic boron nitride ('borazon') which have all the atoms with sp^3 configuration and hence highest stability (with respect to energy), boron carbide has higher wear resistance index. Because of this unique electronic structure (partial conversion of sp^2 to sp^3 configuration of boron) all the remaining compounds are inferior to boron carbide in resistance to wear and other properties.

Improvement in the properties of boron carbide sintered with different metal powders (Chapter 4) will depend upon the stability of electronic configuration of the final product. In its reaction with iron, partial transfer of electrons takes place towards boron carbide, which increases its stability by transition of sp^2 to sp^3 configuration. At the same time the strength in the transition is increased due to an increase in the stability of iron due to transition of $d^6 \longrightarrow d^5$ config-

uration. Thus iron has been found to be most effective sintering additive in the present work (Table 4.10). The effectiveness of other metals will vary according to the ease of electron transfer and the stability of the metal atom as a result of this interchange of electrons. Metals used in this work possess partially filled d-orbitals in their penultimate shell and show variability of oxidation states. It can be assumed that a dominating role will be played either by sp-hybrid states of boron carbide, or the d-state of the metal in the interaction of valence electrons. The precise nature of this phenomenon is still not too clearly understood. However, it would be logical to suggest that transfer of electrons is directed towards boron carbide if they acquire relatively stable configuration as a result of this exchange.

2.5 Bonding and crystal structure of borides and carbides

A comprehensive review discussing the relationship between the bonding and crystal structure of borides and carbides is given by Glasson & Jones (1969a). A summary of this is given below.

It was pointed out (Hägg, 1931) that transition metal binary refractory borides and carbides have simple 'normal' structures if the radius ratio $r_x : r_m$ of the non-metal and metal atoms is less than 0.59 (corresponding to a metal to non-metal radius ratio of over 1.70). Greater non-metal radii cause the unit cell dimensions of the interstitial phases to extend and reduce the radius ratio for normal structures. Despite the fact that decreased metal atom size leads to complex structures, most of these compounds are metallic in nature. Later this limiting radius ratio rule was found to be applicable only to carbides (Schwarzkopf & Kieffer, 1953).

This behaviour of borides has been attributed (Kiessling, 1950)

to the tendency of boron atoms to form chains, sheets or three-dimensional networks. Hägg's rule appears to be confined to phases not containing directly interconnected non-metal structure elements. Accordingly, eight different types of boride crystal structures have been described by Schwarzkhopf and Kieffer (1953) for boride phases in the composition range M_2B to MB_{12}. More variations have been reviewed later (Kieffer and Benesovsky, 1963; Post, 1964; Aronsson, Lundstrom and Rundqvist, 1965) with composition ranges M_4B to MB_{12}, extending to MB_{70}.

Most of the refractories (Hägg, 1931) discovered earlier were monocarbides with radius ratios in the range 0.41-0.59. These were characterised by rock-salt structures irrespective of the parent metal structure. Rundle (1948) assumed the presence of octahedral metal to non-metal bonding, and developed Pauling's original concept of resonance of the bonds of 4- covalent C amongst the 6 positions (Pauling 1940, 1947, 1949). Most of the properties such as hardness, high m.p. and electrical conductivity have been explained in terms of resonating bond structures and ionic structures involving homopolar and heteropolar forces. A different theory, introduced by Ubbelohde (1931, 1937) and Umanskiy (1943) (see also Samsonov & Umanskiy, 1957) have been developed by Samsonov and Neshpor (1958, 1959) and reviewed recently for nitrides (Glasson and Jayaweera, 1968). According to this theory, the non-metal contributes bonding valence electrons to the total system of electrons, at least partially filling the electron defect of the metal atoms. Interatomic bonding is further strengthened by the donor-acceptor interaction forces. Therefore, heats of formation of borides and carbides increase with 'acceptor ability' $^1/_{Nn}$' of the

atoms of the metallic components, where N is the principal quantum number of the partially filled d- (or f-) shell and n is the number of electrons in this shell (Samsonov, 1956). A similar variation in the lattice energy and the hardness with acceptor ability of metallic compounds takes place. Also, the work function of the electrons in the case of thermionic emission rises and electrical resistivity drops with an increase in $1/_{Nn}$ (Samsonov and Neshpor, 1959). The electron density of the bonds also varies with the ionisation energies of the non-metal atoms; their capacity to donate electrons rises in the direction O,N,C,B,Si. This view is repudiated by Rundle (1948), but Schwarzkopf and Kieffer (1953) hold that with lighter atoms in refractory materials, assuming metallic state, fairly strong metal to non-metal bonds can be formed. The Ubbelohde-Samsonov theory leads to comprehensive and quantitative explanation of physical and chemical behaviour. Its scope in rationalising the up-to-date information for borides and carbides is illustrated now; types of experimental information leading to its applicability are indicated.

2.6 Properties of borides and carbides

Properties of borides and carbides have been discussed by Shaffer & Samsonov (1964), Campbell et al (1949), Samsonov & Golubeva (1956), Münster (1959), McDonald & Ansley (1959), Webb et al (1956), Aronsson (1960), Stewart & Cutler (1967), Thompson & Wood (1963), Thompson (1965, 1970a, 1970b, 1970c), Storms (1967, 1972), Toth (1971), Kosolapova (1971), and Glasson & Jones (1969a). Table 2.4 summarises more recent investigations on the various aspects of the properties of borides.

2.7 Sintering of borides and carbides

The duration of sintering in the formation of borides and carbides and their subsequent calcination affects to a large extent their

Table 2.4

Boride	Property	Reference
YB_2	General, reaction with HCl and HNO_3	Markovskii et al, 1969
Scandium and yttrium borides	NMR spectrum	Barnes et al, 1970
ZrB_2	Thermal conductivity	Neshpor et al, 1970a
TiB_2, ZrB_2, HfB_2	Thermal diffusivities	Branscombe & Hunter, 1971
Nb_3B_2, NbB, Nb_3B_4, NbB_2	Physical properties	Kovenskaya & Serebryakova, 1970
IVA-VA metal borides	Thermal expansion	Samsonov et at, 1971a
TiB_2, ZrB_2, HfB_2, NbB_2, TaB_2	Thermal expansion	Keihn & Keplin, 1967
Transition metal borides	Heat capacity	Kuentzler, 1970a, 1971
CrB_2	Calorimetric and resistive magnetic properties	Castaing, 1972
HfB_2	Chemical stability with HCl, H_2SO_4, $HClO_4$, HNO_3, NH_4Cl + HCl, CH_3COOH, H_2O_2, NH_3, Air	Savitskii et al, 1970a
TiB_2, ZrB_2, VB_2, HfB_2, NbB_2, TaB_2	Chemical stability towards HCl, HCl + H_2O_2, HCl + $H_2C_2O_4$, H_2SO_4 + H_2O_2, H_2SO_4 + $H_2C_2O_4$, HNO_3, H_2O_2, H_2O, $H_2C_2O_4$	Kugai & Nazarchuck 1971a
ZrO_2 - ZrB_2 HfO_2 - HfB_2 Nb_2O_5 - NbB_2 Ta_2O_5 - TaB_2 Cr_2O_3 - CrB_2	Reactions at 1000 - 2000°C	Marek et al, 1971

TABLE 2.4 (cont'd)

Boride	Property	Reference
Borides of transition metals TiB_2, ZrB_2, CrB_2, MoB_2	Reaction with $BaCO_3$ or Ca	Kugai & Nazarchuck, 1971b
Molybdenum and tungsten borides	Stability, acid	Kugai, 1971
SrB_6 - LaB_6, BaB_6 - LaB_6	Thermionic properties	Bliznakov & Peshev, 1970
Niobium, tantalum, molybdenum and tungsten borides	Resistance against carbonizing	Samsonov et al, 1970a
TiB_2, ZrB_2, HfB_2, VB_2, NbB_2, TaB_2, CrB_2, MoB, Mo_2B_5, WB, W_2B_5	Heat treatment with carbon	Levenskii et al, 1968
TiB_2, W_2B_5, (Ti, Cr) boride	Wear resistance	Oreshkin et al, 1971
Cobalt and nickel borides	Stability to carbon	Markovskii et al, 1971
LaB_6	Interaction with molybdenum, tantalum and graphite	Gert et al, 1969
LaB_6, CeB_6, PrB_6 NdB_6	Resistance to H_2O, alkalies and acids	Kosolapova & Domasevich, 1970
YB_6, SrB_6, LaB_6, ThB_6	Magnetic susceptibility thermoelectric power, specific heat	Etourneau et al, 1970
LaB_6, NdB_6, SmB_6, DyB_6	Oxidation in air	Timofeeva & Timofeeva, 1971
SmB_6	Reaction with nickel	Romashov et al, 1970
Borides in general	Systematic phase chemical analysis	Vekshina & Markovskii, 1969
FeB, Fe_2B	Effect of temperature on physical properties	Kunitskii & Marek, 1971

TABLE 2.4 (cont'd)

Boride	Property	Reference
FeB, Fe_2B	Resistivity, thermo-emf, thermal conductivity and expansion 70 - 1300K	Kostetskii et al, 1971
FeB, Fe_2B	Anisotropy of thermal expansion	Lyakhovich et al, 1971
(Fe-Co) boride, (Co-Ni) boride	Heat capacity	Kuentzler, 1970b
Rh_3B_3, $RhB_{1.1}$	Hardness	Kosenko et al, 1971
Borides in general	Fusion and heat compression	Pastor, 1969
Boron-coated metal objects	Mechanical properties	Ducrot & Poulain, 1970
AlB_{10}	Crystal structure and electron distribution	Will, 1970
ZrB_2 - Mo	Structural properties	Kislyi & Kuzenkova, 1966
Nb_3B_2, NbB, Nb_3B_4, NbB_2, Cr_4B, Cr_3B_2, CrB, Cr_3B_4, CrB_2	Electrical resistance, thermo electric potential, $\Delta l/L_o$, Hall co-efficient	Samsonov et al, 1971b
$IrB_{1.35}$, $IrB_{1.1}$, $IrB_{0.9}$	Crystal structure	Rogl et al, 1971
SmB_6	Electronic configuration, magnetic and electric properties	Rhyne, 1970 Cohen et al, 1970
General borides	Role of valence electrons	Sleptsov & Kosolapova, 1970

Tables 2.4 (cont'd)

Carbides and mixed borides

Carbide	Property	Reference
ZrC	Hot hardness	Savitskii et al, 1970b
Transition metal carbides	Abrasive wear	Artamonov & Bovkun, 1970
MeC and Me(C,N) of group IVA & VA	Systematic chemical and electrochemical separation	Georgieva et al, 1969
Carbides in general	Systematic phase chemical analysis	Vekshina & Markovskii, 1969
B_4C	Interaction with C + X (fluorides, V_2O_5, MgO, Al_2O_3, SiO_2)	Srborbran, 1969
Pyrolytic B_4C	Electrical resistance, e.m.f., thermal conductivity and microhardness	Neshpor et al, 1970b
B_4C	Optical properties	Werheit et al, 1971
Cr_3C_2 - B_4C, B_4C - SiC, Cr_3C_2 - SiC	Interaction in welding	Oreshkin et al, 1970
Diboride-nitride system	Dry friction and wear	Medvedev & Sin,kov, 1971
C_4AlB_{24}	Crystal structure and electron distribution	Will, 1970
$\int$ - VC, $\int$-NbC, $\int$ - TaC	Crystal structure	Yvon & Parthe, 1970
Carbides in general	Properties of carbides based on electronic configuration	Samsonov, 1970

chemical reactivity. Extensive studies on the sintering of oxides and to a lesser extent of nitrides have been made (Glasson & Jayaweera, 1968). Theories of sintering have been established by Hüttig (1941), Kingery (1960), Coble (1961, 1964), Kuczynski (1961), White (1965) and Fedorchenko & Skorokhod (1967). The rate of sintering is considerably increased by pressing the powdered materials before calcining in vacuo to stop hydrolysis and oxidation (Chiotti, 1952; Geguzin & Partskaya, 1967).

Materials (Schwarzkopf & Kieffer, 1953) can be compacted and pressed to almost theoretical densities by hot pressing them, e.g. oxides such as MgO, CaO, Al_2O_3 (Carruthers & Wheat, 1965; Wheat & Carruthers, 1961). Small amounts of impurities, especially those giving rise to gaseous products such as hydroxides and carbonates hinder the sintering. In the presence of nitrogen, carbides are converted to carbide-nitride solid solutions, e.g. TiC (Zelikman & Loseva, 1947; Zelikman & Gorovits, 1950) and ZrC (Duwez & Odell, 1950). Hot pressing is often carried out in vacuum to avoid such contaminations (Glasson, 1967). Small quantities of low-melting additives generally increase the rate of sintering (Glasson, 1967) usually at the cost of excellent optical and mechanical properties. Cermets (Schwarzkopf & Kieffer, 1960) or surface coatings having superior properties may be obtained by sintering very brittle borides and carbides with metals such as cobalt (Powell et al, 1966).

2.7.1 General principles of the mechanism of sintering and hot pressing

The process of sintering is that by which powders are consolidated into strong, and usually dense polycrystalline aggregates by

heating. Systems undergoing sintering are of two types, namely:

(i) Homogeneous systems consisting of a single component or components which give continuous series of solid solutions.

(ii) Heterogeneous systems consisting of multiple component systems.

In the homogeneous sintering of a powder, distinction can be made between two overlapping stages of sintering. The first stage is characterized by the formation and growth of bonds, i.e. the contact areas between adjacent powder particles. The growth of these contact areas takes place during the early stages of sintering, when the material is densified and the pore volume decreased. Under favourable conditions the pores are practically eliminated. The surface free energy is considered to be the driving force in both stages of sintering. The energy required for sintering is supplied by the decrease of surface areas or by the replacement of high-energy interfacings by those of lower energy, e.g. grain boundaries. The surface free energy is sufficient to account for sintering, provided a suitable mechanism is available for the transport of atoms involved in the consolidation of powder compacts. The following five mechanisms are possible in the case of homogeneous materials:

(i) Evaporation followed by condensation.

(ii) Surface diffusion.

(iii) Volume diffusion.

(iv) Viscous flow (Newtonian flow characterized by a linear relationship between strain rate and stress).

(v) Plastic flow (Bingham flow characterized by the existence of a yield stress).

Different theories of sintering and mechanisms of material and pore transport have attracted much attention of workers in the field of sintering, Alexander et al (1945), Herring (1950), Kingery et al (1955), Murray et al (1954), Nabarro (1948). The sintering of B_4C and other refractory materials has been reviewed comprehensively by Jones (1970). Points arising from this review and recent advances in the technology of sintering are presented here.

2.7.2 Role of volume, Grain boundary and Surface diffusion

The role of volume, grain boundary and surface diffusion during the initial, intermediate and final stages of sintering has been studied by Ristic (1969). Separate equations for all three mechanisms have been formulated. His model for the initial stages of sintering, based on the shrinkage of a wire on a plane, shows considerable discrepancy from the solutions proposed by earlier authors. Accordingly, a solution for an infinite line has been suggested. Comparison of results regarded in the context of some other indicators shows that surface diffusion is responsible for the mechanism of the process in both cases. The intermediate and final stages of sintering are often directly responsible for the physical properties of a sintered body. The equations for models whose systems are composed of units consisting of either cubes, hexagonal prisms, dodecahedrons, or tetrakaidecahedron are given as:-

(a) Bulk diffusion model

$$P_c = \frac{K_1 D\, a_o^3 (t_f - t)}{l^3 kT} \qquad \text{I}$$

(b) Boundary diffusion model

$$P_c = \left[\frac{K_2 D_b W\, a_o^3 t}{l^4 kT}\right]^{2/3} \qquad \text{II}$$

where

P_c = the volume fraction of the pore

D = bulk diffusion coefficient

γ = surface energy

a_o^3 = vacancy volume

t = time

t_f = time at which the pore vanishes

D_b = boundary diffusion coefficient

l = edge of the polyhedron

W = boundary width

K_1, K_2 = constants

k = Boltzmann constant

T = thermodynamic temperature

A comparison of K_1 and K_2 with Coble's model clearly shows the influence of the geometry on densification during intermediate and final stages of sintering. Accordingly it is possible to determine the critical size of the specimen by means of the equation:

$$Z_{kr} \leqslant \sqrt{D_d t} \qquad \text{III}$$

D_d = vacancy diffusion coefficient

t = time

The role of non-stoichiometry in the sintering of ionic solids has been studied by Reijnen (1969). This work deals only with the volume diffusion of vacancies and interstitials, specifically with the flux of vacancies emitted by spherical pores.

Johnson (1969a, 1969b, 1969c, 1970, 1971) has studied extensively the new methods of obtaining volume, grain-boundary and surface diffusion coefficients from sintering data, sintering kinetics for

combined volume, grain boundary and surface diffusions, the intermediate stage of sintering and the methods of determining sintering mechanisms. His model for the determination of sintering is given in Fig. 2.5.

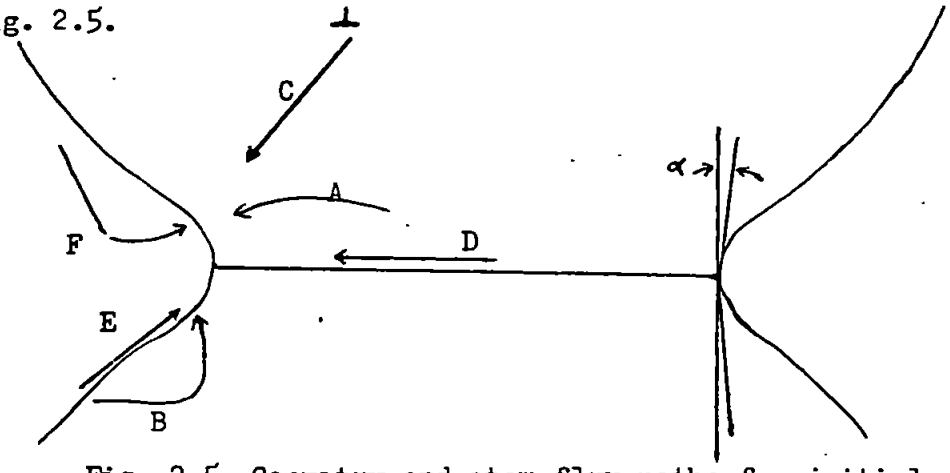

Fig. 2.5 Geometry and atom flux paths for initial stage model. A, B and C are volume diffusion, D is grain boundary diffusion, E is surface diffusion, and F is vapor transport.

(After Johnson, 1971)

It is based on the assumption that all densification is produced by diffusion of atoms from the grain boundary between the particles to the neck surface, by volume or grain boundary diffusion or by both processes acting simultaneously. It is assumed that vacancies are at equilibrium concentration everywhere and that the surface and grain boundary tensions are isotropic. The sintering equation is given by:-

$$\frac{X^3}{X + R\cos\alpha}\dot{y} = \frac{2\gamma\Omega D_v}{kTa^3} \cdot \frac{A}{X} + \frac{4\gamma\Omega bD_b}{kTa^4} \qquad \text{IV}$$

where

X = fractional neck radius

R = normalized minimum radius of curvature of neck surface

α = as defined in Fig. 2.5

y = fractional shrinkage $\Delta L/L_o$

$\dot{y}$ = shrinkage rate

γ = surface tension

Ω = atomic volume

D_v = volume diffusion constant

A = normalized area of neck surface

b = grain-boundary width

D_b = boundary self-diffusion coefficient

a = sphere radius

k = Boltzmann constant

T = thermodynamic temperature

If it is assumed that there is no mass transport from the particle surface to the neck surface, and γ is zero, then all of the geometric parameters can be related to the shrinkage as follows:

$$y^2\dot{y} = \frac{2.48\gamma\Omega D_v}{KTa^3} y + \frac{0.78\gamma\Omega bD_b}{kTa^4} \qquad V$$

If it is assumed further that either grain-boundary diffusion or volume diffusion only occurs, then the following simplifications of equation IV result. For volume diffusion:-

$$L = L_o \left[1 - \frac{2.48\gamma\Omega D_v}{kTa^3} \dot{y}^{-\frac{1}{2}} \right] \qquad VI$$

$$Ty\dot{y} = \frac{2.48\gamma\Omega D_v}{ka^3}$$

and for grain boundary diffusion:

$$L = L_o \left[\left(1 - \frac{0.78\gamma\Omega bD_b}{kTa^4} \right)^{\frac{1}{2}} \dot{y}^{-\frac{1}{2}} \right] \qquad VII$$

$$Ty^2\dot{y} = \frac{0.78\gamma\Omega bD_b}{ka^4} \qquad VIII$$

During the intermediate stage of sintering the individual

particles at the beginning have more or less lost their identity. The pores are interconnected by channels lying along three grain intersections. The densification mechanisms are the same as those that occur during the initial stage but the geometry is more complex. Because of geometric complexities of the compact, a method of averaging the significant geometric parameters is employed. The resulting equation is:

$$\frac{\bar{G}}{\bar{H}L_v}\,\frac{dV}{V^{dt}} = \frac{32\gamma\Omega D_v}{kT}\cdot\frac{S_v}{L_v} + \frac{32\gamma\Omega D_b}{kT} \qquad \text{IX}$$

where

$\bar{G}$ = mean grain diameter

$\bar{H}$ = average mean surface curvature

L_v = length per unit volume of intersection between grain boundaries and pores

S_v = pore surface area per unit volume

V = instantaneous volume of compact

Equation IX is an attempt to analyse sintering data when all changes in the mechanism of mass and pores transport and geometric factors occur. It has been modified further for various states of sintering and for isothermal and non-isothermal sintering.

2.7.3 Role of dislocations

Investigations of sintering processes have included occasionally efforts to observe dislocation motion during sintering. These efforts have been unsuccessful. However, this does not mean that dislocation motion does not contribute to the sintering process. Due to the nature of dislocation slip, it is probable that actual observations of moving dislocations during sintering may be extremely difficult or impossible. The reason is that dislocation generation and motion during sintering

will occur most readily in very small particles or crystallites. In small crystals, dislocation generation will be at the grain boundary, leaving little opportunity for dislocations to be seen by transmission microscopy. The dislocation motion occurs in large particles, where the stress to cause sintering is less only at very high temperatures, which are probably not avilable under the conditions when the microscope is in use. Dislocations can remain in the crystals under certain conditions involving short heating periods. The role of dislocations in the densification of CoO and NiO with a dispersion of MgO or CaO has been studied by Tikkanen and Ylasaari (1969). The dislocations in high-temperature sintering have been observed by Morgan (1971). A comprehensive review based on theoretical and experimental investigations on bubble raft sintering, dislocation nucleation in necks, kinetics of sintering and distinction in the role of dislocations and diffusion flow during sintering has been given by Lenel et al (1971) and Lenel (1972).

2.7.4 Role of atmospheric effects

The atmosphere has an effect on both surface tension and diffusivities. Absorption of gas atoms on metal surfaces lowers the surface tension, while the surface diffusivity is either increased or decreased. The effect of dissolved gas atoms on the volume self-diffusivity is generally quite small. No direct information is available on the atmospheric effect on grain boundary diffusivity. Two effects, which gases trapped at closed pores might exert on the course of microstructure development, have been studied quantitatively (Coble, 1969). The first relates to a change in pore shape, the second to gas solubility.

Because there are few data for gas solubilities or diffusivities in metals or ceramics, there are only few instances for which the final stage of densification can be modelled quantitatively. A comprehensive mathematical treatment of the atmospheric effect on the density decrease with pore coalescense, cylindrical pore equilibration and spheroidization, equilibrium of pore volumes, break up of cylindrical pores to spherical pores and gas solubility, has been presented by Coble (1969).

An interesting problem is the interaction between material transport mechanisms that contribute to surface rounding only, and those which cause densification. The effect of atmosphere on the interaction of two opposing types of material transport mechanism has been studied by Gessinger (1971) using Ag and Fe as model materials. The results are given by two equations:-

$$\frac{\dot{x}_s}{\dot{x}_v} = 0.61 \frac{D_s}{D_v} \frac{\delta}{\ell} \qquad \text{X}$$

$$\frac{\dot{x}_{GB}}{\dot{x}_{DV}} = 0.16 \frac{D_b}{D_v} \frac{\delta}{\ell} \qquad \text{XI}$$

where $\dot{x}_s$ = rate of surface diffusion

$\dot{x}_v$ = rate of volume diffusion

$\dot{x}_{GB}$ = rate of grain boundary diffusion

$\dot{x}_{DV}$ = rate of self-diffusivity

D_s = surface diffusivity

D_v = volume self-diffusivity

D_b = grain boundary diffusivity

δ = surface tension

ℓ = co-efficient of viscosity

In Fig. 2.6 the neck profile required to allow distribution of atoms coming from grain boundary sources is drawn. Only a change in the sign of the curvature would permit such a

Fig. 2.6

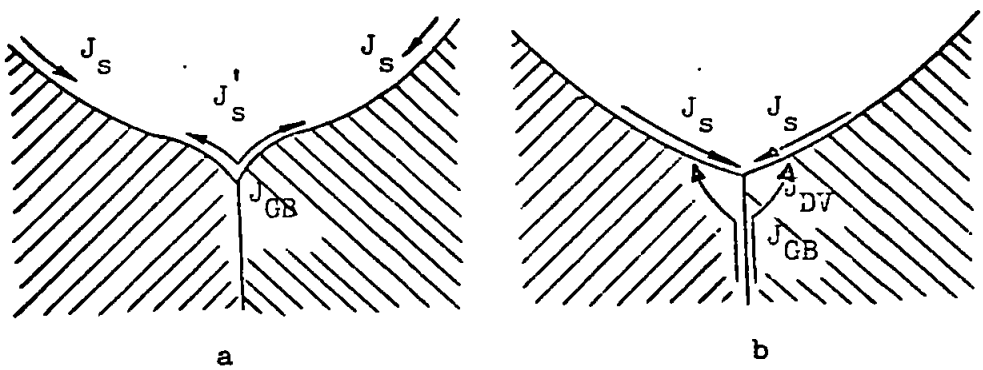

a

Neck profile with sign change in neck curvature

b

Neck profile with same sign of curvature

J_s = surface diffusion flux

J_{GB} = grain boundary flux

J_s' = outward surface diffusion flux

J_{DV} = volume diffusion flux

(After Gessinger, 1971)

hypothetical case, in which surface diffusion could then be densification rate controlling. Due to this convex neck area element, the driving force for shrinkage would, however, be reduced to practically zero. In Fig. 2.6 material from the grain boundary is diffusing along the grain boundary in the direction of the neck surface, but is then channelled through the volume near the surface. Surface diffusion can now proceed from the particle surface to the grain boundary groove at the neck, since the gradient of chemical potential along the surface is unidirectional. This model would predict that volume diffusion is the rate-controlling step in densification and that the effect would be most pronounced when volume diffusion is very slow as compared with grain boundary diffusion.

A mathematical model of sintering has been developed by Tukamoto et al (1970) in which considerations have been given to drying processes of solids, the composition of limestone and the melting and solidifying process of iron ore. Partial differential equations giving numerical values of various parameters have been derived.

2.7.5 Computer-simulated models of sintering

A dynamic volume diffusion model for sintering has been presented using the Laplace equation by Easterling et al (1970). Computed profiles and charts of chemical potential changes are printed out directly. Assuming that there are no internal sources and sinks of vacancies, the chemical potential, μ, of vacancy diffusion can be found by solving the Laplace equation:

$$\frac{\partial^2 \mu}{\partial x^2} + \frac{\partial^2 \mu}{\partial y^2} = 0 \qquad \text{XII}$$

The only boundary values needed for the case of volume diffusion are:

$$\mu = \frac{\gamma \Omega_a}{\rho} \text{ at the neck}$$

$$\mu = -\frac{\gamma \Omega_a}{a} \text{ elsewhere on the surface}$$

where γ = surface tension

Ω_a = atomic volume

intermediate values can be found by the relaxation grid technique. It can be shown that:

$$\mu_i = \frac{1}{4}(\mu_a + \mu_b + \mu_c + \mu_d) \qquad \text{XIII-1}$$

Initially, with only boundary values to work on, the process of calculating the potential distribution is a procedure of iteration. The changes in chemical potential and model profile have been calculated using an IBM 360 computer by this author.

The effects of operating-variables, i.e. temperature and oxygen concentration of gas in ignition furnace, time for ignition, mass velocity of gas, diameter and temperature of solid particles to be fed, on the temperature distribution in the sintering bed have been estimated by Muchi and Higuchi (1970) using numerical techniques with the aid of a computer.

2.7.6 Reaction pressing and pressure sintering

Reaction pressing is based on the fact that many intermetallic compounds can be formed from their constituent elements with rapid evolution of a substantial quantity of heat. This exotherm is often sufficient to render the reaction change. The nascent compound has a transient plasticity so that, provided pressure is applied through a fast-acting system capable of keeping pace with rapid reaction-contraction, a product can be synthesized and shaped quickly and relatively easily at an initiating temperature that is low in relation to conventional fabrication temperatures. Stringer & Williams

(1967) have demonstrated the superiority of reaction pressing over other methods of fabrication. High melting materials, such as borides, carbides, nitrides and silicides as well as oxides and cermets, cannot be compacted to dense pore-free bodies by cold pressing and ordinary sintering. By pressure sintering, on the other hand, it is possible to produce bodies with greater than 95% theoretical densities. Janes & Nixdorf (1969) have compared the two methods of compaction and have shown consolidation to be a function of pressure, temperature and time.

A new predictive densification equation of pressure sintering during the final stage of sintering has been proposed by Shimohira (1971). It is based on polyhedral space-filling bodies. If the size of contact area can be expressed as a function of porosity, f(P) then the effective stress (σ_e), i.e., the compressive stress, may be formulated as:

$$\sigma_e = \sigma_a f(P) \qquad \text{XV}$$

where σ_a = applied stress

f(P) = function of porosity .

A general expression for contact area per polyhedra from geometric considerations is:

$$A = S(1 - kP^{2/3}) \qquad \text{XV(a)}$$

where s = constant equal to total area of polyhedra at zero porosity

k = constant

P = porosity

In a simplified form,

$$A = (1 - P)^{3/2} \text{ when P less than 0.3} \qquad \text{XVI}$$

A linear relationship between A and $(1 - P)^{3/2}$ therefore would be expected. The effective stress may be given as:

$$\sigma_e = \sigma_{a/(1 - P)^{3/2}} \qquad \text{XVII}$$

An isothermal densification equation, derived from a combination of Nabarro-Herring diffusion creep equation and the effective stress, is given as:-

$$d\rho/dt = 10\,\sigma_a D_L \Omega/R^2 kT \rho^{\frac{1}{2}} \qquad \text{XVIII}$$

or

$$\rho^{3/2} = 30\,\sigma_a D_L \Omega/2R^2 kT + \text{constant} \qquad \text{XIX}$$

An apparatus for the automatic measurement of shrinkage during sintering has been developed by Vydrevich (1970). It was used for shrinkage measurement during the sintering kinetics of tungsten powders with small nickel additions. The following empirical formula has been obtained:-

$$\frac{\Delta L}{L_o} = Ae^{-be^{-ct}} \qquad \text{XX}$$

where $\Delta L/L_o$ = shrinkage

t = time

A, b & c = constant

Zaverukha (1970) has investigated the sintering process on the basis of changes in the electrical properties of compacts on heating.

Lindroos (1971) has reported the annihilation of vacancies by small angle grain boundaries during sintering. Pore shape changes during the initial stages of sintering of copper powders has been studied by scanning electron microscopy by Kellam et al (1971).

2.7.7 Effect of wetting on sintering

2.7.7.1 General principles

Wetting is a phenomenon that arises whenever two different phases come into contact. It depends on the contact angle between the phases. In sintering processes, the most common systems are solid-solid, solid-gas, and solid-liquid. Only solid-liquid systems

are dealt with in this section. Wetting is an extremely complex process at high temperatures, and a more comprehensive treatment would be too wide. The solid-liquid and solid-solid systems are of most interest in powder metallurgy and sintering technology, as well as in producing fibre-reinforced materials.

Experience of the development of powdered metal substances based on hard metals, e.g. tungsten, tantalum, molybdenum, niobium, where an interesting combination of properties can be provided by using metals in the iron group as the cementing phase.

The sintering process is the principal technological operation which decides the properties of the finished product. It takes place, in this case, in the presence of a liquid phase which binds the grains of the high-melting compound and of the cementing metal; the latter effectively wets the solid phase. The bonding effect is much greater when there is limited mutual solubility within the system consisting of the high-melting compound and the "cementing" metal (Kermety, 1962). A considerable amount of information has now been accumulated as to the wettability of hard high-melting compounds by molten metals (Naidich,1964; Naidich & Lavrienko, 1965; Eremenko & Naidich, 1959).

This discussion deals with metal boride-metal and metal carbide-metal systems. These classes represent systems used extensively in the production of 'hard metals', which were originally discovered and developed on purely empirical grounds, and whose theoretical principles are still not fully understood.

Multiphase materials of this type are produced through

powder-metallurgical techniques, because conventional methods would not give an equal distribution of the various phases. The choice of system must take into account the properties required for the final product, e.g. density, wetting and non-porous homogeneous character.

A comprehensive treatment of wetting problems in connection with sintering is given by Tikkanen et al (1971). They begin their discussion with the Young-Dupré equation:

$$\gamma_{sv} = \gamma_{sl} + \gamma_{lv} \cos\theta \qquad \text{XXI}$$

where γ_{sv} = solid-vapour interfacial energy (surface tension)
γ_{sl} = solid-liquid " " (" ")
γ_{lv} = liquid-vapour " " (" ")
θ = contact angle

The limitation of this equation and the definition of the terms in it are discussed.

θ is a measure of the degree of wetting and is the only characteristic quantity that can be measured conveniently. The effect on θ of varying each value of γ can be derived from equation XXI, and is summarised by Tikkanen et al (1971).

Since the surface tension of the metals concerned is always appreciably higher than that of the chemically-stable borides and carbides, it is impossible to have complete wetting between these two important groups of materials if sintering is carried out in a neutral atmosphere. Tikkanen et al (1971) define also a term, the spreading co-efficient, S_{ls} in terms of surface tension values. They also give equations to calculate the binding force between two phases.

2.7.7.2 Wetting problems in the sintering of borides and carbides with metals

The refractory borides and carbides of the transition metals are used to make cermets. A metal or alloy which forms the plastic component is in the liquid state during fabrication so that the wetting of a solid ceramic by this liquid is important in ensuring that the product has the required properties.

The metal boride and carbide systems are those with the greatest practical significance. Recently research in this field has been intensified considerably. The effect is related to the larger numbers of free valency electrons in the solid metal surface and metal-boron bond strength.

In general, carbides wet transition metals more than borides. According to Rang, the more stable the carbide the poorer the wetting. The stoichiometric defect structure of carbides plays an important role in this context. However, there is little quantitative information available.

The wetting between a metal and carbide can be altered by making suitable additions. For example, wetting between nickel and TiC is considerably improved by molybdenum; the latter being a powerful carbide former, reacts with TiC and is dissolved in the TiC phase (Tikkanen et al, 1971).

The sintering of ZrB_2 with W has been studied by Kisliy (1971). Shrinkage measurements with time show the formation of solid solutions of W in ZrB_2 as well as new phases, W_2B, (W,Zr)B.

The contact angles of molten metals with refractory borides and carbides are tabulated in Table 2.5.

TABLE 2.5

CONTACT ANGLES OF SOME MOLTEN METALS WITH REFRACTORY BORON COMPOUNDS

Phase	Metal	Temperature °C	θ	Reference
B_4C	Zn	540 - 620	121.5 - 119	Samsonov (1960)
"	Cu	995 - 1,090	130 - 17	"
"	Al	600 - 670	117 - 118	"
"	Al + 1.39 Mg	840	115	Manning et al (1969)
"	Al + 9.98 Mg	"	115 - 114	"
"	Al + 1.62 Cu	"	150	"
"	Al + 9.82 Cu	"	138	"
"	Al + 2.58 Si	"	140	"
"	Al + 10.38 Si	"	120 - 121	"
"	Pb	225 - 395	121 - 113	Samsonov (1960)
"	Brass	905 - 950	54.5 - 30	"
"	Fe	1,780	Strong Reaction	Hamijan (1952)
"	Co	"	90	"
"	Cr	1,820 - 1,830	0	Janes & Nixdorf (1969)
"	Cr/Ni	1,400 - 1,410	0	"
"	Ni	1,470	41	"
TiB_2	Cu	1,500	158	Eremenko (1959)
"	"	1,083 (10^{-4} - 10^{-5} mm.Hg)	158	Tumanov et al (1970)
"	Ni	1,480	100 - 38.5	Eremenko (1959)

TABLE 2.5 (Cont'd)

Phase	Metal	Temperature °C	θ	Reference
TiB_2	Ni	1,455 (10^{-4} - 10^{-5} mm.Hg)	46	Tumanov et at (1970)
"	Al	950 - 1,000	146	Panasyuk et al (1971)
"	"	950 - 50	85 - 150	"
"	"	1,250	90 - 32	"
"	Ag	1,100 - 1,600	120 - 100	Vatolin et al (1969)
ZrB_2	Cu	1,100	60	Panasyuk et al (1969)
"	Ag	1,100 - 1,600	116 - 83	Vatolin et al (1969)
VB_2	Cu	1,300 - 1,350	145	Panasyuk et al (1971)
"	Ag	1,100 - 1,600	109 - 87	Vatolin et al (1969)
NbB_2	Cu	1,450	125	Panasyuk et al (1971)
"	Ni	Metal does melt at 1,550. The surface of the boride under the nickel is corroded		"
TaB_2	Cu	1,100	50	Panasyuk et al (1971)
"	Ni	1,480	43 - 60	"
CrB	Cu	1,083 (10^{-4} - 10^{-5} mm.Hg)	40	Tumanov et al (1970)
"	Ni	1,455 (10^{-4} - 10^{-5} mm.Hg)	0	"

TABLE 2.5 (Cont'd)

Phase	Metal	Temperature °C	θ	Reference
CrB_2	Cu	1,083 (10^{-4} - 10^{-5} mm.Hg)	51	Tumanov et al (1970)
"	Ni	1,455 (10^{-4} - 10^{-5} mm.Hg)	14	"
"	Cu	1,455	85 - 115	Panasyuk et al (1971)
MoB_2	Cu	1,100 - 1,500	8	"
"	Ni	1,480	8 - 15	"
W_2B	Ni	1,200 - 1,400	25 - 16.5	Kiparisov (1970)
WB	Cu	1,083	21	Tumanov et al (1970)
"	Ni	1,455	0	"
WB_2	Cu	1,083	40	Yasinskaya (1966)
TiC	Bi	300 - 700	138 - 118	Livey & Murray (1956)
"	Pb	400 - 1,000	152 - 90	"
"	Ag	980	108	"
"	Al	700	118	Belyaev & Zhemcluzhina (1952)
"	Al	900 - 1,000	142	Panasyuk et al (1971)
"	Al	1,250	85 - 20	"
"	Zn	550	120	Belyaev & Zhemcluzhina (1952)
"	Cu	1,100 - 1,300	108 - 70	Livey & Murray (1956)

TABLE 2.5 (Cont'd)

Phase	Metal	Temperature °C	θ	Reference
ZrC	Cu	1,100 - 1,500	140 - 118	Livey & Murray (1956)
VC	Na	200 - 400	160 - 9	"
"	Cu	1,100	54	"
WC	Bi	500 - 1,200	150 - 80	"
"	Sn	500 - 1,200	120 - 50	"
UC	Na	200 - 400	162 - 122	"
"	Bi	300 - 1,700	140 - 95	"
"	Cu	1,100 - 1,260	113 - 70	"

2.8 Industrial applications of borides and carbides

The applications of borides and carbides in industry have been reviewed by Aronsson (1960), Thompson (1963, 1965), Storms (1967, 1972), Toth (1971) and Kosolapova (1971). Table 2.6 summarises more recent references to such applications. These are tabulated under the following headings:

1. Refractory materials.
2. Corrosion-resistant materials as for the chemical industry.
3. Materials for nuclear energy production.
4. Manufacturing materials for aircraft and rockets.
5. Materials for the electronics industry.
6. Super-hard and wear-resistant materials.

Biddulph, Matterson & Brown (1973) are working on commercial scale applications of boronised objects. Boronised components can be used to advantage in shot blasting equipment, in jigs for industrial polishing, and in machines for handling abrasive dry materials in the chemical industry. In hot dip galvanising and zinc-die-casting use is made of the boronised layer's resistance to attack by molten zinc. Boronising increases life of WC/Co by 250%.

Potential applications for boronising, where the advantage of the wear resistance of the hard layer would be useful, are numerous. For example, in dies and plungers for compacting abrasive powders such as those used in the powder metallurgical industry, the ceramic industry and in the manufacture of pelletised catalysts. Other potential applications are for chain conveyor parts which are subjected to abrasive dust, for bearing surfaces on shafts, especially those subjected to abrasive wear, and for earth-moving equipment.

TABLE 2.6

Feature	Phases	Principal Properties	Fields of Application	Reference
Refractory materials	TiB TiB_2 + TiC	Oxidation resistant, very hard and wear resistant	For coating on graphite to protect against oxidation	Burykina, 1970
	TiC	Extremely hard and wear resistant	As neutron moderator for reactors	Whittemore, 1968
	TiC	Wear and abrasive resistant, high microhardness	Jet mill components	Dan'kin, 1970
	TiC	Hot extruded (worked), high hardness and hard strength	NASA Aerospace applications	Gangler, 1971
	TiC (Cermet TiC-W)	Resistant to molten Na and Na-K alloys at high temperatures ($1050^{\circ}C$) and pressures up to 861 N/m^2 (8.5 atm)	Parts of pumps for transferring Na	Kosolapova, 1971
	ZrB_2	Wear and abrasive resistant, high microhardness	Jet mill components	Dan'kin, 1970
	ZrC	Resistance to molten metals	Crucibles and boats for melting metals, tubes for conveying molten metals	Kosolapova, 1971
	ZrB_2 + ZrC	Oxidation resistant, high hardness and wear resistant	For coating on graphite to protect against oxidation	Burykina, 1970
	HfC	High melting point, resistant to molten metals	In composition of special refractories for lining crucibles for melting metals	Kosolapova, 1971

TABLE 2.6 (Cont'd)

Feature	Phases	Principal Properties	Fields of Application	Reference
	HfC	Very high temperature melting point compound 7,100°F	As incandescent lamps for film	Whittemore, 1968
	NbC	Resistant to molten metals	Crucibles and boats for melting metals, tubes for conveying molten metals	Kosolapova, 1971
	NbC		Parts of plant for evaporating Al and Zn	"
	NbC	Hot extruded (worked), high hardness and bend strength	NASA Aerospace applications	Gangler, 1971
	TaC	High melting point 7,100°F	As incandescent lamps for film	Whittemore, 1968
	TaC	Resistance to molten metals	Parts of plant for evaporating Al and Zn	Kosolapova, 1971
	TaC	High melting point, resistance to molten metals	In composition of special refractories for lining crucibles for melting metals	Kosolapova, 1971
	WC	Extremely hard and wear resistant	As component of cutting tools	Kosolapova, 1971
	B_4C	Hardest and most abrasion resistant material, high neutron-capture cross-section. High strength and elasticity, low density	Sand-blasting nozzle, for control and shielding in nuclear reactors, for the formation of personnel body armour	Whittemore, 1968

TABIE 2.6 (Cont'd)

Feature	Phases	Principal Properties	Fields of Application	Reference
	B_4C		As indenter for studying micro-hardness of materials	Skuratovskii, 1969
	SiC	Very hard, resistant to oxidation ($3000^{o}F$) low thermal expansion high thermal conductivity	As heating element for furnaces ($2800^{o}F$)	Whittemore, 1968
			Abrasive grinding and cutting of wheels	"
	SiC alloys	Resistance to molten metals	Parts of plant for conveying molten Al, linings for baths for the production of Al by electrolysis of molten salts, crucibles for melting non-ferrous and rare metals, protective thermocouple sheaths	Kosolapova, 1971
Corrosion-resistant materials for the chemical industry	TiB_2 ZrB_2 CrB_2	Resistant to non-ferrous metals and chemical attack at high temperatures, high electrical conductivity, hardness, oxidation resistant, high thermal conductivity	For handling molten Pb, Sn, Zn, Mg, Al, Cu, pump impellers, tyres, galvanizing bath components, thermocouple sheaths, troughs chutes, and level indicators in non-ferrous metals, vaporising boats, crucibles for the vacuum evaporation of thermal, electrical contacts, space technology, heat exchangers	Thompson & Wood, 1963

TABLE 2.6 (Cont'd)

Feature	Phases	Principal Properties	Fields of Application	Reference
	Cr_3C_2	High resistance to various chemical reagents and resistance to oxidation	Filters in chemical industry electrodes for use in electrochemical processes, bearings and packing in pumps supplying salt water under high pressure for washing out oil tanks of tanker vessels, parts of pumps for conveying acids, nozzles for corrosive liquids and gases	Kosolapova, 1971
	Cr_3C_2, Cr_7C_3 Mo_2C	Catalytic properties	Catalysts for use in organic synthesis	"
	SiC	High resistance to chemical reagents	Parts of pumps for transferring acid solutions, lining of nozzles for spraying corrosive liquids, condensers and scrubbers working in corrosive gas atmospheres	"
Materials for nuclear energy production	Be_2C	High melting points, strength at elevated temperatures, specific nuclear properties. Addition of Be_2C to metallic Be increases its long-term strength at temperatures of 650-700°C	Constituent of structural materials, material for retarders and biological protection	Kosolapova, 1971
	ZrC	High melting point, low neutron-capture cross-section	Coating for graphite materials containing UC and ThC used as fuel elements in the power reactors for closed-cycle gas turbines	"

TABLE 2.6 (Cont'd)

Feature	Phases	Principal Properties	Fields of Application	Reference
	NbC, TaC	High melting point, chemical resistance	Coatings for dispersion fuel elements with graphite matrices to retain fission fragments.	Kosolapova, 1971
	UC	High melting point and thermal conductivity, absence of phase transformations, specific nuclear properties	Cores of fuel elements of nuclear reactors, fuel materials in reactors with sodium and organic heat carriers. UC-ThC alloys are used as fuel in gas-cooled reactors	
	B_4C	B-10 isotope forms 18.8% total B in B_4C and has 4000 barn cross-section enabling it to arrest thermal neutrons	Fast breeder reactor, the reactor of 80's contains the isotopically enriched boron-ten variety due to this characteristic. Dosimeters for fast-breeder reactor and bomb tests. First commercial gas-cooled reactors powered in 1972 with 330 megawatt has walls produced from hot-pressed B_4C or by carbon bonding a mixture of B_4C and graphite. Used for neutron reactor design tests, as powder in Al_2O_3 pellets for poisons, widely used in nuclear field as a control poison or shielding element. Extremely stable ceramic material, versatile for the demanding reactor applications	Alliegro, 1970

TABLE 2.6 (Cont'd)

Feature	Phases	Principal Properties	Fields of Application	Reference
	B_4C	Large neutron capture cross-section	Absorbent material for regulating rods (B_4C-Al, B_4C-Al_2O_3, B_4C-ZrB_2, B_4C-Zircon alloy)	Kosolapova, 1971
	WC, TiC	High melting point, hardness and heat resistance, strength at elevated temperatures, capacity for recrystallization through molten metals	Constituents of metallo-ceramic hard alloys ensuring higher productivity in the metal-working, mining, coal, and petroleum industries, widely used hard alloys belong to the types KA, TK, WZ, FS and BK	"
	B_4C	Very hard, uniform, strength adherent coatings	In the reactor, rocket nozzles, chemical reaction and process-vessels	Cochran, 1970
	B_4C	Great hardness and abrasive power	Grinding and polishing hard materials, sharpening and finishing of hard-metal tool blades, cutting elements of drilling bits and tools for machining hard materials, tools for turning up grinding wheels, sand spraying jets, gauges, dies for the rod drawing of abrasive materials	Kosolapova, 1971
	CrB, Cr_3C	Very hard and wear resistant coatings	Screw conveyor coatings	Degtev, 1972

TABLE 2.6 (Cont'd)

Feature	Phases	Principal Properties	Fields of Application	Reference
	Cr_3C_2	High melting point, hardness which is retained at elevated temperatures, high chemical resistance	Constituent of filler alloys and also of hard alloys used for nozzles, dies, high-temperature bearing, press dies for forming brass sections jets for sand spraying	Degtev, 1972
	CrC-Mo	High threshhold of oxidation and wear-resistant at elevated temperatures	Coating on the piston rings used in internal combustion engines	Hyde, 1971
Superhard and wear-resistant materials	TiC	Hard and wear-resistant	Cutting tools	Kieffer, 1970
	ZrC	High abrasive power	Polishing materials	Kosolapova, 1971
	VC, NbC, TaC	High melting point, hardness and heat resistance	Alloying addition to hard alloys based on TiC and WC addition of VC increases tool life by 10-210%, addition of 2% TaC to alloy BK6 increases the rate of machining cast-iron by 10% TaC to TK-type alloys increases the rate of machining steel by 20%	"
	NbC, TaC, WC-Co	Hard and wear-resistant	Cutting tools	Kieffer, 1970
	TaC	High emissive power	High-intensity light source suitable for illumination for filming (1400 lm), coating on metallic tungsten and rhenium for special elements of radiation lamps	"

TABLE 2.6 (Cont'd)

Feature	Phases	Principal Properties	Fields of Application	Reference
Materials for electrical and radio purposes	$Cr_{23}C_6$	Metallic character of conduction, small temperature co-efficient of electrical resistivity	Component of standard low-ohmic resistance working at 300-400°C with nominal resistance values of 5-50	Kieffer, 1970
	(80% ZrB_2-SiC) 56% ZrB_2-14% SiC-C) + (a) carbon cloth as reinforcement; (b) nickel as additive	Excellent oxidation resistance, strength, and thermal shock resistance in the temperature range 1600-2800°C	Nuclear rockets, space power systems, re-entry vehicles and aircraft engine components	Gangler, 1971
	ZrB_2 + SiC HfB_2 + SiC	Improved fabricability and enhanced material properties, excellent thermal, physical and mechanical properties.	Nose caps, lifting re-entry leading edges, air breathing engine components, rocket nozzle throats.	Clougherty, 1969
	TiC	High melting point and electrical conductivity, low evaporation rate	Constituent of electrodes for the underwater oxy-electric cutting of steel, thermocouple electrodes for measuring temperatures up to 2000°C in reducing and neutral atmospheres and in vacuum	Kosolapova, 1971

TABLE 2.6 (Cont'd)

Feature	Phases	Principal Properties	Fields of Application	Reference
	TiB_2, ZrB_2	Electric resistance in the order of copper	Tests for use as electrodes for Al reduction. Intergranular corrosion and brittleness caused failure	Whittemore, 1968
	ZrC	High melting point, low evaporation, high emission current density	Thermionic cathodes for electronic devices working in portable equipment under conditions of low vacuum and intensive ionic bombardment, constituent of cathodes (ZrC-UC) of thermionic converters of thermal energy into electrical energy	Kosolapova, 1971
	ThC	High emission current density, low work function of electrons	Cathode material that works stably at 1900°C for 900h	"
	NbC, TaC	High melting point, low vapour tension at high temperatures, metallic nature of conduction, satisfactory mechancial strength	Heating elements of electric resistance furnaces working in reducing and neutral atmospheres up to 3000°C	"
Materials for manufacture of aircraft and rockets	Be_2C	Addition of Be_2C to metallic Be increases its long term strength and fracture resistance	Structural materials used in aviation	Kosolapova, 1971

TABLE 2.6 (Cont'd)

Feature	Phases	Principal Properties	Fields of Application	Reference
	TiC	High melting point, hardness and heat resistance, strength at high temperatures	Constituent of cermets for use in gas-turbine blades, withstanding very well the severe operating conditions experienced in aircarft jet engines, components of friction disks for aircraft construction, protective coatings for rocket components. (ARD nozzles and leading parts.)	
	ZrB_2 + SiC ZrB_2 + SiC + C	Long time high temperature oxidation resistance, high strength, thermal conductivity	Nose caps and leading edges, to fabricate nuts and bolts	Kaufman, 1970
	B_4C, SiC	Highly resistant to abrasive, corrosive and erosive wear in aggressive media at normal and elevated temperatures	Bushings, rings and nozzles in machines and instruments	Varzanov et al, 1969
	SiC	Great hardness and abrasive power	Grinding, polishing, and abrasive parts	Kosolapova, 1971

2.9 The present research

The relatively low thermodynamic stability of boron carbide and its ability to react with most metals or their oxides with or without the addition of B_2O_3 make it a valuable and most important source of boron in the formation of borides. However, although thermodynamically feasible, these reactions may be kinetically unfavourable. Increased surface area in terms of decreased grain size and closer contact of particles brought about by pressing uniform mixtures has been found to promote the rate of solid state reactions as in reactive sintering. Thus, successful reactions of metal hydrides and carbides with boron (Glaser, 1952) for the formation of borides of Ti, Zr, Nb and Ta have been carried out by hot pressing the mixtures at temperatures 1500 - 2780°C. Similarly, borides of V, Cr, Mo and W have been produced by hot pressing at 1500 - 3180°C mixtures of boron and the respective metals or their hydrides or carbides. Likewise, hot pressing studies were later carried out for boron carbide with the respective metals or their hydrides and carbides. Cold pressing of B_4C, some additives (Al, B, Si) and some binders (paraffin wax, evostick, stearic acid, cow-gum) followed by sintering at 1800 - 2200°C has been studied by James and Biddulph (1970). Biddulph (1970)has devised a system for hot pressing and hot pressed TiB_2 at 2000°C up to 97% theoretical densities.

In the present work, the formation of metal borides and carbides is studied at 1000 - 1800°C using very finely divided boron carbide and metals in the form of powder and foil. The research consists initially of a study of the chemical reactivity and subsequent sintering of finely-divided boron carbide with powdered metal additives. Changes in phase composition, surface area, average crystallite and aggregate sizes are to be correlated with temperature and time of heating. Further information

on the sintering processes is obtained from the densification on hot pressing at 1000 - 2100°C boron carbide and some metal borides and carbides.

This research is developed to study the formation of metal boride and carbide coatings on metal surfaces, by reaction with finely-divided boron carbide at different temperatures (1000 - 1800°C). The microstructure of the coatings is examined to ascertain what changes have occurred in phase composition, crystallite and aggregate sizes and microhardness compared with the initial metal surface.

It is hoped that optimum temperatures and times of heating can be found which produce coatings having good crystallinity and microhardness, to prevent any possible galling of the metal surfaces. Nevertheless, for many practical applications, the coatings must have good resistance to oxidation at high temperatures. Thus, further research must be undertaken on the oxidation of boron carbide and some metal borides and carbides, particularly with regard to the effects on scaling resistance and the microhardness of metal coatings containing these materials.

CHAPTER 3

EXPERIMENTAL TECHNIQUES

This chapter contains an account of the experimental techniques used in this research work. Included is a summary of the underlying principles and procedures.

3.1 X-ray diffraction

Peiser et al (1960) have given a comprehensive summary of the theory and practical applications of X-ray diffraction techniques.

3.1.1 X-ray generators

Diffraction studies in the present work were carried out on two X-ray generators of different design, namely, (a) a Hilger & Watts unit connected to a sealed tube containing the filament and target; and (b) a Raymax 60 generator manufactured by Newton Victor Ltd. with the facility that the target can be changed and the filament replaced, and kept continuously pumped by an oil diffusion pump coupled to a rotary vacuum pump. The Hilger & Watts generator has a stabilised X-ray output, with the voltage and the filament current controlled to within 0.1% for a copper target. The radiation used was copper $K\alpha$, wavelength 1.542Å. Where excessive fluorescence was caused by iron or chromium in the test samples, molybdenum radiation (0.711Å) with a zirconium filter was used.

3.1.2 The Counter Diffractometer

The powder diffraction patterns were recorded to identify the phase composition of crystalline substances, in two ways, (a) by a photographic method; and (b) using an X-ray diffractometer equipped with counter and rate meter. For the photographic recording of diffraction patterns, a Debye-Scherrer camera, of 9 cm diameter and manufactured by Unicam Instruments Ltd., was used. A Solus-Schall

diffractometer (diameter 50 cm) was fitted with a Berthold ionisation detector and connected to a Berthold disconnector ratemeter chart recorder. The procedures used are the ones established by other workers, e.g. Jayaweera (1969).

The sample for diffractometer studies was suspended in acetone and the dispersion so formed transferred to a glass slide. The solvent was evaporated from suspension and the powder left behind usually adhered to the slide. For non-adhesive specimens a paste of an adhesive in acetone was used to set these properly on the glass slide.

The glass slide containing the sample was mounted vertically at the centre of the diffractometer and rotated at half the speed of the detector. This arrangement kept the sample in a tangential position to the circle defined by the collimator diaphragm, the centre of the sample and the counter diaphragm. The angles of the diffracting positions were indicated on the circular scale of the table as well as on the chart recorder. The readings on the ratemeter and area surrounded by the peaks on the chart varied according to the intensity of the diffracted beams.

3.1.3 X-ray line (or peak) broadening

Even with a perfect crystal some broadening of the reflections occurs. This instrumental broadening is independent of pure diffraction effects and arises from a variety of causes such as:-

(a) The diameter of the cylindrical specimen and the accuracy of centering, if it is rotated.

(b) The diameter of the camera, and its distance from the X-ray tube.

(c) The absorption of X-rays by the specimen.

(d) The pinhole size or slit system of the camera.

(e) The intensity distribution over the target of the X-ray tube considered from the direction in which the X-rays enter the camera.

Over and above all these instrumental broadenings, the width of X-ray lines may be increased by diffraction effects caused by small crystallite size, by lattice distortion and by structure faults, including inhomogeneities due to variable chemical composition. In order to account for broadening of X-ray reflections from small crystals, Bragg's law has to be extended to cover incomplete reinforcement of the waves scattered by successive lattice planes. For small crystals, especially below 1000Å edge length, the deviations from Bragg's law may be quite large. For parallel monochromatic radiation and a point specimen the breadth of the line is given by

$$\beta = \frac{K\lambda}{t \cos\theta}$$

where β = angular breadth of the line defined by half-peak width corrected to give the intrinsic broadening.

t = edge length of cubic crystal

λ = wavelength of X-radiation

θ = the Bragg angle

K = a constant dependent on crystal symmetry

β is estimated either from the recorder trace as the peak width at half the maximum after subtraction of the background radiation, or by using the scaler and printout to give optimum statistical accuracy. This formula is valid experimentally only with monochromatic radiation and when there is no instrumental line broadening. In order to correct for these factors the method due to Jones (1938) is used. In this

method, the X-ray diffraction lines of the structure under study (m-lines) are compared with those produced by a standard (e.g. calcite) consisting of larger perfect crystallites (s-lines). The observed integral breadths of the lines are first corrected for the fact that they are produced by the $\alpha_1\alpha_2$ doublet of the CuK_α radiation, and then corrected for instrumental broadening. The broadening due to lattice distortion is considered by Stokes & Wilson (1944).

A general method independent of simplifying assumptions, for correcting the above factors is given by Stokes (1948), and described in detail by Lipson & Steeple (1970).

A computer program was written to evaluate particle sizes from X-ray line broadening data; details are given in Appendix II.

3.2 Theory of electron microscopy

A detailed account of the theory and practical applications of electron microscopy and diffraction has been given by Zworykin et al (1945), Kay (1965) and Hirsch et al (1965).

The wavelength of electron beam is given by:

$$\lambda = \frac{h}{\sqrt{2meV}}$$

where h = Plank's constant

λ = wavelength

m = electron mass

e = electron charge

V = accelerating voltage

The above equation is subject to a relativistic correction because of the variation in the mass of the electron with velocity, which in turn depends on the voltage.

The wavelength of the beam can be found from the diffraction

pattern of a substance with known unit cell dimensions and calculating a single factor, the camera constant, λL, where L is the effective camera length.

Electron microscopy is based essentially on the same principle as optical microscopy with the difference that the lens system of the latter for the deflection of the beams is replaced by a combination of magnetic or electric fields having different intensities and directions. The magnifying power of the electron microscope is considerably enhanced due to the far shorter wavelength of the electron beam compared with that of the visible beam. The theoretical limit of resolution, given by half the wavelength of the radiation used, is 0.02Å for the electron microscope and 2000Å for the optical microscope.

A specimen is studied by transmission microscopy by putting it in the focal plane of the lens system and observing its enlarged image on a phosphor screen or by recording on a photographic film held in a cassette within the instrument. Usually, both facilities are employed, one to align and select the image, the other to record it. As the high energy electrons collide with gas molecules, they are dispersed and their energy level is considerably lowered. To avoid such collisions of electrons, the mean free path of the gas molecules is increased by decreasing the working pressure of the electron microscope to about 10^{-6} mm Hg. A special lens system is used, by interposing between objector and projector, to take diffraction patterns of samples being studied on the electron microscope. Diffraction micrographs are obtainable only for very thin crystals and aggregates or elements of low mass number, owing to the high absorption of electron waves by matter. The single crystal diffraction pattern consists of reflections

from a plane of reciprocal lattice points, cf. X-rays. The diffraction pattern of a polycrystalline substance in random orientation consists of typical concentric rings.

3.2.1 Apparatus

Diffraction and direct transmission micrographs of powdered materials and transmission micrographs of surface replicas of sintered refractory materials for the present work were obtained using a Philips EM 100 B model electron microscope (Van Dorsten, Nieuwdorf & Verhoeff, 1950). It has a reasonably good resolution of 25Å. The pumping system of the microscope consists of a prevacuum rotary pump, a mercury diffusion and an oil-diffusion pump. Micrographs of the specimens are taken by means of a camera loaded with 35 mm film and fitted in the microscope. The magnification is controlled by varying the currents to the electro-lenses. Various parts of the grid can be observed by means of controls for focussing and for moving the sample holder. An image of the sample under observation is thrown on the fluorescent screen directly in front of the observer. In order to take a micrograph of the image on the screen, the camera is lowered into position and the shutter opened. The exposure depends upon the illumination of the image and may be up to several seconds. The magnification is determined by reading a scale and then consulting standard tables. A suitable area of the sample for a diffraction micrograph is chosen by means of a diffraction selection diaphragm; the diffraction lens is switched on and the intermediate lens switched off. Longer exposures for diffraction micrographs are required because of their lower intensity. When the electron microscope has started working, samples can be readily changed by removing the grid holder and inserting

another one carrying a different sample. This operation takes a fraction of a minute. The usual voltage of electron microscope was 80kV.

Carbon and metal films were prepared in a "Speedivac" High Vacuum Coating Unit 12 E6, manufactured by Edwards High Vacuum Ltd. The main part of the unit is a glass work-chamber, evacuated by an oil diffusion pump backed by a rotary pump. Electric circuits, to strike an arc across carbon electrodes and for the vapour deposition of metal film from a filament, are fitted inside the chamber. Various gauges for readings of pressure inside the chamber and controls for the electricity supply to the circuits inside are fitted on the panel of the instrument.

3.2.2 Preparation of samples

Microscopic studies of samples were made by scattering the particles on a carbon film supported on a copper grid. The thickness of the carbon film was of the order of 200Å. The copper grid was of 3 mm diameter and had a square mesh. The length of the side of square was 100 μ m. A pair of forceps was used to handle the grid throughout the investigation of specimens.

An electric arc was struck between pure carbon electrodes in the high vacuum coating unit for depositing a carbon film on a mica surface. The arc voltage and current were 10V and 60A respectively. The arc was struck in about eight bursts, with an interval of approximately 3 seconds between successive bursts to cool the electrodes. The pressure inside the chamber was kept below 10^{-4} mm Hg.

The mica plate was held in a slanting position at an angle of about 30° at the surface of a small trough of water and the carbon film floated off on the water surface, by gradually lowering the plate below the water level until it sank. The carbon film is stripped off the surface of mica by water by virtue of its surface tension. It was

facilitated by cutting off the edges of the mica sheet after deposition of the film and contaminating the mica sheet by breathing onto it before deposition. The floating film was deposited on the copper grid and the residual water absorbed by placing it on a filter paper. The grid so prepared was placed in a vertical cylindrical holder and locked in position with a cylindrical cap. The grid was exposed through the open end of the cap. A dispersion of the microcrystalline powder was made in either water or acetone, by keeping it suspended in a liquid tank, vibrating at the extremely high frequency of an ultrosonic unit for about 20 minutes. A drop of the suspension was placed on the copper grid carrying the film and was evaporated to dryness under an infra-red lamp. Then it was placed in a microscope grid holder, and inserted in the electron microscope.

3.2.3 The replica technique and shadow casting

The surface features of solids can be studied in minute details by means of the replica technique. It involves the transfer of a surface topography of a solid body to a thin film which can be examined by transmission electron microscopy. The surface details may be sharpened by shadowing with a heavy metal which absorbs electrons strongly. Carbon replicas with a shadow casting of palladium metal were prepared as follows.

Polystyrene grains were melted on a glass slide over a bunsen burner. The solid surface of the sintered sample was brought into close contact with the melt and pressed very gently onto it. It was then allowed to cool and solidify. This solidified specimen, carrying the surface impression of the sintered sample, was placed in the vacuum unit and deposited with a carbon film as described above. It was then

shadowed, i.e. coated with a film of palladium metal as follows.

A thin palladium metal wire, placed in a tungsten filament, was evaporated by passing through it a heavy current; the metal was allowed to deposit on the film replica. The polymer was dissolved away in 1,2-dichloroethylene. The remaining film was picked up on a copper grid, dried under an infra-red lamp and then observed in the electron microscope. Before each evaporation operation, the filament was "flashed", i.e. its temperature was raised to remove dirt etc. by passing a slightly higher current through it than was subsequently used for metal-evaporation.

After completion of a set of exposures, the film was removed from the electron microscope camera and developed in a fine grain developer to give optimum contrast. Enlarged prints were made from the "negative" onto Kodak bromide paper. In this manner magnifications of over 70,000 times the original were obtained.

3.3 Scanning electron microscopy

Comprehensive accounts of the theory of SEM and its special applications are given by Thornton (1968). A brief summary of its features is given below.

SEM consists mainly of three types of components:

1. Electron-optical column including electronics

   A schematic diagram of the instrument is shown in fig. 3.1. The column comprises an electron gun and two to four electron lenses. The electron beam passing through the system of lenses is demagnified in diameter to 250Å or less. The final lens assembly contains two sets of magnetic scanning coils. They are energized by a suitable scan generator to deflect the

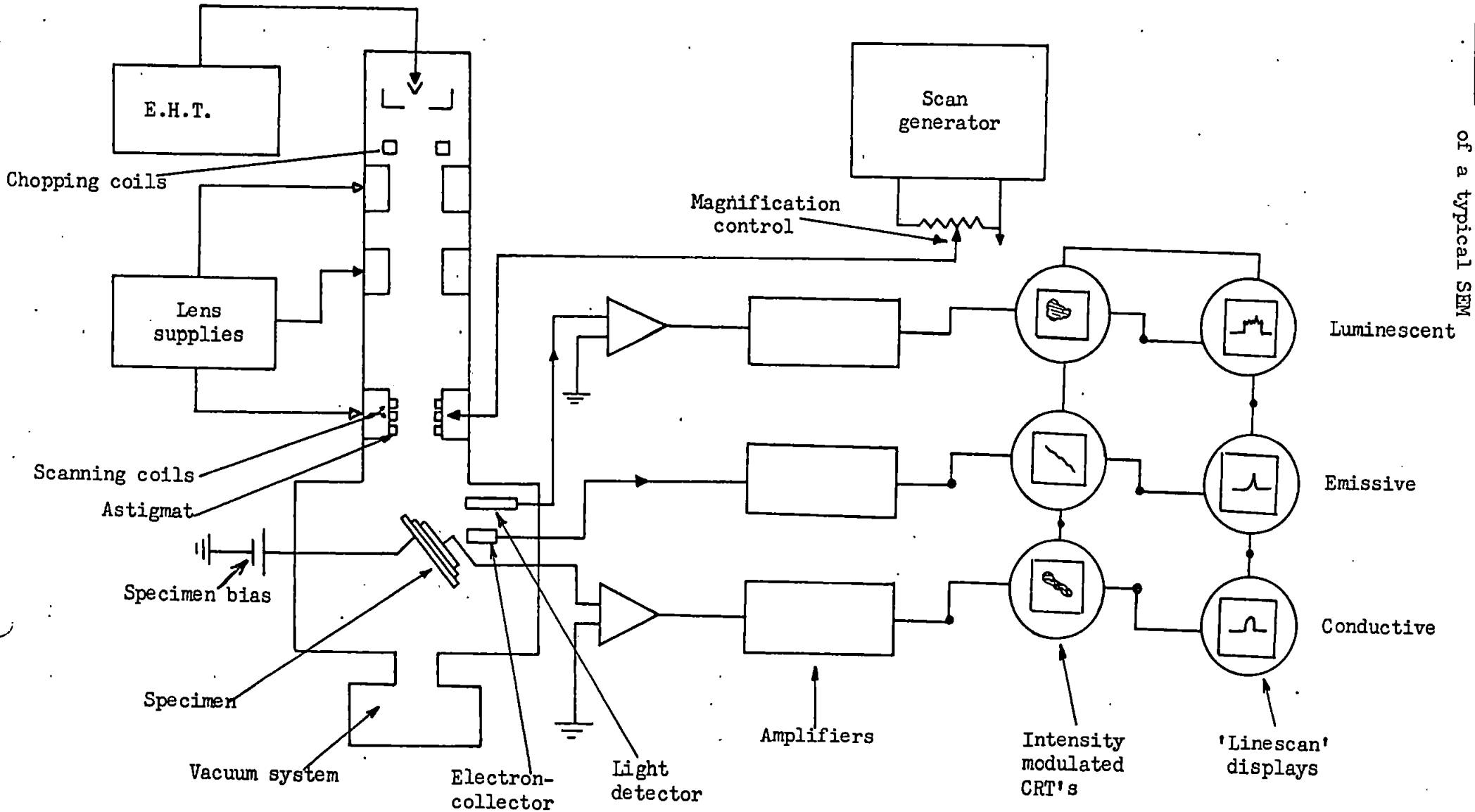

Fig. 3.1 Simplified diagram of a typical SEM

beam on the specimen surface in a raster-like pattern. The electron column contains three more items: (i) A set of apertures for specifying the angular aperture subtended by the beam at the specimen surface. (ii) An 'astigmat', consisting of a set of coils of special design to overcome any astigmatism in the system. (iii) A set of 'chopping' coils or plates for superimposing modulation on the electron beam.

2. Vacuum system, specimen chamber and stage

Vacuum is maintained in the electron column and specimen chamber by a pumping system. The specimen stage in the chamber has the facility to move the specimen in the electron beam and examine at a desirable angle to the beam. The interaction of the electron beam with the specimen gives rise to effects like secondary electron emission, a reflected electron current, beam-induced conduction and often cathodoluminescence.

3. Signal detection and display system

The signals can be deduced and amplified to control the visibility of the bank of cathode-ray tube (CRT). The specification of spot position in CRT and the primary beam on the specimen surface is facilitated by the same scan generator. Usually the signal is fed to the brightness control of a cathode-ray tube with a long persistance phosphor for visual examination. Signal can further be displayed on a tube with short-persistance phosphor for photographic records. The synchronism of cathode-ray tubes with primary beam is manifested by the scan generator controlling the magnification. Its output is introduced to the deflection coils of the CRT to keep the raster size approximately 10 X 10 cm. The raster

size on specimen is smaller than this. In general terms if the specimen raster is 10μ X 10μ in one case, and 1X1mm in another with a certain voltage, then the magnification is X10^4 in the first and X10^2 in the second case.

Additional electronic equipment consists of the high-stability supply for the electron gun, the high-stability current supplies for the magnetic lenses, the control systems for the cathode-ray tubes, the ancillary equipment associated with the various signal detection systems and monitoring systems.

For SEM, samples are simply mounted on the microscope stage and vacuum coated with aluminium to ensure good electrical conductivity and are then placed in the microscope. The Cambridge Stereoscan S4-10 with a resolution of better than 100 Å was used for study of metal foils (Chapter 6). The instrument is situated at The Royal Naval Engineering College, Manadon, Plymouth.

3.4 Thermoanalytical techniques

Of the various analytical techniques known as thermometric analysis, two are most commonly in use. First, thermogravimetry (TG) wherein the weight change of the sample under investigation is followed over given periods of time and the temperature can be varied at any desirable rate. It is specifically useful for studying the reactions of solids involving a change of weight. The atmosphere of the material under study may be controlled, e.g. an inert or reactive atmosphere may be used.

The thermobalance used was a modified version of a double pan analytical balance (Gregg & Windsor, 1945). In the current research programme, a Stanton Model A49 balance was used, sensitive up to weight changes of 10^{-4}g. One pan of the balance was furnished, on its underside, with a hook carrying a length of nichrome wire. The wire passed through a hole in the balance shelf and supported a silica sample bucket, which was suspended in an electric furnace controlled by a Stanton-Redcroft linear

programmer. The measurement of temperature in the vicinity of the sample was made by means of a chromel-alumel thermocouple placed close to the sample bucket and attached to a milli-voltmeter (Baird & Tatlock-Resilia).

Varying amounts of samples, 0.5 - 2.5 g, were weighed accurately into an aluminium crucible (Thermal Syndicate Thermel Alumina). The weight change in the samples were followed at known intervals of time. In the present work, kinetic and heat treatment studies were carried out with air as the reacting medium. The kinetic behaviour of the various reactions was followed by regression analysis (least square fit) over given periods of time.

The second commonly used method for thermometric analysis is differential thermal analysis (DTA), first developed by Houldsworth & Cobb (1922). The test and inert materials had embedded in them separate thermocouples which were connected at their opposite ends. This arrangement enables the measurement of emf produced during the transfer of heat during the reaction process, and temperatures at which such changes take place. Throughout the present research work, apparatus based on the design described by Grimshaw, Heaton & Roberts (1945) was used.

0.5 - 1.5 g of the samples were placed alongside the reference material, recrystallized alumina in a ceramic block. This was heated in an electric furnace (Griffin and George) at a linearly-controlled rate of 10 to 20°/min. by means of a linear programmer (Stanton-Redcroft). An automatic recorder indicated the temperature of the block as well as the heat change over the temperature range of 250° to 1000°C, in order to determine the temperature required for the onset of the reaction.

3.5 Surface area measurement by gas sorption

This method of surface area measurement depends on the fact that the

quantity of a gas adsorbed on the surface of a material is a function of the specific surface, i.e. the surface area per unit mass. From the specific surface, the average crystallite size may be estimated for powders having crystallites of approximately uniform shape and simple geometry. Glasson (1956 and 1958) and Gregg & Sing (1967) have given detailed descriptions of the method.

To obtain the monolayer capacity, x_m, from the adsorption isotherm, the most commonly used method is that given by Brunauer, Emmett and Teller (1938). According to the B.E.T. equation:-

$$\frac{p}{x(p^o - p)} = \frac{c - 1}{x_m c} \cdot \frac{p}{p^o} + \frac{1}{x_m c} \qquad \text{(i)}$$

where: p = pressure of adsorbate vapour in equilibrium with absorbent.

p^o = saturated vapour pressure of vapour adsorbed.

x = amount of vapour adsorbed.

x_m = capacity of filled monolayer.

c = constant.

There are five main types of the adsorption isotherms as classified by Brunauer, Demming, Demming & Teller (1940) (commonly referred to as the B.E.T. classification). Types II and IV are in good agreement with the B.E.T. equation for determing the specific surface of substances, while type IV is applicable for the determination of the pore size distribution. However, type II gives best agreement with the B.E.T. equation over limited ranges of relative vapour pressure (Gregg, 1961). A plot of $\frac{p}{x(p^o - p)}$ VS $\frac{p}{p^o}$ gives a straight line with $\frac{c - 1}{x_m c}$ as slope and $\frac{1}{x_m c}$ as intercept. Values of c and x_m can be calculated from these two

parameters. The linearity of the relationship between $p/x(p^o - p)$ and p/p^o applies only between values of p/p^o from 0.05 to about 0.3. The amount of gas adsorbed can be determined either gravimetrically or volumetrically (Gregg & Sing, 1967 p.310).

The specific surface, S, varies with x_m according to the relationship:-

$$S = \frac{x_m}{M} N. A_m$$

where: M = molecular weight of adsorbate.

N = Avogadro's number.

A_m = Cross-sectional area of an adsorbate molecule in a completed monolayer.

From the specific surface (S) of a powder, the average crystallite size, l, assuming that all the particles are spherical, can be determined easily.

$$S = \frac{6}{\rho l}$$

ρ = density of the solid (adsorbent).

This relationship is applicable for particles of cubic shape also . Expressions for the other shapes (e.g. plate- and needle-shaped particles) can be derived easily.

3.5.1 The apparatus

The sorption balance developed by Gregg (1946, 1955) has been used throughout in the present work. The glass beam of the sorption balance is supported on saphire needles, which are put into a glass cradle. One arm of the balance carries a bucket for the sample with counter-weights, and the other carries a solenoid or magnet enclosed in a glass envelope surrounded by an external solenoid. The whole balance is enclosed in a

glass case and other accessories like vacuum pumps, gauges, and gas reservoirs are connected to it. The glass case can be evacuated and filled with any desirable gas. Descriptions of the sorption balance and the low temperature nitrogen sorption method are given by Gregg (1946) and Glasson (1956). The technique is now an established one for the determination of particle size (BS4359, part I 1969).

3.5.2 Measurement of sorption isotherms

The samples for specific surface studies were outgassed in the specimen bucket to remove adsorbed vapours and moisture on their surfaces. The temperature of the specimen was maintained at 200° by surrounding the glass limb with furnace during this operation (Glasson, 1964). Nitrogen is maintained by boiling liquid oxygen coolant contained in a Dewar flask. The initial weight of samples was determined in vacuo, followd by additions ("dosing") of nitrogen into the apparatus. Observations of sample weight versus corresponding nitrogen gas pressures were taken under conditions of equilibrium. To determine the desorption section of the isotherms, sample weights were recorded at decreasing equilibrium nitrogen pressures, when instalments of nitrogen were pumped out of the balance.

The weight corrections for buoyancy effects of the sample and container had to be applied to all weight changes. Such corrections were determined from experiments carried out under the same conditions with samples of known X-ray density and negligible surface area. The quarter-milligramme sensitivity of the vacuum balance gave an accuracy of $\pm$ 0.1 $m^2 g^{-1}$ on 10 g samples, leading to possible errors of over 3% where the specific surface, S, < 3 $m^2 g^{-1}$. The remaining details of the technique are basically similar to those described in the original paper

involving use of a vacuum balance for low-temperature surface area determination (Glasson, 1956).

Thus, the liquid oxygen bath remained constant within $\pm$ 0.2° and at least 1h was allowed for the sample to attain a constant temperature. In practice, the sample is generally up to about 1° warmer than the liquid oxygen outside the balance limb (as indicated by internal and external thermocouples). The sample shows a temperature constancy similar to that of the bath($\pm$ 0.2°), and dependent to some extent on the sizes of the sample containers and hangdown tubes (up to 30 mm diameter), depth of immersion in the liquid oxygen (over 15 cm) and possibly on the surrounding nitrogen gas pressure. By standardising the equipment and improving the heat insulation at the top of the Dewar flask, the sample temperature was kept within $\pm$ 0.1°, thereby minimising the variation in the s.v.p. of the nitrogen to preserve an accuracy of better than 3% in the surface area determination.

The oxygen isotherms, which extended to a relative pressure, p/p^o, near unity, exhibited little or no hysteresis at $p/p^o < 0.3$. From these and the nitrogen isotherms, S could be calculated by the B.E.T. procedure, using values of 14.1 $\AA^2$ and 17.0 $\AA^2$ for the cross-sectional areas, A_m, of oxygen and of nitrogen respectively; this gave agreement within ca 5% in the values of S obtained from both series of isotherms. The older graphical and newer computer (with line-plotter) methods (O'Neill, 1969) agreed within $\pm$ 1% for values of S from each individual isotherm (Glasson & Linstead-Smith, 1972).

3.6 Sintering of materials

The sintering of boron carbide with and without different additives was carried out in argon as well as in vacuum.

Initially a high temperature furnace P.C.10 (Metals Research, Cambridge) was used for sintering finely-divided boron carbide with metal additives. After some cycles of heating for the sintering of boron carbide with aluminium up to 1,800°C, the inner tube of the furnace failed. Investigation into the cause of failure led to the following explanation. Aluminium, being volatile at such high temperatures (m.p. 659.7°C b.p. 2,057°C), evaporates and reacts with the alumina of the tube to give AlO. The latter is a much more volatile oxide and its formation and evaporation mechanically weakens the tube at high temperatures. After replacement of the tube and element in the P.C.10 furnace, a second start was made with iron as the additive to boron carbide. The furnace again failed, this time due to a technical fault in the manufacture of the element. A third start was made with iron as additive, but this was followed by a tube failure which led to complete closure of this furnace and never was it used again in this work. Investigation by Metals Research engineers suggested the incompatibility of boron carbide with alumina. However, boron carbide was heated with recrystallised alumina from crucibles at 2,000°C later in this work, but X-ray analysis showed no reaction between the components. This alumina was found to be in α - and γ - forms, which may account for its mechanical instability towards thermal shock.

3.6.1 Construction of High Temperature Furnace

After these mishaps, a vacuum furnace was constructed, Fig. 3.2. being powered by a four kilwatt radiofrequency induction heater (Delapena E 4 kW) with the wound coil external to a 1 in. diameter alumina tube. The tube was evacuated by a single stage rotary pump (Edwards Speedivac IS 150) backing a two stage oil diffusion pump (Edwards Speedivac 403A). Vacua of between 10^{-5} to 10^{-6} mm Hg were achieved.

Fig. 3.2 High temperature vacuum furnace of sintering studies

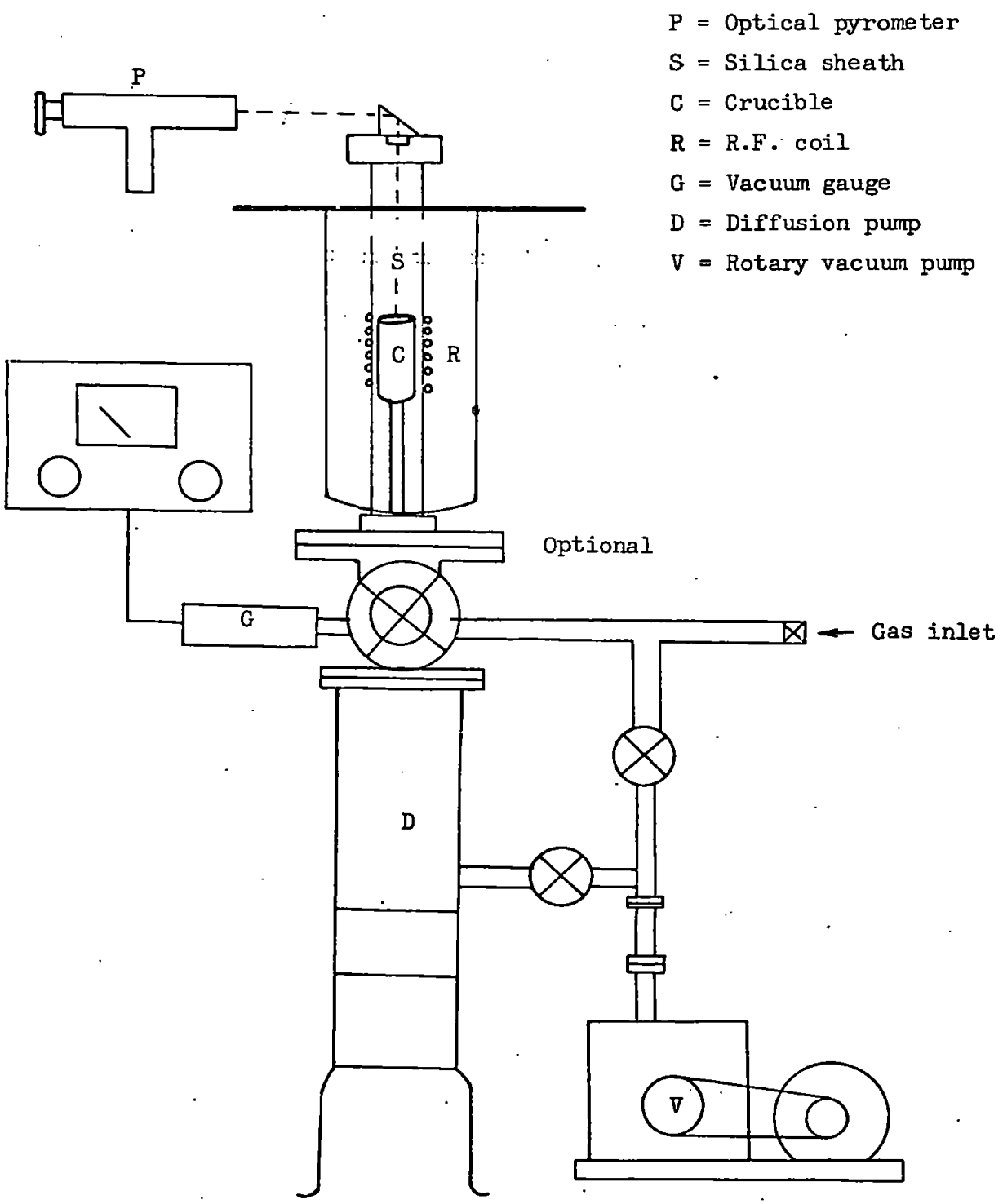

After several failures, the alumina tubes were replaced by fused silica tubes (Thermal Syndicate) having better thermal shock resistance. However, the silica tubes can only be heated to between 1,000° and 1,400°C and for limited times to avoid extensive recrystallisation and cracking when cooled. Contact had to be avoided between the silica tubes and the graphite crucibles for the induction heater.

In order to work at temperatures between 1,000° and 2,000°C, alumina tubes were reintroduced in a modified form. Two tubes were placed end to end in the hottest part of the induction furnace, as shown in Fig. 3.2. This arrangement minimised mechanical strain caused by thermal shock, yet offered thermal resistance to heat radiated towards the walls of the outer tube. The inner tubes were kept vertical by attaching their far ends to asbestos sheets, the top sheet also closing the end of the outer tube. The crucible was supported on an alumina pedestal standing on the bottom of the outer tube. The height of the pedestal was approximately that of the length of the lower inner tube so that the crucible rested near the junction of the two inner tubes, surrounded by the copper coil for R.F. induction heating. The upper parts of the apparatus were sealed with Kos aluminous cement covered also by rubber seals to ensure air-tightness. Porosity to argon was eliminated by coating the cement and asbestos with a uniform thick layer of aluminium paint. The reading of temperature by a disappearing filament optical pyrometer (Foster) was facilitated by having a glass window fastened by a rubber seal to the upper end of the inner tube.

The main features of this furnace are:-

(a) Its design enables it to be resistant to thermal shock, possibly tolerating lower grades of α-Al_2O_3 for the tubes. Samples

can be heated up to 1,800°C in 5 minutes and cooled back to working temperature in 15 minutes; cf. the P.C.10 furnace which requires three hours for similar heating cycles.

(b) The sample can be seen through a glass window at a distance of 6 ins. from it, and photographic methods could be used to follow the course of reactions.

(c) It is more economic to run and does not need a flow of 90% nitrogen-10% hydrogen, as required by the Molybdenum windings of the P.C.10 furnace.

(d) It can be modified for sintering work at higher temperatures, up to 2,500°C using magnesia thoria tubes

3.7 Reaction sintering of boron carbide with metals by hot pressing

Three hot pressing facilities were used for this work.

3.7.1 Laboratory hot-pressing system

A small scale laboratory hot-pressing system (Fig. 3.3) was set up to investiage the pressure sintering properties of small quantities (10g) of powders. The system is based upon a double-acting mechanical press, designed by Roeder and Scholz (1965), capable of working at temperatures up to 3,200°C and pressures up to 1,000 kg cm^{-2}. The resistance-heated graphite die set is held between water-cooled copper electrodes, the power being supplied by a 60 kW single phase transformer which can deliver up to 3,000 A at 20V; the original design employed a smaller (24 kW) transformer. Since the electrical resistance of the die is inversely proportional to its cross-sectional area, the higher power available from the larger transformer will enable different die (and hence sample) geometries to be investigated.

The power supplied to the transformer is regulated by means of a

Fig. 3.3 Laboratory hot pressing system

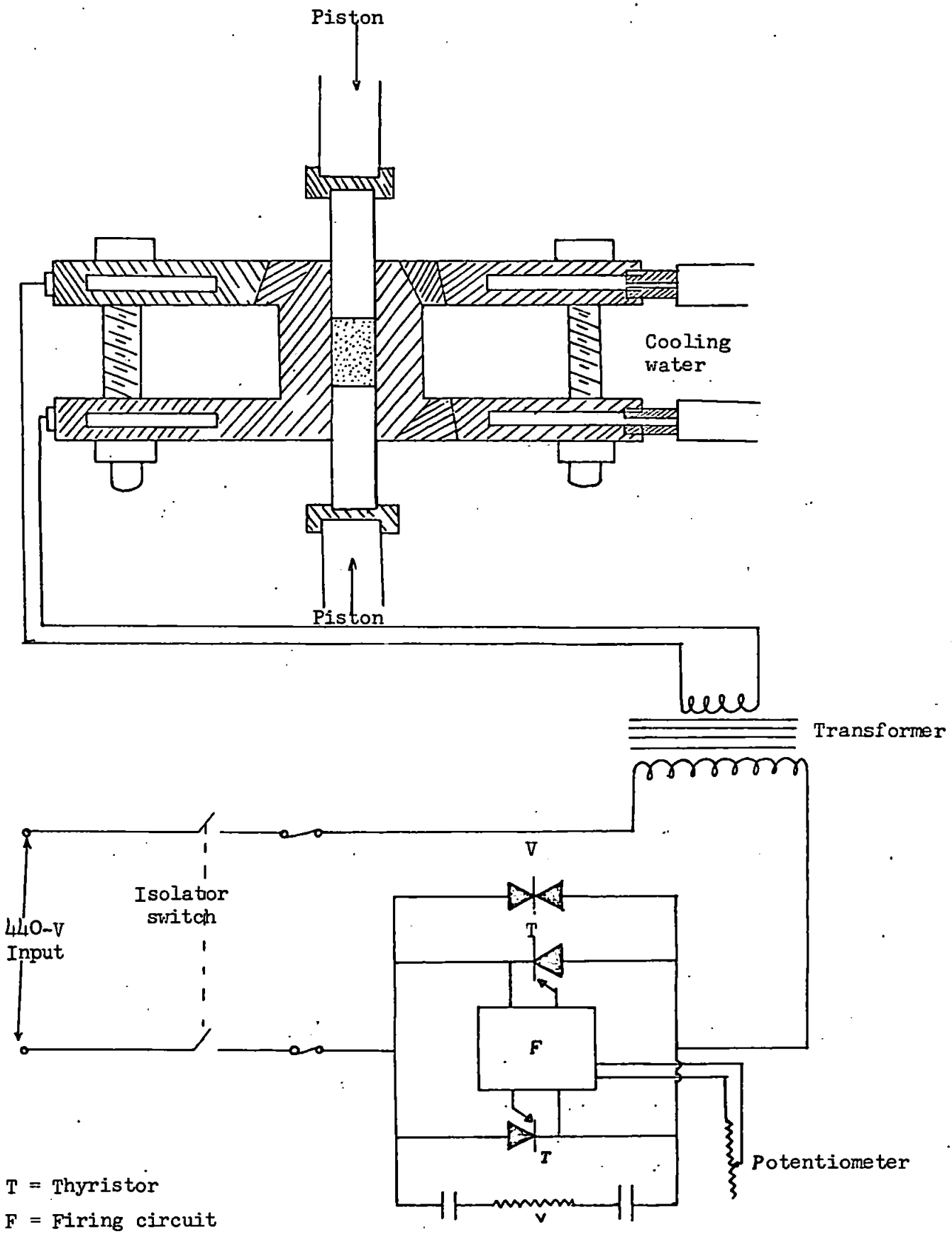

T = Thyristor

F = Firing circuit

V = Transient voltage protectors

thyristor control system designed by Biddulph (1972) and further developed during the present work. The basic circuit consists of two thyristors connected in inverse parallel, mounted on a water-cooled copper bush, and is regulated by a firing circuit. The firing circuit incorporates a potentiometer, the adjustment of which provides a direct control of the power supply. Thyristor control of resistance heating is preferred to the conventional saturation reactor type since a more precise regulation of the sample temperatures can be achieved.

3.7.2 Industrial hot-pressing systems

Samples of borides and carbides were hot-pressed at Bullock Diamond Products Laboratories, Torpoint, using a graphite mould set between hydraulic rams and heated to temperatures lower than the melting point of the respective samples, by a 36 kW R.F. induction heater (Wild-Barfield), Fig. 3.4. The heat of the die set was contained by carbon black powder (charcoal). The temperature and pressure were increased continuously (up to approximately 100 - 150°C below the m.p. of the sample) until the two rams had moved closer to each other by a pre-calculated distance. This calculation was based on the theoretical densities. Hot-pressed samples of up to 80% theoretical density were prepared. A disappearing filament pyrometer (Foster Instrument) was used for temperature measurement. After completion of hot pressing the whole assembly was allowed to cool, before being dismantled to remove the samples. These were tested for chemical composition, phase composition and mechanical properties.

Samples of CaB_6 were hot pressed at Borax Consolidated Research Centre (Chessington). Rams 35.5 - 40.6 cm long and 2.54 cm in diameter were used to press the specimens in a spiral die. The progress of densification was followed by noting the movement of a plunger as the

Fig. 3.4 Hotpressing set up for compaction of boron carbide

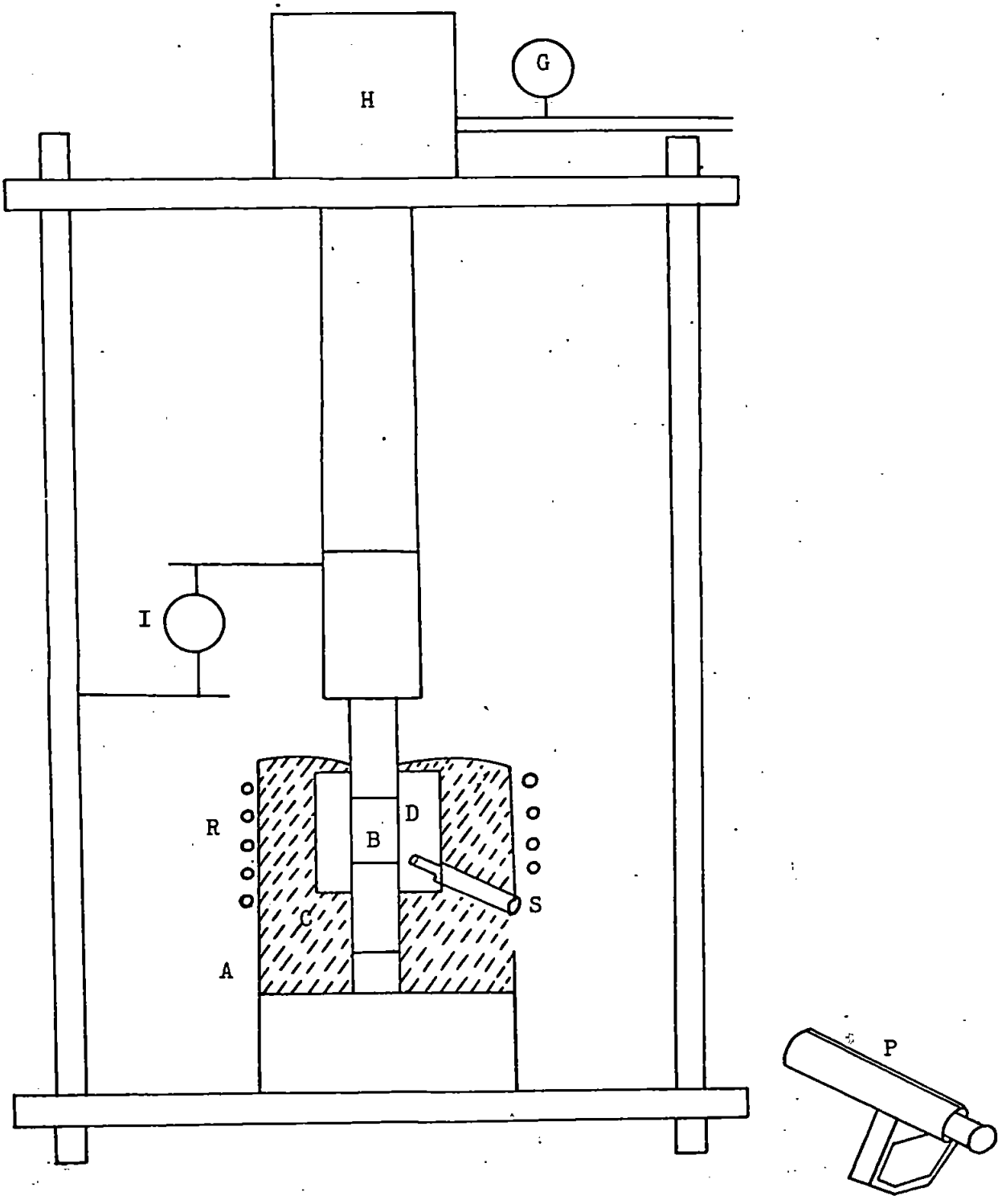

H = Hydraulic ram
G = Pressure gauge
I = Ram-travel indicator
C = Carbon black
B = Boron carbide
R = R.F. coil
A = Asbestos shield
D = Graphitedie
P = Optical pyrometer
S = Sighting tube

temperature and pressure were raised.

3.8 Hardness testing of coatings

3.8.1 Mounting of sample

Hardness tests were performed on the surfaces of metal foils reacted with boron carbide at temperatures 1,000°C - 1,800°C. Some of the specimens were mounted on synthetic resin in the sample mounting machine. The sample was placed at the centre of the bottom of mould and covered with approximately 30 cm^3 of Bakelite. Heating was switched on to cure the Bakelite and pressure was exerted on it slowly and steadily up to 1.37×10^6 Nm^{-2} until it retained shape for a few minutes. The pressure was then raised to 2.75×10^6 Nm^{-2} and kept constant for five minutes. The heater was switched off, the sample cooled by a flow of water for five minutes and then taken out of the mould.

Alternatively some samples were mounted on cold setting resin. Cold setting resin, 'metset resin 'SW'' (Metallurgical Services Ltd.) was mixed with 'metset hardner' in the ratio of 1 drop of hardner to 5 cm^3 of resin in a plastic container and stirred to ensure homogeneity. The samples were placed at the centre of the moulds and filled with this setting mixture. They were left overnight for setting on an even surface and taken out from the moulds the following morning.

3.8.2 Polishing

Mounted specimens were polished by grinding on different grades of silicon carbide paper, fixed on smooth downward slanting glass plates. A continuous flow of water was spread evenly on the paper to ensure wetting during the grinding. Samples were ground on varying grades of rough and smooth papers in the order "Roughes minor" No. 220, No. 320, No. 400 and finally No. 600 (Strues Scientific Instruments).

Alternatively some specimens were polished on an automatic or a hand polishing machine. The specimens, after polishing, were washed,

dried and tested on a Hardness Tester.

3.8.3 Projection microscope and microhardness testing equipment

Detailed description of the equipment is given by Troughton & Simms (1956). A brief account of its important features is given below.

The assembly consists of a projection microscope and is designed for microscopic examinations and photography of:

1. Opaque objects using (a) normal incident illumination with a plain glass reflector; (b) incident illumination with a metallic reflection; (c) dark field illumination; (d) polarized light; (e) phase-contrast; and (f) normal incident and oblique illumination.
2. Translucent objects using (a) transmitted light; (b) polarized light; (c) phase-contrast; and (d) transmitted light

Other facilities include Micro Hardness Tester, equipment for surface topography and ultra-violet light. Present work involves study of opaque surfaces and their hardness values. A brief description of Micro Hardness Tester is given below.

3.8.3.1 Micro Hardness Tester

A Vickers pyramid diamond whose faces have been worked to an angle of 136° is embedded in the outer optical surface of the microscope objective, thus the area to be tested could be selected and the indent made and evaluated without the interchange and exact registration of indenter and objective. The load may vary from 0.1 to 500 g depending on the specimen hardness. A load of 20 g was used throughout the present work. The specimen was secured to one end of an accurately balanced lever and weight was applied to platform above the specimen. The combined objective and diamond indenter were advanced towards the speci-

men by means of the slow motion focussing adjustment of the microscope and contact was indicated by the signal lamp. The measurement of the impression was made with the aid of the Filar Eyepiece. Microhardness was read directly from standard tables.

3.9 Computer programming

Computer programs were written for various calculations carried out in the course of this work. One of these has been discussed already in connection with X-ray line broadening (Section 3.1.4 and Appendix II).

Thermodynamic parameters, i.e. free energy change, heat of reaction and equilibrium constants for various methods of production of borides have been computed from the equations given by Schick (1965). Thermodynamic functions for reactions where the constants are not known, have been calculated from table values. A program for computing free energy change, heat of reaction and equilibrium constant at various temperatures is given in Appendix II, together with specimen output for the reaction:

$$TiO_2 + 2B + 2C = TiB_2 + 2CO$$

The computed values have been plotted as Ellingham diagrams using a graph plotter and a modified version of an existing program. This modified program is given in the Appendix.

Fractional volume changes (Chapters 4, 5 and 6) for conversion of metal to boride (and carbide) and then to oxide have been computed for all known borides and carbides. The program is given in Appendix IV, together with an output sample.

Complete outputs and programs written for calculations during this work are available in a separate folder from Plymouth Polytechnic Library.

PART II

T H E S I S

Chapter 4	Reactivity and sintering of boron carbide with metal powder additives
Chapter 5	Effect of additives on the hot pressing of boron carbide
Chapter 6	The formation and microstructure of boride and carbide coatings on metal surfaces
Chapter 7	Oxidation of boron carbide
Chapter 8	Concluding summary

CHAPTER IV

REACTIVITY AND SINTERING OF BORON CARBIDE WITH METAL POWDER ADDITIVES

4.1 Introduction

Previous researchers (Jones, 1970) have described the production of boron carbide and showed how the sintering was accelerated by chromium metal powder additive (Glasson & Jones, 1969). The sintering was accelerated markedly only at higher temperature, ca. 1800°C. The metal completely wetted the boron carbide surface (Hamijan & Lidman, 1952). Some graphitisation of carbon was noted at this temperature; this could have left some boron in solid solution with the remaining boron carbide or chromium, but no zone of interaction producing crystalline chromium boride or carbide was found. This behaviour of chromium contrasts with that of iron which forms zones of interaction when it accelerates the sintering of boron carbide. Other transition metals, e.g. Co and Ni, give similar zones, apparently consisting of boride and carbide alloys of the corresponding metals.

In the present research the effects of iron and several other metal powders on the sintering of the boron carbide are examined and compared with one another. Possible compound formation during the sintering processes is investigated at a series of temperatures between 1000° and 1800°C.

4.2 Experimental

4.2.1 Materials

The boron carbide used had a specific surface of 20.6 $m^2 g^{-1}$ corresponding to an average crystallite size (equivalent spherical

diameter) of 0.106 μ m. Portions of the material were mixed with known amounts of powdered metal additives of size generally 1 μ m; occasionally metal hydride powders, e.g. titanium and zirconium, were used as additives.

4.2.2 Procedure

The samples were calcined for fixed times usually 5 hours in vacuo at 1000°C and argon at 1000°, 1200°, 1400°, 1600° and 1800°C. The specific surfaces of the cooled samples were determined by the B.E.T. method (Brunauer, Emmett & Teller, 1938) from nitrogen sorption isotherms recorded at -183°C on an electrical sorption balance (Glasson, 1956 and 1964).

The amounts of metal additive were normally 1% and 10% by weight of boron carbide. Although these amounts often accelerated sintering considerably, they were insufficient to give complete X-ray patterns of any metal borides or carbides formed. Thus, it was necessary to compare separately heated mixtures, containing larger amounts of metal additive, generally in stoichiometric amounts required for complete metal boride and/or metal carbide formation. These experiments were carried out and the results are discussed below.

4.2.3 Results

The variations in specific surfaces of the sintered boron carbide samples are shown in Figs. 4.1 - 4.9, where they are compared with the average crystallite sizes (equivalent spherical diamters) calculated from the specific surfaces and the X-ray densities of the products. Tables 4.1 - 4.9 show the main metal boride and carbide phases formed at different temperatures.

Decreases in the number of crystallites during the 5 hour sinterings

of boron carbide with different metal additives at 1800°C in argon are compared in Table 4.10. The multiple changes are calculated from the ratio $(S_1/S)^3$ where S_1 = specific surface of the initial boron carbide (or from the average crystallite size ratio), with allowances being made for up to 10% of metal of comparatively low specific surface and number of crystallites being present initially and for change in density during any chemical reaction between metal and boron carbide.

Further information on the microstructure of the sintered samples is provided by electron-micrographs (Plates 3.1 - 3.22) which show the merging and rounding of the aggregates of crystallites as sintering proceeds at various temperatures (5 hour calcinations) in the presence of different metals. This is discussed in Section 4.4.

4.3 Discussion

As demonstrated earlier (Glasson & Jones, 1970; Jones, 1970), sintering of the boron carbide is enhanced by high temperatures and times of heating. Metal additives are expected to accelerate the sintering generally, by analogy with the previous findings for chromium. The effect of each additive will depend on its ability to form solid solutions or compounds with the boron carbide. The consequent changes in surface properties affect sintering by surface diffusion or crystal lattice diffusion according to temperature conditions.

4.3.1 Iron additive

The extent to which iron additives (1% or 10%) accelerate sintering of boron carbide at different temperatures is illustrated in Fig. 4.1. For more complete comparison, the broken-lined curve in Fig. 4.1a represents the corresponding surface areas for 1g boron carbide samples containing the 10% metal additive of negligible surface area (less than

TABLE 4.10

MULTIPLE CHANGES IN THE NUMBER OF CRYSTALLITES DURING 5 HR. SINTERINGS OF BORON CARBIDE WITH METAL ADDITIVES AT 1,800°C IN ARGON

Additive	Fractional change in total no. of Crystallites (10^{-2})			No. of initial Boron Carbide Crystallites per Crystallite of sintered products		
	0%	1%	10%	0%	1%	10%
Fe	9.2	0.38	0.039	10.9	263	2,550
Ti	9.2	6.0	4.5	10.9	16.7	22.2
Zr	9.2	4.2	2.6	10.9	23.8	38.1
V	9.2	6.3	4.8	10.9	15.9	20.9
Nb	9.2	9.0	7.7	10.9	11.1	12.9
Ta	9.2	6.6	3.6	10.9	15.2	28.0
Mo	9.2	7.0	5.8	10.9	14.3	17.3
W	9.2	9.7	5.8	10.9	10.3	17.3
Al	9.2	8.6	7.6	10.9	11.6	13.2

Fig. 4.1 Sintering of boron carbide with iron additive (5 h. calcination)

Key: (a) and (c) □ Boron carbide only ○ 1% metal additive △ 10% metal additive

Key: (b) and (d) □ 1 000°C ○ 1 200°C △ 1 400°C ▽ 1 600°C ◇ 1 800°C

0.1 m^2), i.e. the specific surfaces that the sample would have had if the iron had not reacted with the boron carbide or accelerated (or retarded) sintering. The position of this broken-lined curve at 1000°C (point A) coincides with that found experimentally, showing that 10% iron has little or no effect on the sintering of boron carbide at this temperature, but considerably accelerates sintering at higher temperatures. This is illustrated also by the curves in Fig. 4.1, which further shows that the effect of the iron usually diminishes considerably after the first 1% has been added.

The iron has correspondingly less effect on the sintering at 1600°C than it has at 1400°C, cf. Fig.4.1a, BC and B'C'. This is ascribed to some activation when the iron reacts more extensively with the boron carbide at 1600°C. Thus, there is more activation with 10% Fe than there is with 1% Fe additive (specific surface changes between 1400° and 1600°C are from 4.9 to 7.2 (BC) and 8.0 to 8.6 $m^2 g^{-1}$ (B'C') respectively).

The above findings are in accord with phase composition identification by X-ray analysis of the sintered mixtures and separate mixtures containing large amounts of stoichiometric metal additives for metal boride and/or carbide formation at similar temperatures. As shown in Table 4.1, there was little or no reaction at 1000°C and only small amounts of iron boride FeB were formed at 1200°C. Most of the 10% iron additive was converted to FeB in 5 hours at 1400°C and larger amounts of iron, viz. 4Fe and 11Fe per B_4C, gave FeB and also some Fe_3C where sufficient iron was present. Formation of both borides FeB and Fe_2B and carbide Fe_3C were much more extensive at 1600°C, while at 1800°C the products were entirely Fe_2B and Fe_3C indicating complete

TABLE 4.1

COMPOSITION OF THE SYSTEM B_4C - Fe AT DIFFERENT CALCINATION TEMPERATURES

Temperature °C	Additive	Products
1 000	10% Fe	No appreciable reaction
	4Fe/B_4C	Small amounts of FeB
1 200	10% Fe	No appreciable reaction
	4Fe/B_4C	Traces of FeB
	11Fe/B_4C	Traces of FeB
1 400	10% Fe	FeB, B_4C
	4Fe/B_4C	FeB, Fe, B_4C
	11Fe/B_4C	Fe_3C, Fe
1 600	10% Fe	FeB, B_4C
	4Fe/B_4C	FeB, Fe_2B, Fe_3C
	11Fe/B_4C	Fe_3C
1 800	10% Fe	Fe_2B, Fe_3C, phase X with peaks d_1 = 2.48, d_2 = 2.71 A.
	11Fe/B_4C	Fe_2B, Fe_3C

reaction:

$$B_4C + 11Fe \longrightarrow 4Fe_2B + Fe_3C$$

The activation opposing the sintering at 1600°C, therefore occurs when the temperature is high enough for both boride and carbide formation to be extensive. This causes maximum changes in molecular volume of the crystal lattice of reactants and products, leading to more extensive strain and crystallite splitting, as often encountered in solid-state thermal reactions. The products are more extensively sintered at higher temperatures (1800°C) , assisted particularly by the comparatively low-melting Fe_2B (m.p. 1390°C), cf. Fig.4.1, CD and C'D'.

4.3.2 Titanium and Zirconium additives

The sintering of boron carbide is accelerated by titanium and zirconium additives at all temperatures between 1000° and 1800°C as shown in Figs.4.2 and 4.3, as found for iron, the effects of the additives diminish considerably after the first 1% present. The surface areas with the 10% additives at 1200°C are slightly higher than expected; this is ascribed to activation caused by crystallite splitting when all of the additive is completely converted to TiB_2 or ZrB_2, compared with only partial conversion within 5 hours at 1000°C. This formation of TiB_2 is analogous to its production by the reaction:

$$B_4C + 2TiC = 2TiB_2 + 3C$$

also occuring extensively at 1,200°C (Nelson, Willmore & Womeldorph, 1951). There may be some carbon formed in the reactions:

$$2Ti + B_4C = TiB_2 + C \text{ and } 2Zr + B_4C = 2ZrB_2 + C,$$

and released form solid solution in the boride-carbide matrix, contributing to the higher surface area. The carbon forms TiC when larger amounts of titanium and zirconium are present in stoichiometric ratios of $2Ti/B_4C$ or $3Ti/B_4C$, cf. Tables 4.2 and 4.3.

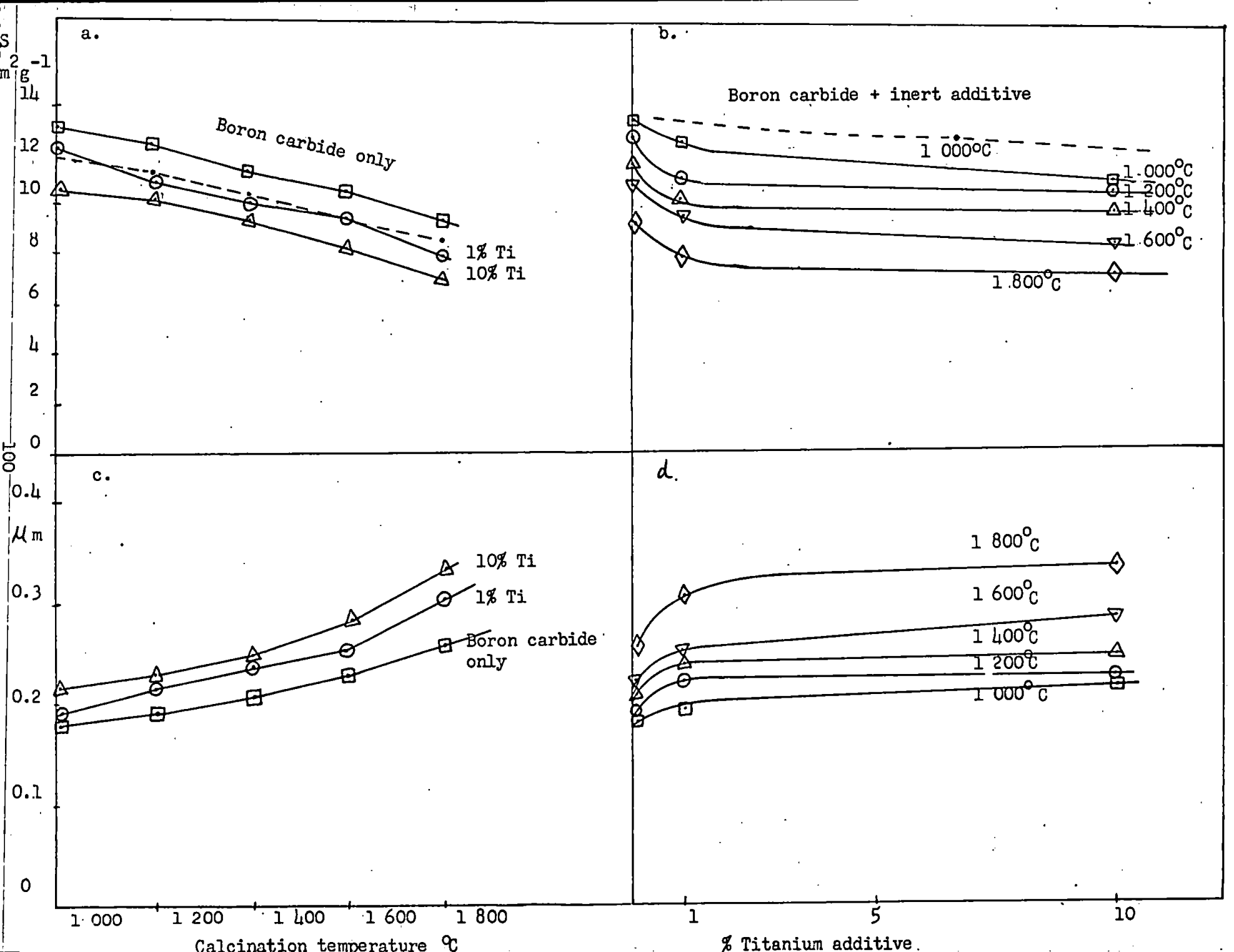

Fig. 4.2 SINTERING OF BORON CARBIDE WITH TITANIUM ADDITIVE (5 h. CALCINATION)

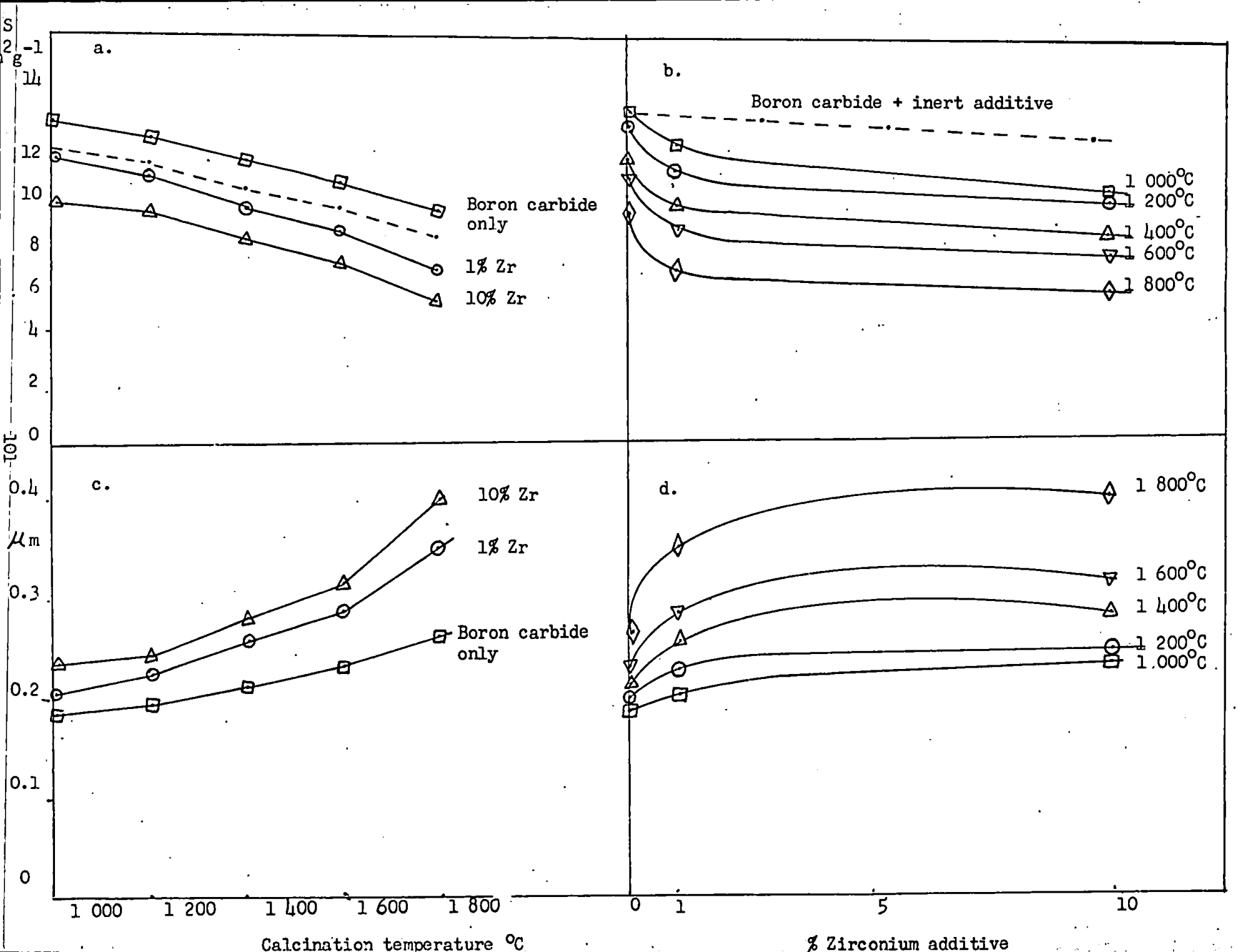

Fig. 4.3 SINTERING OF BORON CARBIDE WITH ZIRCONIUM ADDITIVE (5 h. CALCINATION)

TABLE 4.2

COMPOSITION OF THE SYSTEM B_4C - Ti
AT DIFFERENT CALCINATION TEMPERATURES

Temperature °C	Additive	Product
1 000	10% TiH_2	TiB_2, B_4C
	$2TiH_2/B_4C$	TiB_2, TiC
	$3TiH_2/B_4C$	TiB_2, TiC
1 200	10% TiH_2	TiB_2, B_4C
	$2TiH_2/B_4C$	TiB_2, TiB, TiC
	$3TiH_2/B_4C$	TiB_2, TiB, TiC
1 400	10% TiH_2	TiB_2, B_4C
	$2TiH_2/B_4C$	TiB_2, TiC
	$3TiH_2/B_4C$	TiB_2, TiC
1 600	10% TiH_2	TiB_2, B_4C
	$2TiH_2/B_4C$	TiB_2, TiC
	$3TiH_2/B_4C$	TiB_2, TiC
1 800	10% TiH_2	TiB_2, B_4C
	$2TiH_2/B_4C$	TiB_2, TiC
	$3TiH_2/B_4C$	TiB_2, TiC

TABLE 4.3

COMPOSITION OF THE SYSTEM B_4C - Zr

AT DIFFERENT CALCINATION TEMPERATURES

Temperature °C	Additive	Product
1 000	10% ZrH_2	ZrB_2, B_4C
	$2ZrH_2/B_4C$	ZrB_2, ZrC
	$3ZrH_2/B_4C$	ZrB_2, ZrC
1 200	10% ZrH_2	ZrB_2, B_4C
	$2ZrH_2/B_4C$	ZrB_2, ZrC
	$3ZrH_2/B_4C$	ZrB_2, ZrC
1 400	10% ZrH_2	ZrB_2, B_4C
	$2ZrH_2/B_4C$	ZrB_2, ZrC
	$3ZrH_2/B_4C$	ZrB_2, ZrC
1 600	10% ZrH_2	ZrB_2, B_4C
	$2ZrH_2/B_4C$	ZrB_2, ZrC
	$3ZrH_2/B_4C$	ZrB_2, ZrC
1 800	10% ZrH_2	ZrB_2, B_4C
	$2ZrH_2/B_4C$	ZrB_2, ZrC
	$3ZrH_2/B_4C$	ZrB_2, ZrC

Titanium and zirconium additives are correspondingly less effective than iron additive in promoting sintering of boron carbide mainly because of the higher melting points of TiB_2 (2980°C) and ZrB_2 (3040°C) compared with Fe_2B (1390°C) and FeB(1540°C). Hence, although titanium and zirconium borides can promote sintering by surface diffusion above about 900°C (corresponding to about $\frac{1}{3}$ m.p. in K), they can supplement this by crystal lattice diffusion only above about 1400°C (corresponding to about $\frac{1}{2}$ m.p. in K, i.e. the Tammann temperature) (Glasson, 1967). The carbides formed at the higher temperatures, viz. above 1600°C, behave similarly (m.p. TiC 3150°C, ZrC 3530°C, Fe_3C 1650°C), so that titanium and zirconium carbides can promote sintering by crystal lattice diffusion only above about 1450°C and 1650°C.

4.3.3 Vanadium, niobium and tantalum additives

All of these additives enhance the sintering of boron carbide to varying extents dependent on the melting points of the metal borides and carbides formed and the extent to which the surface activation accompanying the metal boride and carbide formation offsets the loss of surface caused by sintering, cf. Figs.4.4, 4.5 and 4.6. The vanadium additives are the most effective for enhancing sintering especially at 1400°C. Up to this temperature, the vanadium shows a greater tendency to form borides VB_2 (and V_3B_4 when more vanadium is present) than to form its carbide VC, cf. Table 4.4. At higher temperatures, larger amounts of carbide are formed which may account for surface activation at 1600°C. Niobium and tantalum additives are comparatively less effective, but their general behaviour with change of temperature resembles that of vanadium, cf. shapes of curves in Fig. 4.5a and c ; they also tend to form borides rather than carbides at temperatures

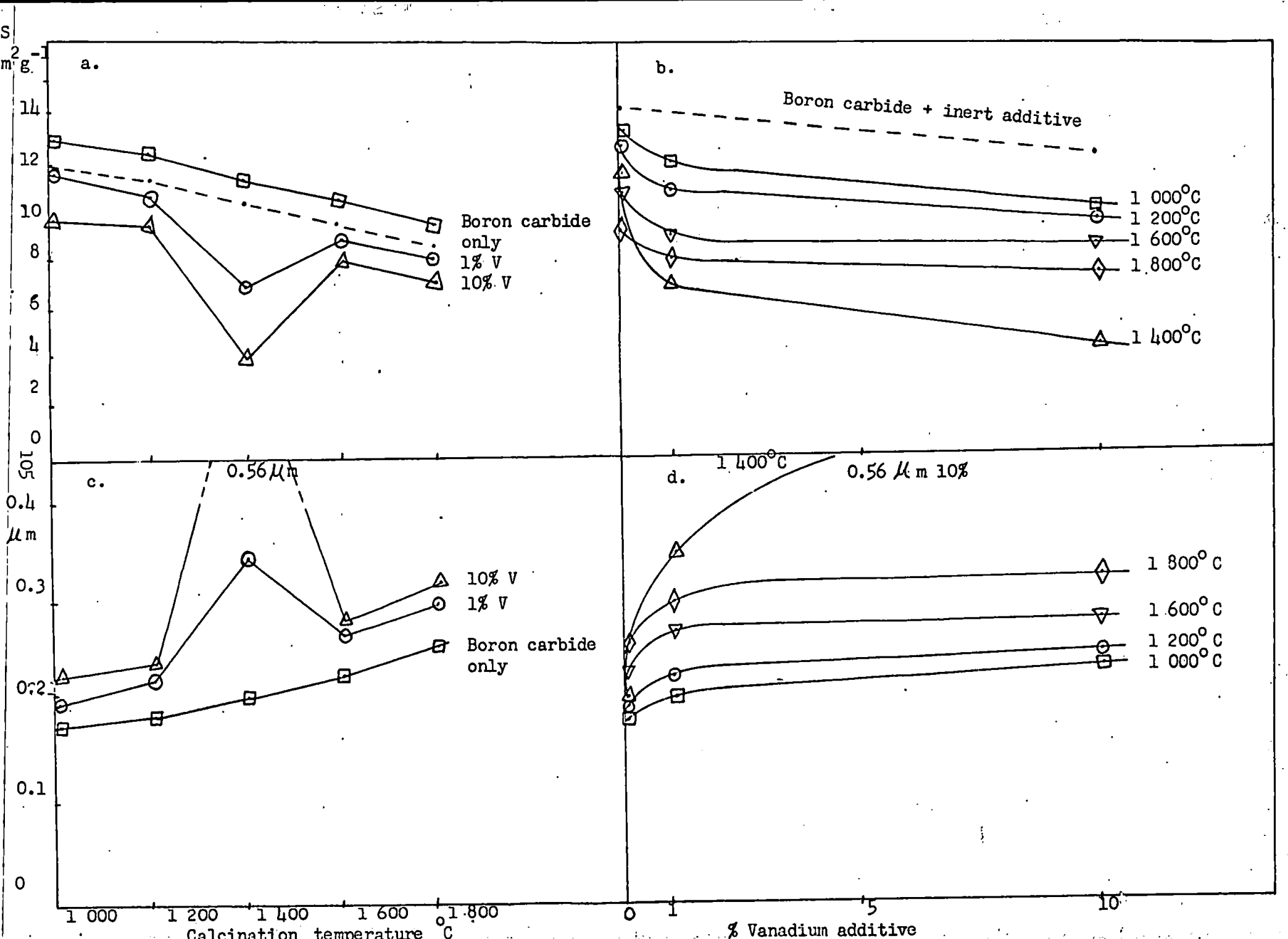

Fig. 4.4 SINTERING OF BORON CARBIDE WITH VANADIUM ADDITIVE (5 h. CALCINATION)

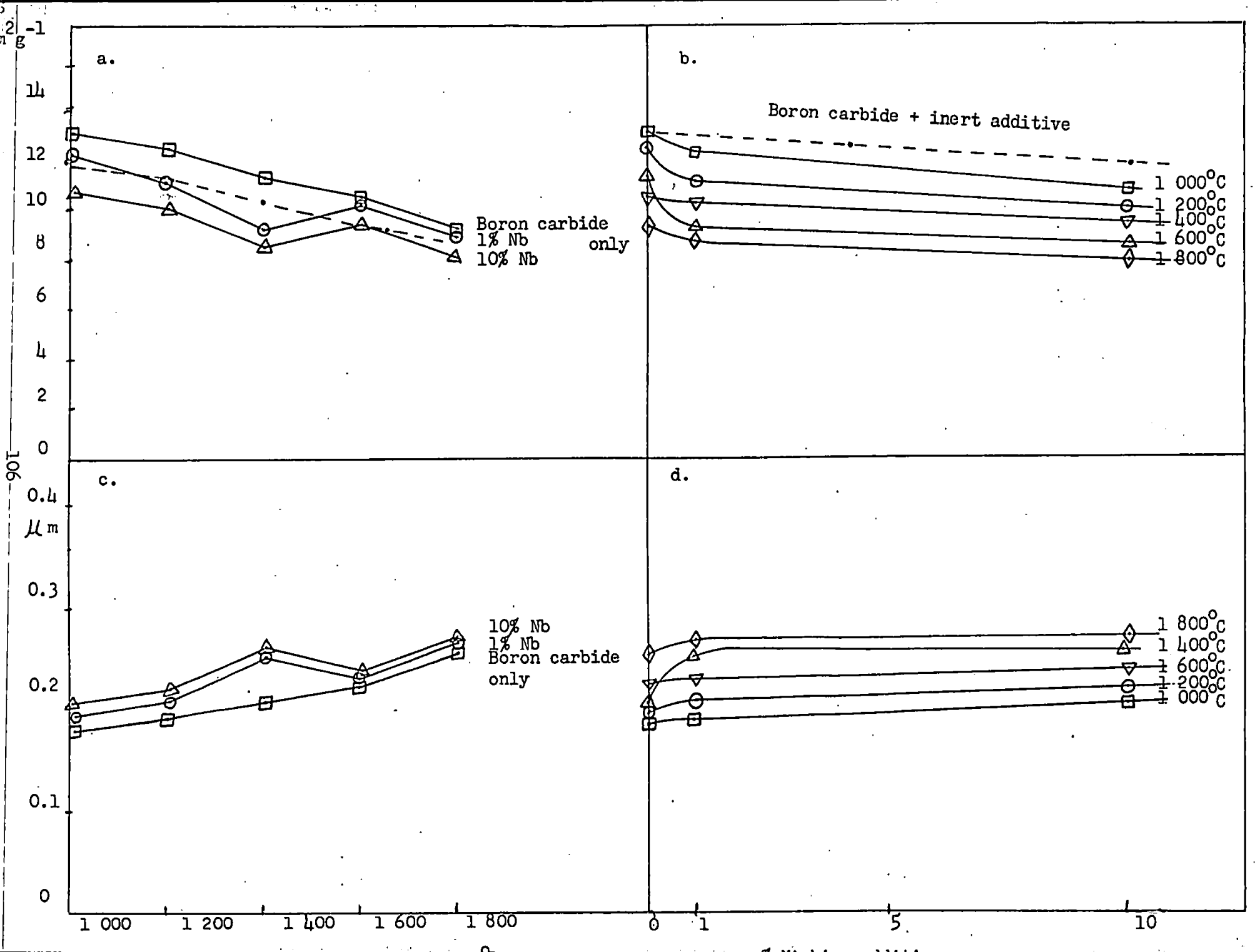

Fig. 4.5 SINTERING OF BORON CARBIDE WITH NIOBIUM ADDITIVE (5 h. CALCINATION)

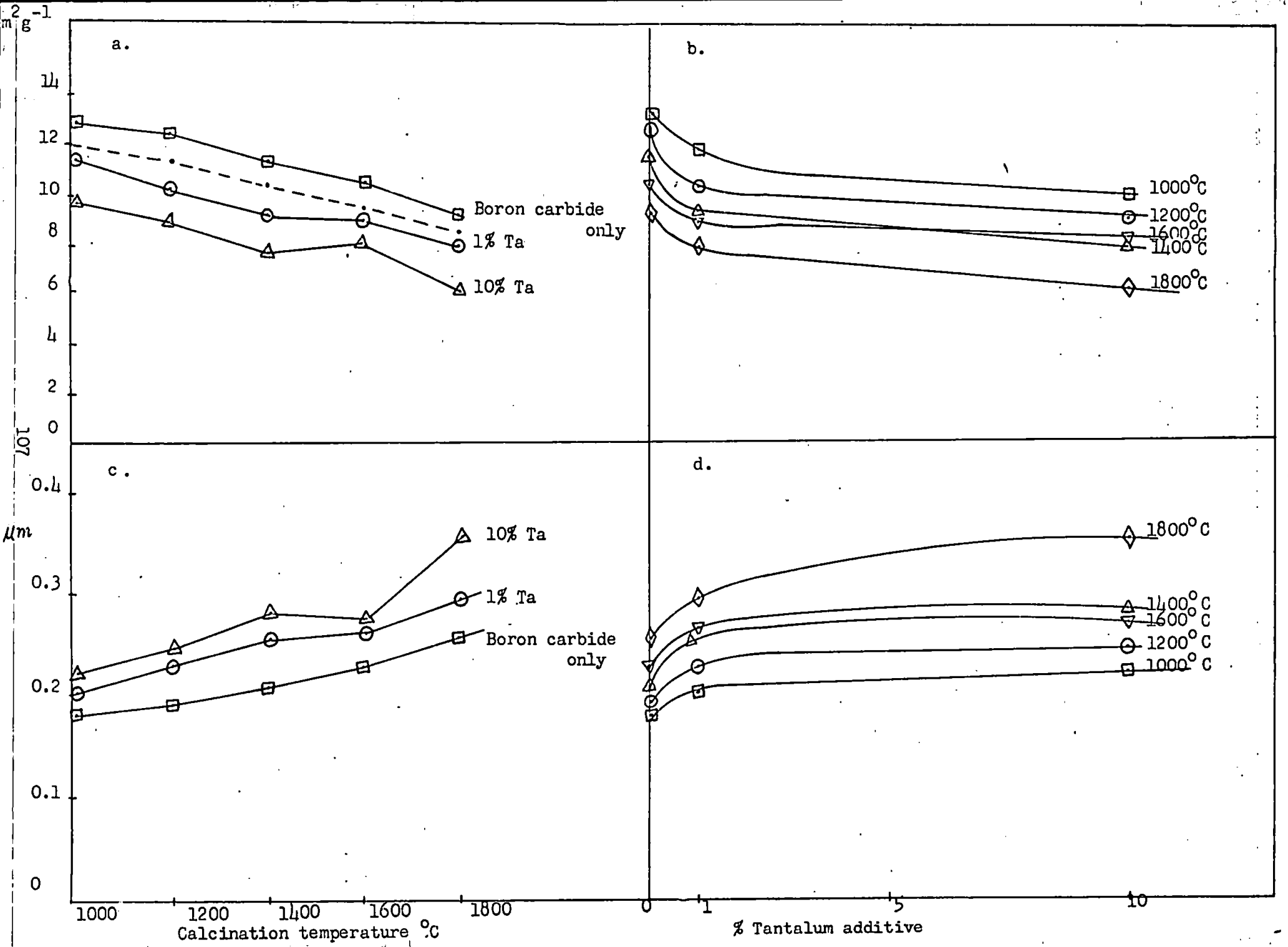

Fig. 4.6 SINTERING OF BORON CARBIDE WITH TANTALUM ADDITIVE (5 h. CALCINATION)

TABLE 4.4

COMPOSITION OF THE SYSTEM B_4C - V

AT DIFFERENT CALCINATION TEMPERATURES

Temperature °C	Additive	Products
1000	10% V	VB_2, B_4C
	2V/B_4C	VB_2, phase X with peaks d_1 = 2.0336, d_2 = 2.06, d_3 = 2.08, d_4 = 2.195, d_5 = 2.386, d_6 = 2.46
1200	10% V	VB_2, B_4C
	2V/B_4C	VB_2, VC
	5V/B_4C	V_3B_4, VC
1400	10% V	VB_2, B_4C
	2V/B_4C	VB_2, V_3B_4, VC
	5V/B_4C	V_3B_4, VC
1600	10% V	VB_2, B_4C
	2V/B_4C	VB_2, V_3B_4, VC
	5V/B_4C	V_3B_4, VC
1800	10% V	VB_2, B_4C
	2V/B_4C	VB_2, VC
	5V/B_4C	V_3B_4, V_3B_2, VC

below 1400°C, cf. Tables 4.5 and 4.6. The above findings are in accordance with the melting points of the vanadium borides, VB_2 and V_3B_4 (2400° and 2350°C) and carbide VC (2810°C) being correspondingly lower than those of the niobium and tantalum borides and carbides, NbB_2 (3000°C), TaB_2 (3100°C), NbC (3480°C), TaC (3880°C). Also, the fractional volume increases when the metals are converted to these borides and carbides are greater for vanadium than for niobium and tantalum: VB_2 (0.713), NbB_2 (0.516), TaB_2 (0.481), VC (0.317).

4.3.4 Molybdenum and tungsten additives

Both metal additives generally promote sintering of boron carbide, the extent depending on the melting points of the metal borides and carbides formed and how far surface activation accompanying the metal boride and carbide formation offsets loss of surface caused by sintering, cf. Figs. 4.7 and 4.8. 10% molybdenum and tungsten additives enhance sintering at 1200°C, 1% Mo is almost as effective. At this temperature, the additives form mainly borides, Mo_2B_5 and W_2B_5; larger amounts of metal, viz. 2Mo or 2W per B_4C or 8Mo and 8W/B_4C, give lower borides, MoB_2, δ- MoB, β- MoB, γ- Mo_2B, WB_2, δ- WB, γ - W_2B with only a trace of a lower molybdenum carbide Mo_2C and no detectable tungsten carbides.

In the sintering experiments the 10% molybdenum additive gives appreciable amounts of MoB_2 as well as Mo_2B_5 at 1600° and 1800°C, which may account for the activation at 1600°C. With larger amounts of metals, the X-ray diffraction traces show that molybdenum and tungsten only begin to form carbides to any appreciable extent at temperatures above 1600°C, cf. Tables 4.7 and 4.8; this accounts for some surface activation of the boron carbide by the tungsten additive even at 1800°C (Fig. 4.8a). The melting points of the borides and carbides are

TABLE 4.5

COMPOSITION OF THE SYSTEM B_4C - Nb

AT DIFFERENT CALCINATION TEMPERATURES

Temperatures ^{o}C	Additive	Product
1000	10% Nb	NbB_2, B_4C
	2Nb/B_4C	NbB_2, NbC
	5Nb/B_4C	NbB_2, NbC
1200	10% Nb	NbB_2, B_4C
	2Nb/B_4C	NbB_2, NbC
1400	10% Nb	NbB_2, B_4C
	2Nb/B_4C	NbB_2, NbC
1600	10% Nb	NbB_2, NbC, B_4C
	2Nb/B_4C	NbB_2, NbC
	5Nb/B_4C	NbB_2, NbC
1800	10% Nb	NbB_2, B_4C
	2Nb/B_4C	NbB_2, NbC
	5Nb/B_4C	NbB_2, NbC

TABLE 4.6

COMPOSITION OF THE SYSTEM B_4C - Ta

AT DIFFERENT CALCINATION TEMPERATURES

Temperature °C	Additive	Products
1000	10% Ta	TaB_2, B_4C
	2Ta/B_4C	TaB_2, TaC
1200	10% Ta	TaB_2, B_4C
	2Ta/B_4C	TaB_2, TaC
	5Ta/B_4C	TaB_2, γ- TaB, TaC
1400	10% Ta	TaB_2, B_4C
	2Ta/B_4C	TaB_2, TaC
	5Ta/B_4C	TaB_2, TaC
1600	10% Ta	TaB_2, TaC, B_4C
	2Ta/B_4C	TaB_2, TaC
	5Ta/B_4C	TaB_2, TaC
1800	10% Ta	TaB_2, B_4C
	10% Ta + Al_2O_3	TaB_2, TaC, $\alpha$and γ- Al_2O_3
	2Ta/B_4C	TaB_2, TaC
	5Ta/B_4C	TaB_2, γ- TaB, TaC

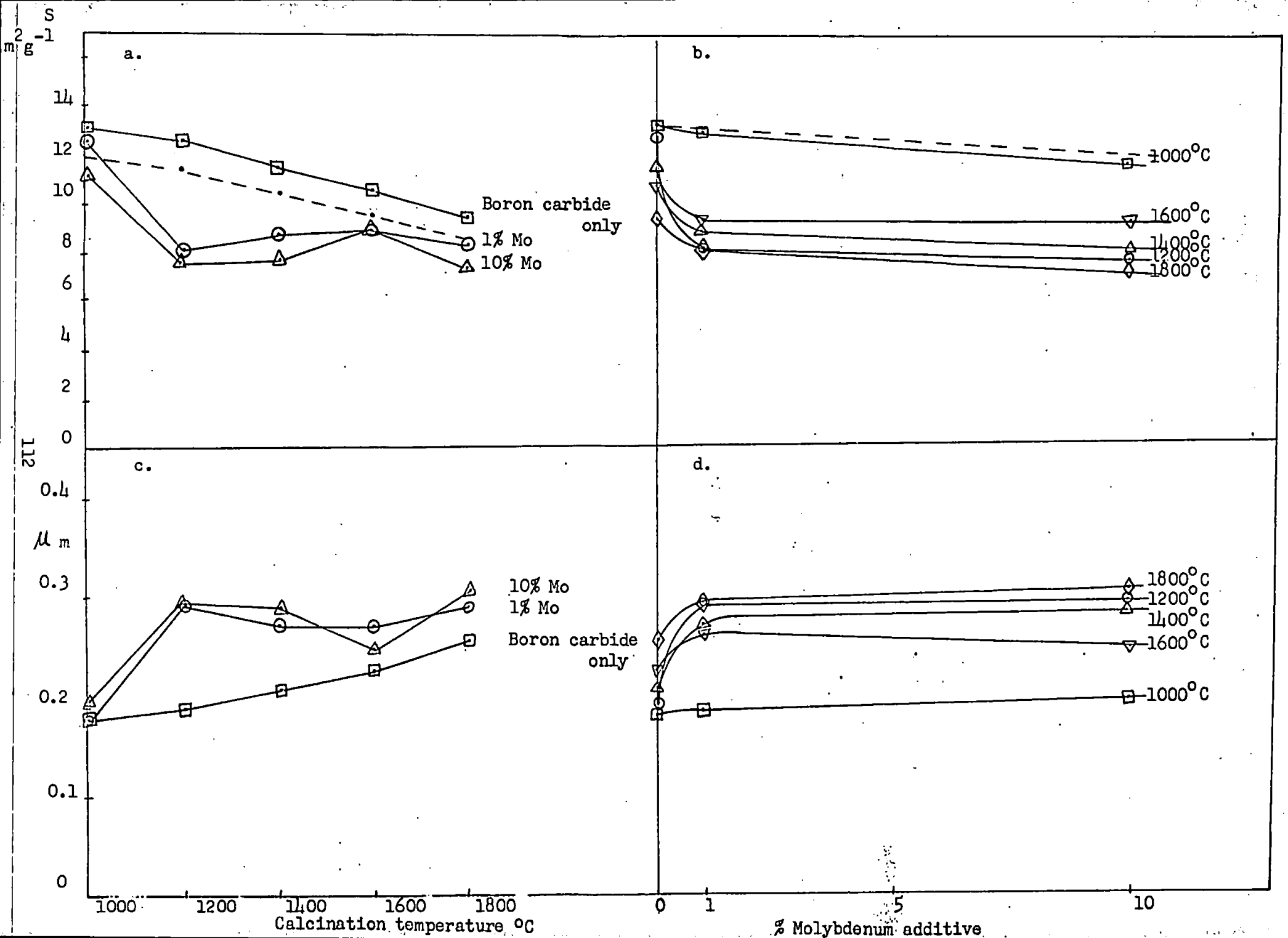

Fig. 4.7 SINTERING OF BORON CARBIDE WITH MOLYBDENUM ADDITIVE (5 h CALCINATION)

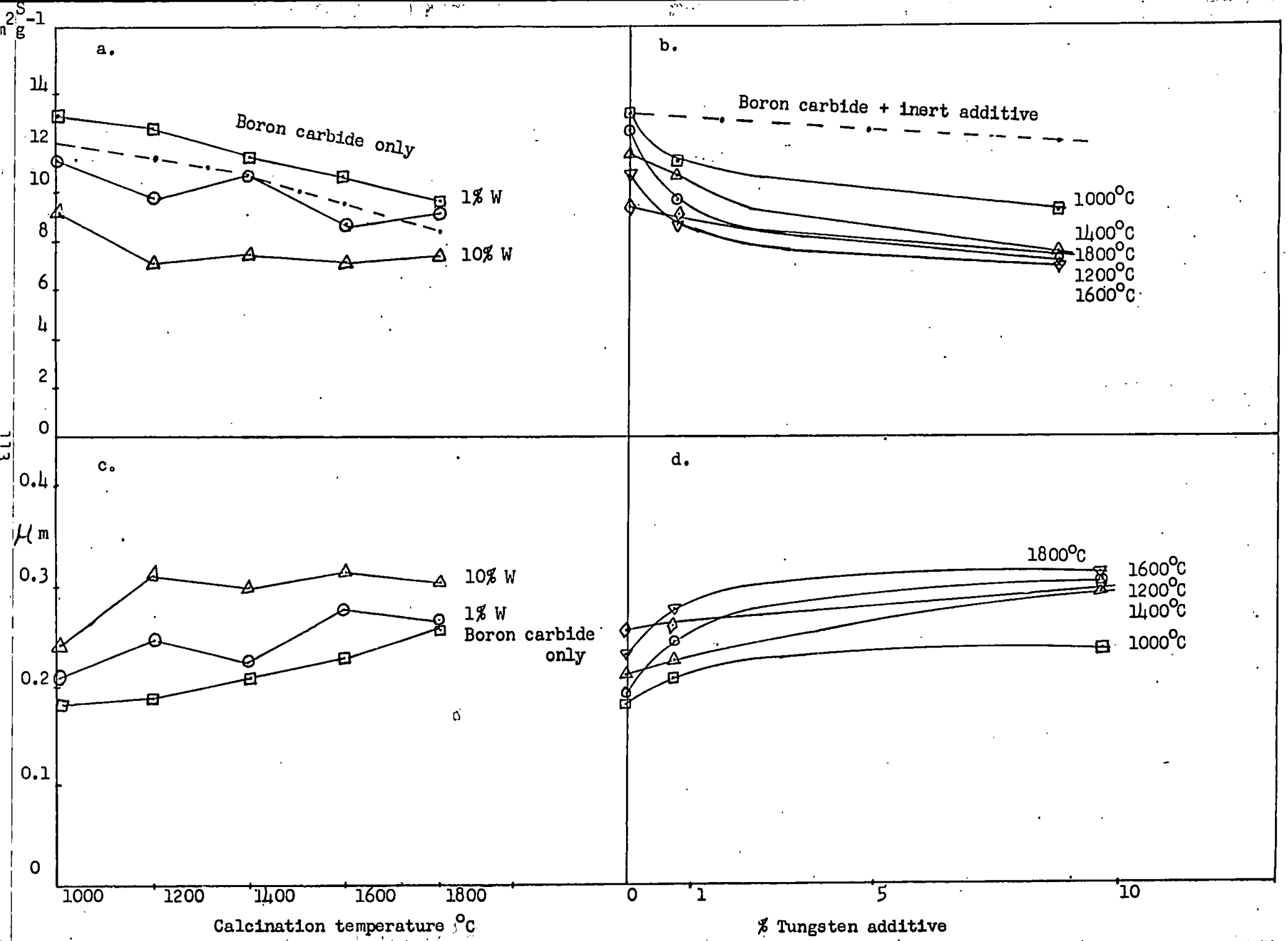

Fig. 4.8 SINTERING OF BORON CARBIDE WITH TUNGSTEN ADDITIVE (5h.CALCINATION)

TABLE 4.7

COMPOSITION OF THE SYSTEM B_4C - Mo

AT DIFFERENT CALCINATION TEMPERATURES

Temperature °C	Additive	Products
1000	10% Mo	Mo_2B_5, B_4C
	$2Mo/B_4C$	δ- MoB, MoB_2, Mo_2B_5
1200	10% Mo	Mo_2B_5, B_4C
	$2Mo/B_4C$	δ- MoB, β- MoB
	$8Mo/B_4C$	γ - Mo_2B, δ- MoB, Mo_2C
1400	10% Mo	Mo_2B_5, B_4C
	$2Mo/B_4C$	δ- MoB, MoB_2
	$8Mo/B_4C$	γ- Mo_2B, δ- MoB, MoC
1600	10% Mo	MoB_2, Mo_2B_5, B_4C
	$2Mo/B_4C$	δ - MoB, β - MoB, MoB_2
	$8Mo/B_4C$	γ - Mo_2B, δ - MoB, Mo_2C
1800	10% Mo	MoB_2, Mo_2B_5, B_4C
	$2Mo/B_4C$	δ- MoB, β - MoB, MoB_2
	$8Mo/B_4C$	δ- MoB, phase X with peaks $d_1 = 2.6$, $d_2 = 2.4856$, $d_3 = 2.36$, $d_4 = 2.1948$, $d_5 = 1.5$, $d_6 = 1.267$, $d_7 = 1.2526$

TABLE 4.8

COMPOSITION OF THE SYSTEM B_4C - W

AT DIFFERENT CALCINATION TEMPERATURES

Temperature °C	Additive	Products
1000	10% W	W_2B_5, B_4C
	2W/B_4C	δ- WB, W_2B_5
1200	10% W	W_2B_5, B_4C
	2W/B_4C	γ- W_2B, δ- WB
	8W/B_4C	γ- W_2B, δ- WB, W
1400	10% W	W_2B_5, B_4C
	2W/B_4C	γ- W_2B, WC
	8W/B_4C	γ- W_2B, δ- WB, W
1600	10% W	W_2B_5, B_4C
	2W/B_4C	δ- WB, W_2B_5
	8W/B_4C	γ- W_2B, W_2C, WC, W
1800	10% W	W_2B_5, B_4C
	2W/B_4C	δ - WB, W_2B_5
	8W/B_4C	γ - W_2B, W_2C, WC

generally lower than those of the niobium and tantalum compounds and more comparable with those of the vanadium compounds, viz. Mo_2B_5 2100°C, MoB_2 2100°C, δ- MoB 2350°C, Mo_2C 2410°C, MoC 2700°C, W_2B_5 2300°C, δ- WB 2400°C, γ- W_2B 2770°C, WC 2720°C. Thus, the borides (except γ - W_2B) can enhance sintering by both surface and crystal lattice diffusion over the whole temperature range studied (1000° - 1800°C); the formation of carbides is confined to temperatures above about 1200°C for crystal lattice diffusion.

4.3.5 Aluminium additive

The effect of aluminium additive (10%) on the sintering of boron carbide in argon at different temperatures is shown in Fig. 4.9a and c. For more complete comparison, the broken-lined curve in Fig. 4.9a represents the specific surfaces if the aluminium had not reacted with the boron carbide or accelerated (or retarded) sintering. The position of this curve indicates that the aluminium has little or no effect on the sintering of the boron carbide at 1000°C. This is confirmed by similar experiments in vacuo where the specific surfaces of the boron carbide sintered for 5 hours alone or with 1% or 10% Al are 12.4, 12.3 and 11.1 m^2g^{-1} respectively: Increasing the amount of additive has little effect on the sintering, cf. values for 1% and 10% Al.

The aluminium considerably accelerates sintering at 1,200°C (Fig. 4.9a and c), even smaller amounts (1%) being quite effective, cf. curves in Fig. 4.9b and d. It has much less effect on the sintering at higher temperatures (1400°C and 1600°C) where there is considerable activation. At these temperatures the aluminium combines with the boron carbide in contrast to temperatures below 1400°C where the wetting of the boron carbide surface by the molten aluminium is difficult and incomplete. The cooled samples now contain no free

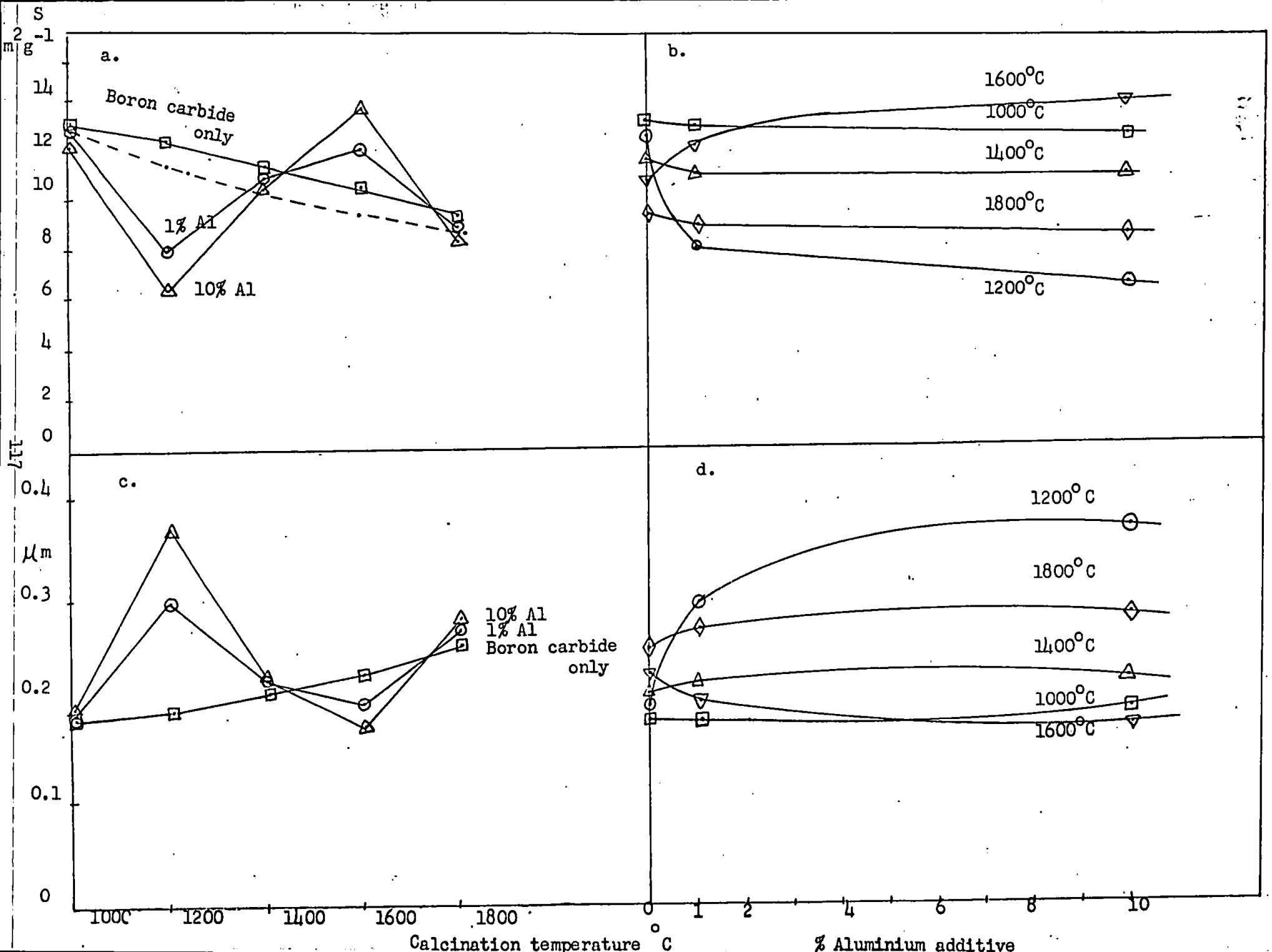

Fig. 4.9 SINTERING OF BORON CARBIDE WITH ALUMINIUM ADDITIVE (5 hr CALCINATION)

globules of solidified aluminium as were found in the samples calcined at 1000°C and 1200°C. This behaviour is in accord with X-ray analysis, no aluminium borides or carbide being found in samples calcined at 1000°C and 1200°C even where there is 2Al per B_4C present. However, there is likely to be some solid solution of Al in B_4C at 1200°C to accelerate sintering, and this is probable at 1400°C where the X-ray traces do not show any crystalline AlB_2, but give somewhat broadened B_4C peaks. These correspond to an average crystallite size of 860 Å compared with 2000 Å estimated from the surface areas. The calculation from surface areas assumes no particular crystallite size distribution but that from X-ray measurements assumes a Gaussian distribution. The direction of the discrepancy indicates that much of the material has a smaller range of crystallite sizes and/or that the aluminium imposes a strain on the boron crystal lattice. The aluminium boride evidently crystallises and splits off at higher temperatures, causing further increases in specific surface as found for the samples calcined at 1600°C, in which AlB_2 has been identified by X-ray analysis, cf. Table 4.9. Some of the carbon formed in the reaction:

$$2Al + B_4C = AlB_2 + C$$

may be released as well from solid solution in the boron carbide matrix (as found in the oxidation of boron carbide (Chapter 7)) and contribute to the increase in specific surface. The products are more extensively sintered at the higher temperature of 1800°C.

4.4 Electron microscopy data

The products of the reactions described above have been examined by electron microscopy, and the data are discussed below.

4.4.1 Iron additive

Comparison with the orginal boron carbide (Plate 4.1) shows that

TABLE 4.9

COMPOSITION OF THE SYSTEM B_4C - Al

AT DIFFERENT CALCINATION TEMPERATURES

Temperature °C	Additive	Products
1000	10% Al	Al, B_4C
	5Al/3B_4C	Al, B_4C
	2Al/B_4C	Al, B_4C
1200	10% Al	Al, B_4C
	5Al/3B_4C	Al, B_4C
	2Al/B_4C	Al, B_4C
1400	10% Al	Al, B_4C
	5Al/3B_4C	Al, B_4C
	2Al/B_4C	Al, B_4C
1600	10% Al	Al, B_4C
	2Al/B_4C	AlB_2, Al, B_4C, phase X with peaks d_3 = 2.496 Å.
1800	10% Al	AlB_2, Al, B_4C
	10% Al + 5% stearic acid	Al, B_4C, phase X with peaks d_1 = 2.93, d_2 = 2.72, d_3 = 2.65, d_4 = 2.52
	2Al/B_4C	(AlN), Al_2O_3, AlB_2, B_4C

Plate 4.1

(a)

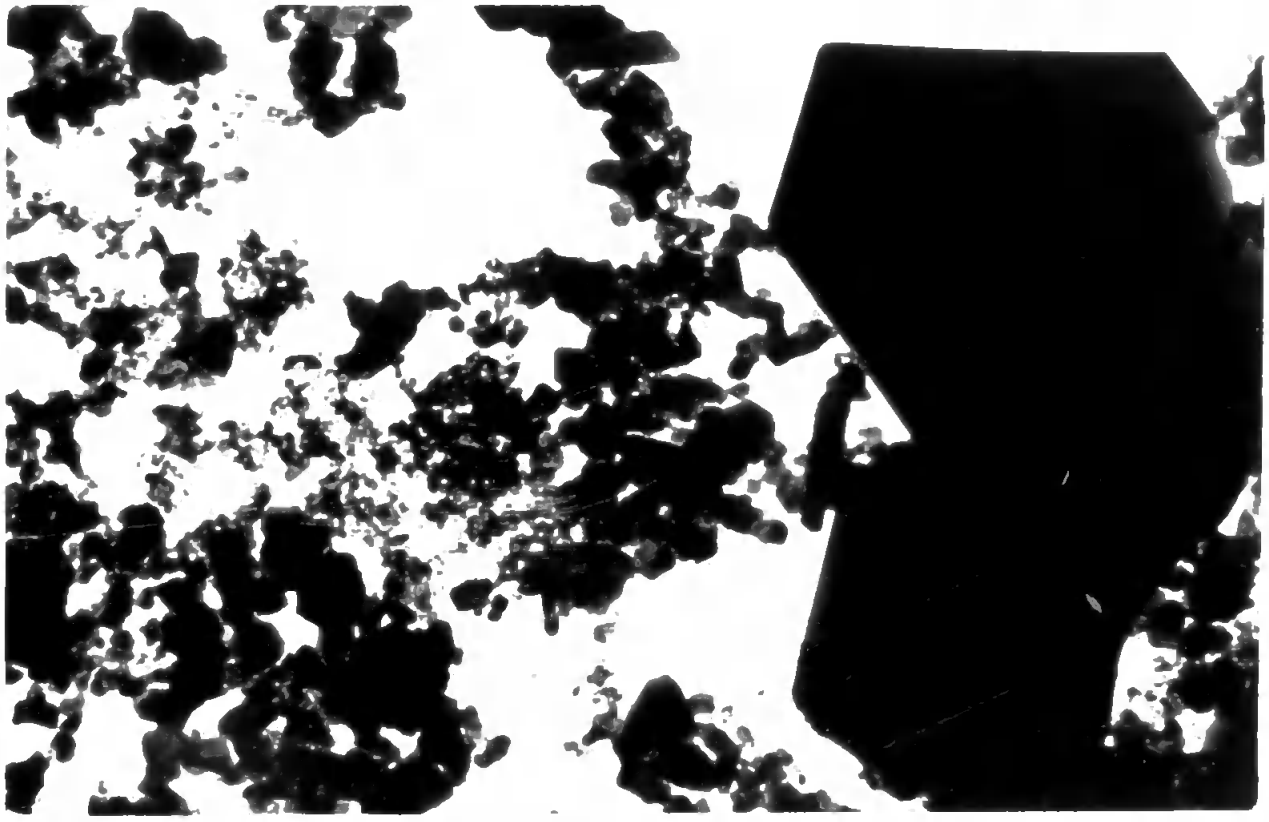

Original boron carbide

Magnification: 12000 X

(b)

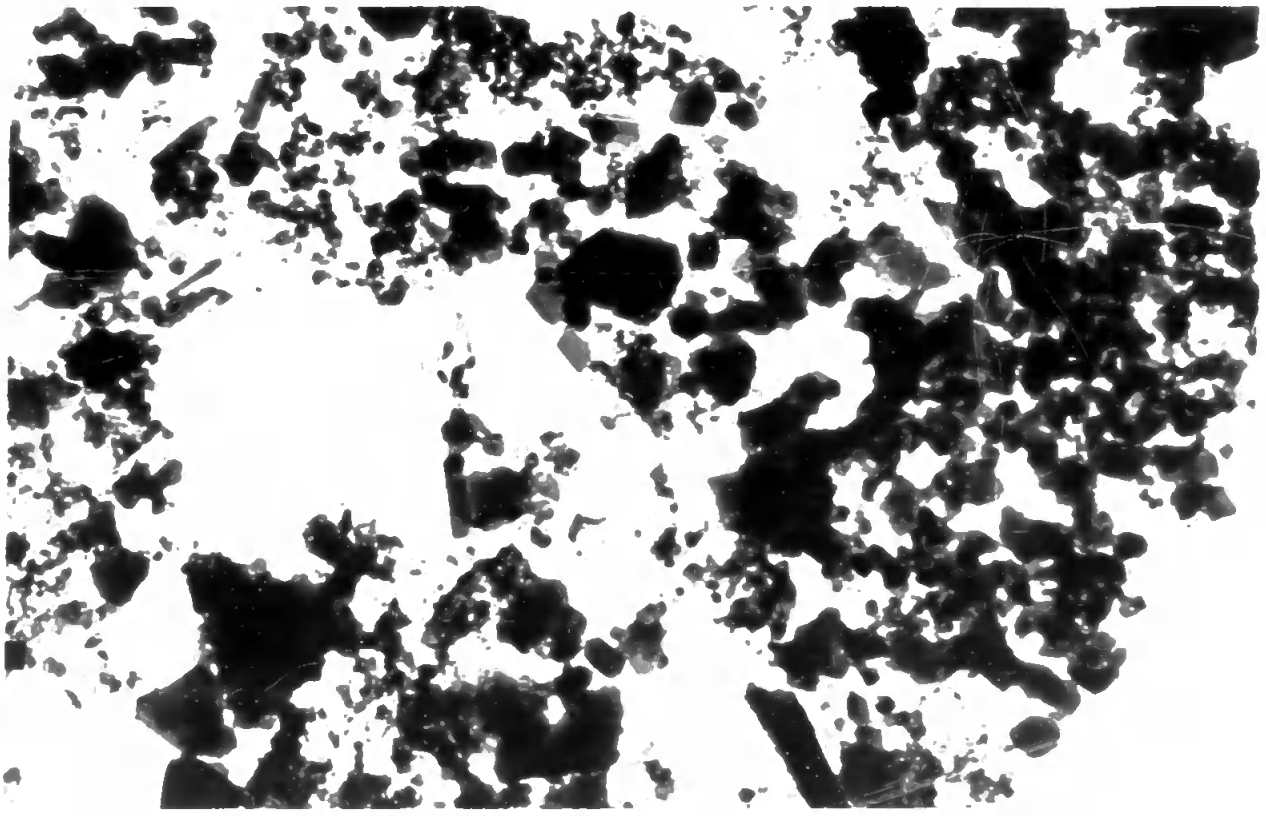

Original boron carbide

at 1400°C (Plate 4.2(a)), the aggregates are becoming larger by coalescing, assisted by the iron boride Fe_2B near its melting point, while the crystallites within the aggregates are merging with loss of surface. There are still some crystals with well defined faces remaining at 1600°C (Plate 4.2(b)). Further sintering occurs with some rounding of aggregates at 1800°C (Plate 4.2(c)). When more iron has been present ($4Fe/B_4C$), the more extensive conversion of the boron carbide to the iron boride, FeB, and carbon, viz. $4Fe + B_4C = 4FeB + C$, has left the material in more disperse form, even at 1800°C (Plate 4.2(d))

4.4.2 Titanium and zirconium additives

Comparison with the original boron carbide (Plate 4.1) shows that sintering has started at 1400°C (Plate 4.3(a)), but there are still wide ranges of aggregate sizes at higher temperatures, 1800°C, most of the smaller aggregates have disappeared as is indicated by Plate 4.3(b). Some rounding of the aggregates has become apparent and extensive sintering set in. Where a stoichiometric amount of titanium has been present ($2Ti/B_4C$), the more extensive conversion of boron carbide to the titanium boride, TiB_2, and carbide or possibly carbon, viz. $2Ti + B_4C = 2TiB_2 + C$, has left a mixture of larger crystals and aggregates at 1200°C (Plate 4.3(c)). There are also some small particles of material in the background, possibly free carbon. There is a similarity in the behaviour of the reaction and sintering of boron carbide by titanium and zirconium additives, cf. Plates 4.3 to 4.4. Excessive amounts of zirconium react with boron carbide to give ZrB_2 and ZrC, viz. $B_4C + 3Zr = 2ZrB_2 + ZrC$, cf. Table 4.3.

4.4.3 Vanadium additive

Much finely-divided material is still present at 1200°C (Plate 4.5(a)), comparable with the original boron carbide (Plate 4.1) and also

Plate 4.2

(a)

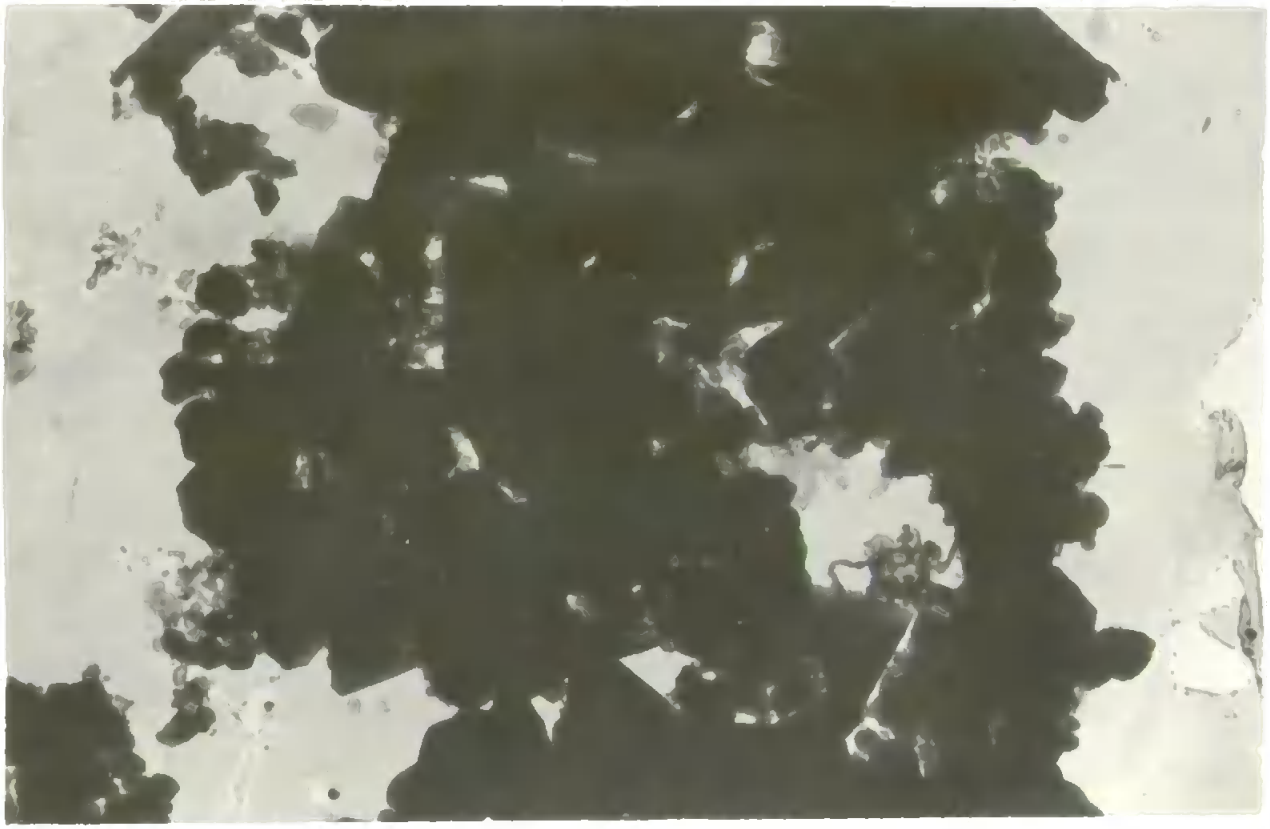

B_4C + 10% Fe sintered at 1400°C for 5 hr.

Magnification: 12000 X

(b)

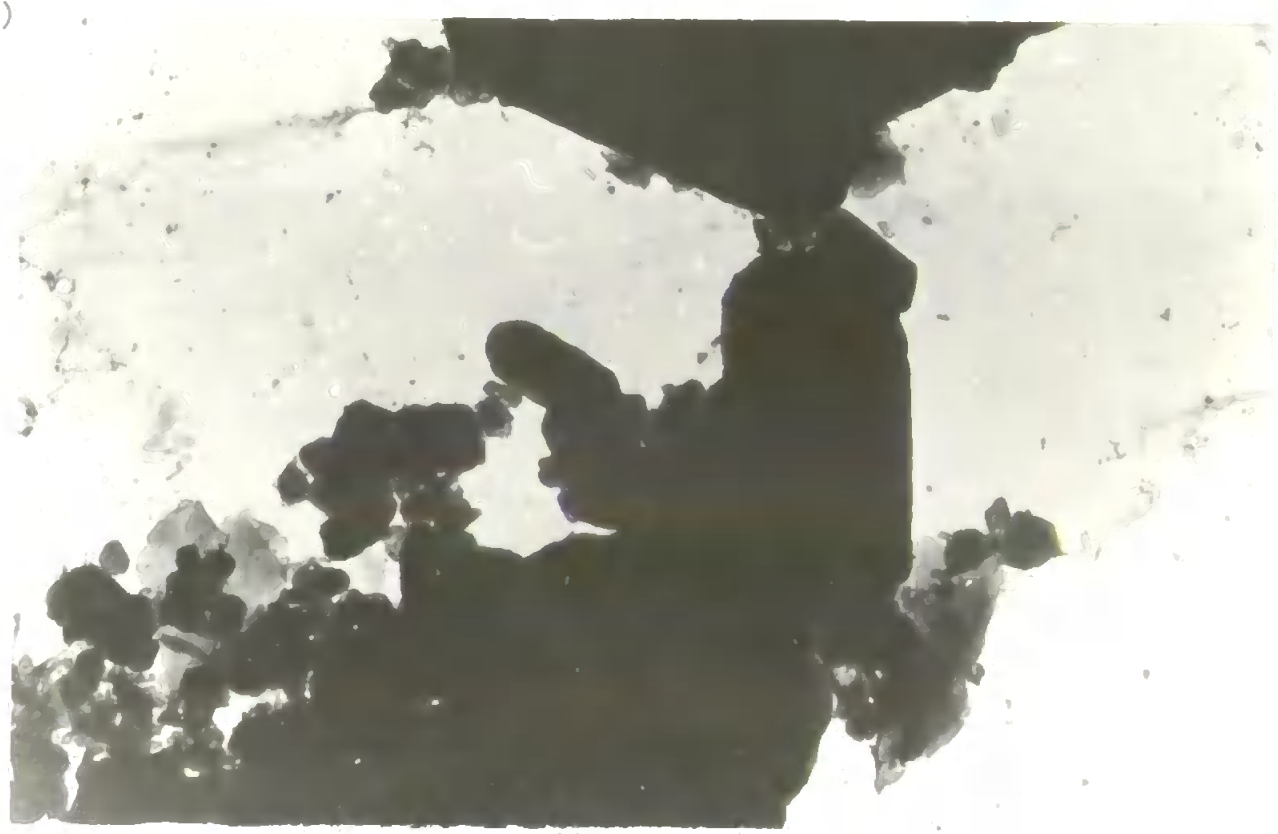

B_4C + 10% Fe sintered at 1600°C for 5 hr.

Plate 4.2

(a)

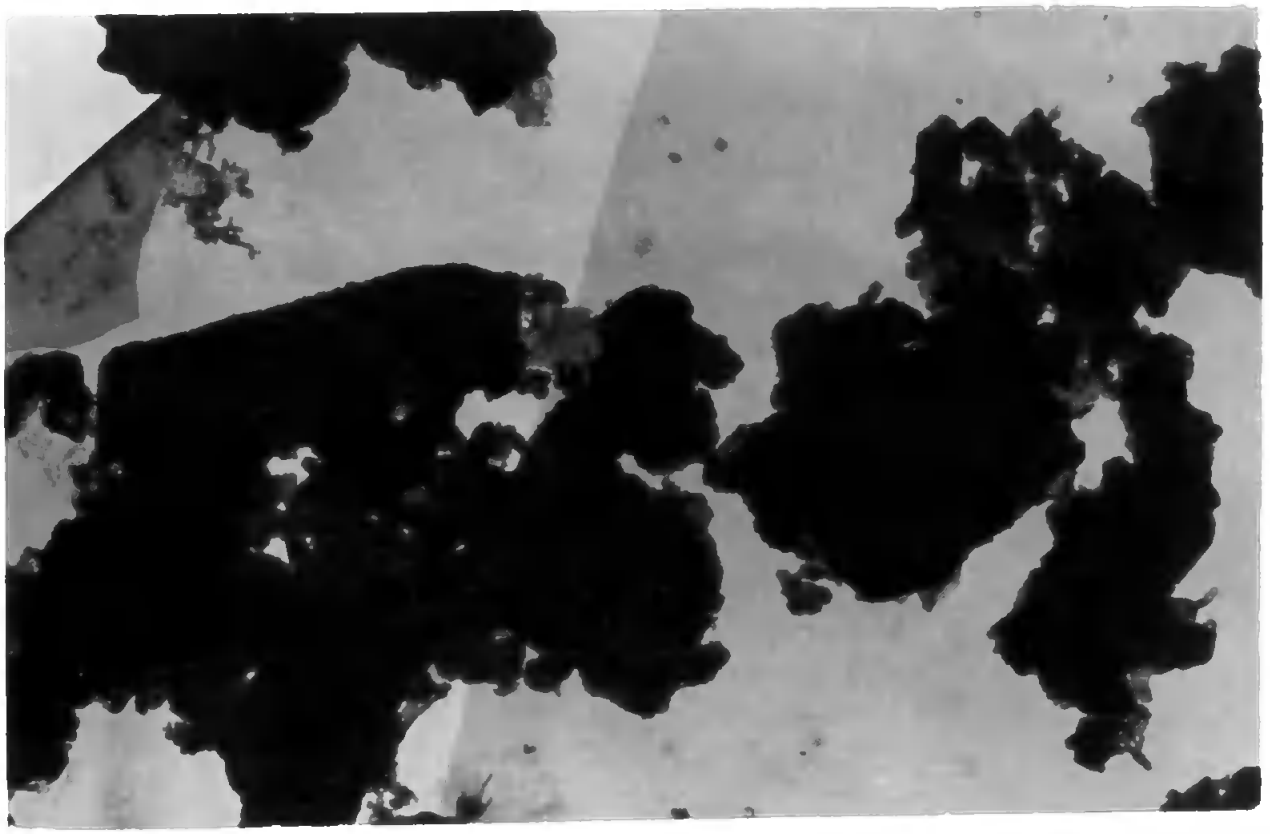

B_4C + 4Fe reacted at 1800°C for 5 hr.

Magnification: 12000 X

(d)

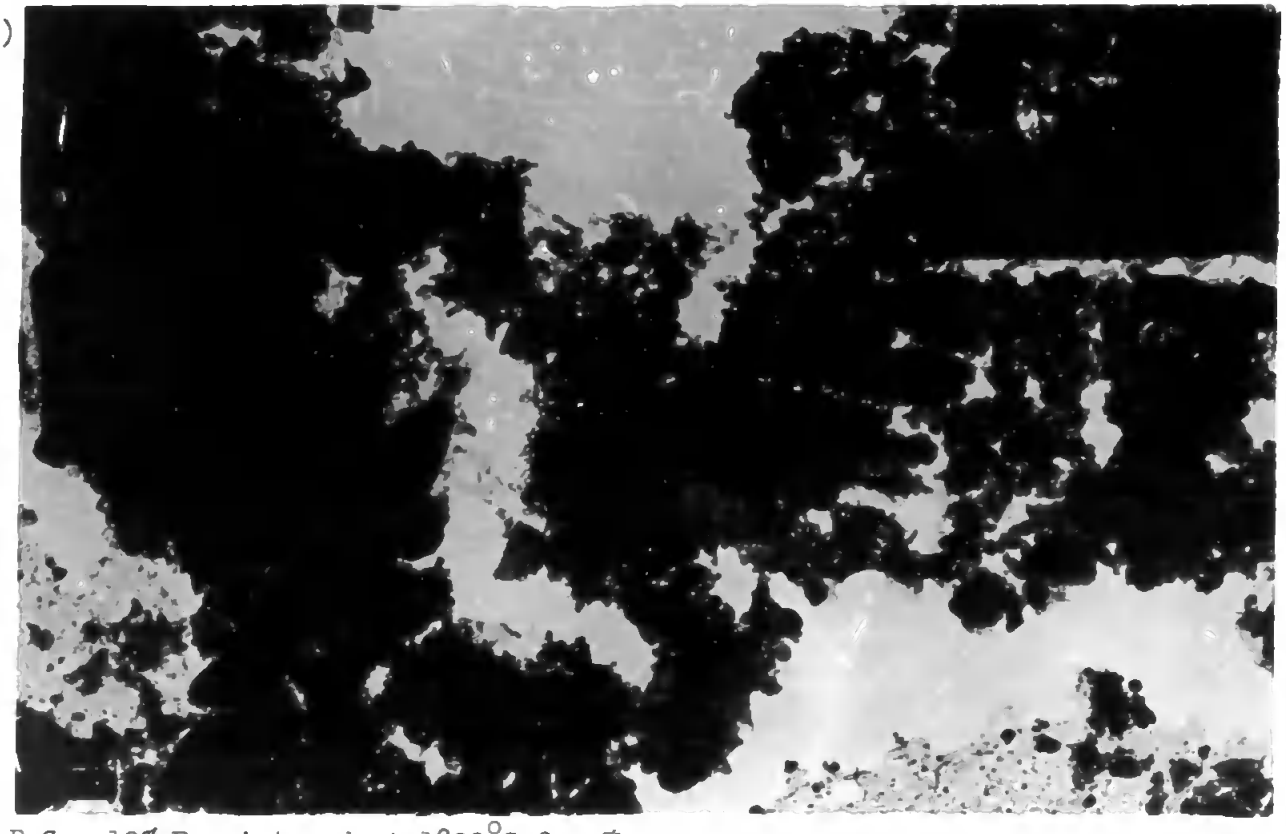

B_4C + 10% Fe sintered at 1800°C for 5hrs.

Plate 4.3

(a)

B_4C + 10% TiH_2 sintered at 1400°C for 5 hr.

Magnification: 12000 X

(b)

B_4C + 10% TiH_2 sintered at 1800°C for 5 hr.

Plate 4.3

(c)

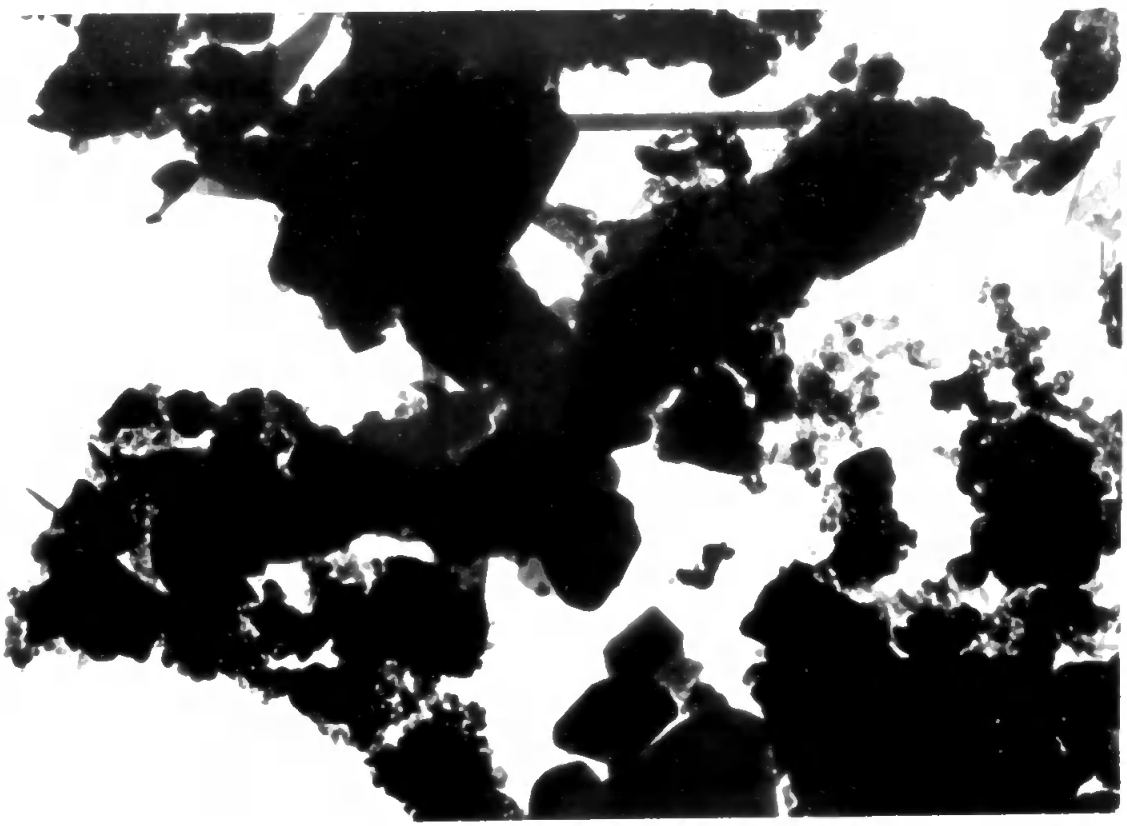

B_4C + 2Ti reacted at 1200°C for 5 hr.

Magnification: 12000 X

Plate 4.4

(a)

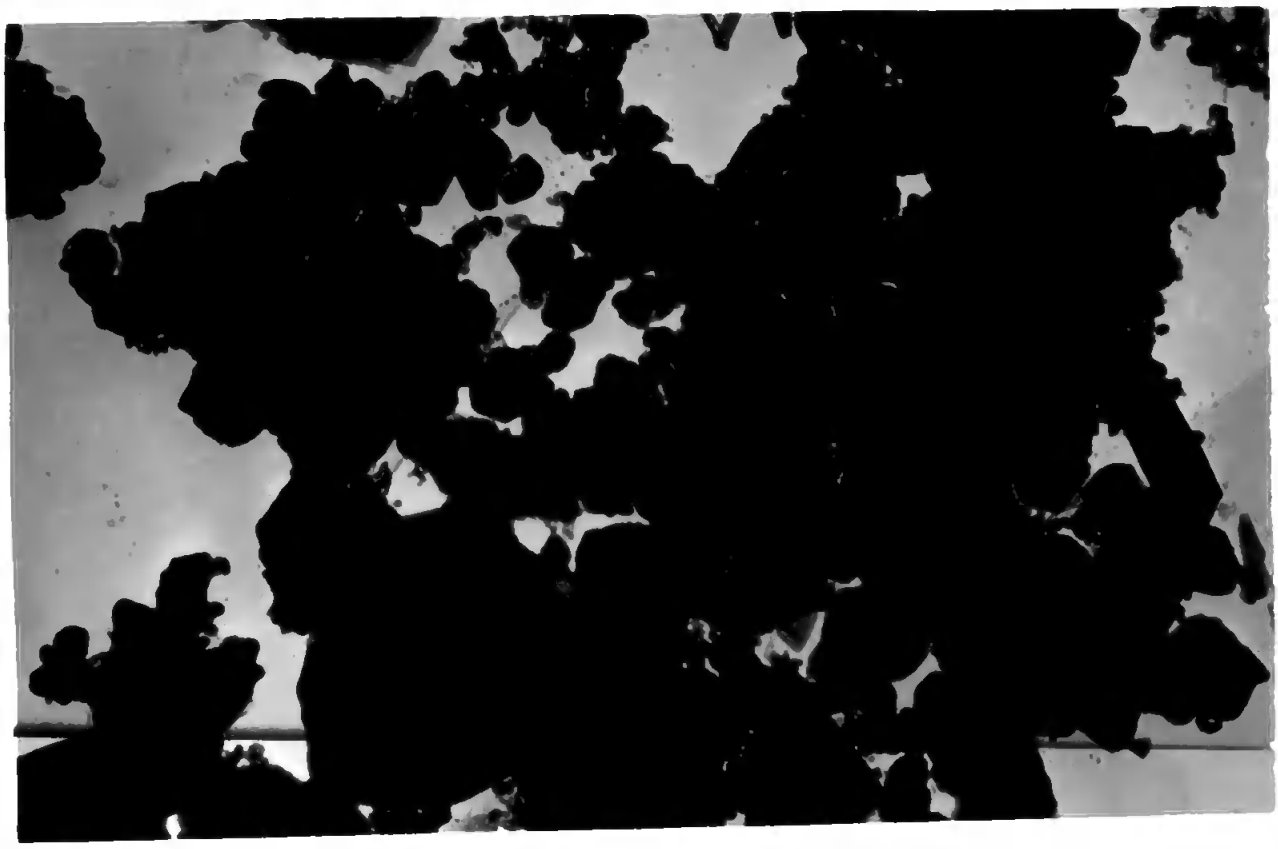

B_4C + 10% ZrH_2 mixture

Magnification: 12000 X

(b)

B_4C + 10% ZrH_2 sintered at 1200°C for 5 hr.

Plate 4.4

(c)

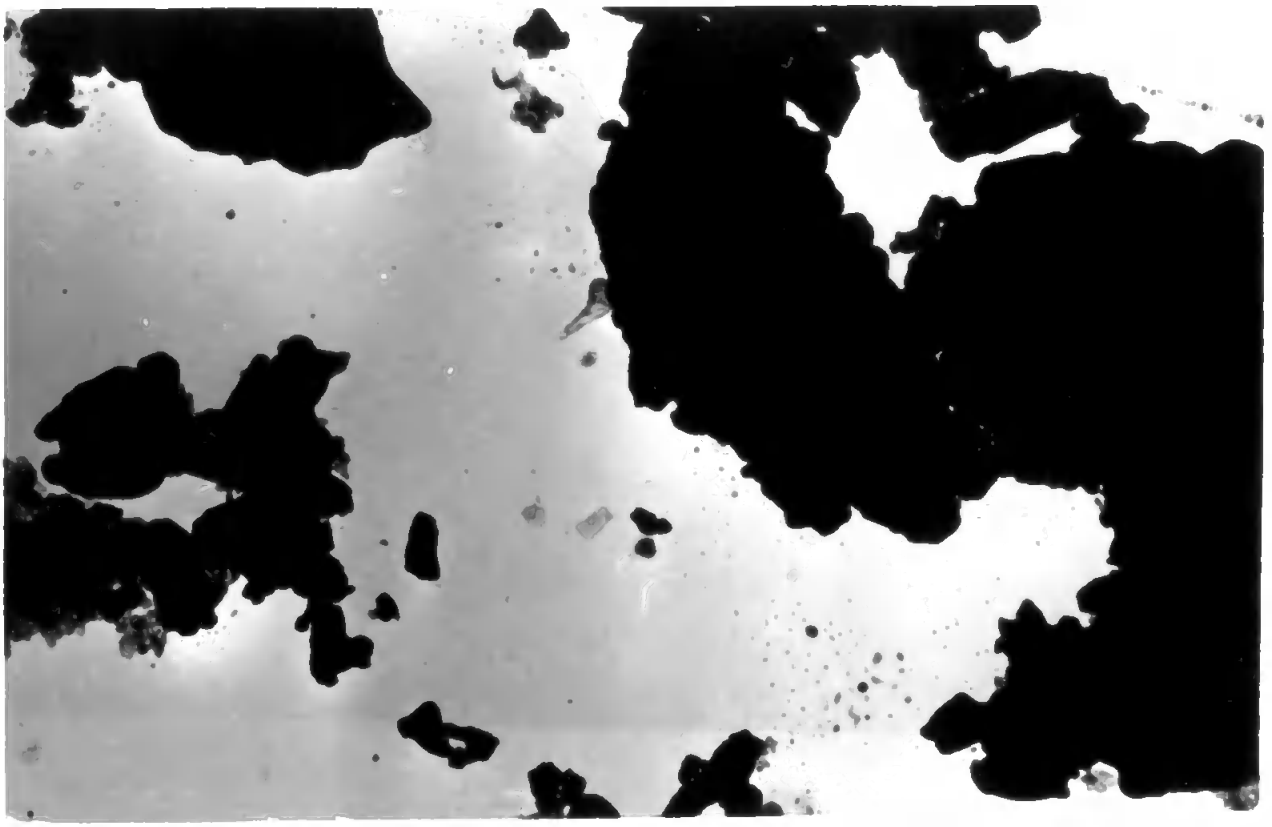

$B_4C + 3ZrH_2$ reacted at 1200°C for 5 hr.

Magnification: 12000 X

(d)

$B_4C + 3ZrH_2$ reacted at 1600°C for 5 hr.

having a wide range of aggregate sizes. At 1400°C the smaller aggregates have disappeared (Plate 4.5(b)), accompanied by a considerable loss of surface area and corresponding proportional increase in average crystallite size. Extensive sintering and rounding of large crystal and aggregates is apparent at 1800°C (Plate 4.5(c)).

4.4.4 Niobium and tantalum additives

With the niobium additive there is still some finely divided material present at 1200°C, cf. Plate 4.6(b). At higher temperatures, smaller particles start to disappear and aggregates increase in size. Considerable rounding of aggregates at 1600° and 1800°C is observed (Plate 4.6(c) and (d)). This behaviour is similar to the sintering of boron carbide with tantalum (Plates 4.7(a) - (f)). Where more tantalum has been present ($2Ta/B_4C$), the conversion of the boron carbide to tantalum boride, TaB_2, and carbon, viz. $2Ta + B_4C = 2TaB_2 + C$, causes progressive disappearance of finely divided material with extensive sintering and rounding of aggregates at higher temperatures (Plates 4.7(c) - (f)).

4.4.5 Molybdenum and tungsten additives

Comparison of the original boron carbide and that calcined with 10% metal additives at 1200°, 1400° and 1600°C indicates sintering and disappearance of smaller aggregates. This also applies to samples calcined with larger amounts of additives in stoichiometric ratios $2Mo/B_4C$ and $2W/B_4C$ as in Plates 4.8 and 4.9.

4.4.6 Aluminium additive

The aluminium has difficulty in wetting the boron carbide surface, especially at the lower temperatures 1000°C and 1200°C. Hence the electron micrographs for the 1000°C calcinations still show wide ranges

Plate 4.5

(a)

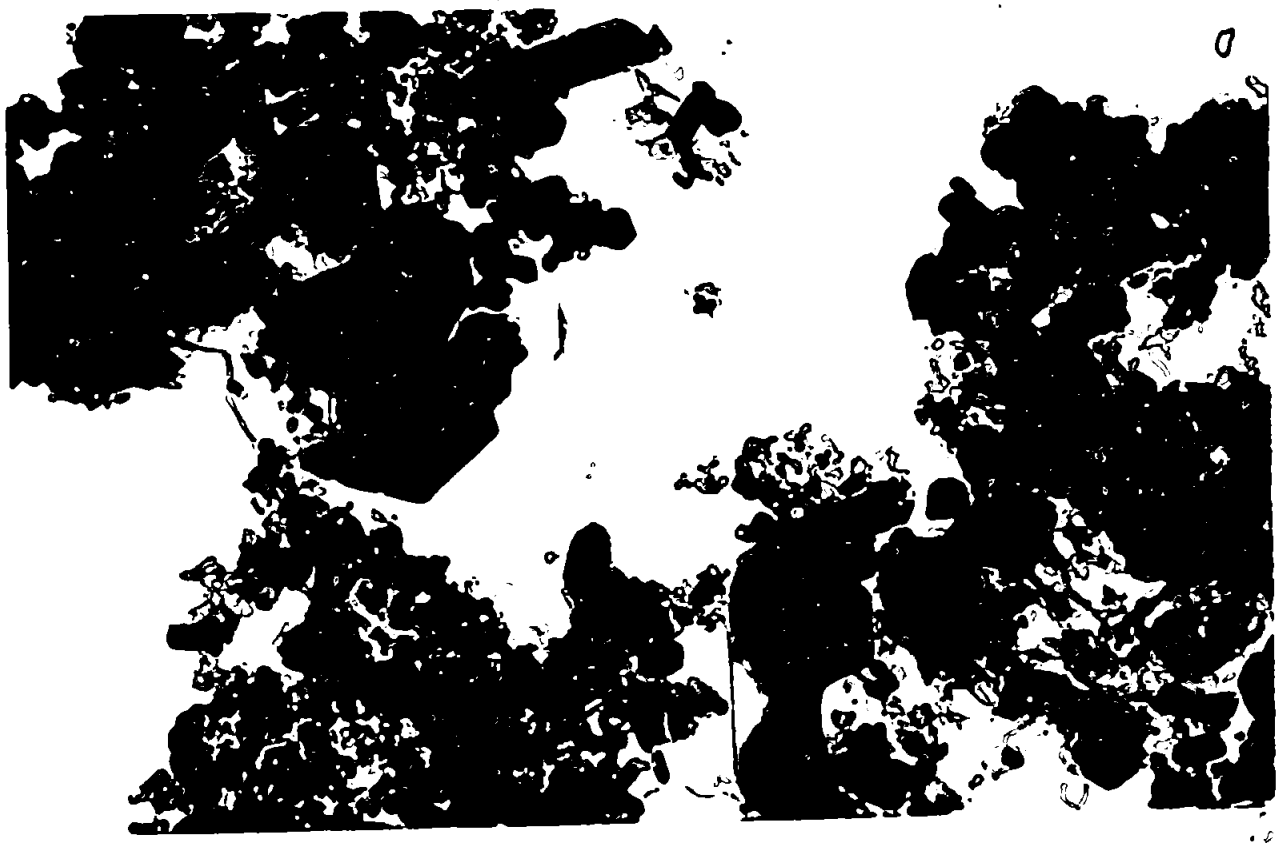

B_4C + 10% V sintered at 1200°C for 5 hr.

Magnification: 16000 X

(b)

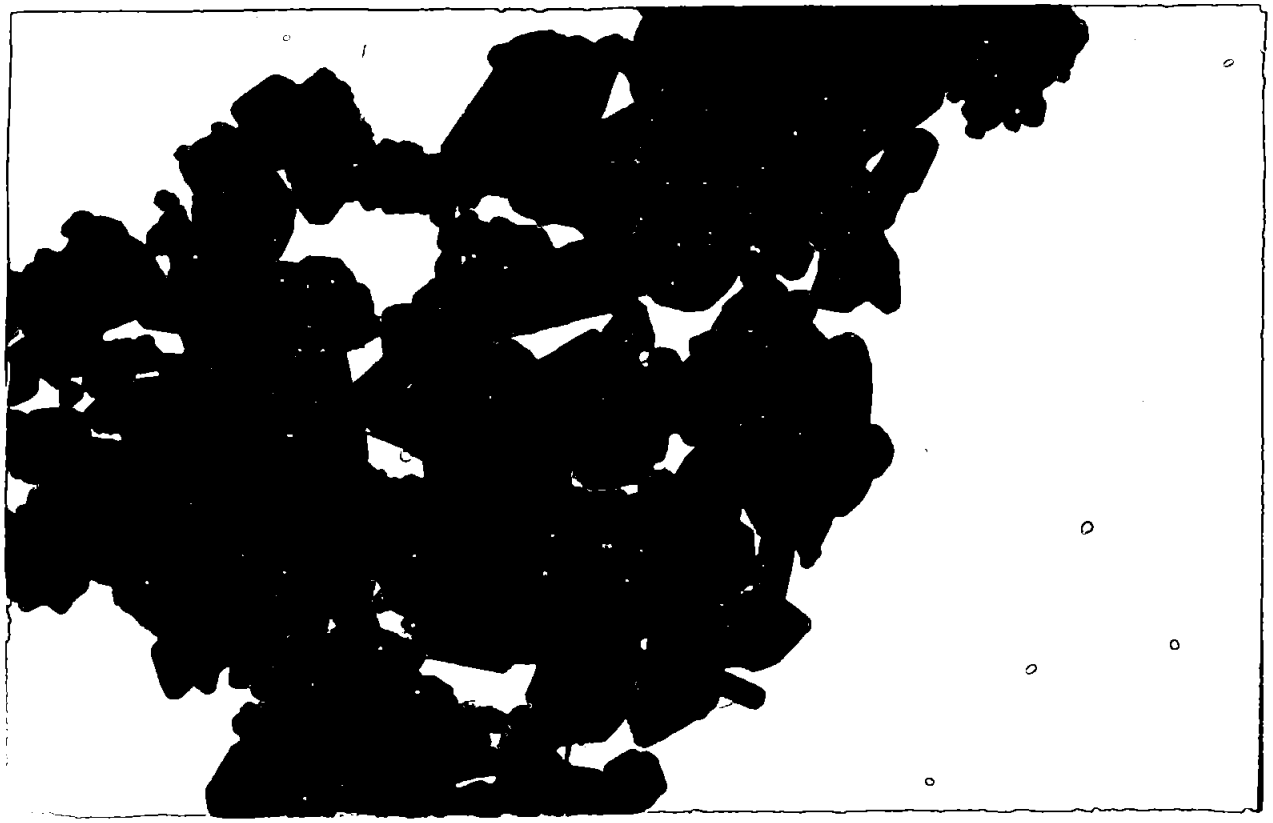

B_4C + 10% V sintered at 1400°C for 5 hr.

Plate 4.5

(c)

B_4C + 10% V sintered at 1800°C for 5 hr.

Magnification: 16000 X

Plate 4.6

(a)

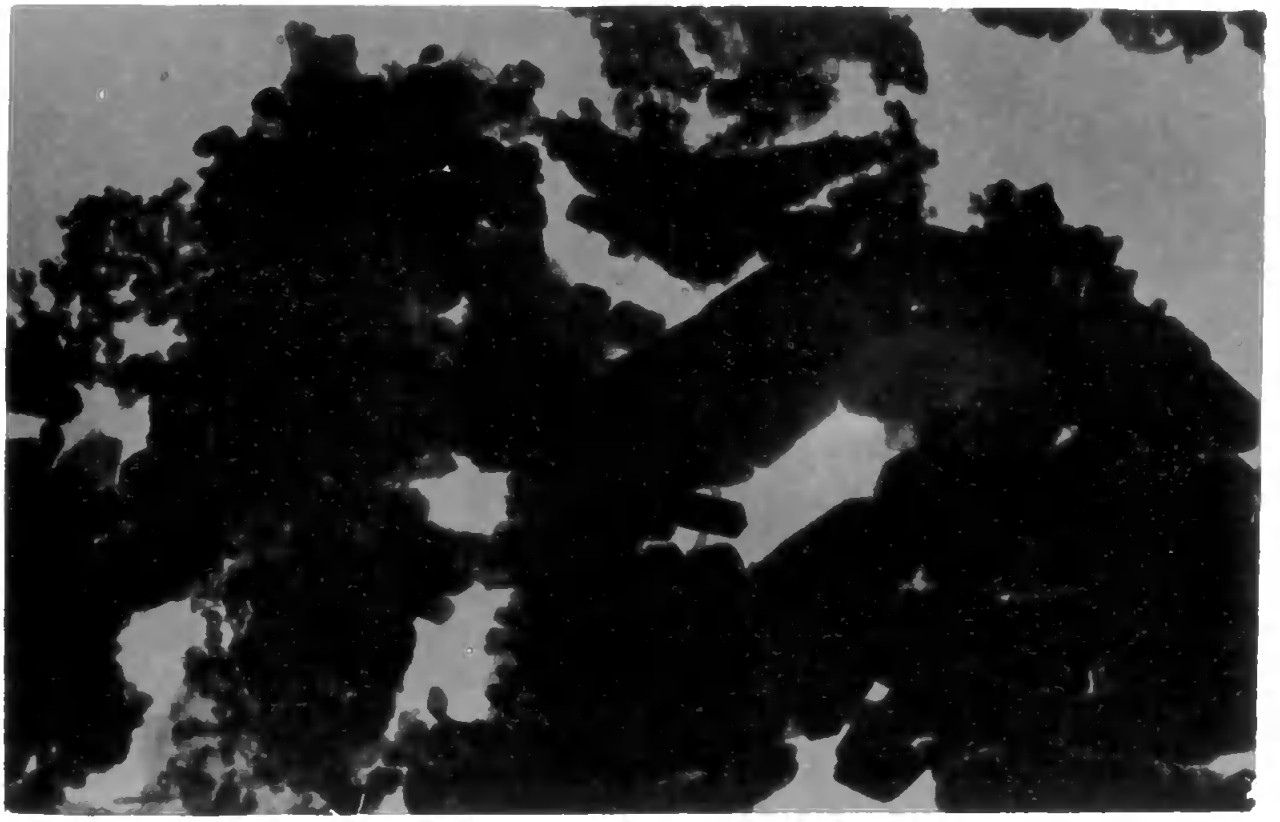

B_4C + 10% Nb mixture

Magnification: 16000 X

(b)

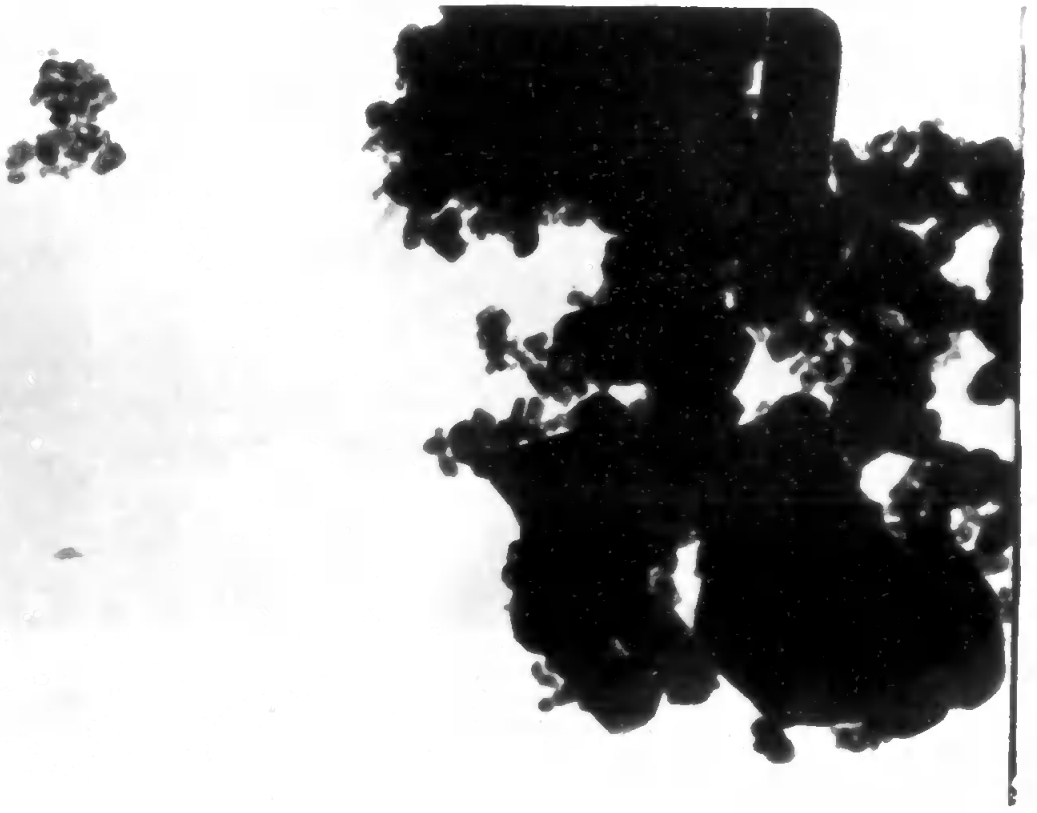

B_4C + 10% Nb sintered at 1200°C for 5 hr.

Plate 4.6

(c)

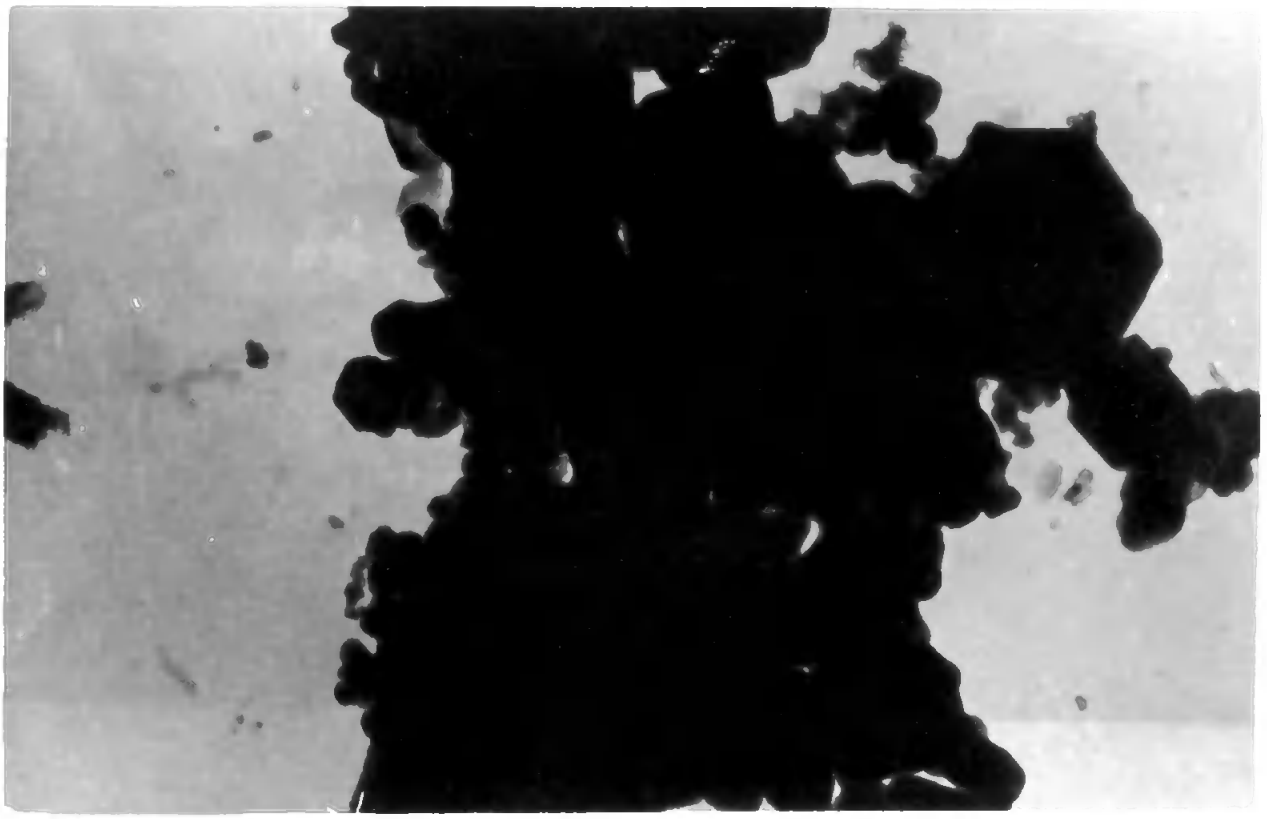

B_4C + 10% Nb sintered at 1600°C for 5 hr.

Magnification 16000 X

(d)

B_4C + 10% Nb sintered at 1800°C for 5 hr.

Plate 4.7

(a)

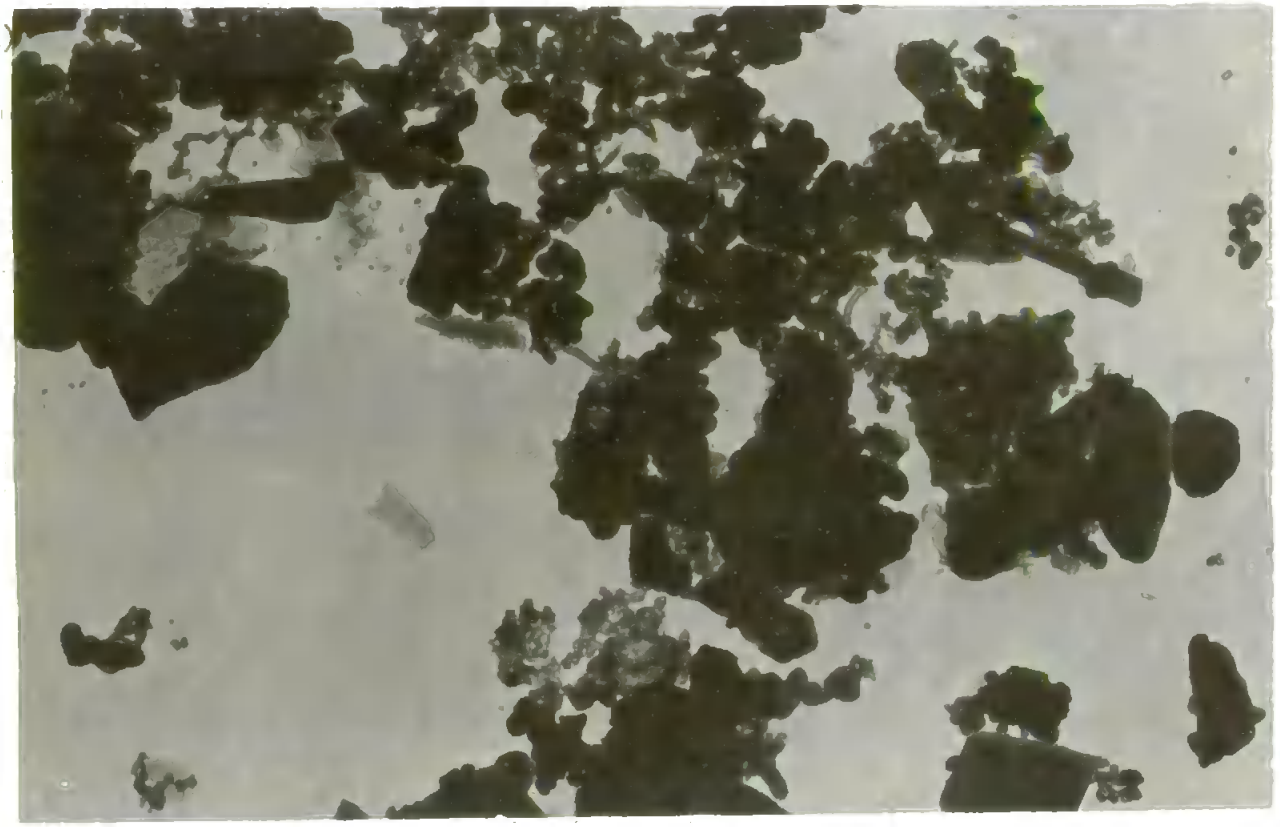

B_4C + 2Ta mixture

Magnification: 12000 X

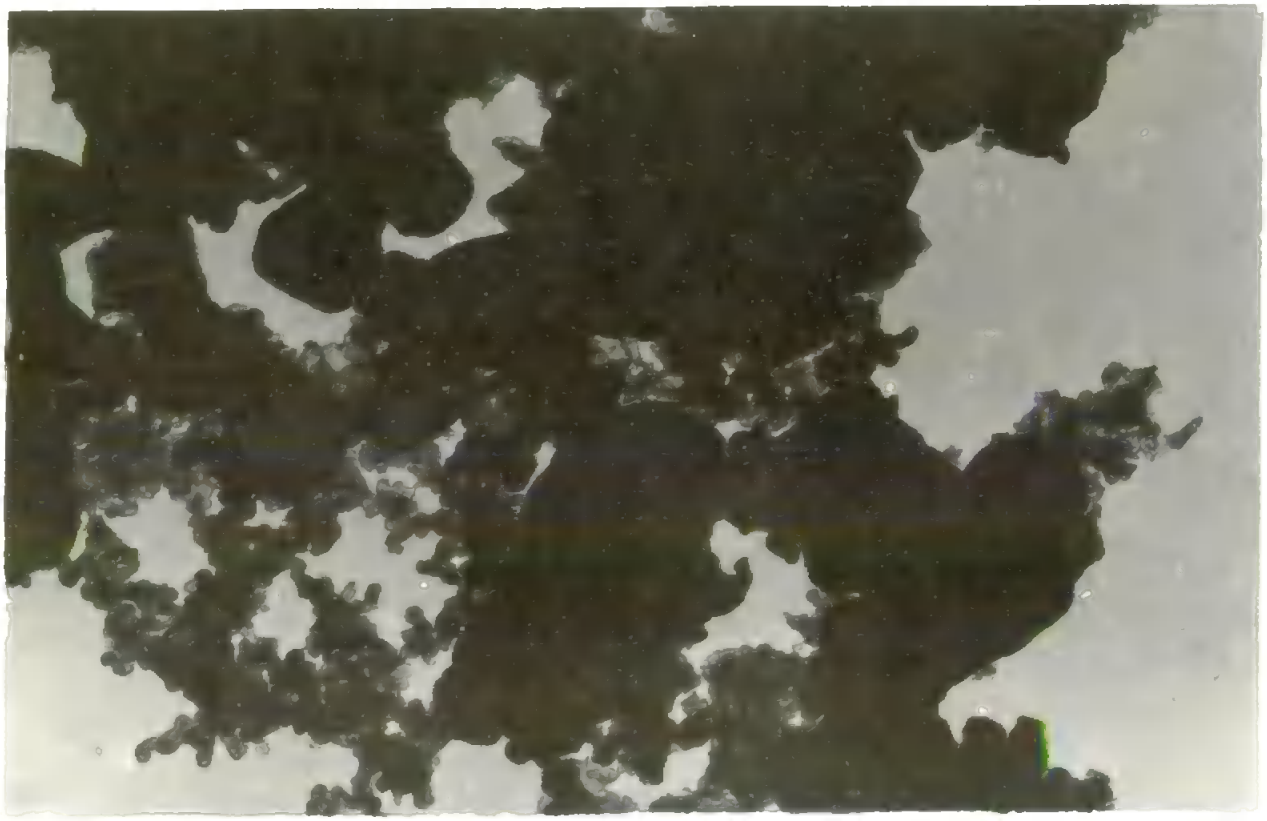

B_4C + 2Ta reacted at 1200°C for 5 hr.

Plate 4.7

(c)

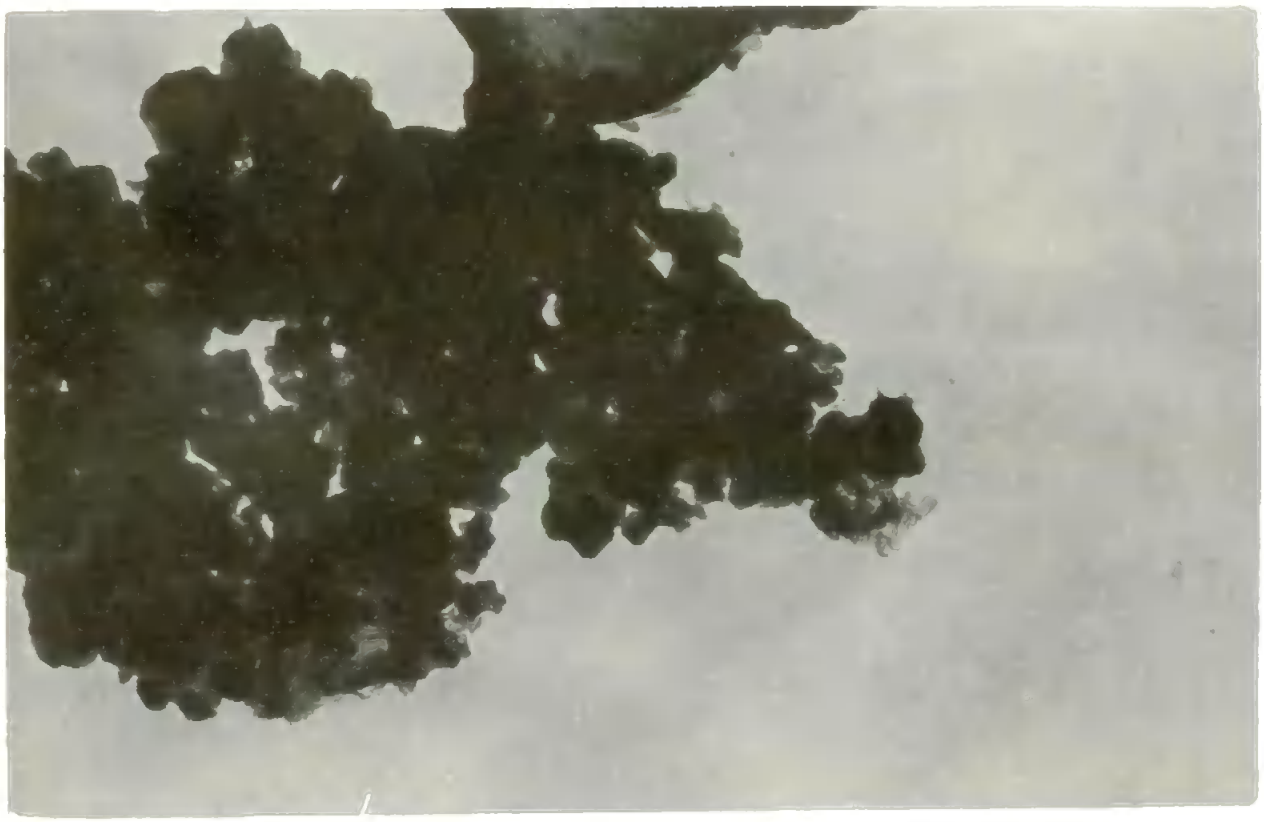

B_4C + 2Ta reacted at 1400°C for 5hr.

Magnification: 16000 X

(d)

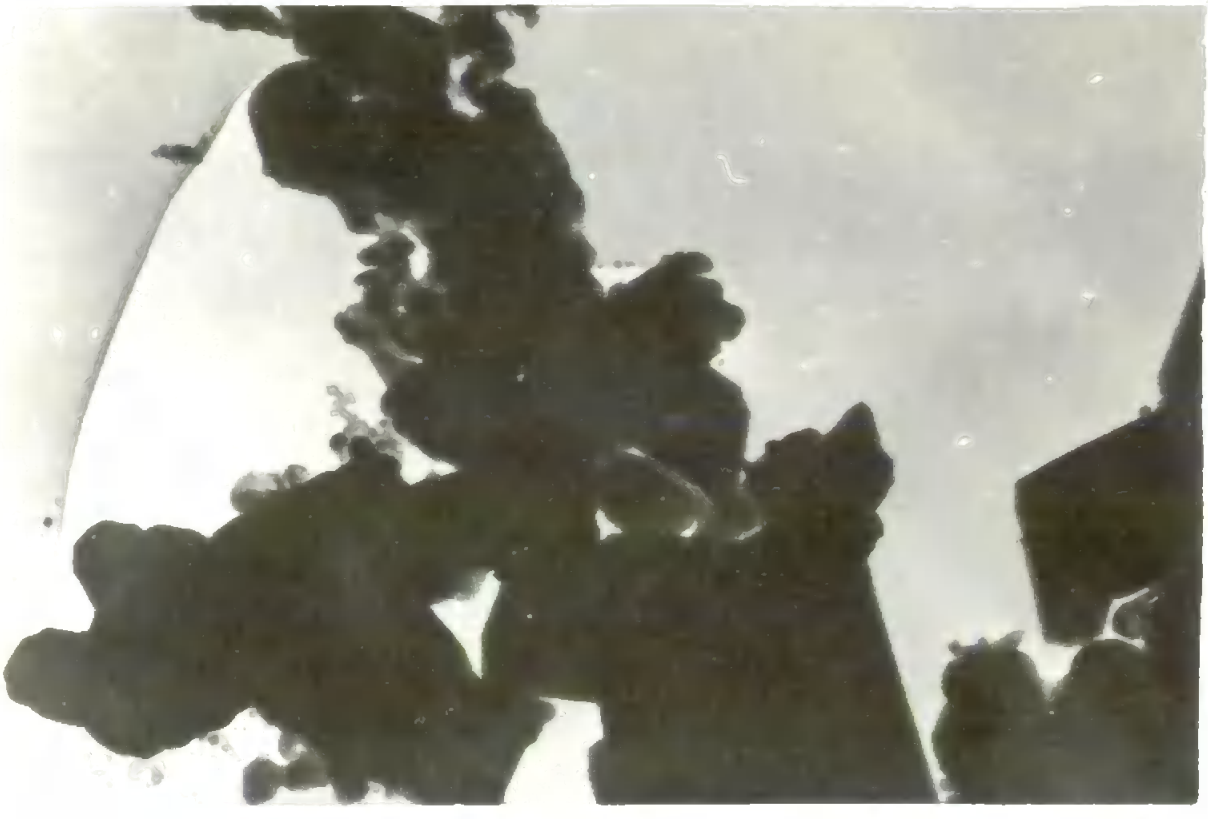

B_4C + 2Ta reacted at 1600°C for 5 hr.

Plate 4.7

(e)

B_4C + 10% Ta sintered at 1600°C for 5 hr.

Magnification: 12000 X

(f)

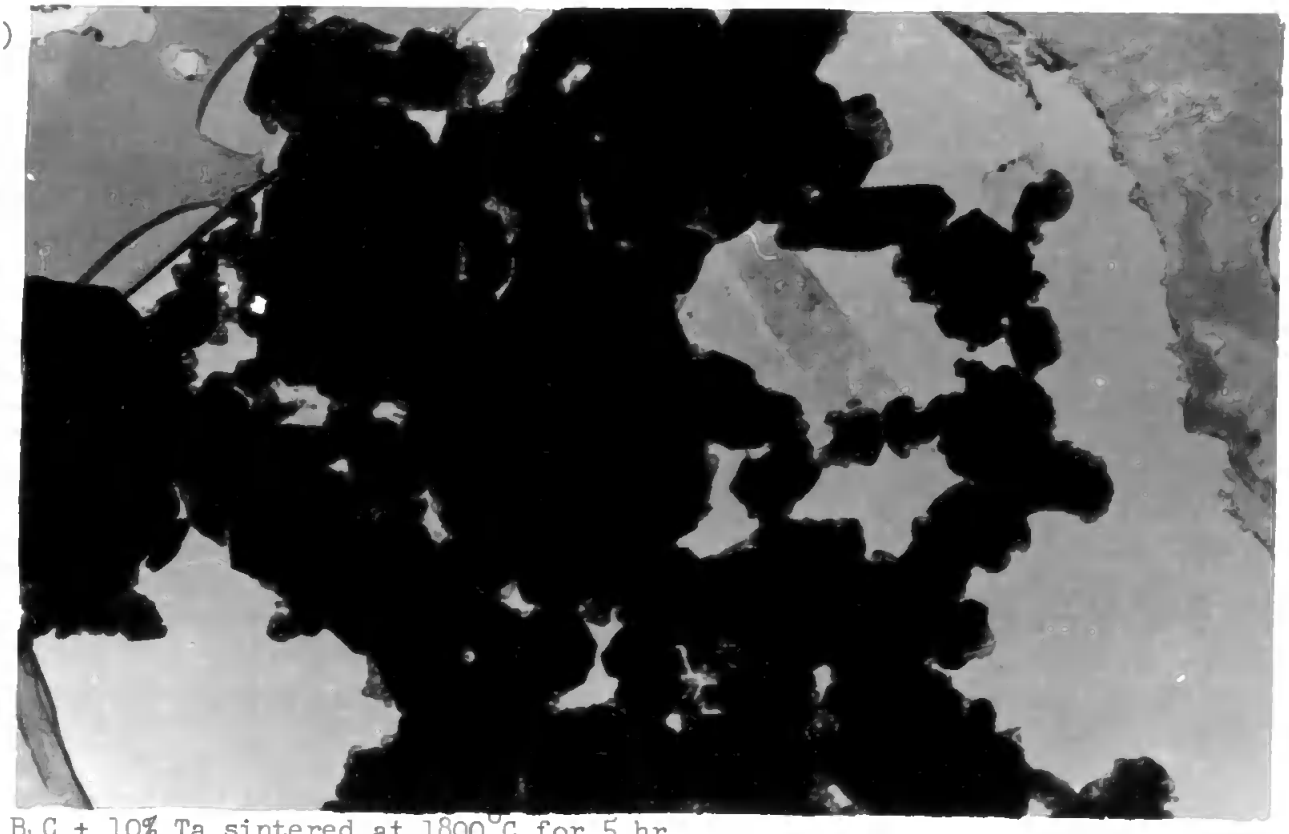

B_4C + 10% Ta sintered at 1800°C for 5 hr.

Plate 4.8

(a)

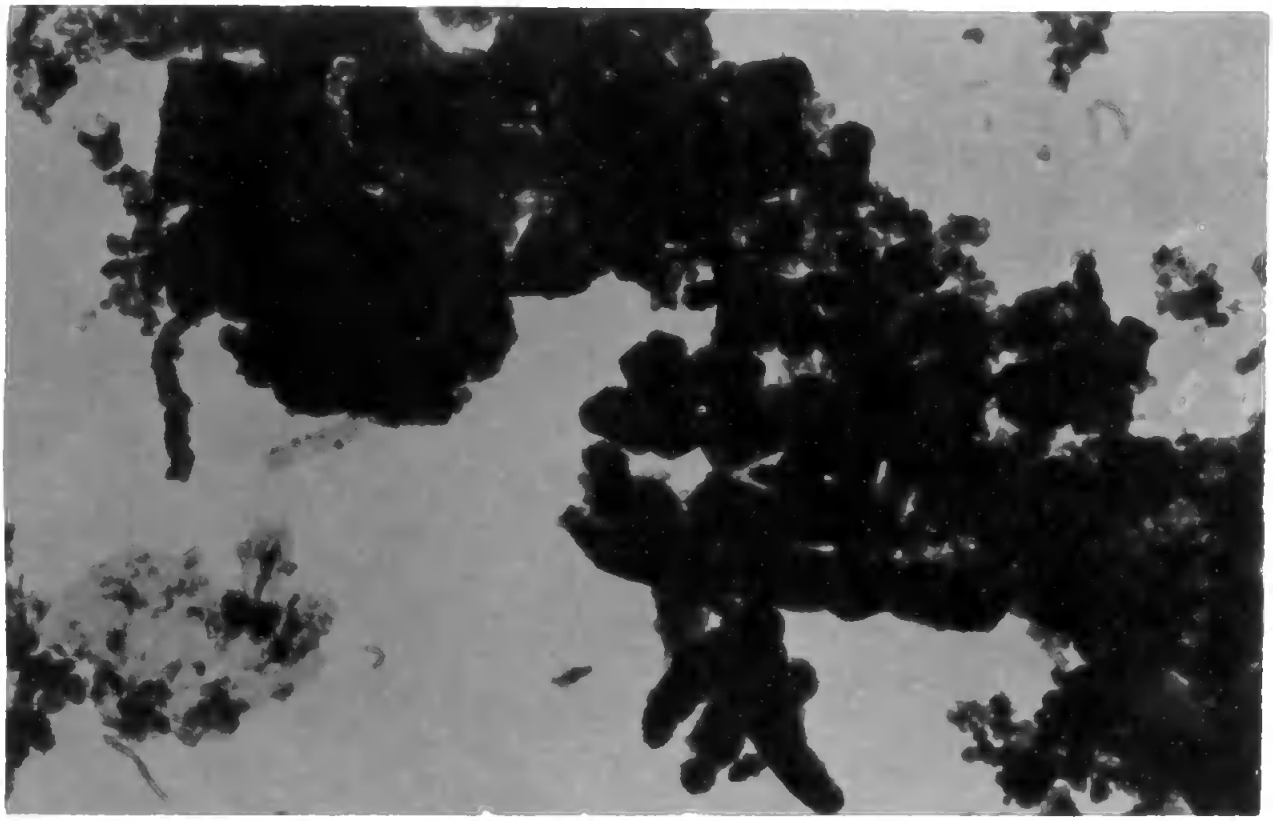

B_4C + 2Mo mixture

Magnification: 12000 X

(b)

B_4C + 2Mo reacted at 1200°C for 5 hr.

Plate 4.8

(c)

B_4C + 2Mo reacted at 1400°C for 5 hr.

Magnification: 12000 X

(d)

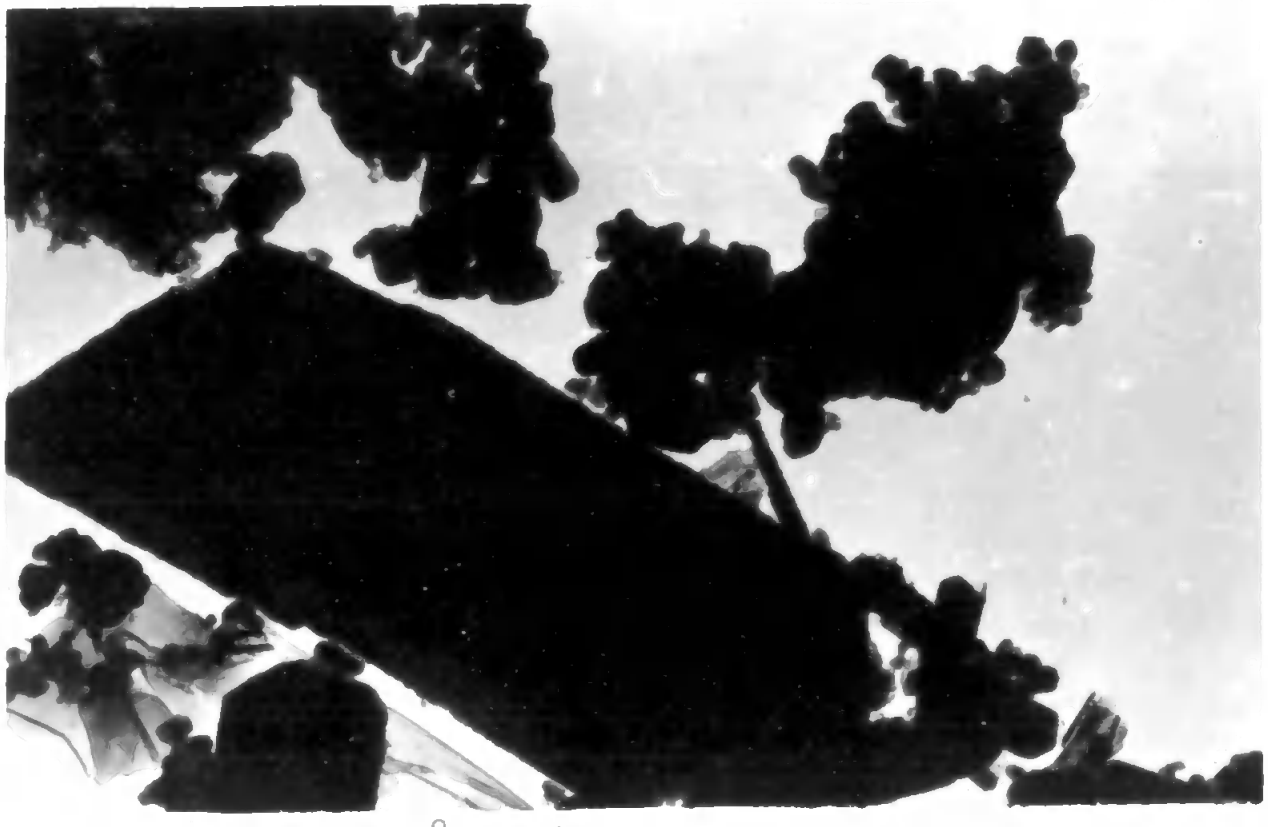

B_4C + 2Mo reacted at 1600°C for 5 hr.

Plate 4.8

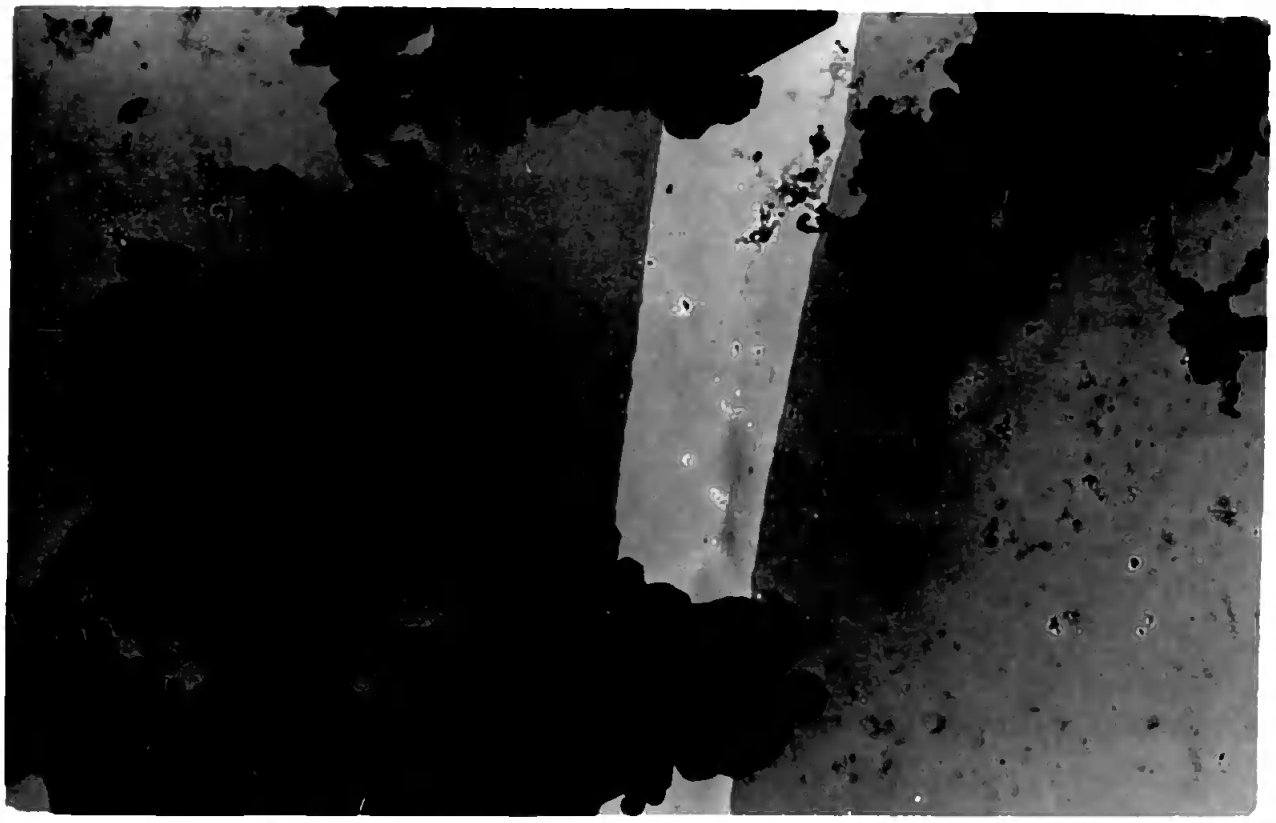

B_4C + 10% Mo sintered at 1400°C for 5 hr.

Magnification: 12000 X

(f)

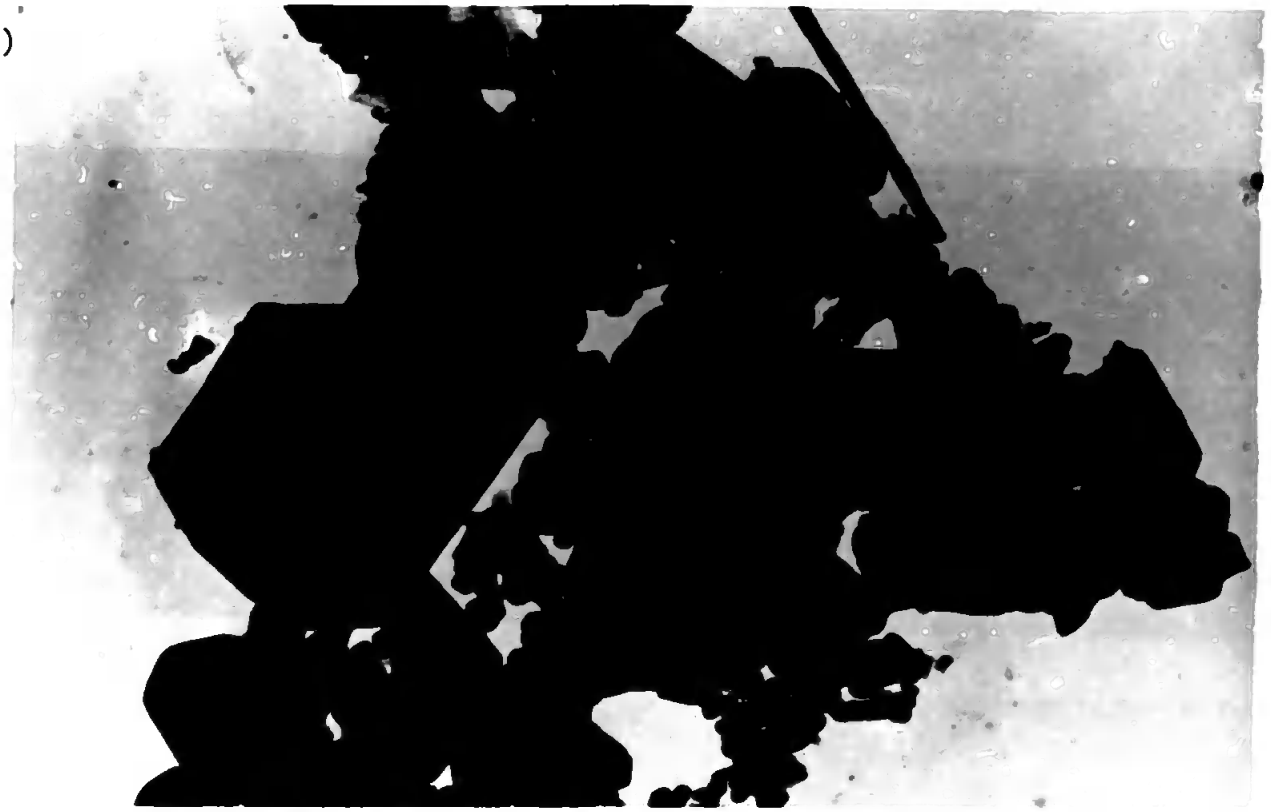

B_4C + 10% Mo sintered at 1600°C for 5 hr.

Plate 4.8

(g)

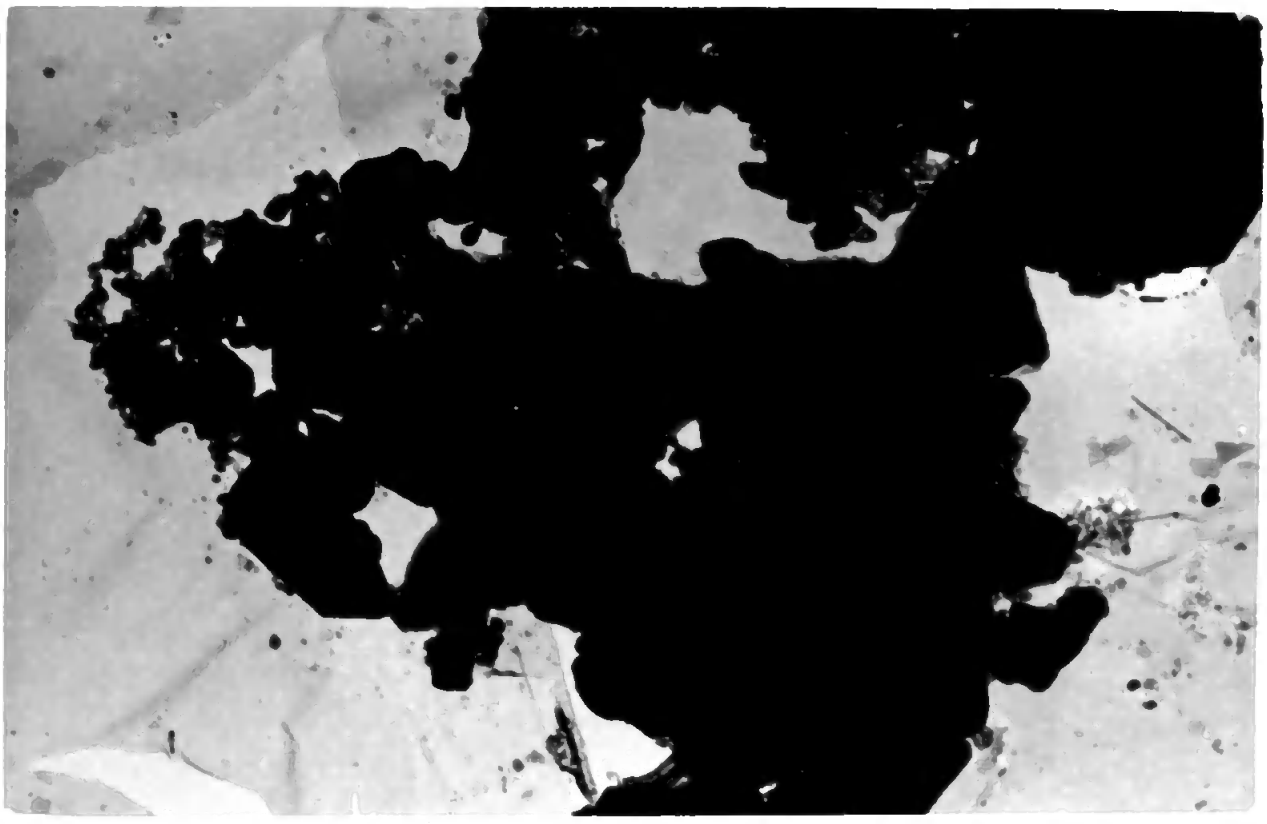

B_4C + 2Mo reacted at 1800°C for 5 hr.

Magnification: 12000 X

Plate 4.9

(a)

B_4C + 10% W sintered at 1200°C for 5 hrs.

Magnification: 16000 X

(b)

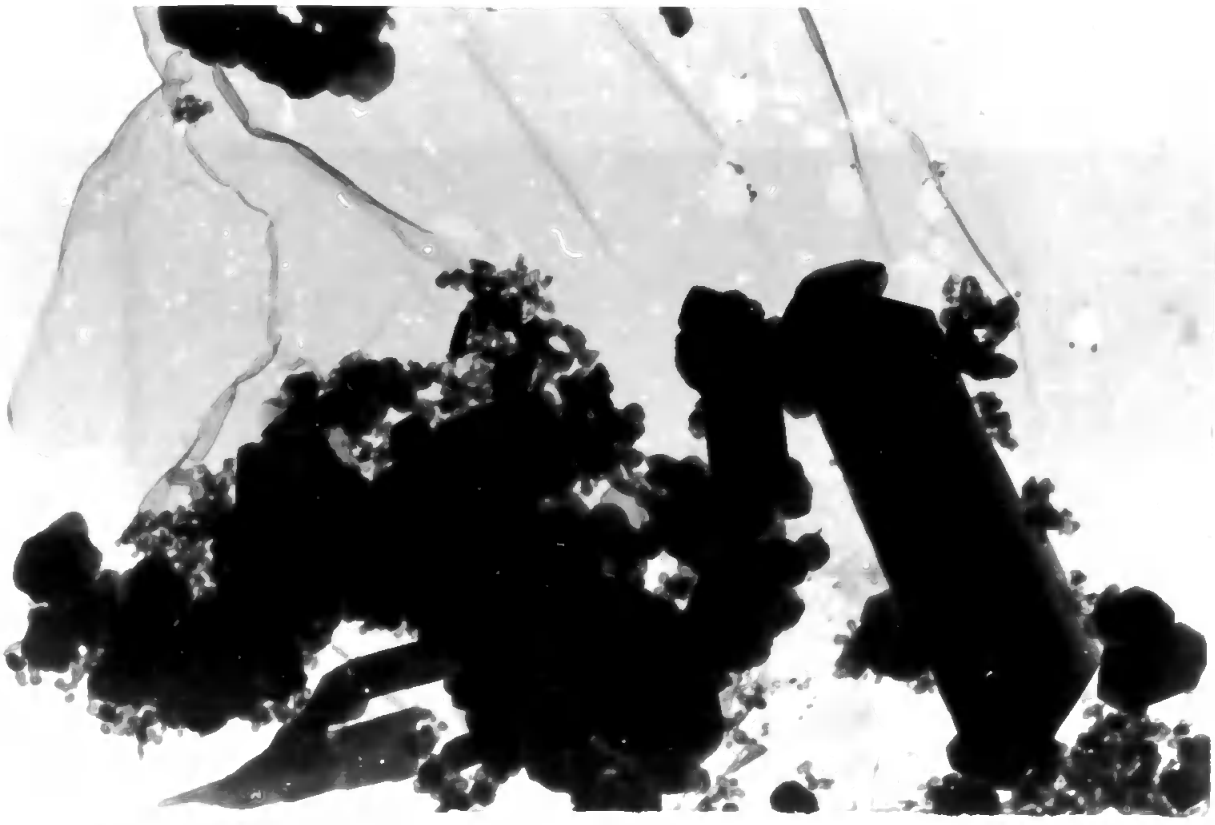

B_4C + 10% W sintered at 1400°C for 5 hr.

Plate 4.9

(c)

B_4C + 2W reacted at 1600°C for 5 hr.

Magnification: 12000 X

(d)

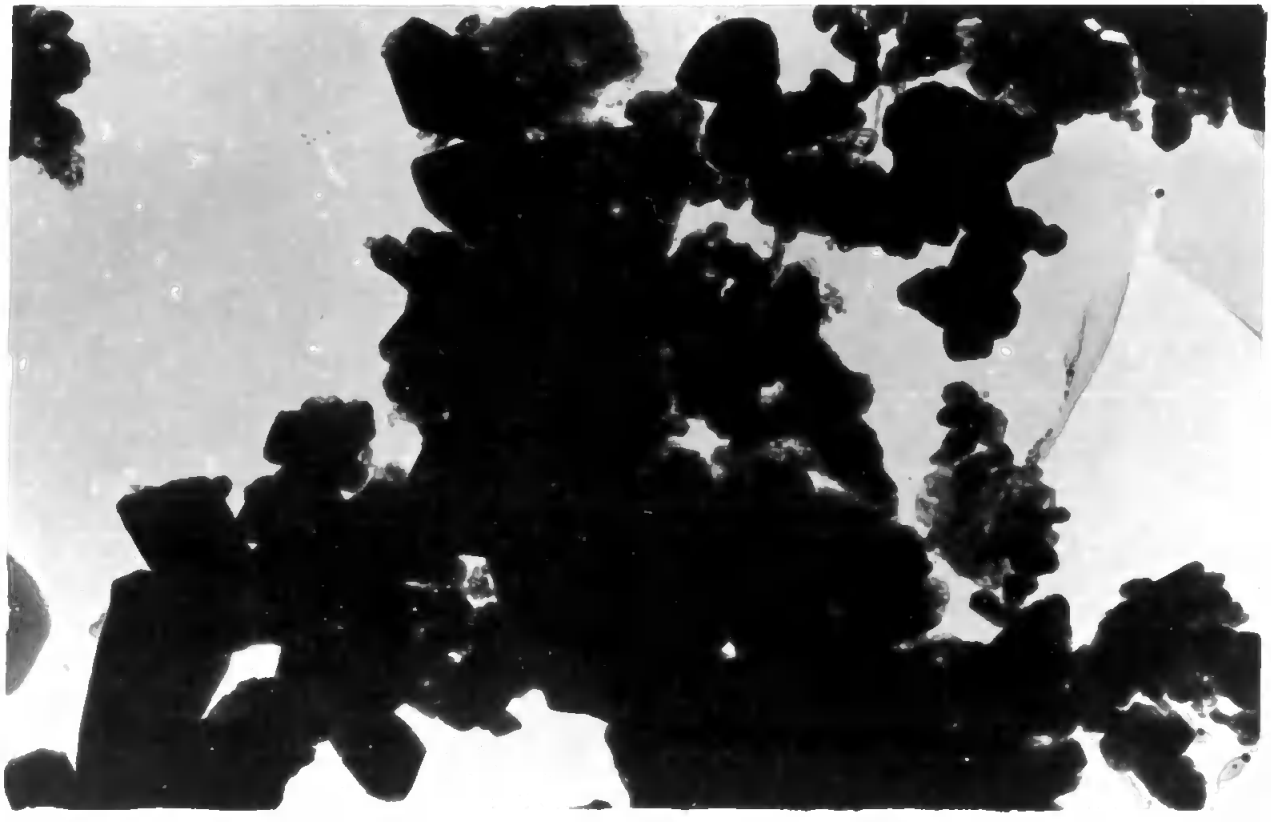

B_4C + 10% W sintered at 1600°C for 5 hr.

of aggregate sizes comparable with the original boron carbide and that sintered without additives for 5 hours at 1000°C (Plates 4.10(a) - (d)).

4.5 Conclusions

At temperatures above 1000°C, metal additives generally promote sintering of the boron carbide. Their effectiveness is occasionally reduced when there is some surface activation caused by the metals reacting with the boron carbide to form metal borides and carbides of different crystal lattice type and molecular volume. With the possible exception of tungsten additive, sintering of the boron carbide with metals at 1800°C is least affected by any surface activation arising from the formation of metal borides and carbides.

Most of the bonding in boron carbide is apparently covalent, whereas bonding in the metal borides and carbides is much more metallic (cf. Chapter 2). The covalency of the boron carbide inhibits diffusion at the surface and at the grain boundaries (discussed in Chapter 2). Thus, boron carbide particles only aggregate and adhere extensively at temperatures above about 80% of the m.p. in K, ($>$1900°C), compared with about 50% of the m.p. in K (Tammann temperature) for metals, metal oxides, metal borides and carbides (Hüttig, 1941), (Glasson, 1967). The Tammann temperatures for the metal borides and carbides produced in this research are all below 1400°C and 1800°C, so that they can promote sintering of boron carbide by crystal lattice diffusion at these temperatures. Of the metal additives investigated, iron is by far the most effective in promoting sintering of the boron carbide at 1800°C, as shown by the much greater changes of crystallites during calcination, cf. Table 4.10. The 5 hour-sintered sample was much harder than those containing the other metal additives, so that the effect of iron additive on further sintering and densification during hot-pressing was investigated. This is described in the next chapter.

Plate 4.10

(a)

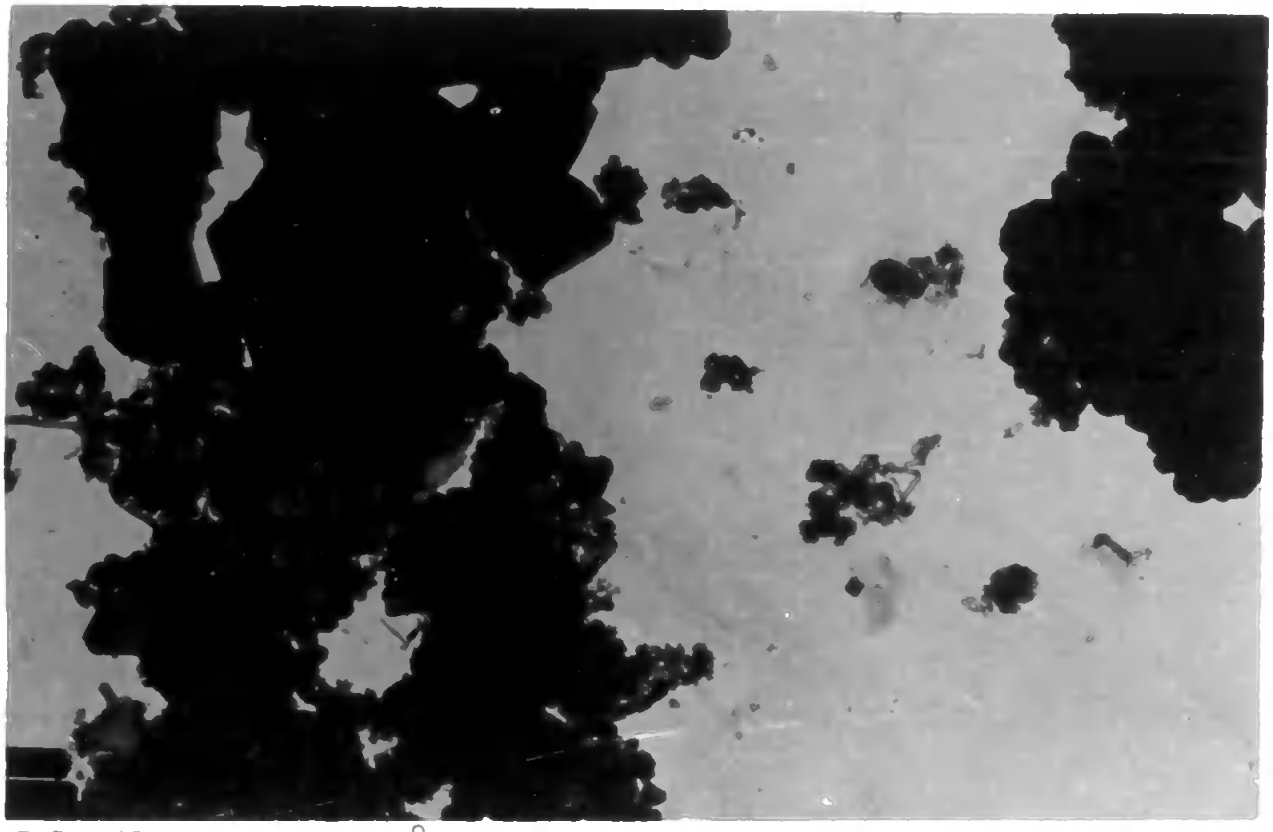

B_4C + Al reacted at 1000°C for 5 hr.

Magnification: 12000 X

(b)

B_4C + 2Al reacted at 1000°C for 5 hr.

Plate 4.10

(c)

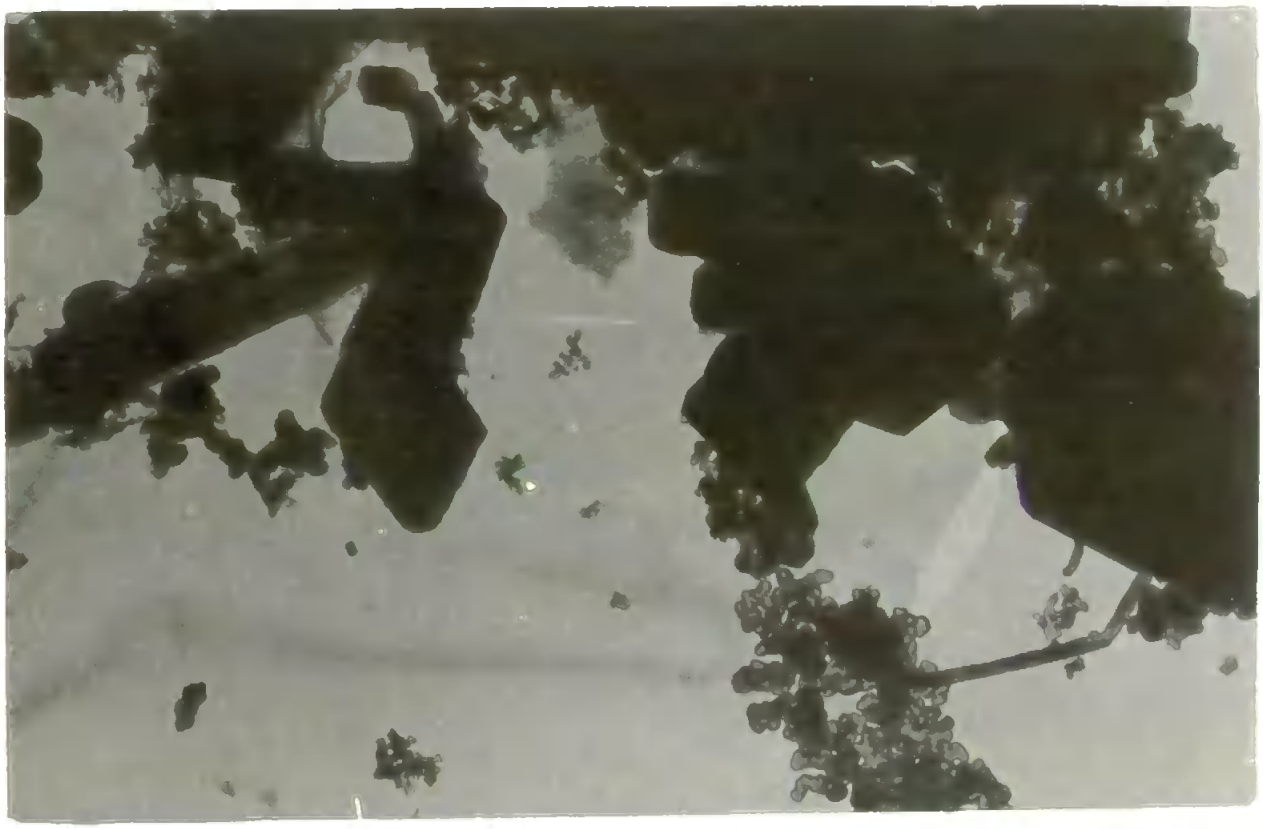

B_4C + 1% Al sintered at 1000°C for 5 hr.

Magnification: 16000 X

(d)

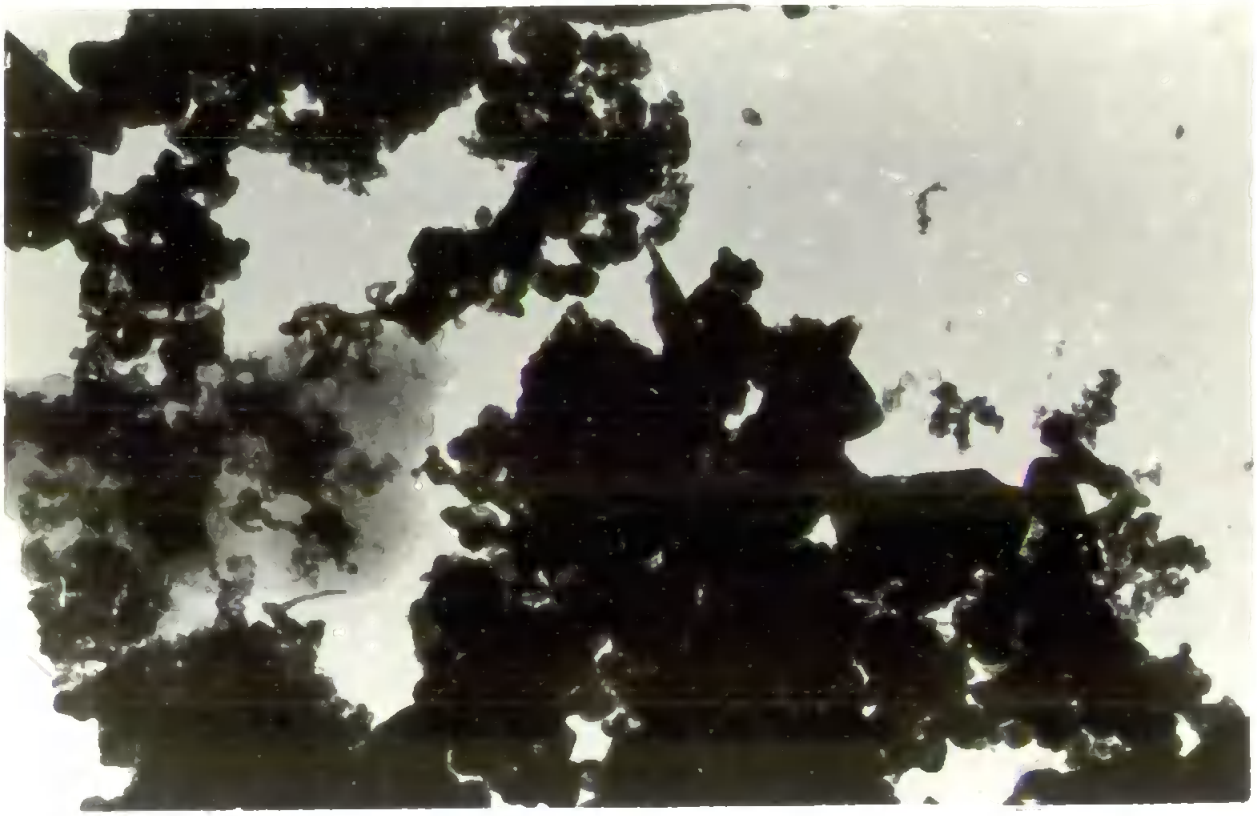

B_4C + 10% Al sintered at 1000°C for 5 hrs.

CHAPTER 5

EFFECT OF ADDITIVES ON THE HOT PRESSING OF BORON CARBIDE

5.1 Introduction

The boron carbide produced on a semi-technical scale (Glasson & Jones, 1969; Jones, 1970) was mainly of submicron size and sintered appreciably when calcined at temperatures between 1000 - 1800°C. Sintering was enhanced by increased temperature and time of calcination and also accelerated by addition of chromium at temperatures above 1600° and especially at 1800°C. More extensive densification was achieved by hot pressing, i.e. heating under a pressure exceeding the critical stress at temperatures relatively close to the m.p. (Dawhil, 1952; Bryjan et al, 1956). The submicron powders from the magnesium reduction process proved more suitable than the coarser samples given by electrothermal carbon reduction, the latter required ball milling (Jones, 1970) to provide suitable grain size composition for effective hot pressing. In the present work changes in phase composition and density in relation to time and temperature of mixtures of B_4C and metal powders when hot pressed have been studied. Mechanism of sintering during hot pressing is discussed in Chapter 2. Correlation of hot pressing with pressureless sintering is discussed by Jones, 1970. Some hot pressing was done on calcium hexaboride also.

5.2 Experimental

5.2.1 Materials

The materials used in this work are the same as those used in sintering studies described in Chapter 4 (Section 4.2.1).

5.2.2 Procedure

Attempts were made to hot press mixtures of boron carbide + metal powder using the laboratory hot-pressing system described in section 3.7.1. Owing to technical difficulties in using this equipment the work was carried out on the industrial system at Chessington and Torpoint described in section 3.7.2.

Samples of CaB_6 were hot pressed at a pressure of 3.00×10^7 N m^{-2} for 20 minutes at temperatures up to 2100°C (0.95 X m.p. in K). They were allowed to cool before removal from the die. The volume of the hot-pressed specimens was determined pycnometrically. The phases present after hot pressing were identified by X-ray diffraction.

5.3 Results

In the development of hot-pressing equipment, thyristor control of resistance heating was found to be preferable to the conventional saturation reactor type, since the former gave a more precise regulation of the sample temperature.

The results obtained when boron carbide is hot pressed with various additives are given in Table 5.1. Densification of the material increased with increasing temperature and time of hot pressing.

In the hot-pressing of CaB_6 alone densification did not start until a minimum temperature was reached; this could be regarded as the yield point or softening point. It then proceeded steadily and reached a maximum of 97% at 2100°C and 2 tons in $^{-2}$.

At each temperature and pressure a maximum density was achieved which did not increase appreciably with time. If the temperature and pressure were increased further, an increase in density followed immediately. Densities of up to 96 - 97% of the theoretical value were

TABLE 5.1

Mixture	Temp. °C	Pressure Nm^{-2}	Time min.	Phases Detected	% Theoretical density
B_4C + 10% Al	1000	1.54×10^7	5	No reaction	-
" "	1200	3.75×10^7	1	β - AlB_2	80%
" "	1200	1.54×10^7	5	No reaction	66%
" "	1200	"	10	"	71%
" "	1400	"	5	"	66%
" "	1400	"	20	"	75%
" "	1800	"	5	β - AlB_{12}	68%
" "	1800	"	20	"	79%
B_4C + 10% Fe*	1400	"	5	FeB, 2.988	49%
" "	1600	"	5	FeC, FeB	54%
B_4C + 10% Fe+	1400	"	5	FeB	55%
" "	1500	"	5	FeB	58%
" "	1700	"	5	FeC, FeB	60%
B_4C + 10% ZrH_2	1200	"	5	ZrB_2, ZrC	58%

* 90 mesh iron

+ finely powdered (reduced) iron

achieved.

5.4 Discussion

Iron additives enhanced sintering during the hot-pressing of boron carbide;—analogous to their effect under pressureless sintering conditions at 1000 - 1800°C. Nevertheless the densities achieved by hot pressing the boron carbide with iron under pressure of up to 1.54×10^7 Nm^{-2} (1 ton in^{-2}) at the temperatures used did not exceed 60% of the theoretical value. It is expected that to reach near maximum densities, temperatures above 0.8T K will be required (where T = m.p. of B_4C) (Jones, 1970). This is in spite of the formation of lower-melting iron borides, and the low wettability of boron carbide by iron.

The densification of boron carbide by hot pressing with aluminium additive is more effective at higher pressure. The combined effect of temperature and pressure help to overcome the critical stresses and non-wettability of boron carbide by aluminium (contact angle 118°) (cf. Section 2.7.7. Pressure helps also to increase the reactivity between the two substances at this temperature. Thus there is very little or no reaction during pressure sintering (cf. Table 4.9). The formation of AlB_2 with a fractional volume increase of 0.5397 results in a higher density than the formation of AlB_{12} (fraction volume change 5.0766, Appendix IV).

Zirconium hydride is a more effective pressure sintering promotor at lower temperature than iron, but less effective than aluminium (Table 5.1).

CHAPTER 6

THE FORMATION AND MICROSTRUCTURE OF BORIDE AND CARBIDE COATINGS ON METAL SURFACES

6.1 Introduction

The formation of coatings of borides on metals, alloys and steel surfaces has been of interest mainly for their wear, abrasion and corrosion resistant properties (Chapter 2). Methods for the formation of such coatings are mainly:-

(1) Direct surface boronizing by boron.

(2) Reaction with boron carbide + alkali metal carbonates.

(3) Gaseous boronizing.

(4) Boronizing by vapour deposition.

In the present research the formation of boride and carbide coatings on the surface of iron and transition metal (Group IVA - VIA) foils by reaction with boron carbide is studied. Improvement in their surface hardness properties and compound formation was investigated at a series of temperatures between 1000° and 1800°C. Possible changes in the reactivity of boron carbide with metals in sheet and fine powder (described in Chapter 4) form are compared.

6.2 Experimental

6.2.1 Materials

Finely-divided boron carbide, produced by Glasson & Jones (1969), corresponding to an average crystallite size of 0.106μm (equivalent spherical diameter) has been used throughout this work. Metal foils of very high purity (Goodfellows Metals Ltd.) were used. The purity and thickness of the metal foils are shown in Table 6.1.

Table 6.1

Metal	Purity, %	Thickness mm
Fe	99.5	0.150
Ti	99.70	0.125
Zr	99.67	0.125
V	99.91	0.150
Nb	99.92	0.150
Ta	99.96	0.150
Mo	99.95	0.150
W	99.97	0.150
Cr	99.995	0.02

6.2.2 Procedure

Pieces of metal foils 1 cm^2 in size were cleaned in trichloropropane vapour to free them of any grease or dust, rinsed with water and stored in argon-filled plastic bags. Stoichiometric weights of boron carbide (sufficient to convert 75% of metal into boride and carbide, cf. Tables 4.1 - 4.9) were dispersed in aqueous ammonia. This suspension was transferred to one side of the metal foil to form a uniform coating. They were dried in an oven (110°C) and then heated for a fixed time, usually 5 h. in argon at different temperatures ranging from 1000° - 1800°C. After X-ray analysis, the reacted samples were polished and their microhardness values determined (Section 3.8). Selected foils were examined by transmission electron microscopy (Plates 6.1 and 6.6) using a replica technique, and also by means of scanning electron microscopy (Plates 6.2 - 6.5).

6.3 Results

Table 6.2 shows the main metal boride and carbide phases formed at different temperatures along with their microhardness values. These values are variable where the reacted surfaces of the metal foils consist of different phases in layers. The electron micrograhs in Plate 6 show that these coatings are somewhat uneven compared with the initial polished uncoated metal surfaces, but nevertheless are generally harder for minimising galling of the metal surfaces.

6.4 Discussion

As demonstrated earlier (Vinczeandras, 1969; Ducrot & Poulain, 1970; Samsonov et al. 1970b; and Oreshkin, 1971), the boriding improves the microhardness and other mechanical properties of metals. The microhardness values determined in the present investigation are expected to

TABLE 6.2 COMPOSITION OF THE SYSTEMS B_4C - METAL FOILS HEATED AT VARIOUS TEMPERATURES

System	Temperature °C	Products		Microhardness kg mm^{-2} coated side	SEM Reference Plate
		Coated side	Uncoated side		
B_4C-Fe	1000	FeB, (*6.36, 2.914)	Fe	1750	
	1200	Fe_3C (*3.51, 3.11, 2.34, 1.18)	Fe	1635	
B_4C-Ti	1000	TiB_2, TiC	Ti	2684	
	1200	TiB_2, TiC	Ti	2744	
	1400	TiB_2, TiC, (*2.86, 2.48, 2.10, 2.033, 1.86, 1.66, 1.52, 1.312, 1.311)	Same as coated side	Did not retain shape	
	1600	TiB_2, TiC	TiB_2, TiC		
B_4C-Zr	1000	ZrB_2, ZrC	Zr	2845	
	1200	ZrB_2, ZrC (*2.60, 2.48, 1.91, 1.47)	ZrC (*2.59, 2.47, 1.91, 1.47, 1.36, 1.30)	2995	6.1
	1400	ZrB_2, ZrC (*2.56, 2.36)	-	2630	
	1600	ZrB_2, ZrC	ZrB_2, ZrC	Did not retain shape	

TABLE 6.2 ....cont'd

System	Temperature °C	Products		Microhardness $kg\ mm^{-2}$ Coated side	SEM Reference Plate
		Coated side	Uncoated side		
B_4C-V	1000	V_3B_2, (*3.2)	V	2225	
	1200	γ- VC, V	γ- VC, Vc, V_3B_2, VB_2	2300	
	1400	V_3B_4, VC (*3.46, 1.74, 1.53, 1.37)	V_3B_4, VC, V (*1.428)	2500	6.2
	1600	γ- VC (*2.37, 2.05, 1.602)	-	-	
B_4C-Nb	1000	NbB_2 (*2.34, 1.59)	Nb	2340	
	1200	NbB_2 (*3.04, 2.00, 1.81)	NbC (*3.01, 1.90, 1.78)	2350	
	1400	NbB_2, NbC (*3.02, 2.53, 2.31, 2.14, 1.77, 1.38	NbC (*1.57, 1.56, 1.41)	2770 2630	
	1600	NbB_2, NbC (*3.21, 2.15, 2.14, 1.63, 1.60, 1.39, 1.29, 1.27)	NbC (*3.65, 2.58, 2.53, 2.29, 2.12, 1.49, 1.43, 1.38, 1.23)	2805 2245	6.3
	1800	NbB_2, NbC	NbC (*1.59, 1.37, 1.28)	2835 3440	

TABLE 6.2 ...cont'd

System	Temperature °C	Products		Microhardness $kg\ mm^{-2}$ Coated side	SEM Reference Plate
		Coated side	Uncoated side		
B_4C-Ta	1000	TaB_2 (*2.17, 1.65, 1.58)	γ-TaB (*3.04, 2.30, 1.35)	2475	
	1200	γ-TaB	-	3100	
	1400	γ-TaB	TaC	3288	
	1600	γ-TaB, TaB_2	TaB_2, δ-Ta_3B_4, TaC, Ta	3542	
	1800	TaB_2 (*3.45, 2.38, 1.73, 1.60, 1.40, 1.34, 1.30)	-	3465 2576	6.4
B_4C-Cr	1600	CrB_2, ζ-CrB, $Cr_{23}C_6$	CrB_2, ζ-CrB, $Cr_{23}C_6$	Did not retain shape	
B_4C-Mo	1000	δ-MoB, MoB_2	Mo	1805	
	1200	δ-MoB, β-MoB	Mo	2250	
	1400	δ-MoB (*2.69, 2.59, 2.35, 2.15, 2.02, 1.89, 1.79)	γ-Mo_2B, Mo_2C	2385 2054	
	1600	δ-MoB, β-MoB, MoB_2	γ-Mo_2B, Mo_2C	1680 1730	6.5
	1800	δ-MoB, β-MoB, MoB_2	γ-Mo_2B, MoC (*2.6, 2.49, 2.36, 2.19, 1.5, 1.27, 1.25)	2130	

TABLE 6.2 ...cont'd

System	Temperature °C	Products		Microhardness kg mm^{-2} Coated side	SEM Reference Plate
		Coated side	Uncoated side		
B_4C-W	1000	γ-W_2B, δ-WB	γ-W_2B (*1.59, 1.58)	2485	
	1200	β-WB	β-WB ("2.76, 2.35)	4486 2822	6.6
	1400	δ-WB, β-WB, W	γ-W_2B, W	4375 2850	
	1600	δ-WB, β-WB	β-WB (*2.36, 2.26)	4500 2910	
	1800	β-WB (*3.76, 2.99, 2.25, 1.90, 1.86, 1.14, 1.09, 1.08)	β-WB, WC	3812 3240	

* Indicates the d spacings in Å of unidentified phases.
Microhardness values were determined only on the coated side of the foils

Plate 6.1

(a)

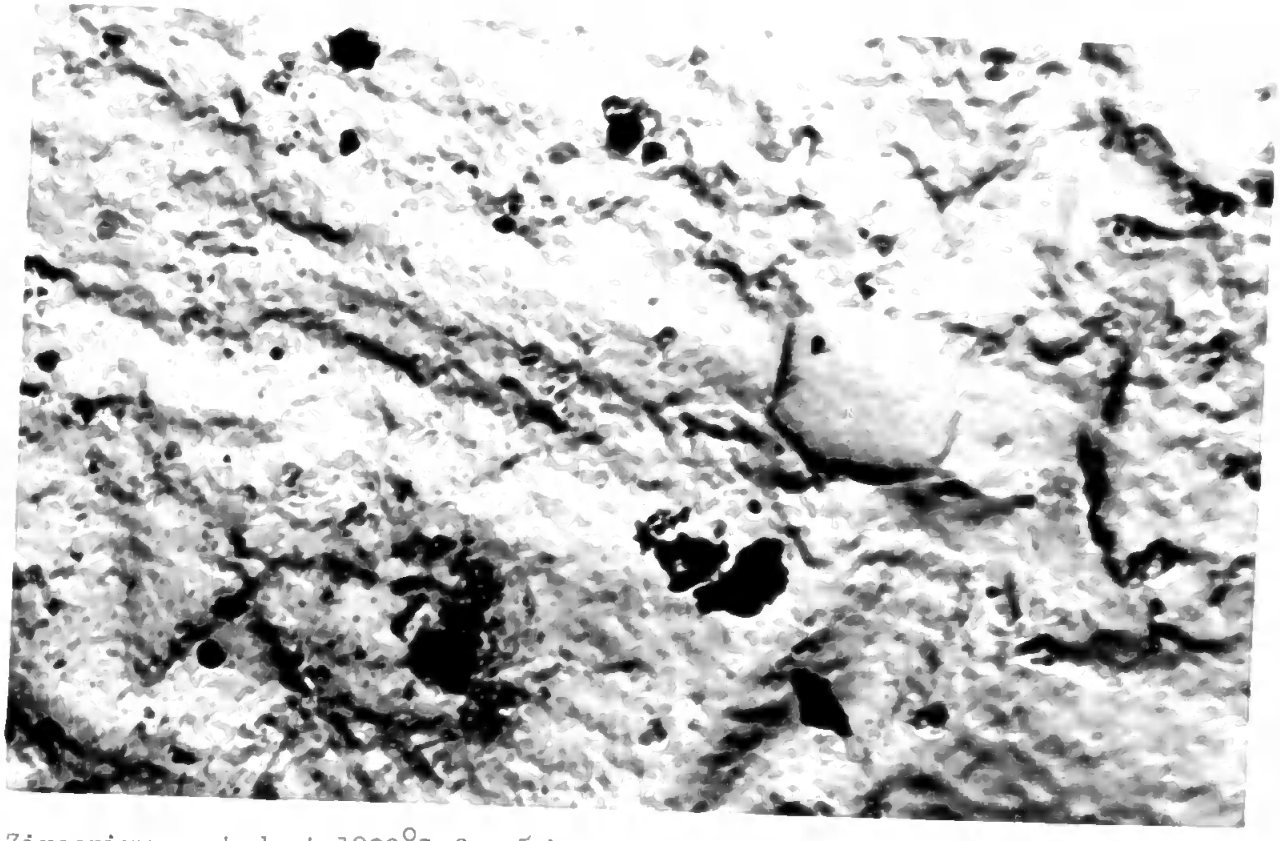

Zirconium coated at 1200°C for 5 hr.

Magnification: 12000 X

(b)

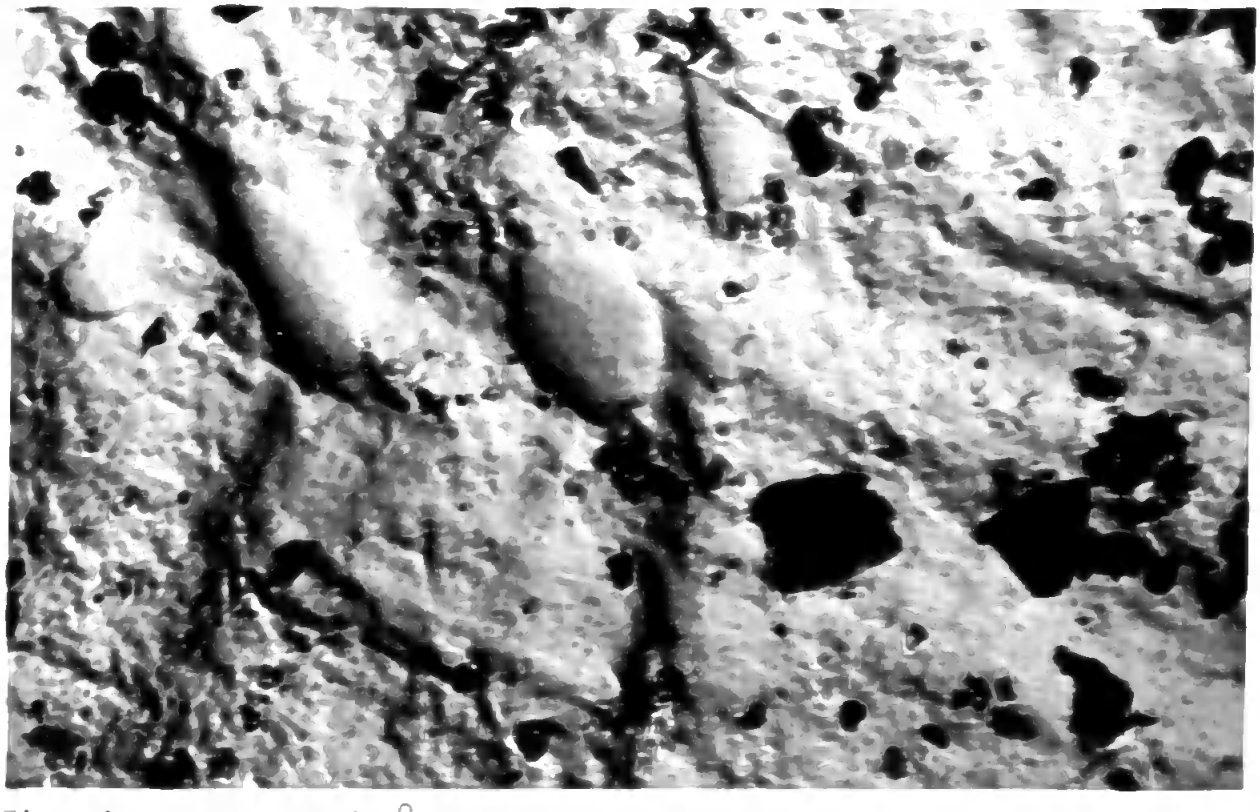

Zirconium coated at 1200°C for 5 hr.

Plate 6.2

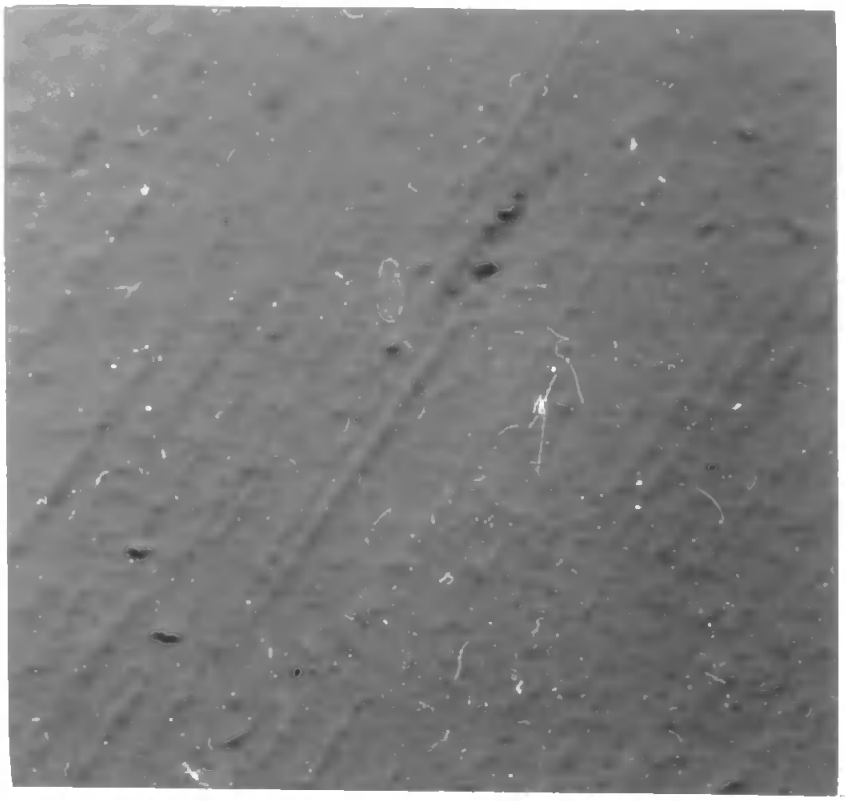

Vanadium uncoated

Magnification: 500 X

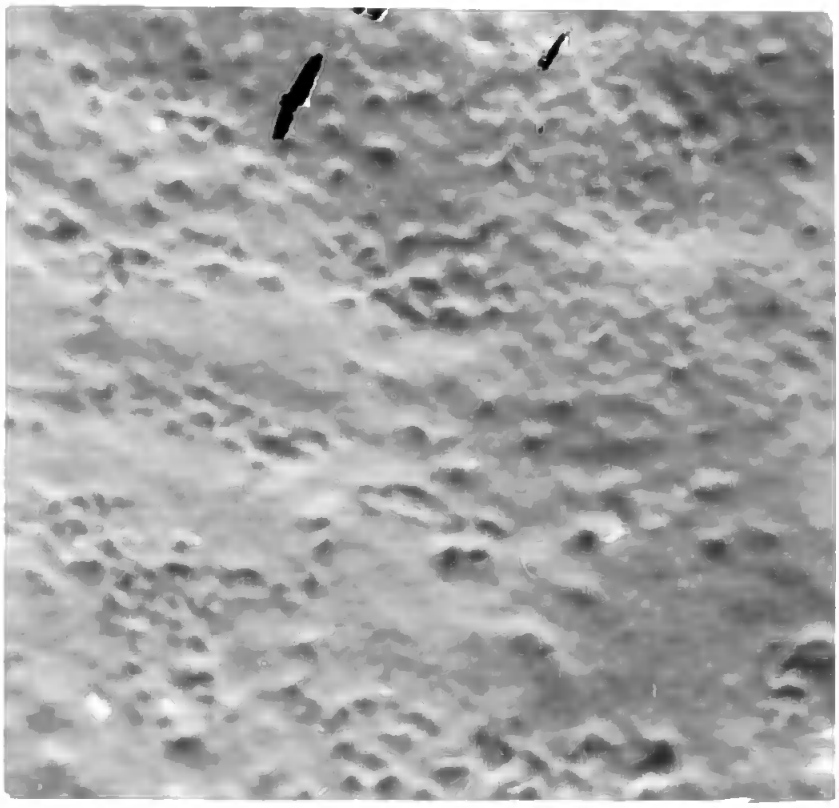

Vanadium coated at 1400 ^{o}C

Plate 6.3

Niobium uncoated

Magnification: 500 X

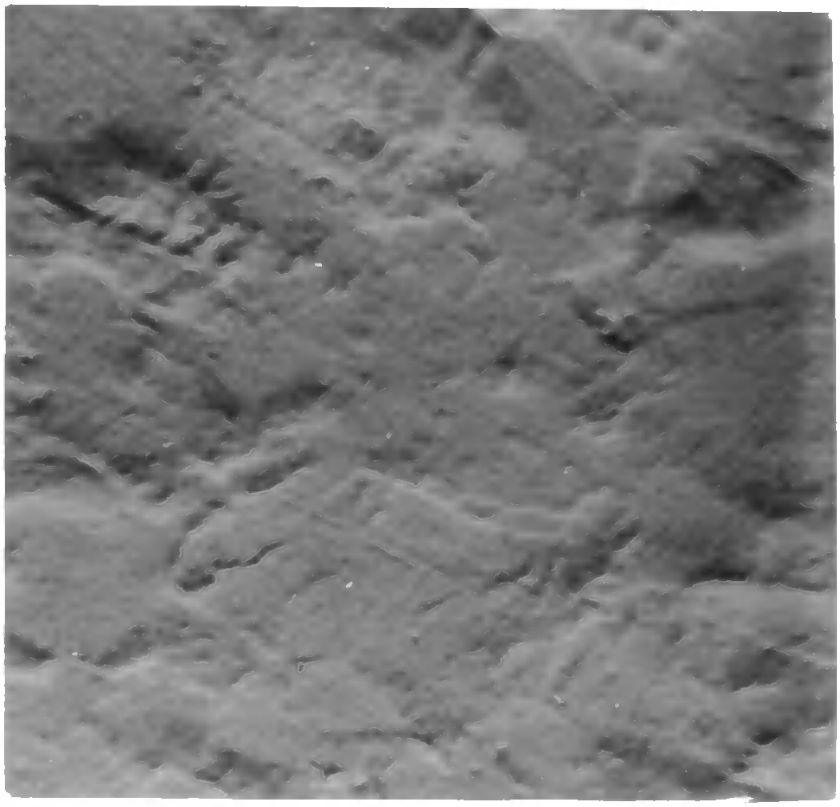

Niobium coated at 1600°C

Plate 6.4

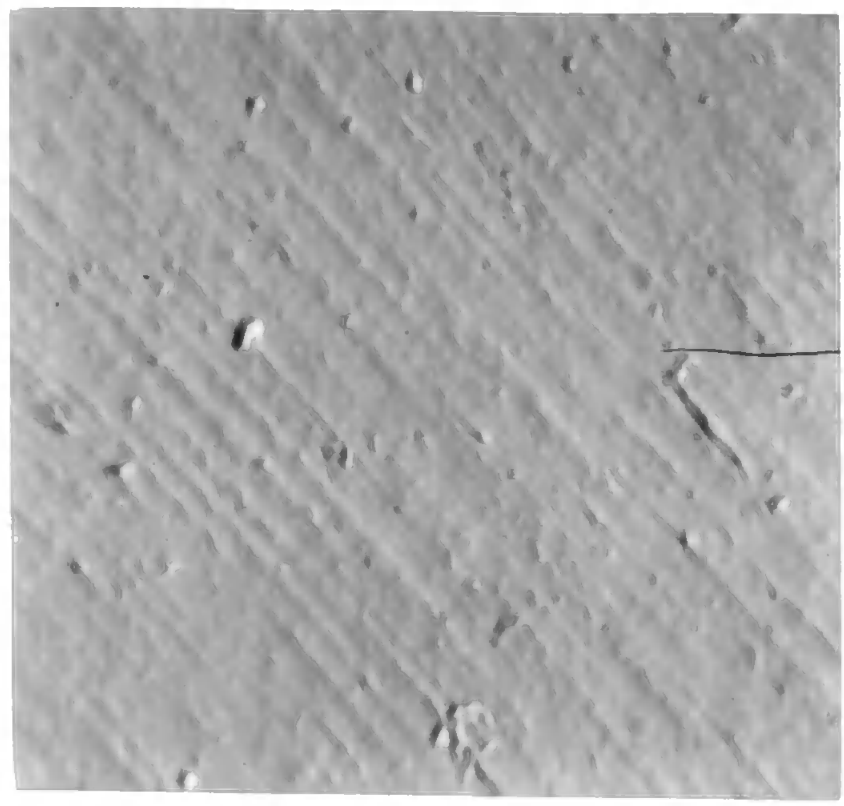

Tantalum uncoated

Magnification: 500 X

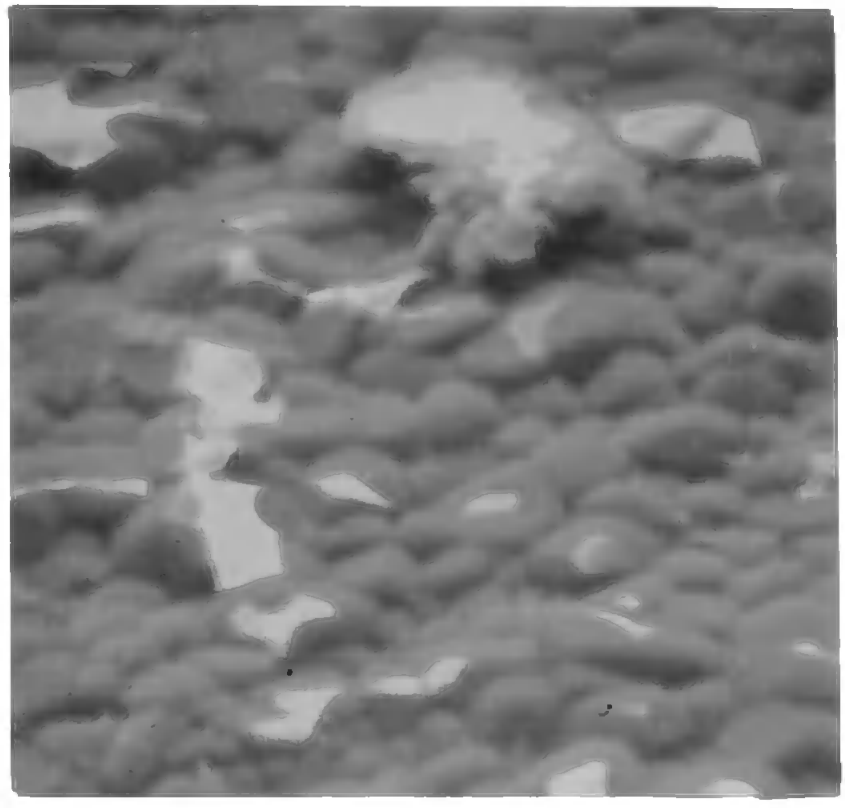

Tantalum coated at 1800 °C

Plate 6.5

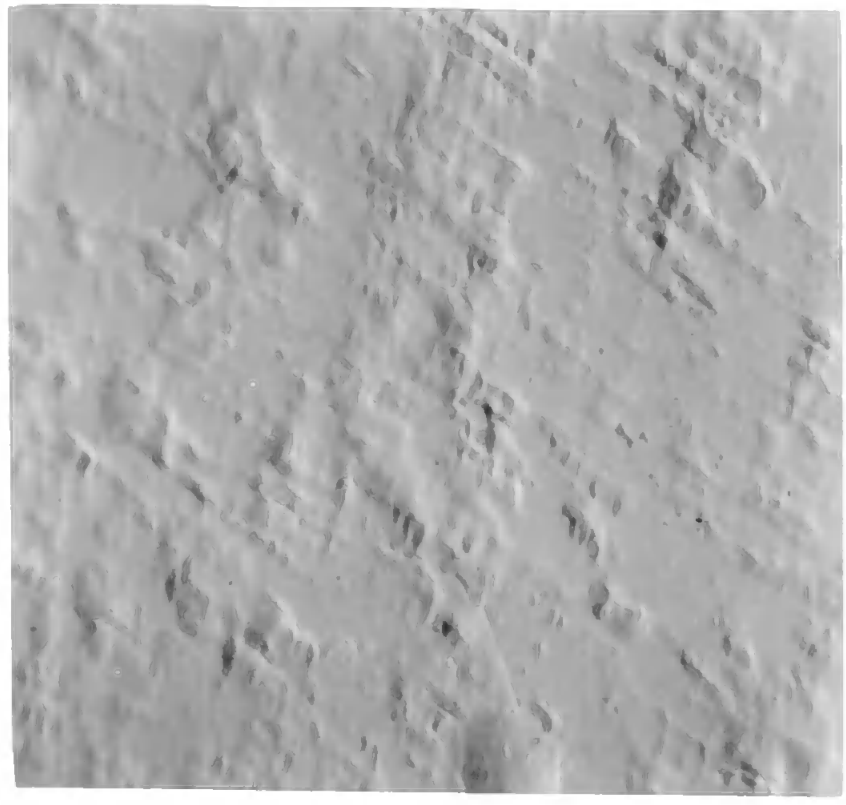

Molybdenum coated at 1600°C

Magnification: 500 X

Molybdenum uncoated

Plate 6.6

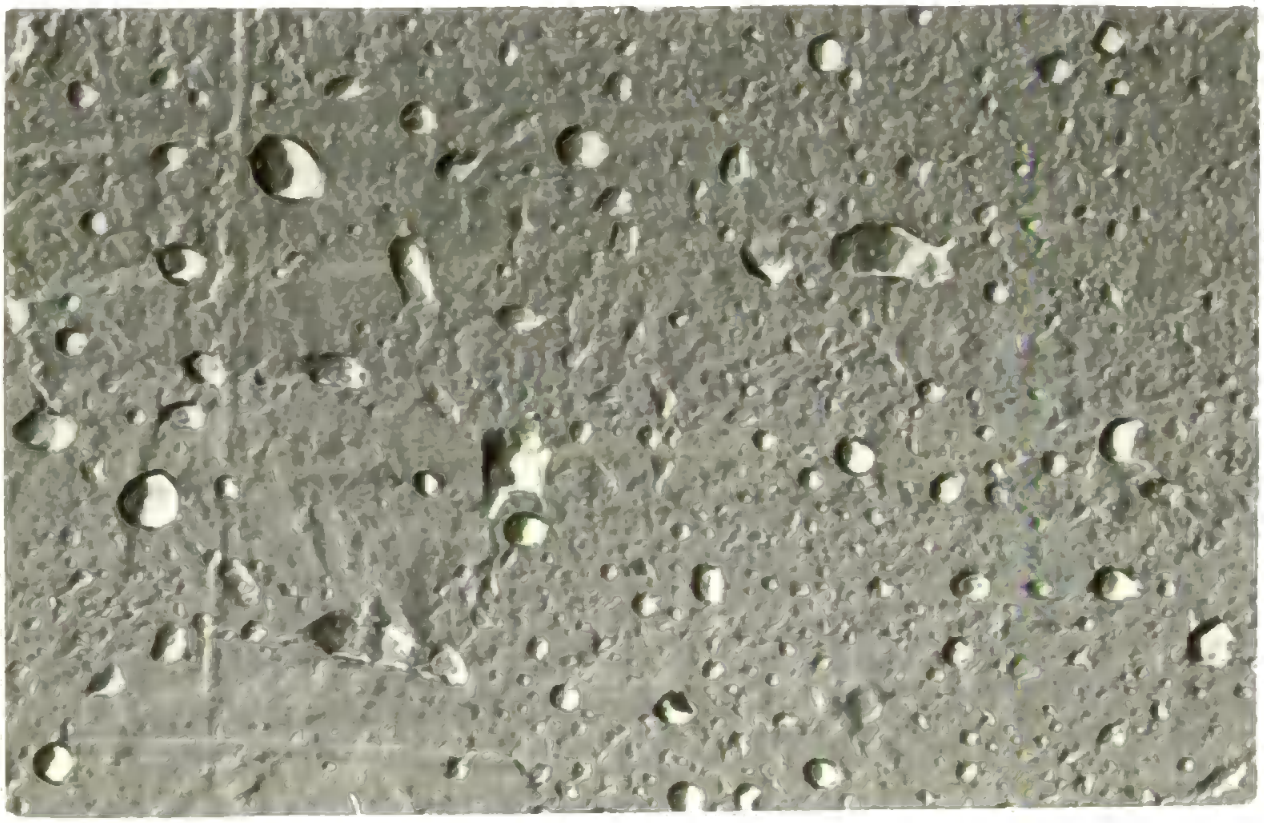

Tungsten uncoated

Magnification: 12000 X

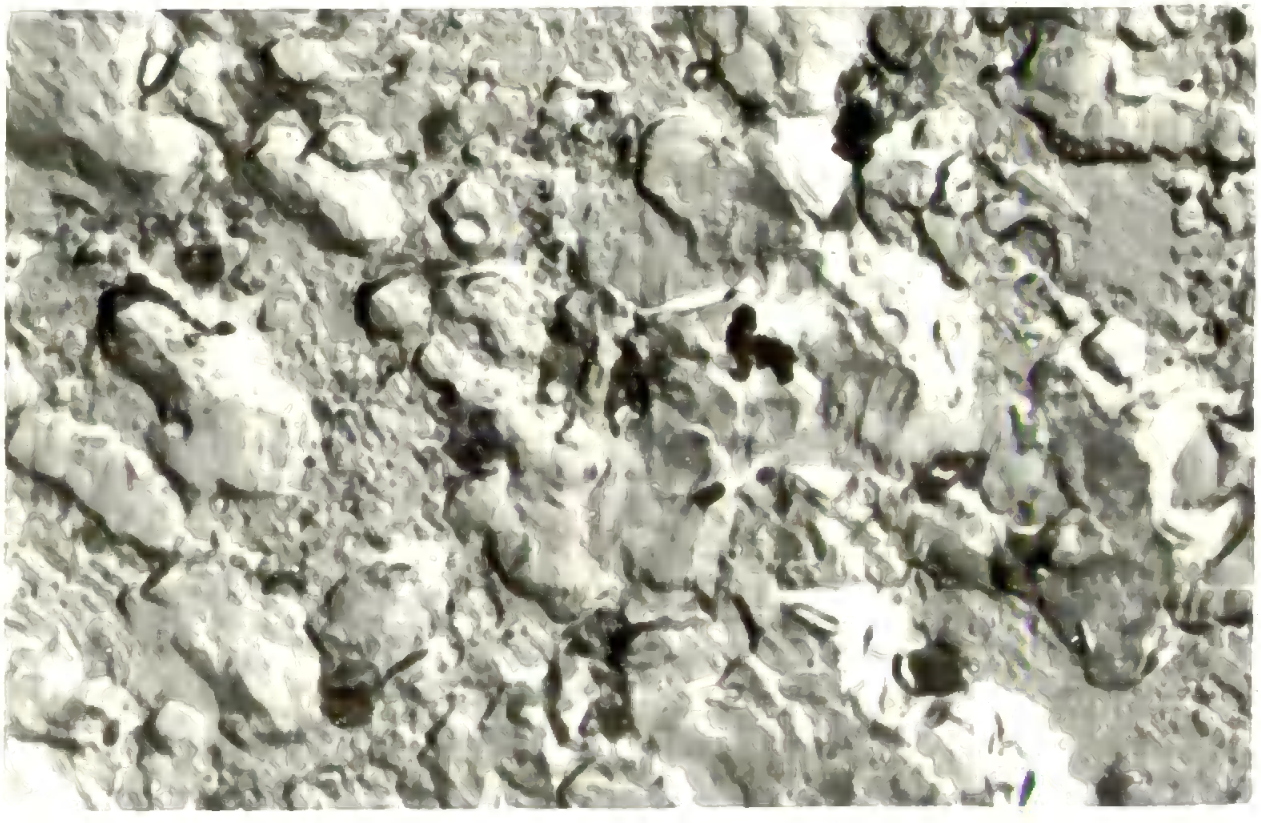

Tungsten coated at 1200°C

differ from those of other workers because of the different compositions of the phases (consisting of borides and carbides) formed on metal surfaces. The variation will depend on the relative proportions of borides and carbides and their solid solutions. The adhesion of the coatings on to the metal surfaces will depend on the volume increases when the metals are converted to borides and carbides (Appendix IV) and the wettability of the components of the system.

The reactions with individual metal foils are discussed below.

6.4.1 Iron

The extent of reaction of boron carbide with iron foil is high compared with that of the powdered metal. The formation of FeB on the coated side and the absence of products on the uncoated side of the metal foil (Table 6.2) indicates incomplete reaction, $B_4C + 4Fe = 4FeB + C$; free carbon possibly forms a solid solution. The microhardness of the coating lies within the values cited in the literature (Katagiri & Fujii, 1971).

6.4.2 Titanium and zirconium

Titanium forms relatively higher proportions of carbide than boride at 1000° and 1200°C with the reaction becoming faster at 1400° and 1600°C, when it is completely converted into boride and carbide.

Zirconium reacts similarly to titanium but tends to form the carbide at a higher temperature and on the uncoated side of the foil. This indicates the preferential diffusion of carbon through the metal and its boride. There is a slight shift in the X-ray diffraction peaks of the products, showing lattice strain in ZrB_2 and ZrC crystals. ZrB_2 and ZrC of fine particle size 3500 Å and 740 Å respectively, are formed on the uncoated side at 1600°C (determined by X-ray line broadening, Section 3.1.3).

6.4.3 Vanadium, niobium and tantalum

The carbide is formed preferentially on the coated side of vanadium in contrast to niobium and tantalum. Vanadium reacts only slightly at 1000°C, the reaction rate becoming faster at higher temperatures. Niobium and tantalum react comparatively faster and form borides in preference to carbides, the latter increasing in proportion at higher temperatures and on the uncoated side of the foils. Vanadium foil forms a higher proportion of carbides compared with the metal powder (cf. Tables 4.4 and 6.2). In the case of niobium and tantalum the products are formed in similar proportions with the foil and powder. Tantalum foil forms lower borides compared with those from the finely powdered metal. A slight shift and broadening of the X-ray diffraction peaks of reaction products of tantalum foil with boron carbide shows crystal lattice strain and formation of very fine crystallites in the range 280 Å - 1050 Å.

6.4.4 Chromium, molybdenum and tungsten

With molybdenum and tungsten foils the reaction products are similar to those formed by the reaction of boron carbide with metal powders (Tables 4.7, 4.8 and 6.2). Carbides are formed only at higher temperatures and on the uncoated side of foils. Chromium foil being very thin does not retain shape and reacts almost completely at 1000°C. This result contrasts with the reaction with metal powder (Glasson & Jones, 1969b).

6.5 Conclusions

At temperatures of 1000°C and above boron carbide reacts with the metal foils selected in this research work. Reaction at 1000°C is comparatively slow and remains incomplete during 5 h heating, being slowest with vanadium. There is a general tendency for the metals of

period IV in the Periodic Table to form carbides in preference to borides. This decreases progressively for periods V and VI. Carbides are formed, in most cases, on the uncoated side of the metal foils (Table 6.2), indicating the preferential diffusion of carbon through the coatings.

The development of crystal lattice strain and the particle size (equivalent spherical diameter) of the crystals is affected by the differences in crystal lattice type and molecular volume of the borides and carbides. X-ray line shifting and broadening show crystal lattice strain in the borides and carbides of zirconium and tantalum and their very fine crystallite size (ZrB_2 3500 Å; ZrC 740 Å; TaC 1959 Å and γ- TaB 280 Å). In some cases the borides and carbides form separate distinct regions on metal foils and have different values of microhardness numbers (Table 6.2). The significance of these results is discussed in Chapter 8 (Section 8.3).

CHAPTER 7
OXIDATION OF BORON CARBIDE, METALS AND METAL BORIDES AND CARBIDES

7.1 Introduction

Information so far available on the oxidation of metal borides and carbides has been summarised in Chapter 2. The kinetics and oxidation products depend mainly on the intrinsic reactivity of the material and available surface at which oxidation could occur. Thus, the chemical reactivity of borides and carbides are controlled generally to a considerable degree by the extent to which they have been sintered during their formation and any subsequent calcination.

The present work extends that of Jones (1970) on the oxidation of finely-divided boron carbide, mainly of submicron crystallite size, used for sintering and hot-pressing with metal powders in Chapters 4 and 5 and for producing metal boride and carbide coatings on metal surfaces in Chapter 6. It compares the oxidation behaviour of coarser boron carbide, mainly above micron crystallite size, with previous work. Further comparison is made with the oxidation of boron suboxide ($B_{6.6}O$), since it was found that below 850°C the oxidation of boron carbide mainly involves boron oxidation only, viz.

$$B_4C + 3O_2 = 2B_2O_3 + C$$

The coated metal surfaces described in Chapter 5 may contain newly-formed metal borides and carbides and also free boron carbide and metal where reaction between the latter material has been incomplete at lower temperatures. Thus, in assessing the susceptibility to oxidation and scaling resistance of the coatings, information is required on the

oxidation of boron carbide in finer or coarser sub-division on the metal surfaces themselves. Oxidation studies have been carried out therefore on a pure metal, its hydride and a substrate of it covered with boron carbide. Titanium has been selected for these studies.

The oxidation of titanium metal surface by reaction with finely divided boron carbide has been described by Jones (1970), and was applied to transition metals generally in the present work (described in Chapter 6). The susceptibility to oxidation and scaling resistance depend primarily on intrinsic reactivity and available surface for oxidation, but additional factors include changes in molecular volume and type of crystal lattice and sintering of the reactants and products. The extent to which the latter factors are important depends on whether the temperature is sufficiently high to permit surface and crystal lattice diffusion, so that increase in surface activity caused by mechanical strain and splitting of crystallites is minimised and sintering is promoted. Changes in molecular volumes when transition metals, metal borides and carbides are oxidised are summarised in Appendix IV. This is complicated if more than one oxide of the metal is formed, which is illustrated in the present research by further investigation of the oxidation of titanium metal compared with its borides and carbides.

7.2 Experimental

7.2.1 Materials

The coarser boron carbide was supplied by Koch Light Industries Limited, titanium hydride by B.D.H. and titanium metal by Alfa Chemicals. The boron sub-oxide ($B_{6.6}O$) was obtained by courtesy of Mr. K.J. Matterson, Borax Consolidated Ltd., Chessington.

7.2.2 Procedure

Samples of the coarser boron carbide (mainly greater than 44 m

crystallite size) were oxidised isothermally in air on a thermal balance (section 3.4). Phases were detected by X-ray powder diffraction.

7.2.3 Results

Oxidation rates for the coarse boron carbide were calculated from weight changes of the samples during calcination shown in Figs. 7.1 - 7.2.

Fig. 7.3 shows the oxidation rates for boron sub-oxide calcined in air isothermally at temperatures between 850° and 1050°C.

Table 7.1 shows the products of oxidation of titanium foil + boron carbide at various temperatures. Fig. 7.4 shows the results of the oxidation of titanium hydride at 850°C.

7.3 Discussion

7.3.1 Oxidation of boron carbide

Below 850°C, the products were mainly boric oxide and carbon, according to the equation $B_4C + 3O_2 = 2B_2O_3 + C$, but at 950 - 1000°C, most of the carbon was oxidised to carbon monoxide and carbon dioxide. The right-hand scales of Fig. 7.1 indicate the percentage oxidation of boron carbide on the basis of (1) no combustion of carbon; and (2) complete combustion of carbon. The limited amount of oxidation recorded at 620°C approximated to first or 2/3-order kinetics (these orders being almost indistinguishable from each other for the limited coverage of the initial stages of the reaction). At higher temperatures, the kinetics become mainly parabolic as indicated by the linearity of the plots in Fig. 7.2 of m^2 vs. time, where m = fractional increase in weight. The parabolic kinetics at temperatures between 720° and 1000°C are in accordance with the mechanism of diffusion through the layers of diboron trioxide and any free carbon surrounding the remaining boron carbide. The energy of activation calculated from the rate constants for the parabolic kinetics at 720° and 850°C for the lower temperature oxidation of the

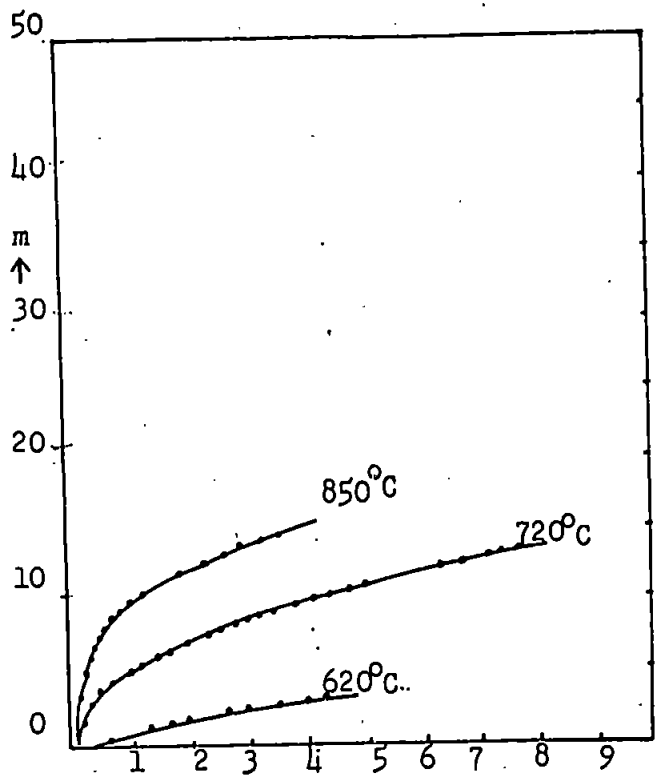

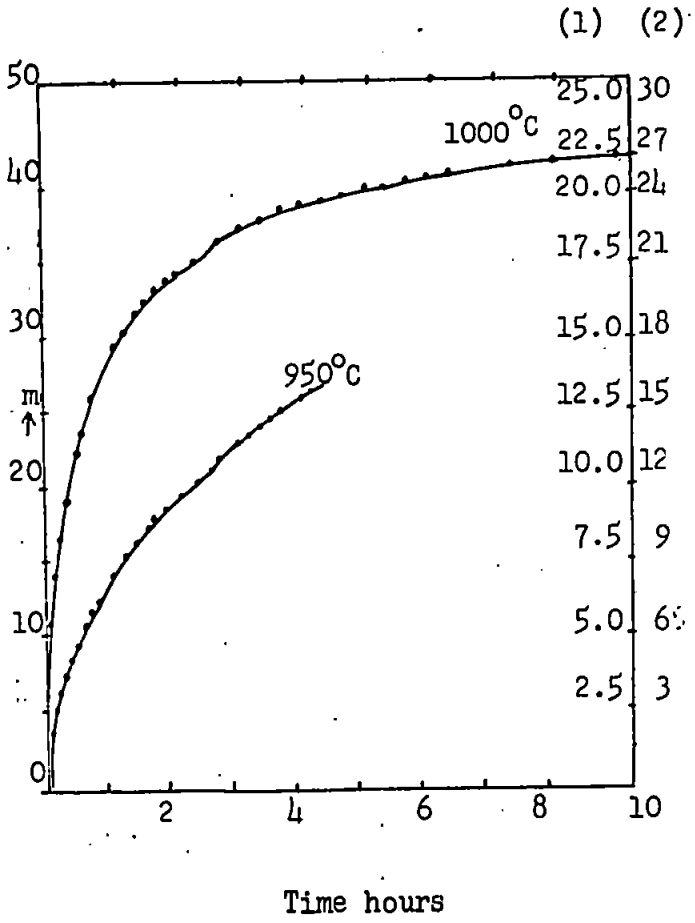

m = fractional increase in weight

Fig. 7.1 Oxidation of boron carbide

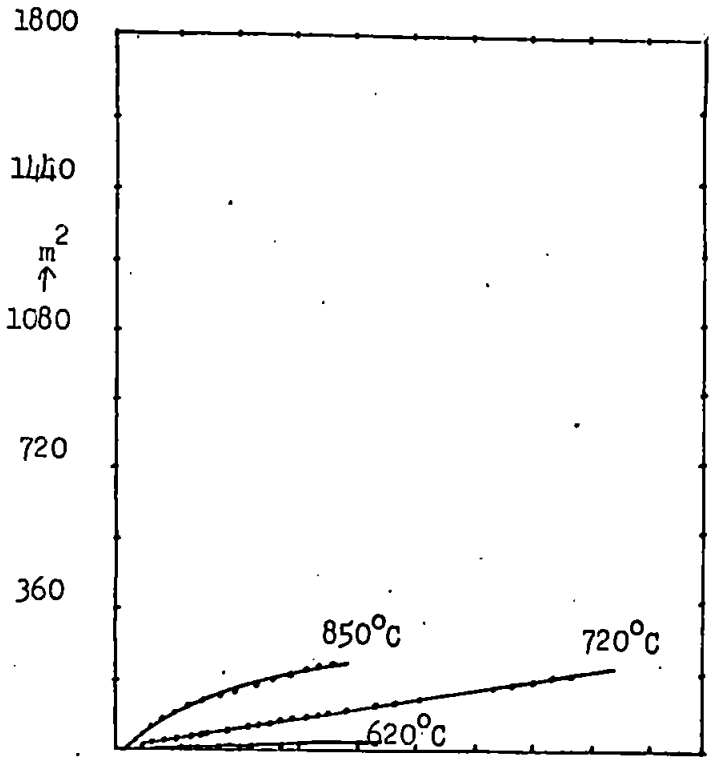

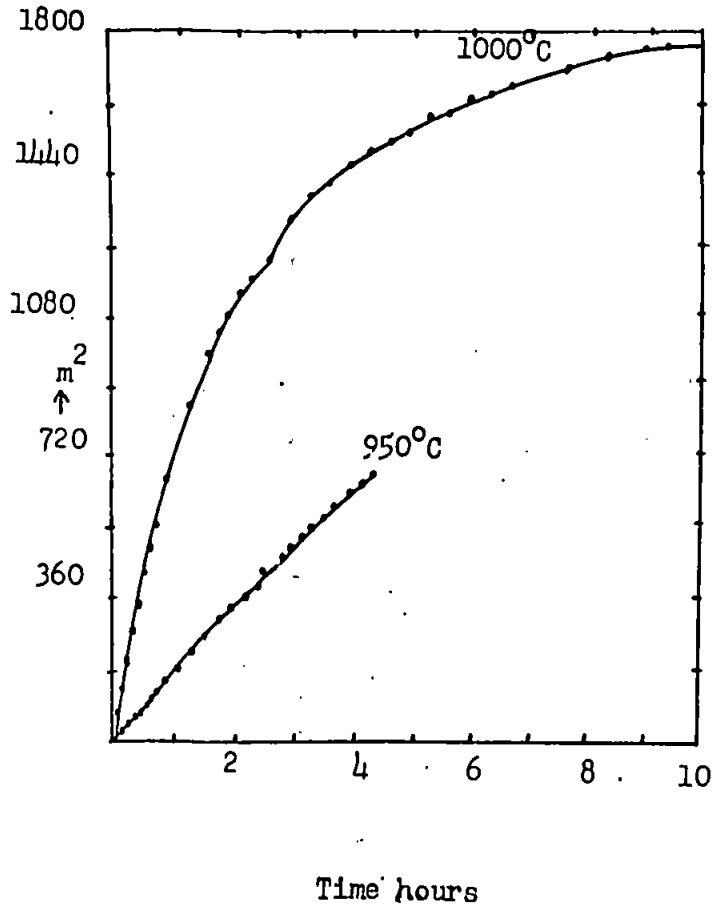

m = fractional increase in weight

Fig. 7.2 Oxidation of boron carbide

Fig. 7.3 Oxidation of $B_{6.6}C$

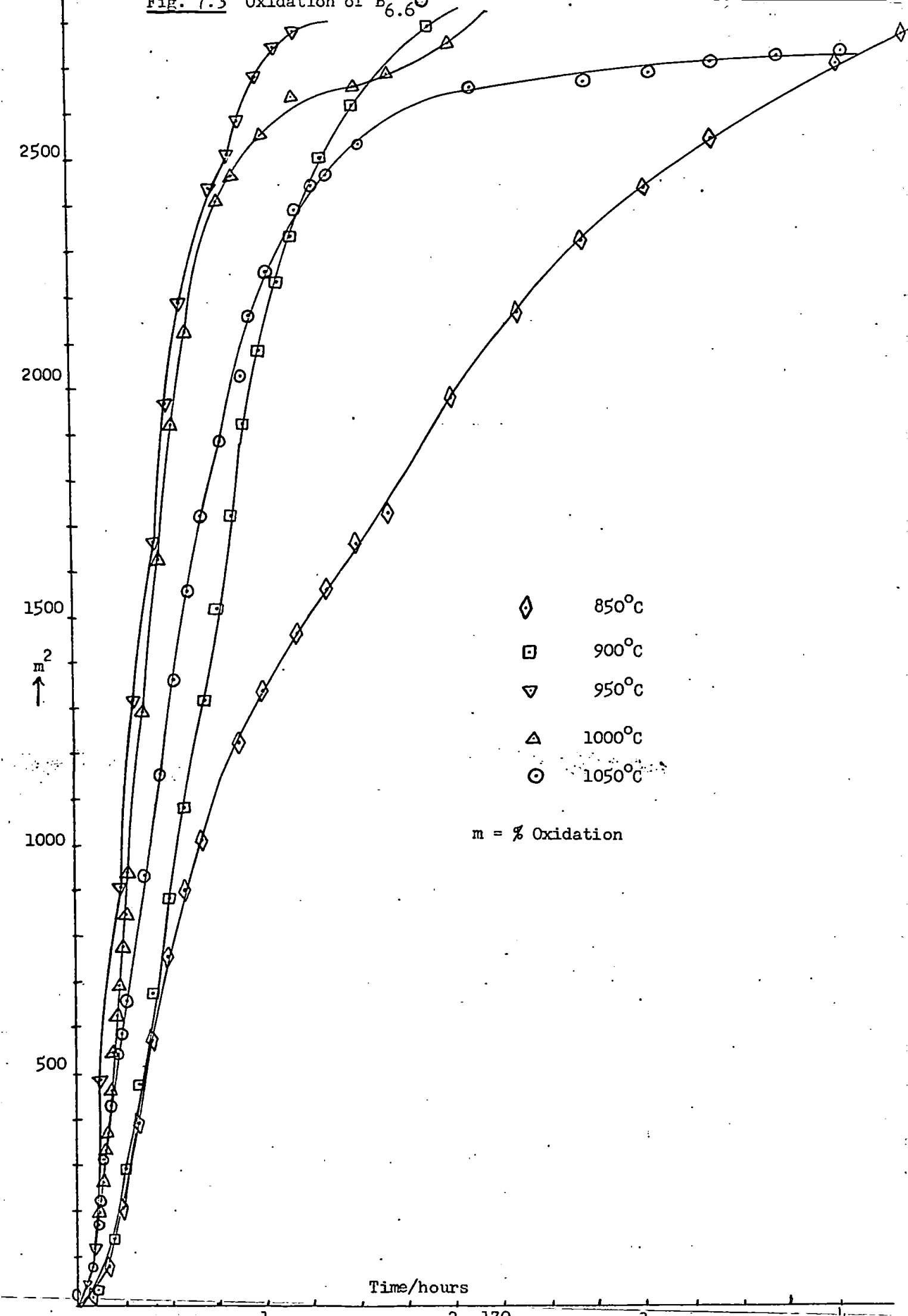

TABLE 7.1

OXIDATION PRODUCTS OF TITANIUM FOIL, SPONGE, AND TITANIUM HYDRIDE AT VARIOUS TEMPERATURES

Temp. °C	Products	Temp. °C	Products
	Titanium foil		Titanium hydride
360	Ti_2O_3	360	TiO
770	TiO, Ti_3O_5	430	TiO
800	TiO_2 (rutile)	500	TiO, TiO_2
910	TiO_2 (rutile)	600	TiO, TiO_2
950	TiO_2 (rutile)	730	TiO, TiO_2 (rutile)
1010	TiO_2 (rutile)	850	TiO, Ti_2O_3, TiO_2
	Titanium foil + B_4C	930	Ti_2O_3, TiO_2 (rutile)
960	TiO_2 (rutile)	1000	TiO_2 (rutile)
1050	TiO_2 (rutile)		
	Titanium sponges		
430	TiO, Ti_2O_3		
480	TiO, Ti_2O_3		
500	TiO, Ti_2O_3		
850	TiO, Ti_2O_3, TiO_2		

Fig. 7.4 Oxidation of titanium hydride at 850°C

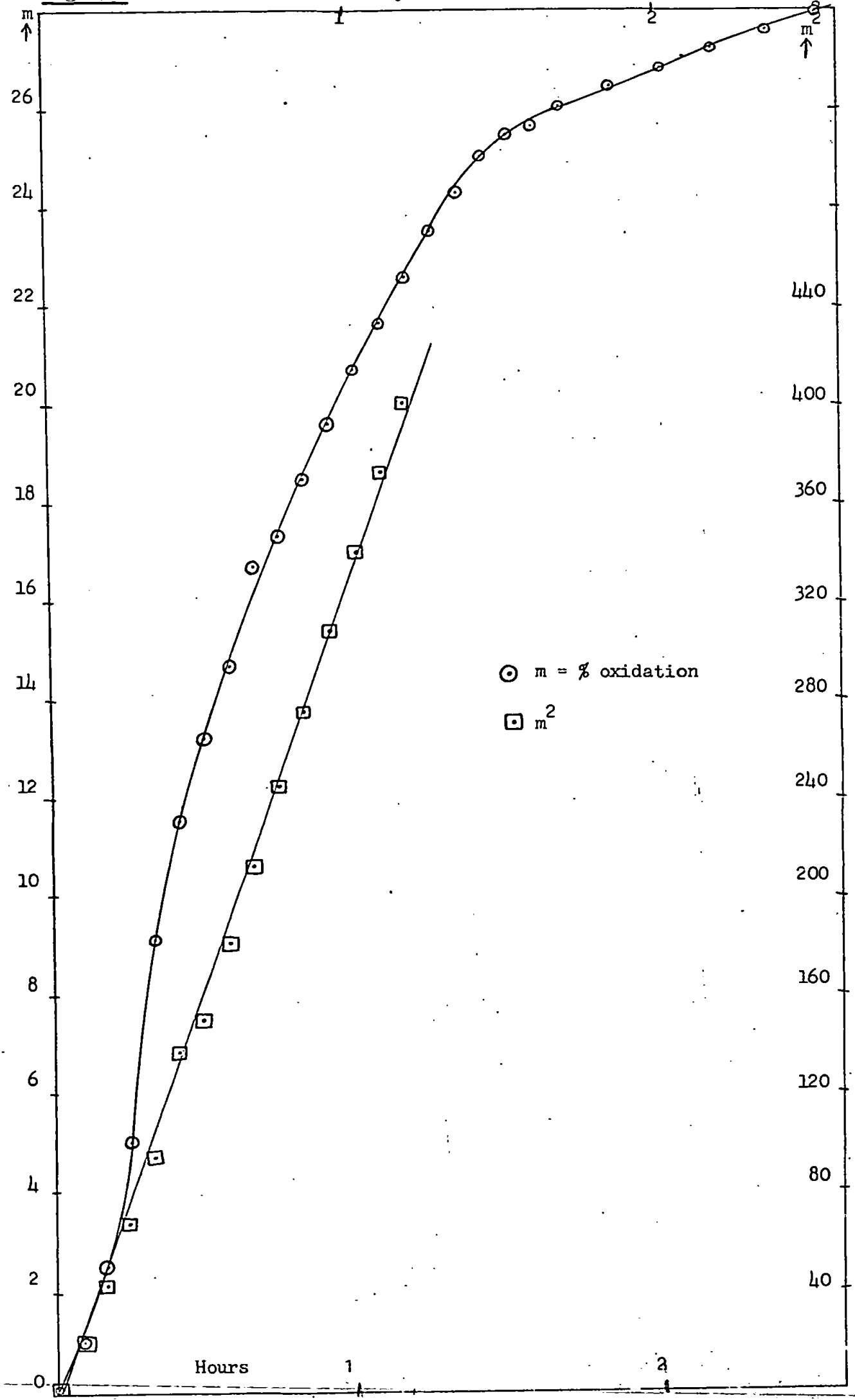

coarser boron carbide is 24 k cal mole^{-1} (5.74 k J mole^{-1}). The value is similar to that obtained by Jones (1970) for the more finely divided sample at 700°, 750° and 850°C.

At higher temperatures, viz. 950° and 1000°C, the rate constants give a value of 95 k cal mole^{-1} (22.73 k J mole^{-1}) for oxidation of the coarser boron carbide sample. The increased activation energy at these higher temperatures corresponds to extensive combustion of the carbon from the boron carbide.

7.3.2 Oxidation of boron sub-oxide

Compared with the boron carbide oxidations, the kinetics of sub-oxide oxidation deviate from the parabolic law at earlier stages especially at the higher temperatures, cf. non-linearity of the plots of m^2 against time (where m = fraction oxidised) in Fig. 7.3. This indicates that the molten boric oxide, B_2O_3, (m.p. 450°C) from the boron sub-oxide causes more rapid coalescence of the particles than in the boron carbide oxidation. The effective thickness of product layer through which the oxygen has to diffuse is more rapidly increased, thereby retarding the reaction, so that the oxidation rates of the boron sub-oxide are almost identical with one another at 950°, 1,000° and 1050°C. The energy of activation between 850° - 1050°C is 13 kcal mole^{-1} (3.1 kJ mole^{-1}) Fig. 7.5. Similar results have been obtained for boron nitride oxidation (Glasson & Jayaweera, 1969; Jayaweera, 1969).

7.3.3 Oxidation of titanium, titanium hydride and titanium + boron carbide

The atmospheric oxidation of titanium foil, sponge or hydride produces mainly lower oxides TiO and Ti_2O_3 at temperatures below 500°C, cf. Table 7.1. Progressively larger amounts of the higher oxide, TiO_2, (rutile) are formed at higher temperatures especially above 850°C when

Fig. 7.5 Arhenius plot for oxidation of $B_{6.6}0$

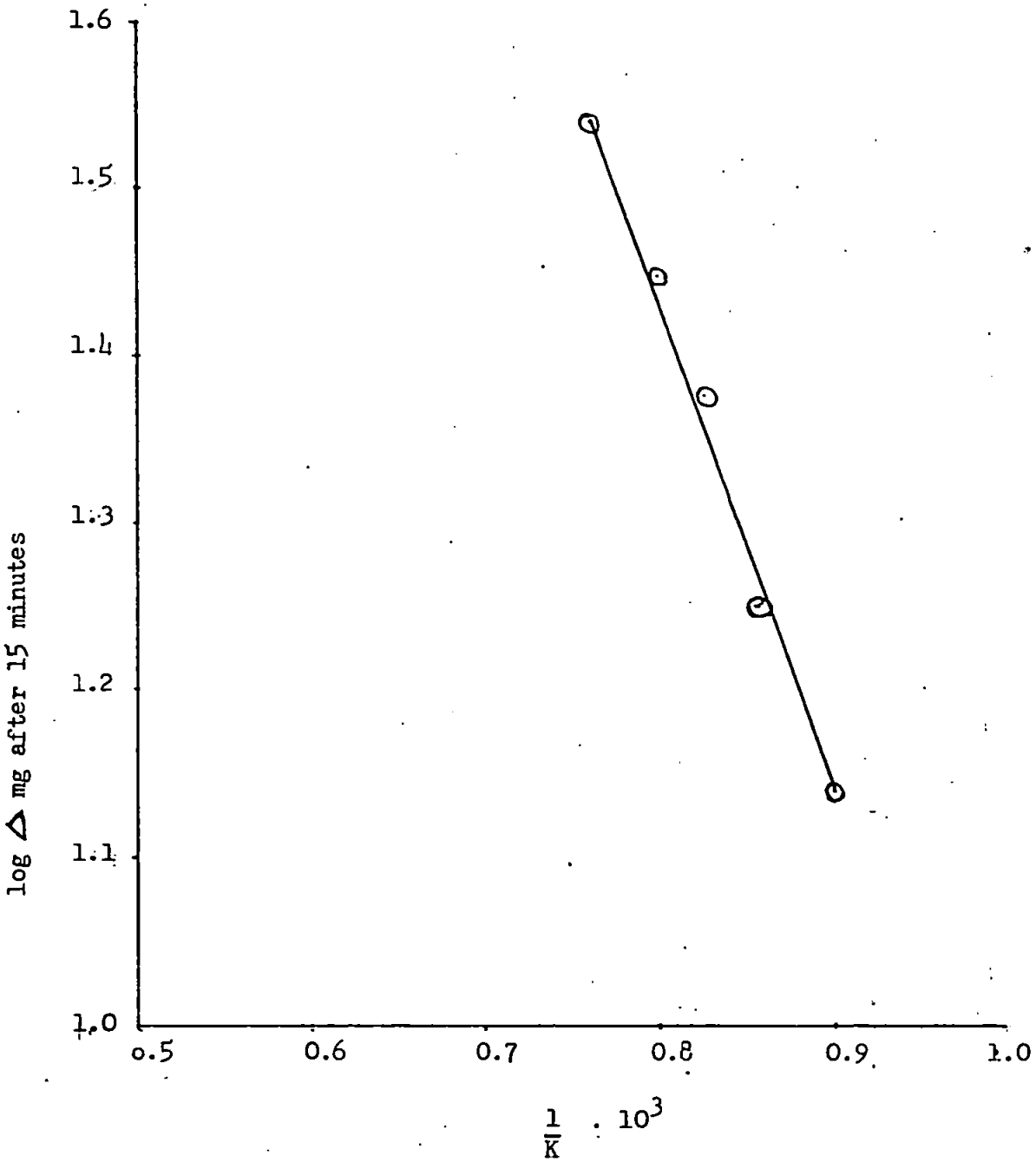

it becomes the main product. Oxidation at these higher temperatures is enhanced by the transformation of the metal from its α to β - crystal form (transition point 882°C) and by crystal lattice diffusion being facilitated above the Tammann temperatures ($\frac{1}{2}$ m.p. in K) of the metal (967K, 694°C) and its dioxide, TiO_2 (1096K, 823°C). This eases strain in the material caused by differences in type of crystal lattice and molecular volume between the metal and its oxide products, cf. Appendix IV. However, the oxidation will be inhibited ultimately by appreciable sintering of the oxide at these temperatures, since this process is enhanced also by crystal lattice diffusion. Accordingly, the kinetics are paralinear with the parabolic law being limited to between about 5 and 25% of the oxidation of the finely-divided titanium hydride, cf. Fig. 7.4. Here, sintering of the oxide product is more significant in that it causes coalescence of the small particles of oxide-coated metal hydride and so more effectively increases the thickness of the oxide layer through which diffusion has to occur to maintain the oxidation of the underlying metal hydride.

The above oxidation behaviour is analogous to that of titanium nitride described by Glasson and Jayaweera (1969) and Jayaweera (1969). The significance of the Tammann temperature in the sintering and agglomeration characteristic of oxide masses during calcination processes has been discussed by Glasson (1967). More recently, Stone (1972) has emphasised its significance for the metal in relation to its oxide during metal oxidation generally, as a basis for relating the oxidation processes to the periodic classification of elements. There is some evidence (Glasson & Maude, 1971) that where a metal, e.g. Ni, has a lower Tammann temperature than its oxide, sintering of the oxide is enhanced.

The oxide layer can sinter also by means of surface diffusion which becomes appreciable above about $\frac{1}{3}$ m.p. in K. Oxidation of titanium boride, TiB_2, and titanium carbide also follow parabolic kinetics at higher temperatures, analogous to titanium metal and nitride and boron carbide. Recent research on oxidation of zirconium boride, ZrB_2, alone (Irving and Worsley, 1968) or with silicon carbide or carbon additives also shows parabolic kinetics (Graham and Tripp, 1970).

Thus, oxidations of the metal coatings containing metal borides, carbides and unchanged boron carbide will follow generally parabolic laws. However, initial rates may be modified by secondary factors described by Gulbransen and Andrews (1951) for oxidation of metals and by Coles, Glasson and Jayaweera (1969) (Jayaweera 1969) for oxidation of nitrides. These factors include decreases in the surface heterogeneity as the reaction proceeds, changes in specific surface or in local surface due to the heat of reaction, solubility effects, impurity concentrations, possible changes in oxide composition and electrical double layer effects. The reactions are initiated by nucleation at defects on the surface after which specific amounts of oxide must be formed, to produce coherent layers. Meanwhile the reactant surfaces (depending on the specific surface of sample) remain exposed to the gas phase, so that the rates increase and approach linearity, cf. the first 5% of the oxidation of titanium hydride (Fig. 7.4). When there is sufficient oxide of rational crystallite size composition, it sinters to form surface films through which normal gaseous diffusion cannot easily occur. The reactions become controlled by solid-state diffusion, with the kinetics becoming parabolic and later linear if sintering becomes extensive, as is the case in the present studies.

CHAPTER 8

CONCLUDING SUMMARY

This thesis describes the results of investigation into the reactivity of boron carbide towards some transition metals and to oxidation. This research forms a part of a wider study of non-oxide ceramics and refractories (nitrides, borides, carbides and silicides) undertaken at John Graymore Chemistry Laboratories, Plymouth Polytechnic (Glasson & Jayaweera, 1969; Jayaweera, 1969; Ali, 1970; Brockington, Glasson, Jayaweera & Jones, 1973; Brockington, 1973).

The reactivity of boron carbide with metal powders and the sintering of the product under normal as well as high pressure is investigated. The boronizing of metal foils with boron carbide with a view to improving their microhardness has been studied. Oxidation of boron carbide and titanium up to 1000°C has been investigated.

8.1 Pressureless sintering of boron carbide with additives

The general effect of metal additives, is to promote the sintering of boron carbide at temperatures above 1000°C and below its melting point. The changes in crystallite size and shape are correlated with temperature and the amount and nature of additive. The differences in the nature of the bonding of the original material and the products bear an effect on the results; so do the differences in the molecular volume and lattice-type. Iron was found to be the most effective sintering agent. The results are discussed in relation to those of earlier workers.

8.2 Hot pressing of boron carbide with additives

Similar reactions under hot pressing conditions were studied and the densities of the products measured. Pressure is an additional factor which promotes sintering and densification.

The simultaneous application of pressure and temperature in an efficient system, where high temperatures are followed immediately by a pressure rise, is the most effective means of achieving maximum densification (Stringer & Williams, 1967).

For most borides and carbides, including boron carbide, final consolidation of the material is not achieved until a temperature of about 0.9 T is reached (where T K = m.p.). This is explicable in terms of their increased covalency compared with many oxides and ionic nitrides inhibiting diffusion at the surface and at the grain boundary, cf. incomplete compaction of diamond and borazon (cubic BN) to a pore-free state by sintering with or without pressure, Compaction of boron carbide without additive to almost theoretical density was achieved only by hot pressing to a temperature above 2300°C (ca 0.95 T) and at pressures between 12 - 19 tons in^{-2} (1.8 - 2.8 x 10^8 Nm^{-2}). This procedure is limited by working pressure of the graphite mould sets, even though the powder rapidly consolidates to about 30% pore density at 1000°C. The results are in accordance with the final densification occuring by a process of plastic flow when the pressure exceeds the critical stresses and causes deformation of asperities at temperatures relatively close to the melting point.

8.3 Microstructure of borides and carbides formed on metal surfaces

The results obtained on the formation of boride and carbide coatings on the metal foils show that there is a considerable variation in the nature and composition of the products depending on the particular metal substrate and the temperature. The boride phases ranged in composition from boron-rich to metal-rich ones with metals such as tantalum, molybdenum and tungsten, where as the metals titanium, zirconium and niobium gave a single boride phase of the MB_2 composition.

Generally, the borides appear to have been formed by the diffusion of metal atoms into the boron network, whilst the reverse mechanism occurs for the production of carbides. This phenomenon could be explained by considering the electron availability of the species involved and free energies of the formation of the product phases.

The increase in microhardness of the metal when subjected to such treatment can be explained in a similar way and is in line with the postulates of Samsonov et al (1970a). The coatings obtained adhered to the metal substrates. The technique represents a process whereby machine parts can be 'case hardened'. Since such systems are readily prone to oxidation at elevated temperatures, the exclusion of oxygen is essential unless a protective coating of the product oxide is maintained, e.g. TiO_2, ZrO_2.

8.4 Oxidation of boron carbide and some metal borides and carbides

Factors influencing the oxidation of the metals, metal borides and carbides and unreacted boron carbide in the metal coatings are investigated. The susceptibility to oxidation and scaling resistance depend primarily on the intrinsic reactivity and available surface for oxidations, but additional factors include changes in molecular volume and the type of crystal lattice and sintering of the reactants and products. The extent to which the latter factors are important depends on whether the temperature is sufficiently high to permit surface and crystal lattice diffusion, so that increase in surface activity caused by mechanical strain and splitting of crystallites is minimised and sintering is promoted. Oxidations of the metals and the components of their coatings are often controlled by solid-state diffusion processes, giving parabolic kinetics which ultimately become linear if the material sinters extensively. Initial rates and

kinetics may be modified by secondary factors, which are discussed. The oxidation behaviour of the above materials is similar to that of metal nitrides. The Tammann temperatures of the reactants and products are significant in the sintering and agglomeration of the oxidised material.

8.5 Future developments

Further research would be advantageous on the hot pressing of boron carbide with iron (and possibly cobalt, nickel or chromium) additives at temperatures between about 1900° and 2300°C (80 - 95% of m.p. boron carbide in K), in which the composition and densification are correlated with the mechanical strength and hardness. The effect of rational grain size composition of the original boron carbide on the densification, and how far an optimum grain size composition could be obtained by sintering during production or subsequent milling, would be of interest also.

Consolidation of metal borides by cold pressing followed by heating the "green" compact should be studied, using suitable additives to give "cermets", cf. earlier examples of "hard" metals and WC/Co system (Schwarzkopf & Kieffer, 1960). Future work should cover the rate of formation of boride coatings on metal substrates, followed ideally by the use of microprobe analysis to identify composition and phase over small regions. The electrical properties of these films deserve some attention for an indication of the electronic states of the phases as well as possible industrial uses. Application of coating by techniques such as flame and plasma spraying, gaseous and salt-bath deposition should be considered. An investigation of resistance of the boride and carbide coatings to wear and oxidation and their comparison with the original metal foils would be an interesting subject for further research.

REFERENCES

Alexander, B.M., & Baluffi, R.W.: J.Metals, 1950, 2, 1219.

Ali, I.: Ph.D. Thesis (CNAA), 1970.

Alliegro, R.A.: Ceramic Age, 1970, 86(12), 32-34.

Aravamuthan, V. et al: Chem.Age, India, 1969, 20(4), 281-296.

Aronsson, B.: "Modern Materials" (Ed. H. Hausner), 1960, Vol.II, p.54 & 143 et sec. (New York: Academic Press).

Aronsson, B., Lundstorm, T., & Rundquist, S.: "Borides, Silicides and Phosphides", 1965, (London: Methuen).

Artamonov, Ya.A., & Bovkun, G.A.: Tugoplavkie Karbidy, 1970, 217-220 (N.L.L. translation, RTS 7289: June 1972).

Bakarinova, V.I., Savitskii, E.M., Arabei, B.G., & Salibekov, S.E.: Izv.Adad.Nauk.SSSR, Neorg.Mater., 1970, 6(11), 2071-2072.

Barnes, R.G., Creel, R.B., & Torgeson, D.R.: J.Chem.Phys., 1970, 53(9), 3762-3763.

Biddulph, R.H.: U.S. patent no. 3,505,438, 1970.

Biddulph, R.H., Matterson, K.J., Brown, A.C.: Private communication.

Bliznakov, G., & Peshev, P.: Izv.Old.Khim.Nauki, Bulg.Akad.Nauk., 1970, 2(3), 391-400.

Branscomb, T.M., & Hunter, O.Jr.: J.Appl.Phys., 1971, 42(6), 2309-2315.

Brewer, L., Searcy, A.W., Templeton, D.H., & Dauben, C.H.: J.Am.Ceram. Soc., 1950, 33, 291.

Brockington, B.J., Glasson, D.R., Jayaweera, S.A.A., Jones, J.A.: Journes d'etude sur les nitrures, Rennes, Brittany, France 10-11 May 1973.

Brockington, B.J.: Ph.D. Thesis (CNAA), 1973.

Brunauer, P.H., Emmett, P.H., & Teller, E.: J.Amer.Chem.Soc., 1938, 60, 309.

Brunauer, P.H., Demming, Demming & Teller, E.: J.Am.Chem.Soc., 1940, 62, 1723.

Bryjan, E., Missol, W., & Bojarskii, Z., Hutnik, Katowice, 1956, 23, 117.

Budnikov, P.P.: "Solid State Chemistry", 1966, p.75, translated Shaw, K., 1968 (Lond.: McLaren).

Burykina, A.L. et al: Zashch.Pokrytiya Metal, 1970, No.3, 178-184.

Burykina, A.L., & Evtushok, T.M.: Zhatostoikie i Teplostoikie Pokrytiya: Trudy 4th Vses. Soveschch.Po.Zharost.Pokrytiyam, 1968. Leningrad, Nauka, 1969, 89-94 (N.L.L. translation, RTS 7322: July 1972).

Campbell, I.E., Powell, C.F., Nowicki, D.H., & Gonser, B.W.: J.Electrochem.Soc., 1949, 96, 318.

Carruthers, T.G., & Wheat, T.A.: Proc.Br.Ceram.Soc., 1965, No.5, p.259.

Castaing, J., Danan, J., & Rieux, M.: Solid State Commn., 1972, 10(6), 563-565

Chiotti, P.: J.Am.Ceram.Soc., 1952, 35, 123.

Clougherty, E.V., Peters, E.T., Kalish, D.: Mater.Process.'s 70's Nat. SAMPE, 1969, 297-308.

Coble, R.L.: J.Am.Ceram.Soc., 1958, 41, 55.

Coble, R.L.: J.Appl.Phys., 1961, 32, 787, 793.

Coble, R.L., & Ellis, J.S.: J.Am.Ceram.Soc., 1963, 46, 493.

Coble, R.L.: "Fundamental Phenomena in Material Sciences", 1964, 1 (New York: Plenum Press).

Coble, R.L.: Phys.Sintering, 1969, 1, 1/3.

Cochran, A.A., & Stephenson, J.B.: Met.Trans., 1970, 1(10), 2875-2880.

Cohen, R.L., Eibshuetz, M., & West, K.W.: Phys.Rev.Lett., 1970, 24(8), 383-386.

Cueilleron, J., Lahet, G., & Thevenot, F., & Paris, R.A.: J.Less-Common Metals, 1971, 24(3), 317-322.

Dan'kin, A.A.: Porosh.Met., 1970, 10(10), 841-844.

Davies, M.W., & Phennah, P.J.: J.Appl.Chem., 1959, 9, 213.

Dawihl, W.: Z.Metallk., 1952, 43, 138.

Davydov, V.S., Ermakov, B.G., Sokolov, V.V.: Tugoplavkie Karbidy, 1970, 20-23 (N.L.L. translation, RTS 7287: Sept. 1972).

Deger, M., Riehle, M., & Schatt, W.: Neue Huette, 1972, 17(6), 341-348.

Degtev, G.F. et al: Izvestiya VUZ Mashinostroenic, 1972, (3), 127-131 (N.L.L. translation, RTS 7940: 1972).

De Vynck, I.: Silicates Ind., 1970, 35(12), 308-314; 1971, 36(1), 1721, 32, (2), 49-54.

Dominey, D.A.: J.Chem.Soc., 1968, A. 712.

Ducrot, A., & Poulain, J.C.: Ger.Offen. 1,960,973 (Cl. $C_{23}b$), 25 June 1970.

Duwez, P., & Odell, F.: J.Electrochem.Soc., 1950, 97, 299.

Easterling, K.E., & Tholen, A.R.: Planseeber Pulvermet., 1970, 18, 81.

Easterling, K.E., & Tholen, A.R.: Z.Metallk., 1970, 61(12), 928-934.

Ellingham, H.J.T.: J.Soc.Chem.Ind., 1944, 63, 125.

Eremenko, V.N., & Naidich, Yu.V.: Zh.Neorgan Khimii, 1959, (9), 2052.

Etourneau, J., Mercurio, J.P., Naslain, R., & Hagenmuller, P.J.: Solid State Chem., 1970, 2(3), 332-342.

Fedorchenko, I.M., & Skorokh, V.V.: Porosh.Metall., 1967, No.10(58), 29; "Progress in Inorganic Materials", 50th Anniversary Publication, Akud.Nauk SSSR, Oct. 1967, p.1.

Fisk, Z., Cooper, A.S., Schmidt, P.H., & Castellano, R.N.: Mater. Res.Bull., 1972, 7(4), 285-288.

Fomichev, O.I., Zhluktanko, E.I., Katkov, V.F., & Spiridonova, I.M.: Zh.Fiz.Khim., 1971, 45(10), 2688-2689.

Frenkel, J.: J.Phys., 1945, 9, No.5.

Gangler, J.J.: High temp. - High pressure, 1971, 3, 487-502.

Geguzin, Y.E., & Partskaya, L.N.: Porosh.Metall., 1967, No.1(49).

Georgieva, G.G., Lashko, N.F., & Sorokina, K.P.: Khim.Svoistva Metody Anal. Tugoplavkikh Soedin., 1969, 91-97 (N.L.L. translation, RTS 7318: June 1972).

Gert, L.M., Babadzakhryapin, A.A., Minashkin, V.I.: Izv.Akad.Nauk. Neorg.Mater., 1969, 5(12), 2198-99.

Gessinger, G.H.: Z.Metallk., 1970, 61(1), 53.

Gessinger, G.H.: Mod.Develop.Powder Met., 1971, 4, 267-279.

Gingerich, K.A.: J.Chem.Phys., 1970, 53(2).

Glaser, F.W.: J.Metals, N.Y., 1952, 4, 391.

Glaser, F.W., Moskowitz, D., & Post, B.: J.Appl.Phys., 1953, 24, 731.

Glasson, D.R.: J.Chem.Soc., 1956, 1506.

Glasson, D.R.: J.Appl.Chem., 1958, 8, pp. 793-797.

Glasson, D.R.: J.Appl.Chem., Lond., March, 1964, 14, 121, 125.

Glasson, D.R.: J.Appl.Chem., Lond., 1967, 17, 91.

Glasson, D.R., & Jayaweera, S.A.A.: J.Appl.Chem., Lond., 1968, 18, 65.

Glasson, D.R., & Jayaweera, S.A.A.: J.Appl.Chem., Lond., 1969, 19, 178

Glasson, D.R., & Jones, J.A.: J.Appl.Chem., 1969, 19, 125.

Glasson, D.R., & Jones, J.A.: J.Appl.Chem., 1969, 19, 37.

Glasson, D.R., & Lindstead-Smith, D.E.D.: 10th Conference on vacuum microbalance techniques, Brunel University, Uxbridge, England, July 1972.

Goldschmidt, H.J.: "Interstitial Alloys", 1967 (London: Butterworth).

Graham, H.C., & Tripp, W.C.: AGARD Conf.Proc., 1970, 52, 9.

Graham, H.C.: U.S.Nat.Tech.Inform.Serv., AD, Rep. 1972, No.740941.

Gregg, S.J., & Windsor, G.W.: Analyst, Lond., 1945, 70, 336.

Gregg, S.J.: J.Chem.Soc., 1946, 561.

Gregg, S.J.: J.Chem.Soc., 1955, 1438.

Gregg, S.J., & Sing, K.S.W.: "Adsorption, Surface Area and Porosity", Academic Press, London (1967).

Grimshaw, R.W., Heaton, E., & Roberts, A.L.: Trans.Ceram.Soc., 1945, 44, 76.

Groshev, V.I., Maskayev, A.S., Nezhevenko, L.B., & Plotoratsky, N.I.: Porosh.Met., 1967, No.1(49), 108.

Gulbransen, E.A., & Andrew, K.F.: J.Electrochem.Soc., 1951, 98, 241.

Gurin, V.N., Obukhov, A.P., & Korsukova, M.M.: Terent, eva, S.p., Kozlova, I.R., Planseeber. Pulvermet. 1971, 19(2), 86-90.

Hägg, G.: Metallwirt., Metalwiss., Metaltech., 1931, 10, 387.

Hägg, G.: Z.Phys.Chem., 1931, (B), 12, 33.

Hamijan, H., & Lidman, W.: J.Am.Ceram.Soc., 1952, 35, 44.

Hansen, M., & Anderko, K.: "Constitution of Binary Alloys", 1958, p.14 et seq. (New York: McGraw-Hill).

Harvey, M.R.: Diss.Abs., 1965, 25, 6510.

Herring, C.: J.Appl.Phys., 1950, 21, 437.

Higashi, I., & Atoda, T.: J.Cryst.Growth, 1970, 7(2), 251-253.

Hirsch, P.B., Howie, A., Nicholson, R.B., Pashley, D.W., & Whelan, M.J.: "Electron Microscopy of Thin Crystals", 1965 (London: Butterworth).

Hosokaiva, K., Kogakubu, K.D.: Kinzoku hyomen gijutsu, 1972, 23(4) 211-6.

Houldsworth, H.S., & Coble, J.W.: Trans.Ceram.Soc., 1922, 22, 111.

Hüttig, G.F.: Kolloidzeitschrift, 1941, 97, 281.

Hyde, G.F., et al: U.S. Patent No. 3,556,747, 1971.

Irving, R.J., & Worsley, I.G.: J.Less-Common Metals, 1968, 16(2), 103.

James, F.W., & Biddulph, R.H.: Private communication.

JANAF, Thermochemical Tables, 1960-1971, P.B. 168,370 (New York: Dowchemical Co.).

Janes, S., & Nixdorf, J.: Ber.Ceut.Keram.Ges., 1969, 46(2), 60-64.

Jayaweera, S.A.A.: Ph.D. Thesis (London University) 1969.

Johnson, D.L.: Mater.Sci.Res., 1969a, 4, 331-348.

Johnson, D.L.: J.Am.Ceram.Soc., 1969b, 52(10), 562-563.

Johnson, D.L.: Phys.of Sintering, 1969c, 1(1-3), B_1-B_{22}.

Johnson, D.L.: J.Am.Ceram.Soc., 1970, 53(10), 574-577.

Johnson, D.L.: Mod.Develop.Powder Met., 1971, 4, 189-198.

Jones, F.W.: Proc.Roy.Soc. 166A, 16, 1938.

Jones, J.A.: Ph.D. Thesis (CNNAA), 1970.

Karev, V.N., Klyucharev, A.P., Lishenko, L.G., Nazarova, T.S., & Rozen, A.A.: Izv.Adad.Nauk SSSR, Neorg.Mater., 1967, 3(9), 1676-1678.

Katagiri, Toshio,& Fugii, K: Kinzoku Hyamen Gijutsu, 1971, 22(5), 238-245. (N.L.L. translation, RTS 7002: April 1972).

Kaufman, L.: SAMPE Quart., 1970, 2(1), 46-52.

Kawashina, C.: Taika, Zairyo, 1970, (112), 16-26. (N.N.L. translation, RTS 7657: Nov. 1972).

Kay, D.H.: "Techniques for Electron Microscopy", 1965 (Oxford: Blackwell).

Keihn, F.G., & Keplin, E.J.: J.Am.Ceram.Soc., 1967, 50(2), 81-84.

Kellam, D., & Nicholson, P.S.: J.Am.Ceram.Soc., 1971, 54(2), 127-128.

"Kermety" (Metal - Ceramics). Izv-vo IL, Moscow, 1962.

Kieffer, R., & Benesovsky, F.: "Hartstoffe", 1963 (Wien: Springer-Verlag).

Kieffer, R., Reister, N., & Fister, D.: Iron Steel Inst. Lond., 1970, No. 126, 156-161.

Kiessling, R.: Acta Chem. Scand., 1950, 4, 209.

Kingery, W.D., & Berg, B.: J.Appl.Phys., 1955, 26, 1205.

Kingery, W.D.: "Introduction to Ceramics", 1960, p.353 (N.Y. Wiley).

Kiparisov, S.S., Nikiforov, O.A., & Kuz'mina, Yu.K.: Izv.Vyssh.Ucheb. Zaved., Tsvet.Met., 1970, 13(5), 93-95 (N.L.L. translation, RTS 7202: May 1972).

Kisliy, P.S., & Kuzenkova, M.A.: Izv.Akad.Nauk. SSSR, Neorg.Mater., 1966, 2(12), 2139-2144.

Kisliy, P.S., Kuzenkova, M.A., & Zaverukha, O.V.: Phys.Sintering, 1971, 3, 29-43.

Kosenko, V.A., Rud, B.M. & Sidorova, V.G.: Izv.Akad.Nauk. SSSR, Neorg.Mater., 1971, 7(8), 1455-1456.

Kosolapova, T.Ya., & Domasevich, L.T.: Porosh.Met., 1970, 10(5), 1-5.

Kosolapova, T.Ya., Makarenko, G.N.: Tugoplavkie Karbidy, 1970, 16-20 (N.L.L. translation, RTS 7315: July 1972).

Kosolapova, T.Ya.: Carbides, Properties, Production and Applications, 1971.

Kostetskii, I.I., L'vov, S.M. & Kunitskii, Yu.A.: Izv.Akad.Nauk SSSR, Neorg.Mater., 1971, 7(6), 951-955.

Kovenskaya, B.A., & Serebryakova, T.I.: Porosh.Met., 1970, 10(5), 79-82.

Kowalewski, M., & Bogkaszewska, K.: Hutnik, 1971, 38(3), 131-137 (N.L.L. translation, RTS 7174: Oct. 1972).

Kuchima, A.Ya., & Samsonov, G.V.: Neorg.Mater., 1966, No.11, p.1970.

Kuczynski, G.C.: "Theory of Solid State Sintering", 1961 (N.Y., Wiley; Interscience).

Kuentzler, R.: Phys.Status Solidi, 1970a, 41(1), 291-296.

Kuentzler, R.: J.Appl.Phys., 1970b, 41(3), 908-909.

Kuentzler, R.: J.Phys.(Paris), Collog., 1971, 1(2), C1, 634-635.

Kugai, L.N., & Nazaruchuk, T.N.: Porosh.Met., 1971a, 11(3), 51-55.

Kugai, L.N., & Nazaruchuk, T.N.: Porosh. Met., 1971b, 11(4), 50-53.

Kugai, L.N.: Porosh.Met., 1971, 11(12), 54-57.

Kunitskii, Yu.A., & Marek, E.V.: Porosh.Met., 1971, 11(3), 56-59.

Kuz'ma Yu.B., Serebryakova, & Plakhina, A.M.: Zk.Neorg.Khim., 1967, 12(2), 559.

Lenel, F.V., Ansell, G.S., & Morris, R.C.: Modern Develop.Powder Met., 1971, 4, 199.

Lenel, F.V.: Phys.Sintering, 1972, 4(1), 120.

Levinskii, Yu.V., Portnoi, K.I., & Salibekov, S.E.: (USSR). Vzaimodeistvie Mater. Vysoko-temp. Naznacheniya Sredoi, Sb.Tr.Vses. Nauk.Semin., 1967 (pub.1968), 175-185 (N.L.L. translation, RTS 7425: Aug. 1972).

Lindroos, V.K.: Met.Trans., 1971, 2(11), 3231-3233.

Lipson, H., & Steeple, H.: Interpretation of X-ray powder diffraction patterns, 1970, St. Martin's Press, N.Y.

Lyakhovich, L.S., Surkov, V.V., Dolmanov, F.V., & Turov, Yu.V.: Metalloved.Term.Obrab.Metal., 1971, (7), 72-73.

MacDonald, N.F., & Ransley, C.E.: Powder Metall.Bull., 1959, No.3, p.172.

MacKinnon, I.M., & Wickens, A.J.: Chemistry and Industry, 1973, No.16, 18th August.

Maire, J., Slonina, J.P., & Schrer, A.: Fr. 1,568,883 (Cl.$C_{22}C$, $B_{22}f$), 30 May 1969.

Manning, C.R., JR., Gurganus, T.B.: J.Am.Ceram.Soc., 1969, 52(3), 115

Marek, E.V., Kuz'ma, Yu.B., & Kosolapova, T.Ya.: Porosh.Met., 1971, 11(2), 70-73.

Markovskii, L.Ya., & Bezruk, E.T.: Izv.Akad.Nauk. SSSR, Neorg. Mater. 1967.

Markovskii, L.Ya., Vekshina, N.V., Kondrshev, Yu.D., Voevodskaya, T.K., & Pitirimov, B.Z.: Zh.Prikl.Khim (Leningrad) 1969, 42(12), 2690-2695.

Markovskii, L.Ya., Bezruk, E.T., & Berlova, G.E.: Izv.Akad.Nauk. SSSR Neorg.Mater., 1971, 7(1), 56-58.

Maron, F.S., & Germaidze, M.S.: Zh.Prikl.Khim. (Leningrad), 1970, 43(8), 1826-1827.

Matkovich, V.I., & Giese, R.F. Jr.: Economy J., Z.Kristallogr. Kristallgeom., 1965, 122, 116.

Matkovich, V.I., Giese, R.F. Jr., Economy, J., & Barrett, R.: Acta Crystallogr., 1965, 19, 1056.

Maude, : M.Phil. Thesis (London), 1970.

McDonald, R.J., & Stuart, W.J.: Acta Crystallogr., 1960, 13, 447.

Medvedev, O.A., & Sin'kov, V.A.: Porosh.Met., 1971, 11(7), 63-67.

Medvedev, O.G., Trunov, L.V., Chernyak, L.V., & Shlyuko, V.Ya.: Poroshkovaya Metallurgiya, 1971, No.3 (99), 101-102.

Meerson, G.A., & Gorbunov, A.E.: Izv.Akad.Nauk. SSSR, Neorg.Mater. 1969, 5(12), 2075-2082.

Meerson, G.A., Manelis, R.M., & Nurmukhamedov, V.: Kh. (USSR). Izv. Akad.Nauk.SSSR, Neorg.Mater., 1970, 6(7), 1219-1223.

Minkevich, A.N., Rastorguev, L.N., & Yusfina, L.I.: Metal Science & Heat Treatment, Nos.3-4, March-April, 1967, 191-193.

Morgan, C.S.: High temp. - High pressure, 1971, 3(3), 317-324.

Muchi, I., & Higuchi, J.: Tetsu To Hagane, 1970, 56(3), 371-381.

Münster, A.: Z.Electrochem., 1959, 63, 807.

Murray, P. et al: Trans.Brit.Ceram.Soc., 1954, 53, 474.

Muta, A., Toda, G., & Shimanoki, H.: Nippon Kinzokii Gakkaishi, 1968, 32(5), 440-443 (N.L.L. translation, RTS 7197: July 1972).

Nabarro, F.R.N.: "The Strength of Solids", Physical Soc., 1948.

Naidich, Yu.V.: Porosh.Met., 1964, (2), 50.

Naidich, Yu.V., & Lavrienko, I.V.: Porosh.Met., 1965, (10), 61.

Naumenko, V.Ya.: Porosh.Met., 1970, 10(10), 20-22.

Nelson, J.A., Willmore, T.A., & Womeldorph, R.C.: Refractory Borides composed of B & Ti Carbides bonded with Metals. Presented at 99th meeting Electrochem.Soc., Wash. April 1951.

Neshpor, V.S., Friedlender, B.A., & Sharupin, B.: N.Inzh.-Fix.Zh., 1970a, 18(3), 527-530.

Neshpor, V.S., Nikitina, V.P., & Rahotnov, V.V.: (USSR). Tugoplavkie Karbidy, 1970b, 132-138 (N.L.L. translation, RTS 6961: Jan. 1972).

Niihara, K.: Bull.Chem.Soc.Jap., 1971, 44(4), 963-967.

Nowotny, H.: MTP.Int.Rev.Sci.Inorg.Chem., Ser.One, 1972a, 10, 151-188.

Nowotny, H.: Angew.Chem.Internat.Edit., 1972b, 11(10).

Odintsov, V.V., & Paderno, Yu.B.: Izv.Akad.Nauk. SSSR, Neorg.Mater., 1971, 7(2), 333.

O'Neill, P.: M.Sc. Thesis, 1969, Newcastle University.

Ordan'yan, S.S., et al: Porosh.Met., 1970, 10(8), 665-668.

Oreshkin, V.D., Svetlopolyanskii, V.I., & Kochkin, P.V.: (USSR) Issled.Naplavochnykh Splavov Csn.Tugoplavkikh Soedin., 1970, 63-72 (N.L.L. translation, RTS 7682: Nov. 1972).

Oreshkin, V.D., Svetlopolyanskii, V.I., & Serebryakova, T.I.: Porosh. Met., 1971, 11(3), 78-82.

Paderno, Yu.B., Yupko, V.L., Rud, B.M., Kvas, O.F., & Makarenko, G.N.: Neorg.Mater., 1967, No.2, pp.395, 398.

Panasyuk, A.D., Kozina, G.K., Borovikova, M.S., & D'Yakonova, L.V.: (USSR) Fiz.Khim.Poverkh.Yavlenii Vys.Temp., 1971, 185-188 (N.L.L. translation, RTS 7975: Feb. 1973).

Pastor, H.: Ind.Ceram., 1969, 615, 89-104.

Pauling, L.: "Nature of the Chemical Bond", 1940, p.420 (Ithaca, N.Y.: Cornell Univ.Press).

Pauling, L.: J.Am.Chem.Soc., 1947, 69, 542.

Pauling, L.: Proc.R.Soc.(A), 1949, 196, 343.

Pearson, W.B.: "A Handbook of Lattic Spacings and Structures of Metals and Alloys", 1958, p.7 et seq (Oxford: Pergman).

Peisser, H.P., Rooksby, A.J.C., & Wilson (Ed.): "X-Ray Diffraction of Polycrystalline Materials", part I, Chapman & Hall, London, 1960.

Pilling, N.B., & Bedworth, R.E.: J.Inst.Metals, 1923, 29, 529.

Ploog, K., Schmidt, H., Amberger, E., Will, G., & Kossobutzki, K.H.: J.Less-Common Metals, 1972, 29(2), 161-169.

Podmore, H.L., & Beasley, E.S.C.: Chemy.Ind., 1967, p.1443.

Portnoi, K.J., & Romashov, V.M.: Porosh.Met., 1968, 8(2), 41-44.

Post, B.: "Boron, Metallo-Boron Compounds and Boranes" (Ed.R.M.Adams), 1964, p.301 (New York: Interscience).

Powell, C.F., Oxley, J.H., & Blocker, J.M.: "Vapour Deposition", 1966, p.343 (New York: Wiley).

Protasevich, G.F., Novik, F.S., & Voroshnin, L.G.: Vesti AN Bel. USSR ser.fiz.-tekh.Navik, 1972, 1, 20-26 (N.L.L. translation, RTS 7758: Dec.1972).

Reijnen, P.: Reactive Solids, Proc.Int.Symp., 6th, 1968 (Pub. 1969), 99-114.

Richardson, L.S., & Grant, N.J.: Trans.Metall.Soc. A.I.M.E., 1954, 200, 69.

Richardson, F.D., & Jeffes, J.H.E.: J.Iron and Steel, 1948, 160, 261.

Ristic, M.M.: Phys.Sintering, 1969, 1(1-3), A_1-A_{14}.

Roeder, E., & Scholtz, S.: "Special Ceramics", Proc.Symp.Br.Ceram. Res.Ass., 1964, p.269 (London. Academic Press).

Rogl, P., Nowotny, H., & Benesovsky, F.: Monatsh.Chem., 1971, 102(3), 678-686.

Romashov, V.M., Timofeeva, N.I., Frolova, K.I., & Romanovich, I.V.: Sov.Powder Metall.& Met.Ceram., 1970, (9), 762-776.

Rose, H.E.: Chemy.Ind., 1967, p.1383.

Rundle, R.E.: Acta Crystallogr., 1948, 1, 180.

Salibekov, S.E., Levinskii, Yu.V., & Lobankov, V.V.: (USSR). Izv.Akad. Nauk. SSSR, Neorg.Mater., 1970, 6(9), 1622-1624.

Samsonov, G.V., & Golubeva, N.K.: Zh.Fiz.Khim., 1956, 30, 1258.

Samsonov, G.V.: Zh.Fiz.Khim., 1956, 30, 2058.

Samsonov, G.V., & Grodshtein, A.E.: Zh.Fiz.Khim., 1956, 30, 379.

Samsonov, G.V., & Umanskiy, Y.S.: "Solid Compounds of Refractory Metals", 1957, p.1 (Moscow: Metallurgizdat).

Samsonov, G.V., & Neshpor, V.S.: Dokl.Akad.Nauk. SSSR., 1958, 122, 1021.

Samsonov, G.V.: Usp.Khim., 1959, 28, 189 (U.K.A.E.A. translation, report AERE, Trans. 849).

Samsonov, G.V., & Neshpor, V.S.: "Subjects of Powder Mettallurgy and Strength of Materials", 1959, Issue 7, p.99 (Kiev: Izdvo Akad.Nauk. SSSR).

Samsonov, G.V., Markovskiy, L.Ya., Zhigach, A.F., & Valyashko, M.G.: "Boron, its Compounds and Alloys", 1960, p.60 (Kiev: Izdvo Akad.Nauk Ukr. SSR).

Samsonov, G.V., Markovskiy, L.Ya., Zhigach, A.F., & Vlyashko, M.G.: "Bor, Ego Soedineniya i Splavy", 1960, p.179 (Kiev: Izdvo Akad.Nauk. Ukr. SSR).

Samsonov, G.V.: "Refractory Transition Metal Compounds", 1964a (London: Academic Press).

Samsonov, G.V.: "High-Melting Compounds of the Rare-Earth Metals", 1964b, p.1 (Moscow: Metallurgizdat).

Samsonov, G.V.: Ukr.Khim.Zh., 1965, 31(10), 1005 (N.L.L. translation, RTS 4233: Dec. 1967); Summarised in Izv.Akad.Nauk. SSSR, 1967, 58(10), 76.

Samsonov, G.V.: Dokl.Akad.Nauk. SSSR., 1953, 83, 689; Neorg.Mater., 1967, No.1, p.17.

Samsonov, G.V., & Neronov, V.A.: Electron Technology, 1970, 3(1-2), 67-72.

Samsonov, G.V., Zhunkovskii, G.L., & Evtushok, T.M.: Izv.Akad.Nauk. SSSR, Neorg.Mater., 1970a, 6(9), 1617-1621.

Samsonov, G.V., Yurchenko, D.Z., & Bovkun, G.A.: (USSR). Automatic Welding, 1970b, 23(10), 70-71.

Samsonov, G.V.: (USSR). Tugoplavkie Karbidy, 1970, 9-15 (N.L.L. translation, RTS 7334: July 1972).

Samsonov, G.V., & Kunits'kii, Yu.A.: Dopovidi AN Ukr. RSR.Ser.A.Fiz. Tekh.Met.Nauki, 1970, 32(11), 1048-1050.

Samsonov, G.V., Kovenskaya, B.A., Serebryakova, T.I., & Tel'nikov, E.Ya.: Teplofiz.Vys.Temp., 1971a, 9(1), 195-197.

Samsonov, G.V., Koven'ska, B.O., & Serebryakova, T.I.: Dopovidi - AN Ukr. RSR.Ser.A., 1971b, 33(12), 1127-1129 (N.L.L. translation RTS 7528: Oct. 1972).

Savitskii, E.M., Timofeeva, N.I., & Bakarinova, V.I.: Izv.Akad.Nauk. SSSR, Neorg.Mater., 1970a, 6(1), 120-121.

Savitskii, E.M., Kul'hakh, A.A., & Evstyukhin, N.A.: (USSR). Tugoplavkie Karbidy, 1970b, 211-214. (N.L.L. translation RTS 7288: Sept. 1972).

Savitskii, E.M., & Arabei, B.G.: Izv.Akad.Nauk. SSSR, Neorg.Mater., 1971, 7(4), 617-619).

Schick, H.L.: "Thermodynamics of certain Refractory Compounds", 1966, Vols. I and II (Lond. Academic Press).

Scholtz, S.: "Special Ceramics", Proc.Symp.Br.Ceram.Res.Ass., 1962, p.293 (Lond. Academic Press).

Schwarzkoph, P., & Glaser, F.W.: Third Int.Cong.Electrohead Electro-Chem., Paris, 1953, Paper 4.

Schwarzkopf, P., & Kieffer, R.: "Refractory Hard Metals", 1953 (New York: Wiley).

Schwarzkopf, P., & Kieffer, R.: "Cemented Carbides", 1960 (Lond. Macmillan).

Serebryakova, T.I., & Samsonov, G.V.: Zh.Prikl.Khim., 1967, 40(1), 1-6.

Shaffer, P.T.B., & Samsonov, G.V.: "High Temperature Materials", 1964, Handbooks 1 and 2 (New York: Plenum).

Shimohira, T.: Yogyo Kyoki Shi, 1971, 79(908), 132-138.

Skuratovskii, V.N., Dzhemelinskii, V.V., Borisenko, V.A.: Problemy Prochnosti, 1969, No.6, pp.100-101.

Sleptsov, V.M., & Kosolapova, T.Ya.: Sovrem.Probl.Porosh.Met., 1970, 224-242.

Sosnowskii, L.: Electron Techno., 1970, 3(1-2), 15-19.

Srbobran, Rajic: Z.Anal.Chem., 1969, 246, 111-115.

Stewart, R.W., & Cutler, I.B.: J.Am.Ceram.Soc., 1967, 50(4), 176.

Stokes, A.R., & Wilson, A.J.C.: Proc.Phys.Soc., 1944, 56, 174.

Stokes, A.R.: Proc.Phys.Soc., 1948, 61, 382

Stone, H.E.N.: Fournal of Materials Science, 1972, 7, 1147-1153.

Storms, E. .: "The Refractory Carbides", Refractory Materials Monogrs. (Ed. J.L. Margrave), 1967, Vol.II (London Academic Press).

Storms, E.K.: MTP (Med.Tech.Publ.Co.) Int.Rev.Sci.Inorg.Chem., Ser. One, 1972, 10, 37-49.

Stringer, R.K., & Williams, L.S.: Fourth Symposium on Special Ceramics", (Stoke-on-Trent) July, 1967.

Sugya, T., & Watanabe, O.: J.Less-Common Metals, 1972, 26(1), 25-31.

Takahashi, T., Sugiyama, K., & Suzuki, Y.: J.Cryst.Growth, 1971, 10(2), 139-143.

Telegus, V.S., & Kuz'ma, Yu.B.: Porosh.Met., 1968, 8(2), 68-75.

Thompson, R., & Wood, A.A.R.: The Chemical Engineer, Feb. 1963.

Thompson, R.: Lecture Series, R.I.C., 1965, No.5.

Thompson, R.: Process Common W.Mining Met.Conr., 9th 1969 (Pub.1970a), 563-571, Edited by Jones, M.J., Inst. Mining & Met.

Thompson, R.: Endeavour, 1970b, 29(106), 34-38, Boron and its Refractory Binary Compounds.

Thompson, R.: Progress Boron Chemistry, 1970c, 2, 173-230.

Thompson, R.: Chemistry in Britain, 1971, 7, No.4, April.

Thornton, P.R.: "Scanning Electron Microscopy", 1968, Willmer Brothers Limited, Birkenhead.

Tikkanen, M.H., & Ylasarri, S.: Phys.Sintering, 1969, 1, 1-10

Tikkanen, M.H., Ylasaari, S., & Blonster, K.: Phys.Sintering, 1971, 3(1), 1-28.

Timofeeva, E.N., & Timofeeva, N.J.: (USSR). Zh.Prikl.Khim.(Leningrad), 1971, 44(6), 1400-1402.

Torkar, K., Krischner, H., & Hitsch, E.: Monatsh.Chem., 1971, 102(1), 249-255.

Toth, L.E.: Transition Metal Carbides and Nitrides, April 1971.

Troughton, C., & Simms Ltd.: "Photomicrography with the Vickers Projection Microscope" handbook, 1956.

Tukamoto, T., Shimada, S., Taguchi, T., Higuchi, J.: Tetsu To Hagane, 1970, 56(6), 661-670.

Tumanov, V.I., Gorbunov, A.E., & Kondratenko, T.M.: Zh.Fiz.Khim., 1970, 44(2), 540.

Ubbelohde, A.R.: Trans.Faraday Soc., 1931, 28, 284.

Ubbelohde, A.R.: Proc.R.Soc.(A), 1937, 159, 295.

Umanskiy, Y.S.: J.Phys.Chem., Wash., 1943, 26, 127.

Varzanov, M.A., Dombrova, I.V., Kalirina, A.A.: U.K. Patent No.1,243,569, 1969.

Varzanov, M.A., Dombrova, I.V., Kalirina, A.A.: British 1,243,569, 1971

Vatolin, N.A., Ukhov, V.F., Eston, O.A., & Dubinin, E.I.: (USSR). Tr. Inst.Met., Sverdlovsk, 1969, 20(2), 42-45 (N.L.L. translation, RTS 7321: Aug. 1972).

Vekshina, N.V., & Markovshkii, L.Ya.: (USSR). Khim.Svoistva Metody Anal. Tugoplavkikh Soedin., 1969, 132-142 (N.L.L. translation, RTS 7319: July 1972).

Vekshina, N.V., Markovskii, L.Ya., Kondrashev, Yu.D., & Voevdskaya, T.K.: (USSR). Prikl.Khim. (Leningrad), 1971, 44(5), 959-963.

Vincze, A.: Banyasz.Kohasz.Lapok.Kohsz., 1969, 102(11), 480-482.

Voroshilov, Yu.V., & Kuz'ma, Yu.B.: Porosh.Met., 1969, 9(11), 94-98.

Vydrevich, L.A.: Sov.Powder Metall. and Met.Ceram., 1970, (12), 980-985.

Wallbaum, H.J.: Z.Metallk., 1941, 33, 778.

Webb, W.W., Norton, J.T., & Wagner, C.: J.Electrochem.Soc., 1956, 103, 112.

Werheit, H., Binnenbruck, H., & Hausen, A.: Phys.Status Solidi B., 1971, 47(1), 153-158.

Wheat, T.A., & Carruthers, T.G.: "Science of Ceramics", 1968, Vol.IV, p.34 (Stoke-on-Trent: British Ceram.Soc.).

White, J.: "Science of Ceramics", Proc.Br.Ceram.Soc., 1962, 1, 305, ibid., 1965, 3, 155.

Whittemore, O.J.: Trend Eng.Univ.Wash., 1968, 30(2), 28-33.

Wicks, C.E., & Block, F.E.: Thermodynamics Properties of 65 Elements - Their Oxides, Halides, Carbides and Nitrides, 1965, U.S. Bureau of Mines Bull. No.605.

Will, G.: Nature, Lond., 1966, 212, 175.

Will, G.: Electron Technol., 1970, 3(1-2), 119-126.

Yukin, G.I.: Metalloved. Term Obrab.Metal., 1971, No.8, 662-664.

Yvon, K., & Parthe, E.: Acta Crystallogr., Sect.B., 1970, 26(2), 149-153.

Zaverukha, O.V.: Porosh.Met., 1970, 10(6), 41-43.

Zelikman, A.N., & Loseva, S.S.: Tsvet Metally, Mosk., 1947, 20(4), 41.

Zelikman, A.N., & Gorovits, N.N.: Zh.Prikl.Khim. SSSR, 1950, 23, 689.

Zworykin, V.K., Morton, G.A., Ramberg, E.G., Hillier, J., & Vance, A.W.: "Electron Optics and the Electron Microscope". J. Wiley, N.Y., 1945.

APPENDICES

1. Computer programme for particle size measurement by X-ray method and table of values of particle size.

2. Computer programme for calculation of thermodynamic functions and tables of thermodynamic data for borides and carbides.

3. Computer programme for graph plotting.

4. Computer programme for calculation of fractional volume change for conversion of metals to borides and carbides and their subsequent conversion to oxides. Fractional volume change tables for borides and carbides.

APPENDIX I

PARTICLE SIZE MEASUREMENT BY X-RAY LINE BROADENING

Let b_o and B_o be the observed breadths of a s-line and a m-line respectively, and Δ the doublet spearation given by:

$$\Delta = 0.285 \tan \theta$$

θ being the angle for maximum diffraction (Bragg angle). The corrections for the α-doublet to the s-line and the m-line are given by Jones (1938) graphic form, b/b_o as a function of Δ/b_o, and B/B_o as a function of Δ/B_o, where b and B are the respective breadths after correction for the α-doublet. In this programme, b and B were expressed as an exponential function which was made to fit the curve.

These values of b and B were used to calculate β, the intrinsic broadening, from the following relation between b/B and β/B:

$$b/B = kp \qquad \beta/B = 2p$$

where

$$p = \frac{2k^3 - 3k^2 + 1}{2(1-k^2)^2}$$ and k is a parameter of particle size..

This equation was solved by the Newton Raphson numerical method to find k values over the desired range of b/B, in this case 0 to 1. The k value was back substituted to evaluate β, thus giving t the particle size. The particles were assumed to be in the form of cube or spheres; t is then the cube edge or equivalent spherical diameter.

The programme calculates particle sizes from values of θ from 16° to 24° in increments of 0.1°, and for B_o from 0.27° to 0.40° in increment of 0.01°. These ranges for θ and B_o were the ones usually dealt with in the application of the programme to the work described in this thesis. The ranges of θ and B_o as well as their increment can be changed by

slight modification to the programme.

The computer programme is given below together with a page of specimen output. Complete tables are available in a separate folder from Plymouth Polytechnic Library.

```
      DIMENSION N(14)
   30 FORMAT(40X,'MEASUREMENT OF PARTICLE SIZE BY THE X-RAY METHOD')
      WRITE(3,30)
   40 FORMAT(///,' THE UNITS OF PARTICLE SIZE ARE ANGSTROMS')
      WRITE(3,40)
    5 FORMAT('1',7X,'B0',3X,'0.50',3X,'0.60',3X,'0.70',3X,'0.80',3X,'0.9
     *0',3X,'1.00',3X,'1.10',3X,'1.20',3X,'1.30',3X,'1.40',3X,'1.50',3X
     *,'1.60',3X,'1.70',3X,'1.80')
      WRITE(3,5)
   14 FORMAT(/,1X,'THETA')
      WRITE(3,14)
      LINES=0
      WAVEL=1.54
      DELTS=0.285*(SIN(14.717*3.1429/180.0)/COS(14.717*3.1429/180.0))
      BS0=0.24
      XS=DELTS/BS0
      YS=EXP(0.195-XS)
      BS=YS*BS0
      ANGLE=15.9
      DO 25 I=1,86
      IF(LINES-15)65,60,60
   60 WRITE(3,11)
   11 FORMAT(1H)
      LINES=0
   65 THETA = ANGLE +0.1
      ANGLE=THETA
      THETA=THETA*3.1429/180.0
      DELTL=0.285*(SIN(THETA)/COS(THETA))
      L=1
      DO 15 J=50,180,10
      BL0=0.01*J
      XL=DELTL/BL0
      YL=EXP(0.195-XL)
      BL=YL*BL0
      BSBL=BS/BL
      IF(BSBL-0.9)45,45,50
   50 SIZE=0.0
      GO TO 55
   45 RK=0.5
    8 U=2.0*RK**4-3.0*RK**3+RK
      V=2.0*(1.0-RK**2)**2
      FV=U/V-BSBL
      DU=8.0*RK**3-9.0*RK**2.+1.0
      DV=4.0*(1.0-RK**2)*(-2.0*RK)
      FKD=(V*DU-U*DV)/(V**2)
      DIF=-FK/FKD
      RKD=RK+DIF
      IF(ABS(DIF)-0.0001)4,4,10
   10 RK=RKD
      GO TO 8
    4 BTBL=(2.0*RKB**3-3.0*RKB**2+1.0)/(1.0-RKB**2)**2
      BT=BTBL*BL
      BT=BT*2.0*3.143/360.0
      SIZE=WAVEL/(BT*COS(THETA))
   55 N(L)=SIZE
      L=L+1
   15 CONTINUE
      LINES = LINES+1
   25 WRITE(3,20)ANGLE,(N(L),L=1,14)
   20 FORMAT(/,F6.2,3X,14F7)
      CALL EXIT
      END
```

```
FEATURES SUPPORTED
 TRANSFER TRACE
 ARITHMETIC TRACE
 ONE WORD INTEGERS
 EXTENDED PRECISION
 IOCS

CORE REQUIREMENTS FOR
 COMMON      0 VARIABLES    106 PROGRAM    686

END OF COMPILATION

// XEQ
```

THETA	B0	0.27	0.28	0.29	0.30	0.31	0.32	0.33	0.34	0.35	0.36	0.37	0.38	0.39	0.40
16.00		2413	1726	1346	1104	937	814	721	647	587	537	495	460	429	402
16.10		2455	1748	1359	1113	944	819	725	650	589	539	497	462	431	404
16.19		2498	1770	1373	1122	950	824	729	653	592	542	499	463	432	405
16.29		2543	1793	1386	1132	957	836	733	656	595	544	501	465	434	406
16.39		2589	1816	1400	1141	968	835	737	658	597	546	503	467	435	408
16.49		2637	1839	1415	1151	971	840	741	663	600	549	505	468	437	409
16.59		2686	1864	1429	1160	978	845	745	666	603	551	507	470	438	411
16.69		2737	1889	1444	1170	985	851	749	670	606	553	509	472	440	412
16.79		2791	1914	1459	1180	992	856	753	673	609	556	511	474	441	413
16.89		2846	1940	1474	1190	999	862	758	677	612	558	513	476	443	415
16.99		2904	1967	1490	1201	1007	867	762	680	614	561	515	477	445	416
17.09		0	1995	1506	1211	1014	873	766	684	617	563	518	479	446	417
17.19		0	2023	1523	1222	1022	878	771	687	620	565	520	481	448	419
17.29		0	2053	1539	1233	1029	884	775	691	623	568	522	483	449	420
17.39		0	2083	1556	1244	1037	890	780	695	626	570	524	485	451	422

Units of particle size are Angstrom

PAGE 2 A A CHAUDHRY

```
      DIMENSION REAC(8), SYS(5), DGT(40),EK(40), NT(40)
      READ(2,90)NS
   90 FORMAT(I2)
      WRITE(3,92) NS
   92 FORMAT(///////,30X,'NUMBER',2X,'OF',2X,'SYSTEMS=',I2)
      L=0
    2 READ(2,95)(SYS(J),J=1,5)
   95 FORMAT( 5A2)
      WRITE(3,97)(SYS(J),J=1,5)
   97 FORMAT(//,30X,5A2)
      READ(2,90)NR
      WRITE(3,99)NR
      J1=0
   99 FORMAT(//,10X,'NUMBER',2X,'OF',2X,'POSSIBLE',2X,'REACTIONS=',I2)
    5 READ(2,100)(REAC(J),J=1,8)
  100 FORMAT(8A4)
      WRITE(3,102)(REAC(J),J=1,8)
  102 FORMAT('1',10X,'REACTION',2X,8A4///)
      READ(2,105)AR1,BR1,CR1,DR1,HR1,GR1,R1M
      READ(2,105)AR2,BR2,CR2,DR2,HR2,GR2,R2M
      READ(2,105)AR3,BR3,CR3,DR3,HR3,GR3,R3M
      READ(2,105)AP1,BP1,CP1,DP1,HP1,GP1,P1M
      READ(2,105)AP2,BP2,CP2,DP2,HP2,GP2,P2M
      READ(2,105)AP3,BP3,CP3,DP3,HP3,GP3,P3M
  105 FORMAT(F10.2,F10.5,F10.6,4F10.1)
      DA = P1M*AP1+ P2M*AP2+P3M*AP3- R1M*AR1-R2M*AR2-R3M*AR3
      DB = P1M*BP1+ P2M*BP2+P3M*BP3- R1M*BR1-R2M*BR2-R3M*BR3
      DC = P1M*CP1+ P2M*CP2+P3M*CP3- R1M*CR1-R2M*CR2-R3M*CR3
      DD = P1M*DP1+ P2M*DP2+P3M*DP3- R1M*DR1-R2M*DR2-R3M*DR3
      DHS= P1M*HP1+ P2M*HP2+P3M*HP3- R1M*HR1-R2M*HR2-R3M*HR3
      DHO= DHS-298.0*DA-(298.0**2)*DB/2-(298.0**3)*DC/3.0 + DD/298.0
      DGS= P1M*GP1+ P2M*GP2+P3M*GP3- R1M*GR1-R2M*GR2-R3M*GR3
      COI= (DHO-DA*298.0*ALOG(298.0)-DB*(298.0**2)/2.0 -DC*(298.0**3)/6.
     10 - DD/(2.0*298.0)-DGS)/298.0
      DO 120 I=3 ,42
      NT(I)=100*(I-2)
      T=NT(I)
      DHT=DHO+DA* T    +DB*( T    **2)/2.0+DC*( T    **3)/3.0-DD/ T
      DGT(I)= DHO- T    *DA*ALOG( T    )-DB*( T    **2)/2.0-DC*( T    **3)/
     16.0-DD/(2.0* T    )-COI* T
      EK(I)= EXP(-DGT(I)/(1.986* T    ))
  120 WRITE(3,125)NT(I),DGT(I),EK(I),DHT
  125 FORMAT(4X,I4,8X,F16.1,8X,E25.7,8X,F16.1)
      J1=J1+1
      IF(NR-J1)130,130,5
  130 L=L+1
      IF(NS-L)135,135,2
  135 CALL EXIT
      END
```

FEATURES SUPPORTED
ONE WORD INTEGERS
IOCS

CORE REQUIREMENTS FOR
COMMON 0 VARIABLES 352 PROGRAM 934

END OF COMPILATION

REACTION TiO2+2B+2C = TiB2+2CO

Temp. K	ΔG kcal	Eq. Constant	ΔH k cal
100	97191.5	0.0000000E 00	104272.3
200	89325.7	0.0000000E 00	105798.0
300	80993.2	0.0000000E 00	106152.8
400	72597.9	0.0000000E 00	106174.3
500	64217.4	0.8205725E-28	106029.9
600	55877.2	0.4313191E-20	105775.5
700	47586.7	0.1361607E-14	105434.9
800	39350.1	0.1752030E-10	105020.2
900	31169.6	0.2670293E-07	104538.1
1000	23046.2	0.9126171E-05	103992.4
1100	14980.5	0.1051726E-02	103385.7
1200	6972.6	0.5362511E-01	102719.8
1300	-977.3	0.1466178E 01	101995.8
1400	-8869.4	0.2420808E 02	101214.5
1500	-16703.6	0.2723627E 03	100376.5
1600	-24480.1	0.2217143E 04	99482.4
1700	-32199.0	0.1386412E 05	98532.4
1800	-39860.3	0.6955914E 05	97526.9
1900	-47464.3	0.2902979E 06	96466.0
2000	-55010.9	0.1034769E 07	95349.9
2100	-62500.4	0.3723435E 07	94178.8
2200	-69932.8	0.1238468E 08	92952.7
2300	-77308.2	0.3948103E 08	91671.8
2400	-84626.8	0.1138574E 09	90336.2
2500	-91889.5	0.3098437E 09	88945.9
2600	-99093.6	0.8140023E 09	87500.9
2700	-106242.0	0.4024764E 09	85801.4
2800	-113333.9	0.7100585E 09	84447.3
2900	-120369.2	0.1192860E 10	82839.8
3000	-127348.2	0.1917577E 10	81175.7
3100	-134270.9	0.2962387E 10	79456.2
3200	-141137.2	0.4414433E 10	77680.3
3300	-147947.3	0.6366915E 10	75848.0
3400	-154701.3	0.8911210E 10	73959.3
3500	-161399.2	0.1213750E 11	72044.2
3600	-168041.0	0.1612362E 11	70054.7
3700	-174626.7	0.2093225E 11	68010.9
3800	-181156.5	0.2660629E 11	65912.8
3900	-187630.4	0.3316470E 11	63760.4
4000	-194048.3	0.4059994E 11	61553.6

```
PAGE   1

// JOB

LOG DRIVE   CART SPEC   CART AVAIL  PHY DRIVE
   0000         0006        0006        0000
                            0001        0001
                            0021        0002

V2 M09   ACTUAL 16K  CONFIG 16K

// FOR
*LIST SOURCE PROGRAM
*IOCS(DISK,CARD,1132 PRINTER,TYPEWRITER,KEYBOARD,PLOTTER)
*ONE WORD INTEGERS
      DIMENSION  X(100),Y(100)
      CALL SCFOR(1,7.0,8.0,-1.0,0.0)
      CALL SCFOR(2,0.0,40.0,-270.0,-39.0)
      N=1
      L=0
      READ(2,35)
   35 FORMAT(I2)
   25 READ(2,3)XMAX,YMAX,YMIN
    3 FORMAT(3F10.3)
      READ(2,5)(X(I),I=1,41)
      READ(2,6)(Y(J),J=1,41)
    6 FORMAT(10F8.3)
      X(1)=X(1)
    5 FORMAT(16F5.1)
      CALL FPLOT(1,X(1),Y(1))
      IF(L-N)45,50,50
   50 WRITE(1,400)
      PAUSE
   45 DO 10 I=1,41
   10 CALL SCFOR(5,X(I),Y(I),235.,0.)
      CALL FPLOT(-2, X(1),Y(1))
      DO 20 I=1,41
   20 CALL FPLOT(0, X(I),Y(I))
      CALL FPLOT(1,XMAX,YMAX)
      L=L+1
      IF(L-M)40,30,30
   40 GO TO 25
  400 FORMAT(//,' PLEASE CHANGE PEN')
   30 CALL SCFOR(7,SCFX,SCFY,0.,0.)
      CALL ECHAR(XMIN+2.5/SCFX,YMIN+4/SCFY,0.1,0.2,0.)
      CALL EXIT
      END

FEATURES SUPPORTED
 ONE WORD INTEGERS
 IOCS

CORE REQUIREMENTS FOR
 COMMON       0  VARIABLES    426  PROGRAM    372

END OF COMPILATION

// XEQ
```

```
PAGE   1
// JOB
LOG DRIVE   CART.SPEC   CART AVAIL  PHY DRIVE
  0000        0006        0006        0000
                          0012        0001
                          0024        0002

V2 M09   ACTUAL 16K  CONFIG 16K

// FOR
*LIST SOURCE PROGRAM
*ONE WORD INTEGERS
      SUBROUTINE OXIDE( R,VFCO)
      DIMENSION NAME(9,3),CLASO(9,3),AO1(9),BO1(9),CO1(9)
     1   ,AO(9),BO(9),CO(9),NUO(9),NAO(9)
      COMMON I,AO ,BO,CO,AO1,BO1,CO1,NUO,NAO,O,NAME,CLASO
      R=(AO(I)*BO(I)*CO(I)+SQRT(1.0-COS(AO1(I))**2-COS(BO1(I))**2-COS(CO
     1(I))**2+2.0*COS(AO(I))*COS(BO1(I))*COS(CO1(I)))/(NUO(I)*NAO(I))
      VFCO = (R-Q)/Q
      WRITE(3,121)(NAME(I,J),J=1,3),VFCO,(CLASO(I,J),J=1,3),AO(I)
  121 FORMAT(69X,3A2,2X,F7.4,2X,3A4,8X,F7.4)
      WRITE(3,123)BO(I)
  123 FORMAT(106X,F7.4)
      WRITE(3,123)CO(I)
      RETURN
      END

FEATURES SUPPORTED
 ONE WORD INTEGERS

CORE REQUIREMENTS FOR OXIDE
 COMMON     212  VARIABLES     26  PROGRAM     254

RELATIVE ENTRY POINT ADDRESS IS 002F (HEX)

END OF COMPILATION

// DUP

*STORE      WS  UA  OXIDE
CART ID 0006   DB ADDR  5594   DB CNT   0013
```

```
      DIMENSION NAME(9,3),NAMEB(3),CLASO(9,3),CLASM(3),CLASB(3),AO1(9)
     1    ,AO(9),BO(9),CO(9),NUO(9),NAO(9),BO1(9),CO1(9)
      COMMON I,AO ,BO,CO,AO1,BO1,CO1,NUO,NAO,O,NAME,CLASO
      WRITE(3,99)
   99 FORMAT('1 BORIDE',2X,'FRAC.VOL.',2X,'CRYST.LATT.',2X,'LATT.CONST',
     *2X,'CRYST.LATT.',2X,'LATT.CONST.',2X,'OXIDE',2X,'FRAC.VOL.',2X,'CRY
     *YST.LATT.',2X,'LATT.CONST.')
      WRITE(3,98)
   98 FORMAT(9X,'CHANGE',6X,'ELEMENT',18X,' BORIDE',38X,'OXIDE'///)
    1 READ(2,100)AM,BM,CM,AM1,BM1,CM1,NUM,(CLASM(J),J=1,3)
      AM1=AM1*3.143/180.0
      BM1=BM1*3.143/180.0
      CM1=CM1*3.143/180.0
  100 FORMAT(3F6.4,3F4.1,I2,3A4)
      READ(2,106)NO,NB
      READ(2,102)(AO(I),BO(I),CO(I),AO1(I),BO1(I),CO1(I),NUO(I),NAO(I),(
     )NAME(I,J),J=1,3),(CLASO(I,J),J=1,3),I=1,NO)
      DO 140  I=1,NO
      AO1(I)=AO1(I)*3.143/180.0
      BO1(I)=BO1(I)*3.143/180.0
  140 CO1(I)=CO1(I)*3.143/180.0
  102 FORMAT(3F6.4,3F4.1,I2,I1,3A2,3A4)
    3 READ(2,102)AB,BB,CB,AB1,BB1,CB1,NUB,NAB,(NAMEB(J),J=1,3),(CLASB(J)
     1,J=1,3)
      AB1=AB1*3.143/180.0
      BB1=BB1*3.143/180.0
      CB1=CB1*3.143/180.0
  106 FORMAT(2I1)
      I=1
      NI=1
      P=    AM*BM*CM*SQRT(1.0-COS(AM1)*COS(AM1)-COS(BM1)*COS(BM1)-COS(CM1
     *)*COS(CM1)+2.0*COS(AM1)*COS(BM1)*COS(CM1))/NUM
      Q =    (AB*BB*CB*SQRT(1.0-COS(AB1)*COS(AB1)-COS(BB1)*COS(BB1)-COS(C
     *B1)*COS(CB1) + 2.0*COS(AB1)*COS(BB1)*COS(CB1)))/(NUB*NAB)
      VFCB =  (Q-P)/P
      R=(AO(I)*BO(I)*CO(I)*SQRT(1.0-COS(AO1(I))*COS(AO1(I))-COS(BO1(I))*
     1COS(BO1(I))-COS(CO1(I))*COS(CO1(I))+2.0*COS(AO1(I))*COS(BO1(I))*CO
     1S(CO1(I))))/(NUO(I)*NAO(I))
      VFCO=  (R-Q)/Q
      WRITE(3,107)(NAMEB(J),J=1,3),VFCB,(CLASM(J),J=1,3),AM,(CLASB(J),J=1,0
     11,3),AB,(NAME(I,J),J=1,3),VFCO,(CLASO(I,J),J=1,3),AO(I)
  107 FORMAT(/3A2,4X,F7.4,2X,3A4,2X,F7.4,2X,3A4,3X,F7.4,5X,3A2,2X,F7.4,2X
     1X,3A4,8X,F7.4)
      WRITE(3,109)BM,BB,BO(I)
  109 FORMAT(33X,F7.4,17X,F7.4,42X,F7.4)
      WRITE(3,111)CM,CB,CO(I)
  111 FORMAT(33X,F7.4,17X,F7.4,42X,F7.4)
  112 IF(NO-I)115,113,115
  113 NB=NB-1
      IF(NB-0.0001)117,117,119
  117 GOTO1
  119 GOTO3
  115 I=I+1
      CALL OXIDE(R,VFCO)
      IF(NT-90)125,125,128
  125 GOTO112
  128 CALL EXIT
      END

FEATURES SUPPORTED
 ONE WORD INTEGERS
 IOCS

CORE REQUIREMENTS FOR
 COMMON     212  VARIABLES      90  PROGRAM    1058

END OF COMPILATION

// XEQ
```

BORIDE	FRAC.VOL. CHANGE	CRYST. LATT. ELEMENT	LATT.CONST	CRYST. LATT. BORIDE	LATT.CONST.	OXIDE	FRAC.VOL.	CRYST. LATT. OXIDE	LATT.CONST.
ALB2	0.5397	CUBIC	4.0496 4.0496 4.0496	HEXAGONAL	3.0090 3.0090 3.2620	AL2O	-0.2300	HEXAGONAL	3.0160 3.0160 5.0000
						α-AL2O3	1.4768	HEXAGONAL	4.7580 4.7580 12.9250
						β-AL2O3	0.0142	HEXAGONAL	5.6400 5.6400 22.6000
						γ-AL2O3	-0.1902	CUBIC	7.9200 7.9200 7.9200
						η-AL2O3	-0.1810	CUBIC	7.9500 7.9500 7.9500
ALB12	5.0766	CUBIC	4.0496 4.0496 4.0496	TETRAGONAL	12.5800 12.5800 10.2000	AL2O	-0.0049	HEXAGONAL	3.0160 3.0160 5.0000
						α- AL2O3	-0.3724	HEXAGONAL	4.7580 4.7580 12.9250
						β-AL2O3	-0.7430	HEXAGONAL	5.6400 5.6400 22.6000
						γ-AL2O3	-0.7948	CUBIC	7.9200 7.9200 7.9200
						η- AL2O3	-0.7924	CUBIC	7.9500 7.9500 7.9500
ALB12	4.7230	CUBIC	4.0496 4.0496 4.0496	TETRAGONAL	10.3000 10.3000 14.3300	AL2O	-0.7928	HEXAGONAL	3.0160 3.0160 5.0000
						α-AL2O3	-0.3336	HEXAGONAL	4.7580 4.7580 12.9250
						β-AL2O3	-0.7271	HEXAGONAL	5.6400 5.6400 22.6000
						γ-AL2O3	-0.7821	CUBIC	7.9200 7.9200 7.9200
						η - AL2O3	-0.7796	CUBIC	7.9500 7.9500 7.9500
BAB6	0.2254	CUBIC	5.0250 5.0250 5.0250	CUBIC	4.2680 4.2680 4.2680	BAO	-0.4535	CUBIC	5.5391 5.5391 5.5391
						BAO2	-0.3585	TETRAGONAL	5.3958 5.3958 6.8513
BE2B	0.2264	HEXAGONAL	2.2856 2.2856 3.5843	CUBIC	4.3000 4.3000 4.3000	BEO	0.3960	HEXAGONAL	2.6990 2.6990 4.4010
CAB6	0.6378	CUBIC	5.5820 5.5820 5.5820	CUBIC	4.1450 4.1450 4.1450	CAO	-0.6120	CUBIC	4.7990 4.7990 4.7990
CEB4	0.5440	CUBIC	5.1615 5.1615 5.1615	TETRAGONAL	7.2050 7.2050 4.0900	CEO2	-0.2542	CUBIC	5.4100 5.4100 5.4100
						CE2O3	-0.1617	CUBIC	11.2500 11.2500 11.2500
						CE2O3	-0.2561	TRIGONAL	3.8800 3.8800 6.0000
CEB6	1.0626	CUBIC	5.1615 5.1615	CUBIC	4.1300 4.1390	CEO2	-0.4417	CUBIC	5.4100 5.4100

XXXX